

ABSTRACT

Title of Dissertation: DIFFERENTIAL MODULATION FOR
BROADBAND SPACE-TIME/COOPERATIVE
WIRELESS COMMUNICATIONS

Thanongsak Himsoon, Doctor of Philosophy, 2006

Dissertation directed by: Professor K. J. Ray Liu
Department of Electrical and Computer Engineering

Among various diversity techniques to combat fading in wireless channels, spatial diversity through MIMO coding scheme is an effective way to increase link capacity and system reliability without sacrificing bandwidth efficiency. Recently, cooperative diversity has been introduced as an efficient alternative to improve system performance without the requirement of additional antennas. However, most of existing works on MIMO and cooperative communications are based on an assumption that the destination has perfect knowledge of channel state information of all transmission links and hence introduces high complexity to the receiver.

To overcome such problems, this thesis proposes differential modulation schemes for space-time coded MIMO and cooperative communications. By exploiting spatial/cooperative diversity without the requirement of channel state information,

the proposed schemes provide an excellent tradeoff between receiver complexity and system performance. First, a matrix rotation based signal design for differential space-time modulation is investigated to minimize the union bound on block error probability. Next, a robust differential scheme for MIMO-OFDM systems is proposed by which the signal transmission of each differentially encoded signal is completed within one OFDM block rather than multiple blocks as in existing works. Then, a differential scheme for UWB systems employing MIMO multi-band OFDM is proposed to explore all available diversities by jointly encoding across spatial, temporal, and frequency domains. To exploit cooperative diversity, an amplify-and-forward differential cooperative scheme and a threshold-based decode-and-forward differential cooperative scheme are proposed. The proposed differential cooperative schemes are first considered in a two-node cooperation system, and the proposed works are extended to a general multi-node scenario. Finally, a general framework to improve lifetime of battery-operated devices by exploiting cooperative diversity is proposed such that the device lifetime can be greatly improved by efficiently taking advantages of both different locations and energy levels among distributed nodes in wireless networks.

Differential Modulation for
Broadband Space-Time/Cooperative Wireless Communications

by

Thanongsak Himsoon

Dissertation submitted to the Faculty of the Graduate School of the
University of Maryland, College Park in partial fulfillment
of the requirements for the degree of
Doctor of Philosophy
2006

Advisory Committee:

Professor K. J. Ray Liu, Chairman
Professor Carlos A. Berenstein
Professor Rama Chellappa
Professor Sennur Ulukus
Professor Steven A. Tretter

©Copyright by
Thanongsak Himsoon
2006

DEDICATION

To my parents, Boonsong and Boonsri, and my brother and sisters, who offered me unconditional love and support throughout my graduate studies.

To my love, Wipawee (Pam) Siriwongpairat, for her immense love, patience, and unwavering confidence in me made this thesis come true.

ACKNOWLEDGEMENTS

It is my great honored to have an opportunity to work with many distinguished colleagues during the development of this thesis. My experience as a graduate student at the University of Maryland has been unique and invaluable. I owe my heartfelt thanks to all that supported me along the way.

The first person I would like to thank is my advisor Dr. K. J. Ray Liu for his invaluable guidance and support through the years. His endlessly enthusiasm and integral view on research as well as his mission on providing high-quality state-of-art research has made a real deep impression on me. He set high standards for me, and showed me how to maintain them. He guided me through tough times, and never doubted my abilities, not even when I doubted myself. He was with me at every phase of the learning process, patiently watching over my progress. He set a great example for me as a researchers, teacher and advisor. His array signal processing course induced my peaked initial interest in this field. Without his encouragement to continue my studies and his supportive during my difficult time, I would certainly not have accomplished many things that I am proud of today.

I also would like to express my great gratitude to Professor Carlos A. Berenstein, Professor Rama Chellappa, Professor Sennur Ulukus, and Professor Steven A. Tretter for their agreement to serve as my thesis committee and for sparing their times in reviewing the thesis manuscript.

I would also wish to thank Professor Robert Wayne Newcomb, my former advisor, for his kindness, generous, and valuable support.

I would like to thank Dr. Weifeng Su for his guidance and discussion which are highly informative but yet concise. This thesis can not be theoretically completed without his strong mathematics background. I also thank Dr. Zhu Han for his helpful discussion and innovative idea. His way of quick thinking and finishing an almost unfinishable work in a short time are role models to follow.

I also would like to express my gratitude to all of my colleagues at the Communications and Signal Processing Laboratory (CSPL), which is now changed to the Signal and Information Group (SIG), for their useful discussions, interaction as a family, and informative presentations of their research works during our group meeting.

I would like to thank all of my friends from the past until present who always share thoughts and opinions, and they partly made me become myself. A very special big thank is directed to Mr. Prateep Kongprat who is very supportive and sincerely helps when it needed be.

I feel a deep sense of gratitude for my mother, Boonsri Himsoon, and father, Boonsong Himsoon, for their life-long love and support, understanding, and long-awaiting for my successful return to our homeland. They have formed part of my vision and have taking care of me to become a mature and disciplined man. I also thank my uncle, Sutham Nutakom, for his guidance and support. I am also grateful for my sisters and brother, for rendering me the senses and the values of sisterhood and brotherhood. I am glad to be one of the family members.

Finally, I would like to express my biggest and profound thanks to my beloved small-little girl, Wipawee (Pam) Siriwongpairat, who have shared invaluable ex-

periences in research and life during our graduate studies. The sincere bonding among us inspires hope for prosperous future and bring us powerful strength to overcome several difficult moments. Her love and support allow me to finish this thesis.

TABLE OF CONTENTS

List of Tables	ix
List of Figures	x
1 Introduction	1
1.1 Differential Modulation for Multiple-Antenna Communication Systems	2
1.2 Motivations	5
1.3 Dissertation Overview and Contributions	9
2 Background and Related Literature	15
2.1 Wireless Channel Fundamentals	15
2.1.1 Attenuation for Wireless Systems	16
2.1.2 Input/output Model of the wireless channels	17
2.1.3 Fading Parameters	18
2.1.4 Types of Fading	22
2.1.5 Statistical Channel Models	22
2.2 Diversity Techniques to Combat Multipath Fading	24
2.2.1 Space Diversity	25
2.2.2 Polarization Diversity	26
2.2.3 Angle/Directional Diversity	26
2.2.4 Frequency Diversity	26
2.2.5 Time Diversity	27
2.3 Diversity Combining Techniques	27
2.3.1 Selection Combining	27
2.3.2 Switched Combining	28
2.3.3 Maximum Ratio Combining	28
2.3.4 Equal Gain Combining	30
2.4 MIMO Techniques	30
2.5 Cooperative Diversity	34

3	Differential Modulations for MIMO systems	37
3.1	Differential Unitary Space-Time Signal Design for MIMO systems	37
3.1.1	Channel Model and DUST Scheme	38
3.1.2	Design Method	39
3.1.3	Simulation Results	44
3.2	Differential Modulation for Frequency Selective MIMO-OFDM systems	48
3.2.1	System Description	50
3.2.2	Single-Block Differential Transmit scheme	53
3.2.3	Pairwise Error Probability and Design Criteria	59
3.2.4	Simulation Results	64
3.3	Chapter Summary	71
4	Differential Modulation for UWB Communication Systems	73
4.1	System Model	74
4.2	Differential Scheme for Multiband UWB Systems	75
4.2.1	Transmit Signal and Differential Encoding Structures	76
4.2.2	Differentially Decoding	78
4.3	Pairwise Error Probability	80
4.4	Simulation Results	84
4.5	Chapter Summary	87
5	Differential Modulations for Cooperative Communications	89
5.1	Differential Modulation for Amplify-and-Forward Cooperative Communications	89
5.1.1	Amplify-and-Forward Differential Cooperation Scheme	90
5.1.2	Analysis and Discussions	92
5.1.3	Simulation Results	97
5.2	Differential Modulation for Decode-and-Forward Cooperative Communications	102
5.2.1	Threshold-Based Decode-and-Forward Differential Cooperation Scheme	103
5.2.2	BER Analysis for the DF Differential scheme	109
5.2.3	BER Upper Bound and BER Lower Bound	125
5.2.4	Optimum Decision Threshold and Power Allocation	130
5.2.5	Simulation Results	133
5.3	Chapter Summary	139
6	Differential Modulations for Multi-Node Cooperative Communications	141
6.1	Differential Modulation for Multi-Node Amplify-and-Forward Cooperative Communications	141
6.1.1	Multi-Node AF Differential Scheme	142

6.1.2	BER Performance Analysis for the Multi-Node AF Differential Scheme	145
6.1.3	Optimum Power Allocation for Multi-Node AF Differential Scheme	151
6.1.4	Simulation Results	159
6.2	Differential Modulation for Multi-Node Decode-and-Forward Cooperative Communications	163
6.2.1	Signal Models for the Multi-Node DF Differential Scheme	164
6.2.2	Approximate BER formulation	167
6.2.3	Optimizing Power Allocation and Thresholds	177
6.2.4	Simulation Results	179
6.3	Chapter Summary	182
7	Device Lifetime Maximization in Cooperative Communications	185
7.1	System Model	186
7.1.1	Non-Cooperative Wireless Network	187
7.1.2	Cooperative Wireless Network Employing the DF Protocol	189
7.2	Lifetime Maximization by Cooperative Node Employment	193
7.2.1	Problem Formulation	193
7.2.2	Analytical Solution for a Two-Node Wireless Network	195
7.2.3	Suboptimal Algorithm for Multi-Node Wireless Network	200
7.3	Lifetime Maximization by Cooperative Relay Deployment	204
7.4	Simulation Results and Discussions	209
7.5	Chapter Summary	214
8	Conclusions and Future Research	216
8.1	Conclusions	216
8.2	Future Research	223

LIST OF TABLES

3.1	Comparison of constellation parameters and union bounds for the MRB space-time signal design with $M_T = 2$ transmit antennas. . .	42
6.1	Optimum power allocation for cooperation system with one relay based on exhaustive numerical search.	156
6.2	optimum power allocation for cooperation system with one relay based on approximate closed-form formulation.	156
6.3	Optimum power allocation for cooperation system with two relays based on exhaustive search.	157
6.4	Optimum power allocation for cooperation system with two relays based on approximate formulation (6.55).	157
6.5	Optimum power allocation and thresholds for a cooperation system with two relays.	178
7.1	Suboptimal algorithm for maximizing the minimum device lifetime of wireless network with multiple cooperative nodes	204
7.2	Suboptimal algorithm to determine device lifetime when relay locations are fixed	208
7.3	Algorithm to determine relay locations	209

LIST OF FIGURES

2.1	A generic MIMO communication system.	31
2.2	A generic two-user cooperation system.	34
3.1	Performance for $L = 4$, $M_T = 2$, and $M_R = 1$	45
3.2	Performance for $L = 4$, $M_T = 2$, and $M_R = 2$	45
3.3	Performance for $L = 32$, $M_T = 2$, and $M_R = 1$	46
3.4	Performance for $L = 32$, $M_T = 2$, and $M_R = 2$	46
3.5	Performance for $L = 64$, $M_T = 2$, and $M_R = 1$	47
3.6	Performance for $L = 64$, $M_T = 2$, and $M_R = 2$	47
3.7	Description of the differential MIMO-OFDM system.	50
3.8	An example of a code structure for $\Gamma = 2$ and $M_t = 2$ at the p^{th} sub-matrix.	55
3.9	Performance for $M_t = 2$, $M_r = 1$, $R = 1$ b/s/Hz, and $\Gamma = 1, 2$, and 3 under the TU power delay profile.	66
3.10	Performance for $M_t = 2$, $M_r = 1$, $\Gamma = 2$, and $R = 1.5$ b/s/Hz under the two-ray power delay profile.	67
3.11	Performance for $M_t = 2$, $M_r = 1$, $\Gamma = 2$, and $R = 1$ b/s/Hz under the TU power delay profile.	68
3.12	Performance for $M_t = 3$, $M_r = 1$, $\Gamma = 2$, and $R \approx 1$ b/s/Hz under the two-ray power delay profile.	70
3.13	Performance for $M_t = 3$, $M_r = 1$, $\Gamma = 2$, and $R \approx 1$ b/s/Hz under the TU power delay profile.	70
4.1	Example of differential encoded signal matrix and transmit signal structure for the UWB system employing multiband OFDM, $K = 2$, $G = 2$, and $M_t = 2$	77
4.2	Performance under CM1, $M_t = 1$, $M_r = 1$, $R = 1$ b/s/Hz.	84
4.3	Performance under CM1 and CM2, $M_t = 1$, $M_r = 1$, $R = 1/K$ b/s/Hz.	85
4.4	Performance comparison of the proposed differential scheme under CM1 employing SISO and MIMO processing, $K = 1$ and $R = 1$ b/s/Hz.	87
5.1	Cooperative communication system with DQPSK signals, $\sigma_{s,d}^2 = \sigma_{s,r}^2 = \sigma_{r,d}^2 = 1$, $P_1/P = 0.7$ and $P_2/P = 0.3$	98
5.2	Performance comparison of the proposed scheme and that with optimum weights.	99

5.3	Asymptotically tight of the BER formulations with optimum weights to the simulated performance of the proposed scheme with DQPSK signals, $\sigma_{s,d}^2 = \sigma_{s,r}^2 = \sigma_{r,d}^2 = 1$	100
5.4	Cooperative communication system with DQPSK signals for different power allocation schemes, and different channel variances.	101
5.5	Performance comparison of optimum power allocation scheme and equal power allocation scheme, $\sigma_{s,d}^2 = \sigma_{s,r}^2 = 1$ and $\sigma_{r,d}^2 = 10$	101
5.6	The threshold-based differential scheme for decode-and-forward cooperative communications.	105
5.7	Two possible differential detection techniques at the destination; single-channel differential detection or two-channel differential detection, with six possible scenarios based on the currently received signal and the signal stored in memory M_2	111
5.8	DQPSK: BER performance versus P/\mathcal{N}_0 : $\sigma_{s,d}^2 = 1, \sigma_{s,r}^2 = 1$	128
5.9	DQPSK: Performance comparison of theoretical BER curves and simulated curves. (a)-(c) $\sigma_{s,d}^2 = \sigma_{s,r}^2 = \sigma_{r,d}^2 = 1$. (d)-(f) $\sigma_{s,d}^2 = 1, \sigma_{s,r}^2 = 1, \sigma_{r,d}^2 = 10$	132
5.10	DQPSK with or without CRC at relay node, and with or without threshold at destination node, $P_1 = P_2 = 0.5P, \sigma_{s,d}^2 = 1, \sigma_{s,r}^2 = 1, \sigma_{r,d}^2 = 10$	135
5.11	DQPSK: Different thresholds with fixed power allocation.	138
5.12	DQPSK: Different power allocations with fixed threshold.	138
5.13	DQPSK: Different power allocations and different thresholds.	138
6.1	Multi-node differential AF scheme.	143
6.2	DBPSK : Two relays, equal power allocation strategy, and $\sigma_{s,d}^2 = \sigma_{s,r_i}^2 = \sigma_{r_i,d}^2 = 1$	160
6.3	DQPSK : Two relays, equal power allocation strategy, and $\sigma_{s,d}^2 = \sigma_{s,r_i}^2 = \sigma_{r_i,d}^2 = 1$	161
6.4	DQPSK : Two and three relays, equal power allocation strategy, and $\sigma_{s,d}^2 = \sigma_{s,r_i}^2 = \sigma_{r_i,d}^2 = 1$	161
6.5	DQPSK : Two relays, optimum power allocation strategy, and $\sigma_{s,d}^2 = 1, \sigma_{s,r_i}^2 = 10, \sigma_{r_i,d}^2 = 1$	162
6.6	DQPSK : Two relays, optimum power allocation strategy, and $\sigma_{s,d}^2 = \sigma_{s,r_i}^2 = 1, \text{ and } \sigma_{r_i,d}^2 = 10$	163
6.7	System descriptions of the multi-node differential DF scheme.	165
6.8	DQPSK: equal power allocation, $\sigma_{s,d}^2 = \sigma_{s,r_i}^2 = \sigma_{r_i,d}^2 = 1$, and $\zeta = 1$	175
6.9	DQPSK: optimum power allocation, $\sigma_{s,d}^2 = \sigma_{s,r_i}^2 = \sigma_{r_i,d}^2 = 1$, and $\zeta = 1$	176
6.10	DQPSK : different number of relays, equal power allocation, threshold = 1, and $\sigma_{s,d}^2 = \sigma_{s,r_i}^2 = \sigma_{r_i,d}^2 = 1$	180
6.11	DBPSK : three relays, fixed power allocation but different thresholds, and $\sigma_{s,d}^2 = \sigma_{s,r_i}^2 = 1$, and $\sigma_{r_i,d}^2 = 10$	181
6.12	DQPSK : two relays, different power allocation and thresholds, and $\sigma_{s,d}^2 = \sigma_{s,r_i}^2 = 1, \sigma_{r_i,d}^2 = 10$	182

7.1	An example of non-cooperative wireless network with a destination (denoted by d).	187
7.2	The proposed cooperative wireless network: (a) A cooperative wireless network with 4 nodes. (b) The corresponding power allocation matrix. . .	190
7.3	Lifetimes of the two cooperative nodes as functions of the transmit power of the helped node (P_{22}).	196
7.4	Cooperative wireless network with relay deployment: (a) One cluster with 4 nodes, 2 relays, and 1 destination. (b) The corresponding power allocation matrices (\mathbf{P}) and ($\hat{\mathbf{P}}$) for the nodes and the relays, respectively.	206
7.5	Lifetimes of nodes in the two-node wireless network.	210
7.6	Device lifetime with different number of randomly-located nodes.	211
7.7	Device lifetime for a wireless network with a cooperative relay deployment.	213
7.8	Device lifetime of the proposed cooperative wireless network where different number of cooperative relays are deployed.	214

Chapter 1

Introduction

In conventional single-antenna wireless communication systems, the channel capacity can be very low and bit error rate is high when fading occurs. Various techniques can be utilized for fading mitigation, e.g. robust modulation, coding and interleaving, error-correcting coding, equalization, and diversity. Different kinds of diversities such as space, time, frequency, or any combination of them are possible. Among these diversity techniques, space diversity is of a special interest because of its ability to improve performance without sacrificing delay and bandwidth efficiency. Recently, the space diversity has been intensively investigated in point-to-point wireless communication systems by the deployment of multiple input multiple output (MIMO) concept together with efficient coding and modulation scheme. The MIMO systems with proper coding techniques, such as space-time codes [4], nicely convert independent fading channels into benefits to users. The study of MIMO channel capacity [5] shows that MIMO coding frameworks yield much higher capacity than that of the conventional single-antenna systems. Specifically, the MIMO channel capacity increases in linearly proportional to the minimum among the number of transmit (M_T) and receive (M_R) antennas. In addition, it was shown in [4] that pairwise error probability (PEP) is inversely

proportional to $SNR^{M_T M_R}$ which is greatly improved over that for single antenna systems. In recent year, cooperative communication [19] has been proposed as an alternative communication system that explores MIMO-like diversity to improve link performance without the requirement of additional antennas. However, most of existing works [4]- [18] on MIMO systems and [19]- [23] on cooperative communications are designed based on an assumption that the receivers have full knowledge of the channel state information (CSI). In this case, the schemes must incorporate reliable multi-channel estimation which inevitably increases the cost of frequent retraining and the number of estimated parameters to the receivers. Although the channel estimates may be available when the channel changes slowly comparing with the symbol rate, they may not be possibly acquired in fast fading environment. To develop practical schemes that omit such CSI requirements, we propose in this thesis differential modulations for MIMO systems and cooperative communications.

In the rest of this Chapter, we present an introduction to differential modulation for MIMO systems. Then, we provide motivations of this dissertation to overcome such design challenges. After that, we address the organization of this dissertation as well as our research contributions.

1.1 Differential Modulation for Multiple-Antenna Communication Systems

In conventional single-antenna systems, non-coherent modulation is useful when the knowledge of CSI is not available. The non-coherent modulation simplifies the receiver structure by omitting channel estimation and carrier or phase trackings. Some examples of the non-coherent modulation techniques are non-coherent frequency shift keying (NFSK) and differential modulation [3]. Among these mod-

ulation techniques, the differential scheme is preferred to the SFSK because it provides better performance at the same operating SNR. Two classes of differential modulation schemes are available; differential M-ary quadrature amplitude modulation (DMQAM) and differential M-ary phase shift keying (DMPSK). In the DMQAM scheme, information is modulated through the amplitude difference among two consecutive symbols. The DMPSK, however, modulates information through the phase difference among two consecutive symbols. The merit of the differential detection can be described as follows. Define x_τ as the differentially encoded symbol to be transmitted at time τ , α^τ as the fading coefficient, and n^τ as additive noise, then the received signal for DMPSK modulation system can be written as

$$y^\tau = \alpha x^\tau + n^\tau, \quad (1.1)$$

where $x^\tau = v^\tau x^{\tau-1}$ results from differentially encodes information symbol (v^τ) with the previously transmitted symbol $x^{\tau-1}$. The DMPSK demodulator uses two consecutive received signals to decode the transmitted information by calculating

$$\begin{aligned} y^\tau (y^\tau)^* &= |\alpha|^2 x^\tau (x^{\tau-1})^* + \alpha x^\tau (n^{\tau-1})^* + n^{\tau-1} \alpha^* (x^{\tau-1})^* + n^\tau (n^{\tau-1})^*, \\ &\approx |\alpha|^2 v^\tau x^{\tau-1} (x^{\tau-1})^* + \alpha x^\tau (n^{\tau-1})^* + n^{\tau-1} \alpha^* (x^{\tau-1})^*, \\ &= |\alpha|^2 v^\tau + \tilde{\mathcal{N}}, \end{aligned} \quad (1.2)$$

where $\tilde{\mathcal{N}}$ is Gaussian noise, α is assumed constant over time τ and $\tau - 1$, and $(\cdot)^*$ stands for the complex conjugate. The result in the last equality of (1.2) is obtained by discarding $n^\tau (n^{\tau-1})^*$. Therefore, the differential decoder estimates the transmit information using the following decoding rule:

$$\hat{v}^\tau = \arg \min_{v^\tau} |y^\tau (y^\tau)^* - v^\tau|^2, \quad (1.3)$$

by which the successful differential decoding does not requires CSI. In (1.3), $|\alpha|^2$ is

removed because it does not effect the decision region of the DMPSK modulation. Note that the decoding rule in (1.3) depends only on two consecutive received signals, and it does not depend on previous decoding results. Therefore, decoding error does not propagate. The sufficient statistic (1.2) gives an intuitive idea on the performance of the differential detection in comparison to its coherent counterpart. Specifically, the signal power is $|\alpha|^4$ and the noise power is approximately $2|\alpha|^2$, so the obtained SNR is half of that with coherent detection. Therefore, in case of Rayleigh fading, there is about 3 dB performance gap between the differential detection and coherent detection.

A good tradeoff in receiver complexity and performance has driven the differential scheme to be deployed in the IEEE IS-54 standard [24] for cellular systems. Recently, the merit of bypassing multi-channel estimation attracted many researchers to naturally extend the conventional single-antenna differential scheme for MIMO systems. For narrowband systems, a research work on MIMO coding that does not require CSI at either the transmitter or the receiver is proposed in [25] as unitary space-time modulation. It was shown in [25] that the unitary space time modulation achieves the same diversity order of $M_T M_R$ as that of general space time codings. In addition, the unitary signaling concept [25] has been generalized to a differential modulation for MIMO systems, coined as differential unitary space-time (DUST) modulation [26] [27]. The DUST scheme, which utilizes unitary group constellation, are suitable for MIMO systems with arbitrary number of transmit antennas. The other class of differential MIMO systems is based on differential orthogonal space time block codes (DSTBC) have been proposed in [28] for two transmit antennas and in [29] for more than two transmit antennas. A special case of the proposed works in [28] and [29] has been reported in [30, 31].

The related works in [32, 33] utilized multilevel amplitude modulation for DSTBC to improve the MIMO link performance. In case of wideband systems, an idea of employing DUST or DSTBC modulations with orthogonal frequency division multiplex (OFDM) have been introduced as differential space-time-frequency (DSTF) MIMO-OFDM systems [34]- [41].

1.2 Motivations

The proposed design of DUST signals is based on minimizing pairwise block error probability (PBEP). In particular, at asymptotically high signal-to-noise ratio (SNR), the PBEP performance of a good DUST constellation is determined by the so-called diversity product [26]. Based on the design criterion of maximizing the diversity product, a large number of DUST codes have been proposed, for example, diagonal codes or cyclic group codes [26] and [27], generalized quaternion codes or dicyclic group codes [27], fixed-point-free group codes [42] using representation theory, and a non-group signal constellation called parametric codes [43]. The parametric codes was specifically designed for two transmit antenna communication systems. Recently, the matrix rotation based (MRB) space-time signals [44], with a similar concept to [43], have been proposed for a MIMO system with even number of transmit antennas. It was argued recently in [45] that the main target of the performance evaluation is block error probability (BEP), not the PBEP. The codes optimized over the worst case PBEP do not guarantee to provide optimum performance in terms of the BEP. Thus, in [45], a code design criterion of minimizing the union bound on BEP was proposed, and some new cyclic codes were obtained.

Recently, a technique of incorporating the DST modulation with OFDM transmission, called differential space-time-frequency (DSTF) MIMO-OFDM [34]- [41],

was introduced for wideband systems under frequency-selective fading channels. The DSTF scheme differentially encodes across spatial, temporal, and frequency domains such that both spatial and frequency diversities can be explored. However, a complete transmission of one DSTF codeword expands several OFDM symbol periods which are, in fact, proportional to the number of transmit antennas. In order to perform successful differential decoding, all of the existing DSTF schemes [34]-[41] assumed that the fading channels keep constant within several OFDM blocks and slowly change from a duration of several OFDM blocks to another OFDM blocks. Therefore, the constant fading assumption depends directly on the number of transmit antennas. Nevertheless, such channel condition may not valid in practical situations since the channel coefficients would change before two entire DSTF codeword matrices are completely transmitted. The related work on non-coherent SF coding has been investigated in [47], however, a set of SF codes was obtained through random searching, and the scheme introduced high decoding complexity.

Ultra-wideband (UWB) is an emerging technology that offers great promises to satisfy the growing demand for low cost and high-speed digital wireless home networks. A traditional UWB technology, which occupies the available bandwidth of 7.5 GHz, is based on single-band approaches that directly modulate data into a sequence of impulse-like waveforms. Recently, multiband UWB scheme has been proposed [48] by which the UWB frequency band is divided into several subbands, each with a bandwidth of at least 500 MHz in compliance with the FCC regulations. Since many UWB applications are expected to be in portable devices, low complexity becomes a fundamental requirement. This indicates the important need of a simple transceiver design. However, UWB system with coherent detection

requires channel estimation and hence introduces complexity to the receiver. An alternative approach to overcome such problem is the use of non-coherent detection techniques. In recent years, non-coherent UWB systems have been proposed, e.g. in [49], [50]. Nevertheless, most of the existing works are based on single-band impulse radio technology. Most of the current works for multiband UWB, on the other hand, are confined to the coherent detections [51], [52].

In some applications such as wireless networks, e.g. cellular networks or ad-hoc networks, the implementation of multiple antennas at each terminal might be cumbersome or not possible. Therefore, an idea of antenna sharing among users in the networks to form virtual antenna array has been introduced [19]- [22] as a cooperative communications system. By taking advantage of the broadcasting nature of wireless networks, the cooperative communications is able to explore the inherent spatial diversity through relay channels. Two possible transmission protocols have been proposed based on relay processing: amplify-and-forward (AF) and decode-and-forward (DF) [19]. In the AF protocol, users can act as relay nodes that amplify and retransmit their partner's received signal to its intended destination. The DF protocol, on the other hand, users decode and decide based on the received signal quality whether to retransmit the received signal to the destination. In [21], [22] a specific two-user CDMA cooperative diversity has been proposed. Most of the works in [19]- [23] assume that the destination has perfect knowledge of CSI of all transmission links. While in some scenarios, e.g. slow fading environment, the CSI is likely to be acquired by the use of pilot symbols, it may not be possible in fast fading environment. In addition, it is questionable on how the destination can obtain source-relay channel perfectly through pilot signal forwarding without noise amplification. Moreover, the computational overhead for

channel estimation increases in proportional to the product of number of transmit antennas and number of relaying nodes. To overcome such problems, a specific two-hop relay system using differential modulation has been investigated [53]. Recently, a framework of non-coherent cooperative diversity has been proposed [54] for the DF protocol employing frequency shift keying modulation. However, the framework does not fit to the differential phase shift keying (DPSK) and the AF cooperation protocol.

The research works in [19]- [59] have proved the significant potential of cooperative diversity in wireless networks. However, most of the existing works on cooperative communications focus on improving physical layer performance or minimizing link energy consumption. Previous works on extending lifetime, on the other hand, concentrate on non-cooperative transmission in which the received signals from the source and the relay are not combined to exploit the cooperative diversity. Wireless networks comprise heterogeneous devices such as mobile phones, laptop computers, and personal digital assistants. These devices are equipped with limited energy, and hence have limited lifetimes. Nevertheless, each device may have different advantages due to its location or remaining energy. For instance, a device might be located in some ideal location so that the energy can be saved, or a device with high initial energy may have energy advantage. The devices with such advantages tend to have longer lifetimes. By allocating some energy of these devices with longer lifetimes to help the energy depleting devices through the employment of cooperative protocols, the lifetime of the helped devices can be greatly improved which in turn increasing the minimum device lifetime of the network. This motivates us to extend the device lifetime by introducing cooperation among nodes.

1.3 Dissertation Overview and Contributions

In this dissertation, we propose various differential modulation schemes that exploit spatial and cooperative diversities to improve system performance without the requirement of channel state information. First, we improve the signal design for differential unitary space-time modulation for narrowband MIMO system. Then, we propose differential modulation schemes for MIMO-OFDM system and MIMO-UWB systems in which all transmit antennas are closely located. Next, we develop differential schemes based on amplify-and-forward and decode-and-forward protocols for more general cooperative communications systems. Lastly, we develop a framework on maximizing device lifetime for the cooperative communication systems, by which for mathematical convenience, the framework is based on coherent detection. The organization of this dissertation is given as follows.

In Chapter 2, we provide some background and related literature which will be used in developing our main contributions and results contained in Chapters 3-7. We begin with wireless channel characteristics and related fading parameters. The basic channel models are also considered. Then, we present mathematical background for MIMO wireless communications. Diversity and coding advantages are discussed. Finally, a general overview on cooperative communication paradigm is given.

In Chapter 3, we consider differential modulations for MIMO systems. In the first part of the Chapter, for narrowband MIMO systems, we consider the design of matrix rotation based space-time signals based on the design criterion of minimizing the union bound on block error probability. We further propose to design the signal parameters via non-integer searching to get better signals. Superior performance of our improved design over the previous design are demonstrated

through numerical calculations and performance simulations. With our proposed design for two transmit antennas and one or two receive antennas, we achieve the coding gain of about 1 *dB* over that of the previous design. In the second part of the Chapter, for wideband MIMO systems, we propose a differential encoding and decoding scheme for MIMO-OFDM system which is able to transmit the differentially encoded signal matrix within one OFDM symbol period, regardless of the number of transmit antennas. The scheme allows us to relax the channel fading assumption to vary from a duration of one OFDM block to the next, but remain approximately constant over only two OFDM symbol periods. The pairwise error probability analysis in case of frequency-selective fading channels with arbitrary power delay profiles is also given. We address design criteria of the proposed scheme, and it reveals that the diagonal cyclic codes [26] can be used to achieve the maximum diversity order.

In Chapter 4, we propose a differential encoding and decoding scheme for multi-band UWB systems. The proposed scheme incorporates frequency-domain differential en/decoding with the hopping multiband OFDM modulation. To capture the effect of multipath-rich clustering property of UWB channels, we characterize the pairwise error probability performance of the proposed scheme in terms of cluster and ray arrival rates. It turns out that the diversity advantage does not strongly depend on the random-clustering of UWB channels, and we can achieve the same diversity gain in different channel environments. However, the system performance relies on the clustering behavior through the coding gain. The maximum diversity order is found to be the product of the number of transmit and receive antennas, the number of jointly encoded subcarriers, and the number of jointly encoded OFDM symbols, regardless of the clustering property of UWB

channels. Simulation results show that the proposed differential scheme achieves good performance in the short-range line-of-sight scenarios. In addition, the jointly encoded differential multiband UWB scheme is able to yield superior performance to the uncoded coherent multiband UWB system at high SNR.

In Chapter 5, we consider differential modulations for cooperative communications. In the first part of the Chapter, we propose a differential amplify-and-forward transmission scheme for a two-user cooperation system. By efficiently combining signals from both direct and relay links, the proposed scheme provides superior performance compare to those of direct transmissions with either differential detection or coherent detection. While the exact bit error rate (BER) formulation of the proposed scheme is not available currently, we provide, as a performance benchmark, an exact BER formulation and its simple bounds for a case of optimum-combining cooperation system with differential M-ary phase shift keying (DMPSK) signals. The optimum power allocation is also determined based on the provided BER formulations. We show that the proposed differential cooperative transmission scheme together with the optimum power allocation yields comparable performance to the optimum-combining scheme. Simulation results show that a significant performance improvement is obtained for a case of optimum power allocation strategy comparing to the performance with equal power allocation scheme.

In the second part of the Chapter 5, we consider a threshold-based differential decode-and-forward cooperative scheme that not only alleviates the problems of synchronization and rate limitation, but also efficiently exploits the cooperative relay channels through the use of a pre-determined decision threshold. In the proposed scheme, the source information is forwarded by the relay only if it is cor-

rectly decoded. The properly-designed threshold enables the destination to decide whether the received signal from the relay contains information such that the received signals from the source and the relay can be efficiently combined and jointly decoded. The BER performance analysis of the proposed scheme is analyzed in case of DMPSK signals. A tight BER approximation is established, and BER upper bound and lower bound are determined. Based on the tight BER approximation, joint optimum decision threshold and power allocation are numerically evaluated. Both analytical and simulation results reveal that the decision threshold and the power allocation depend on qualities of the communication channels. Interestingly, when the link quality between relay and destination is very good, the effect of the threshold dominates the effect of the power allocation at high signal-to-noise ratio. For example, in case of DQPSK signals with equal power allocation, the proposed scheme with a properly-designed threshold leads to more than 5 dB performance improvement over the scheme without the threshold at a BER of 10^{-4} . When the transmitted power is allocated optimally, the performance is further improved by 0.5 dB at the same BER. Extensive simulation results are provided to validate the merit of the proposed scheme and confirm the theoretical analysis.

In Chapter 6, we generalize the proposed differential schemes in Chapter 5 to multi-node scenario. In the first part of the Chapter, we consider a differential scheme for multi-node amplify-and-forward cooperation system. The proposed scheme efficiently combines signals from the direct and multiple relay links to improve communication reliability. BER analysis for DMPSK is provided as performance measure of the proposed scheme, and optimum power allocation is investigated. While the exact BER formulation of the proposed scheme is not available currently, we provide as a performance benchmark a tight BER formu-

lation based on optimum combining weights. A simple BER upper bound and a tight BER approximation show that the proposed scheme can achieve the full diversity which equals to the number of cooperating nodes. We further provide simple BER approximation in order to provide analytical result on power allocation scheme. A closed-form optimum power allocation based on the tight simple BER approximation is obtained for single-relay scenario. An approximate optimum power allocation scheme is provided for multi-relay systems. The provided BER formulations are shown to closely match to the simulation results. Moreover, simulation results show that the optimum power allocation scheme achieves up to 2 dB performance gain over the equal power allocation scheme.

In the second part of the Chapter 6, we propose a multi-node decode-and-forward cooperation system. By utilizing a decision threshold at each relay-destination link and combining only the received signal whose amplitude is larger than the threshold, the proposed scheme enables efficient combining at the destination. The BER performance of the proposed scheme is analyzed for DMPSK signals. We provide an approximate BER formulation of the proposed scheme, and then derive a tractable BER lower bound to provide more insights. Based on the obtained BER lower bound, we jointly optimize the power allocation and decision thresholds to further enhance the system performance

In Chapter 7, we propose a general framework is proposed to improve lifetime of battery-operated devices by exploiting cooperative diversity. The framework efficiently takes advantages of both different locations and energy levels among distributed nodes. First, a lifetime maximization problem via cooperative nodes is considered. With an objective to maximize the minimum device lifetime under a constraint on BER performance, we determine which nodes should cooperate

and how much powers to allocate for cooperation. To solve the formulated problem which is NP hard, a closed-form solution for a two-node network is derived to obtain some insights. Based on the two-node solution, a fast suboptimal algorithm is developed for multi-node scenarios. Moreover, the device lifetime is further improved through the cooperative relay deployment by which additional cooperative relays are deployed to help forward information of nodes in the network. The optimum location of each relay and the power allocation are determined with an aim to maximize the minimum device lifetime. A suboptimal algorithm is proposed for the wireless network with multiple cooperative relays and multiple cooperative nodes. Simulation results show that the minimum device lifetime of the network with cooperative node employment improves 2 times compared with that of the non-cooperative network. In addition, deploying one cooperative relay in a proper location leads up to 3 times longer network lifetime than that of the non-cooperative network.

In Chapter 8, conclusions are provided and some possible future directions are discussed.

Chapter 2

Background and Related Literature

This chapter presents background on wireless fading channels and conventional fading mitigation techniques. In addition, various kinds of contemporary fading mitigation techniques are discussed.

2.1 Wireless Channel Fundamentals

Because there are obstacles and reflectors in the wireless propagation channel, the transmitted signal arrives at the receiver from various directions over a multiplicity of paths. Such a phenomenon is called multipath. It is an unpredictable set of reflections and/or direct waves each with its own degree of attenuation and delay. Multipath is usually described by

- **Line-of-sight (LOS)**: the direct connection between the transmitter and the receiver.
- **Non-line-of-sight (NLOS)**: the path arriving after reflection from reflectors

The signal multipath components generally have different carrier-phase offsets and, hence, they may add destructively at times, resulting in a phenomenon called signal fading. Moreover, the speed that the mobile (automobile, train, etc.) is traveling results in frequency offsets, called Doppler shifts, of the various frequency components of the signal.

There are basically two distinct characteristics of the types of radio channels described above. The first characteristic is that the transmitted signal arrives at the receiver via multiple propagation paths, each of which has an associated time delay. We model this kind of channel as linear time invariant channel. A second characteristic of the types of radio channels is concerned with the time variations in the structure of the medium. As a result of such time variations, the response of the channel to any signal transmitted through it will change with time. Such changes include variations in the relative delays of signals from the multiple scatterers. In general, the time variations in the received signal appear to be unpredictable to the user of the channel. This leads us to characterize the time-variant multipath channel statistically.

2.1.1 Attenuation for Wireless Systems

- **Path Loss** : The path loss of a radio link is the loss over the considered transmission path that would be measured between the transmit and receive antennas. The average received power diminishes with the distance between transmitter and receiver. Assuming that there is a direct path from the transmitter and receiver, and denoting P_T and P_R as the transmitted power and received power, respectively. The free space propagation can be described by

the following relation,

$$P_R \propto \frac{GP_T}{f^2 d^\alpha}, \quad (2.1)$$

where f is the carrier frequency, G is the gain between the transmitter and receiver, d represents distance of the transmission link, and α denotes the path loss component. Based on the relation in (2.1), we can interpret that higher operating frequency results in shorter operating range.

- **Shadowing :**

In case that the communication link has some obstructions, then the received power is randomly attenuated. Shadowing describes behavior of variations of received signals which can be different if the communication links are surrounded by different obstructions. The log normal shadowing can be written as

$$PL(\text{dB}) = PL(d_0) + 10\alpha \log(d/d_0) + X_\sigma, \quad (2.2)$$

where d_0 denotes the reference distance, X_σ represents a zero mean Gaussian random variable with variance σ^2 , and σ and α are obtained from measured data.

2.1.2 Input/output Model of the wireless channels

In order to design reliable wireless communication systems, it is important to construct a mathematical model for the multipath effects such that the most important characteristics of the wireless medium can be included in the design. In this subsection, we show that the multipath effect can be model as a time-varying system.

- **Wireless Channel as Time-Varying System**

The linear time-variant filter channel with additive noise can be expressed as the following. For an input signal $s(t)$, the channel output signal is

$$y(t) = s(t) \star h(\tau; t) + n(t) = \int_{-\infty}^{+\infty} h(\tau; t) s(t - \tau) d\tau + n(t), \quad (2.3)$$

where \star denotes convolution, $h(\tau; t) = \sum_{k=1}^L a_k(t) \delta(\tau - \tau_k)$ represents the time-variant impulse response, $a_k(t)$ represent the possibly time-variant attenuation factors for the L propagation paths, and $n(t)$ is an additive noise.

- **Wireless Channel as Time-Invariant System**

In a scenario that the channel impulse response is not vary with time. This is a reasonable assumption when the transmitted signals do not exceed specified bandwidth limitations and, thus, do not interfere with one another. We can write the channel output as

$$y(t) = s(t) \star h(\tau) + n(t) = \int_{-\infty}^{+\infty} h(\tau) s(t - \tau) d\tau + n(t). \quad (2.4)$$

2.1.3 Fading Parameters

To obtain a statistical description of the channel, let us consider the transmission of an unmodulated carrier

$$c(t) = A \cos(2\pi f_c t), \quad (2.5)$$

and the received signal in the absence of noise can be expressed as

$$\begin{aligned} x(t) &= A \sum_n \alpha_n(t) \cos(2\pi f_c (t - \tau_n(t))), \\ &= A \operatorname{Re} \left[\sum_n \alpha_n(t) e^{-j2\pi f_c \tau_n(t)} e^{j2\pi f_c t} \right], \end{aligned} \quad (2.6)$$

where $\alpha_n(t)$ is the time-variant attenuation factor associated with the n^{th} propagation path and $\tau_n(t)$ is the corresponding propagation delay. The complex-valued signal

$$\begin{aligned} z(t) &= \sum_n \alpha_n(t) e^{-j2\pi f_c \tau_n(t)}, \\ &= \sum_n \alpha_n(t) e^{-j\phi_s(t)}, \end{aligned} \quad (2.7)$$

represents the response of the channel to the complex exponential $\exp(j2\pi f_c \tau_n(t))$. We note that, although the input to the channel is a signal at a single frequency, the output of the channel consists of a signal that contains many different frequency components. These new components are generated as a result of the time variations in the channel response.

- **Delay Spread** It is defined as the difference in propagation delay between the longest and shortest path which has significant energy:

$$T_d \triangleq \max_{i,j} |\tau_i(t) - \tau_j(t)|, \quad (2.8)$$

where $\tau_i(t)$ denotes the propagation delay of the i^{th} path. It is a metric to characterize the multipath delay in terms of second order moment of the channel delay power profile.

- **Coherence Bandwidth**

The other useful parameter is the reciprocal of the multipath spread, which has units of frequency. This quantity is a measure of the bandwidth over which the channel characteristics (magnitude $\alpha(t)$ and phase $\phi(t)$) are highly correlated. In other words, all frequency components of a signal within this bandwidth will fade simultaneously. We call this parameter the coherence

bandwidth of the channel and define it as Coherent bandwidth is used to measure how flat the channel bandwidth is. It is given by

$$W_s = \frac{1}{2T_d} \quad (2.9)$$

- **Doppler Shift** Due to movement of devices, the frequency of received signal is different than the frequency of the original signal. The change in frequency of the received signal is called the Doppler shift. In case of a mobile is moving with velocity v on an x-axis, and the angle between the transmitter and receiver is θ from the x-axis. At time t , the mobile moves for a distance of $d = v\Delta t$, then the phase change is $\Delta\phi = 2\pi d/\lambda$. Therefore, the Doppler shift is given by

$$F_d = \frac{1}{2\pi} \frac{\Delta\phi}{\Delta t} = \frac{v}{\lambda} \cos(\theta) \quad (2.10)$$

- **Doppler Spread**

Doppler spread is the measure of maximum broadening of the spectrum due to Doppler shift which is $f_m = v/\lambda$ which is the maximum of (2.10).

- **Coherence Time**

This quantity is a measure of the time interval over which the channel characteristics will change very little, i.e. a time period that two received signals have high amplitude correlation. We call this parameter the coherence time of the channel, and define it as $T_c \approx 1/f_m$.

- **Coherence Distance**

The coherent distance measures a minimum distance between point in space for which the signals are uncorrelated. It is $\lambda/2$ for wide beamwidth receive

antennas, and about $10 - 20\lambda$ for low-medium and high BTS antenna heights, respectively.

- **Channel Spread Factor** The product $T_s F_d = T_s / T_c$ is usually called the channel spread factor. If $T_s F_d < 1$, the channel is called underspread and if $T_s F_d > 1$, the channel is said to be overspread. The spread factor usually provides some indication on whether or not phase-coherent demodulation is possible at the receiver. In general, if the channel is overspread, due either to a large multipath spread or a large Doppler spread or both, the estimation of the carrier phase is extremely difficult because of the rapid time variations ($T_c \ll T_s$) in the channel that occur in the time interval T_s . On the other hand, if the channel is underspread, the channel-time variation is slow relative to the multipath spread ($T_c \gg T_s$) and, hence, the carrier phase of the received signal can be estimated with good precision. Fortunately, most physical time-varying channels encountered in practice are underspread.

The multipath propagation model for the channel, embodied in the received signal $x(t)$ or, equivalently, $z(t)$ given by (2.7), results in signal fading. The fading phenomenon is primarily a result of the time-variant phase factors $\phi_n(t)$. At times, the complex-valued vectors in $z(t)$ add destructively to reduce the power level of the received signal. At other times, the vectors in $z(t)$ add constructively and, thus, produce a large signal value. The amplitude variations in the received signal due to the time-variant multipath propagation in the channel are usually called signal fading.

2.1.4 Types of Fading

Based on multipath time delay spread, there are two types of fading, namely flat fading channel or frequency selective fading channel. In terms of doppler spread, fading is separated into two types as fast fading or slow fading. Description of these four channel characteristics are described as follows:

- **Flat Fading Channel**

The signal will suffers from flat fading if the channel bandwidth is greater than the signal bandwidth ($B_c > B_s$). In this way, spectral shape of the signal is preserved but the gain is changed due to fading. Distortion in gains may cause deep fade, hence it requires more power in some frequencies.

- **Frequency Selective Fading**

In this case, The signal will suffers from fast fading if the bandwidth of the signal is greater than the coherence bandwidth of the channel ($B_s > B_c$), or the delay spread is greater than the symbol period ($T_d > T_s$).

- **Fast Fading or Slow Fading**

In this case, The signal will suffers from fast fading if the bandwidth of the signal is greater than the coherence bandwidth of the channel ($B_s > B_c$), or the delay spread is greater than the symbol period ($T_d > T_s$).

2.1.5 Statistical Channel Models

- **Rayleigh Fading**

In case that the channel coefficient is characterized as complex-valued Gaus-

sian random processes. We may express each of the coefficients as

$$h(t) = h_r(t) + jh_i(t), \quad (2.11)$$

where $h_r(t)$ and $h_i(t)$ represent real-valued Gaussian random processes. We assume that $h_r(t)$ and $h_i(t)$ are stationary and statistically independent. By re-expressing in polar form as $h(t) = \alpha(t)e^{j\phi(t)}$ in which $\alpha(t) = \sqrt{h_r^2(t) + h_i^2(t)}$ and $e^{j\phi(t)} = \tan^{-1}(h_i(t)/h_r(t))$. In this representation, if $h_r(t)$ and $h_i(t)$ are Gaussian with zero-mean values, the amplitude $|h(t)|$ is characterized statistically by the Rayleigh probability distribution and $\phi(t)$ is uniformly distributed over the interval $(0, 2\pi)$. As a consequence, the channel is called a Rayleigh fading channel. The Rayleigh fading signal amplitude $|h(t)|$ is a Rayleigh random variable with probability density function (PDF) described

$$f(\alpha) = \frac{\alpha}{\sigma^2} e^{-\alpha^2/2\sigma^2}, \quad \alpha \geq 0, \quad (2.12)$$

and $f(\alpha) = 0$ for $\alpha \leq 0$ where $\sigma^2 = E[h_r^2(t)] = E[h_i^2(t)]$ in which $E[\cdot]$ represents the expectation operator. The square magnitude $|h(t)|^2$ is exponentially distributed with density

$$f(\beta) = \frac{1}{\sigma^2} e^{-\beta/2\sigma^2}, \quad \beta \geq 0. \quad (2.13)$$

- **Rician Fading**

On the other hand, if $h_r(t)$ and $h_i(t)$ are Gaussian with nonzero mean, the amplitude $|h(t)|$ is characterized statistically by the Rice probability distribution and the phase $\phi(t)$ is also nonzero mean. In this case the channel is called a Rician fading channel and the PDF of $|h(t)|$ is given by

$$f(\alpha) = \frac{\alpha}{\sigma^2} e^{-(\alpha^2+s^2)/2\sigma^2} I_0(s\alpha/\sigma^2), \quad \alpha \geq 0, \quad (2.14)$$

where s^2 represents the power of the received nonfading signal component and $\sigma^2 = VAR[h_r(t)] = VAR[h_i(t)]$ in which $VAR[\cdot]$ denotes the variance.

- **Channel gain auto-correlation function**

The channel gain auto-correlation function is used to measure how the channel gain vary with time. As it will be apparent in the rest of the book that this quantity has significant impact on the performance of the wireless communication system. The channel gain auto-correlation function for the channel coefficient at time τ apart is defined as $R(\tau) \triangleq E[h^*(t)h(t + \tau)]$. This definition is used to find the auto-correlation of the Jakes's Model for flat fading. Suppose the communication bandwidth F_d is much smaller than the reciprocal of the delay spread, we have

$$R(\tau) = 2\alpha^2\pi J_0(2\pi F_d T_s \tau), \quad (2.15)$$

where $J_0(\cdot)$ represents the zeroth-order Bessel function of the first kind:

$$J_0(x) = \frac{1}{\pi} \int_0^\pi e^{jx \cos(\theta)} d(\theta), \quad (2.16)$$

and $T_s = f_c v/c$ is the Doppler spread in which f_c is the carrier frequency and θ is angle of the arriving signal.

2.2 Diversity Techniques to Combat Multipath Fading

Diversity technique refers to a method for improving reception of a transmitted signal, by receiving and processing multiple versions of the same transmitted signal that pass through over independent fading paths. This means that the diversity

method requires that a number of transmission paths be available, all carrying the same message but having independent fading statistics. The success of diversity schemes depends on the degree to which the signals on the different diversity branches are uncorrelated. In a Rayleigh fading channel, the probability that the signal power A^2 is less than a certain value γ is given by

$$P(A^2 < \gamma) = 1 - e^{-\frac{\gamma}{\gamma_m}}, \quad (2.17)$$

where γ_m is an average received signal power. Accordingly, at high SNR region, the probability in (2.18) can be approximated as

$$P(A^2 < \gamma) \approx \frac{\gamma}{\gamma_m} \propto SNR^{-1}, \quad (2.18)$$

From (2.18), we can see that the probability of error is high when deep fade occurs for a system without diversity reception. A simple remedy against this is to introduce L diversity reception. In this way, L replicas of the same information reach the receiver via L channels with statistically independent fading amplitudes. Hence, the probability that the whole received information is affected by a deep fade will be proportional to SNR^{-L} . We refer L as the **diversity order** or the number of diversity branches. The way in which those multiple versions of the signal are received, characterizes various diversity techniques as follow:

2.2.1 Space Diversity

If the receiver has multiple antennas, the distance between the receiving antennas is made large enough to ensure independent fading. This arrangement is called space diversity. Space separation of half of the wavelength is sufficient to obtain two uncorrelated signals for a mobile receiver. In the case of wired transmission, this can be achieved by transmitting via multiple wires. In the case of wireless

transmission, this can be achieved by transmitting to multiple receiving antennas (antenna diversity).

2.2.2 Polarization Diversity

Antennas can transmit either a horizontal polarized wave or a vertical polarized wave. When both waves are transmitted simultaneously, received signals will exhibit uncorrelated fading statistics. This scheme can be considered as a special case of space diversity because separate antennas are used. However, only two diversity branches are available, since there are only two orthogonal polarizations.

2.2.3 Angle/Directional Diversity

Since the received signal arrives at the antenna via several paths, each with a different angle of arrival, the signal component can be isolated by using directional antennas. Each directional antenna will isolate a different angular component. Hence, the signals received from different directional antennas pointing at different angles are uncorrelated.

2.2.4 Frequency Diversity

Signals with different carrier frequencies far apart with each other are possibly independent. The carrier frequencies must be separated enough so that the fading associated with the different frequencies are uncorrelated. For frequency separations of more than several times the coherence bandwidth, the signal fading would be essentially uncorrelated. The use of RAKE receiver, OFDM transmission, or equalization are possible techniques to explore frequency diversity. However, it can not be used over frequency-flat fading channel.

2.2.5 Time Diversity

When the same data are sent over the channel at different time instants, the received signals can be uncorrelated if the time separations are large enough. The required time separation is at least as great as the reciprocal of the fading bandwidth, which is two times the speed of the mobile station divided by the wavelength. Hence, the time separation is inversely proportional to the speed of the mobile station. In case that the mobile station is stationary, time diversity is useless. This is in contrast to all of the other diversity types discussed above because they are independent of the speed of the mobile station.

2.3 Diversity Combining Techniques

A diversity combining technique is applied to combine the multiple received signals of a diversity reception device into a single improved signal before further signal processing takes place. Proper combining the multiple signals will greatly reduce severity of fading and improve reliability of transmission. We will briefly consider some basic diversity combining methods here.

After receiving the multiple versions of the signal, a diversity combining technique is applied before further signal processing takes place. Proper combining the multiple signals will greatly reduce severity of fading and improve reliability of transmission. Various diversity combining techniques can be distinguished:

2.3.1 Selection Combining

Because deep fades seldom occur simultaneously during the same time intervals on two or more paths. Selection combining is the simplest combining scheme, which

is based on the principle of selecting the best signal (the largest energy or SNR) among all of the signals received from different branches.

Since different receive signals are independent from each other, the probability that all of them have an SNR smaller than γ is

$$P[\gamma_1, \gamma_2, \dots, \gamma_L \leq \gamma] = [1 - e^{-\gamma/\gamma_m}]^L. \quad (2.19)$$

Hence, the probability that at least one receive signal has SNR greater than γ is $P_L(\gamma) = 1 - [1 - e^{-\gamma/\gamma_m}]^L$, and the corresponding PDF is $f(\gamma) = \frac{L}{A} [e^{-\gamma/\gamma_m}]^{L-1} e^{-\gamma/\gamma_m}$. Therefore, the average SNR at the combiner output is

$$\bar{\gamma} = \int_0^\infty \gamma f(\gamma) d\gamma = A \sum_{l=1}^L \frac{1}{L}. \quad (2.20)$$

Therefore, the selection combining offers SNR improvement of $\sum_{l=1}^L \frac{1}{L}$ times without increasing the transmit power. However, this amount of SNR improvement is less than the maximum improvement ratio of L . Therefore selection combining does not provide an optimal diversity gain and as a result an optimal performance enhancement. However, its complexity is low since it only requires one RF chain. In other words, selection combining provides a trade-off between complexity and performance.

2.3.2 Switched Combining

In case of the switch combining scheme, the receiver switches to another signal when current signal drops below a predefined threshold.

2.3.3 Maximum Ratio Combining

In Maximum Ratio combining each signal branch is multiplied by a weight factor that is proportional to the signal amplitude. That is, branches with strong

signal are further amplified, while weak signals are attenuated.

Considering a system that receives L replicas of the transmitted signal through L independent paths. Let us assume $r_l, m = 1, 2, \dots, L$, as the l^{th} received signal:

$$r_l(t) = \alpha_l s(t) + w(t). \quad (2.21)$$

We consider a coherent detection scheme where the receiver knows the channel path gains, α_l . Based on the received signal (2.21), the conditional joint density function of the received signals can be written as

$$f(r_1, r_2, \dots, r_L | s, \alpha_1, \dots, \alpha_L) = \frac{1}{\pi N_0} \exp \frac{-\sum_{l=1}^L |r_l - \alpha_l s|^2}{N_0}, \quad (2.22)$$

where N_0 is the noise variance. For a constellation with equal energy symbols, for example PSK, the optimal maximum likelihood detector is given by

$$\hat{s} = \arg \min_s \left| \sum_{l=1}^L \alpha_l^* r_l - s \right|^2. \quad (2.23)$$

To summarize, MRC uses a matched filter, that is optimum receiver, for each received signal and using the optimal weights $w_l = \alpha_l^*$ combines the outputs of the matched filters. If the average power of the transmitted symbol is E_s , the SNR of the l^{th} receiver is $\gamma_l = |\alpha_l|^2 (E_s/N_0)$. To derive the SNR of the output of the maximum ratio combiner, first we calculate

$$\sum_{l=1}^L \alpha_l^* r_l = \sum_{l=1}^L \alpha_l^* (\alpha_l s(t) + w_l(t)) = \sum_{l=1}^L |\alpha_l|^2 s(t) + \sum_{l=1}^L \alpha_l^* w_l(t). \quad (2.24)$$

Then, the SNR at the output of the maximum ratio combiner is

$$\gamma = \frac{\left(\sum_{l=1}^L |\alpha_l|^2 \right)^2 E_s}{\sum_{l=1}^L |\alpha_l|^2 N_0} = \sum_{l=1}^L |\alpha_l|^2 \frac{E_s}{N_0} = \sum_{l=1}^L \gamma_l. \quad (2.25)$$

Therefore, the effective receive SNR of a system with diversity L is equivalent to the sum of the receive SNRs for L different paths. The importance of this L -fold increase in SNR is in the relationship between the average error probability and the average receive SNR.

2.3.4 Equal Gain Combining

Equal gain combining is similar to MRC but the diversity branches are not weighted or weighted with the same factor, irrespective of the signal amplitude. However, co-phasing of all signal is needed to avoid signal cancelation. EGC is particularly useful for modulation techniques that use equal energy symbols such as M-PSK.

2.4 MIMO Techniques

Multiple-input-multiple-output (MIMO) has recently emerged as one of the most technical advances in wireless communications. The MIMO system significantly improves performance with no extra spectrum requirement but trades off with added hardware and complexity at both the transmitter and receiver. An ability of resolving the bottleneck of traffic capacity makes the MIMO systems a viable candidate for bandwidth-consuming applications. Under narrowband communication systems, space-time (ST) codes have been proposed [4], [6]- [9]. The main concept of the ST MIMO system is the joint spacetime signal processing through the use of multiple spatially distributed antennas such that both spatial and temporal diversities can be explored. Under wideband communication systems in which the wireless channels are frequency-selective, space frequency (SF) codes [10]- [15] have been introduced to incorporate with orthogonal frequency division multiplexing (OFDM) transmission. By jointly encoding across spatial and frequency domain, SF codes are able to explore the available spatial and frequency diversity in the MIMO-OFDM system. Recently, an idea of jointly encoding across spatial, temporal, and frequency diversity has been proposed as a

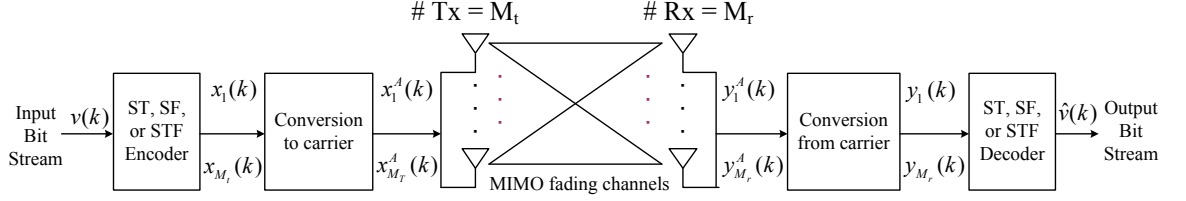


Figure 2.1: A generic MIMO communication system.

space-time-frequency (STF) codes [16]- [18]. By proper coding design, the STF is able to simultaneously explore the spatial, temporal, and frequency diversity which significantly improves system performance and increases bandwidth efficiency.

Figure 2.1 shows a generic MIMO communication system that employs ST, SF, or STF codes. Suppose there are M_T transmit and M_R receive antennas in the systems. In what follows, we consider a transmission and a reception of ST codes over narrowband MIMO systems as example, the transmission of SF or STF codes over MIMO-OFDM systems can be obtained in a similar way. From the figure, every input symbol x_t is fed into the ST encoder and generates M_T ST coded symbols $s_t^1 s_t^2 \dots s_t^{M_t}$. All of these ST coded symbols are transmitted simultaneously over M_T transmit antennas. Define $\mathbf{s}_t \triangleq [s_t^1 s_t^2 \dots s_t^{M_t}]$ as a $1 \times M_T$ row vector of ST coded symbols, then the ST codeword matrix can be expressed by stacking L consecutive rows of ST coded symbol together as

$$\mathbf{S} = [\mathbf{s}_1 \mathbf{s}_2 \dots \mathbf{s}_T]^T, \quad (2.26)$$

which is of dimension $T \times M_T$. For T consecutive time intervals, the received signals are formulated in matrix form as

$$\mathbf{Y} = \sqrt{\rho} \mathbf{S} \mathbf{H} + \mathbf{W}, \quad (2.27)$$

where \mathbf{Y} is the $T \times M_R$ received signal matrix, \mathbf{S} is the $T \times M_T$ transmitted signal matrix. In (2.26), \mathbf{H} represents the $M_T \times M_R$ fading-coefficient matrix whose

each $(i, j)^{th}$ element $\alpha_{i,j}$ is the channel coefficient between the i^{th} transmit and the j^{th} receive antenna. Also in (2.26), \mathbf{W} is the $T \times M_R$ additive noise matrix. The transmitted signal is normalized to have unit energy during one transmission period to ensure that ρ is the averaged SNR per receiver, i.e., $\mathbb{E}[\sum_{i=1}^{M_T} |s_t^i|^2] = 1$, where \mathbb{E} represents expectation operator.

If we assume that the channel state information (CSI), i.e. \mathbf{H} , is available at the receiver, then the receiver uses the maximum likelihood decoding rule to recover the transmitted symbol as

$$\hat{\mathbf{S}} = \arg \min_{\mathbf{S}} \|\mathbf{Y} - \sqrt{\rho} \mathbf{S} \mathbf{H}\|_F^2, \quad (2.28)$$

where $\|\mathbf{A}\|_F^2$ represents the Frobenius norm [84] of the $T \times M_R$ matrix \mathbf{A} which is defined as $\|\mathbf{A}\|_F^2 = \text{tr}(\mathbf{A}^H \mathbf{A}) = \text{tr}(\mathbf{A} \mathbf{A}^H) = \sum_{i=1}^T \sum_{j=1}^{M_R} |a_{ij}|^2$ in which $(\cdot)^H$ denotes the conjugate transposition.

To find the error probability, define the $M_T \times M_T$ error matrix \mathcal{E} as

$$\mathcal{E}(\mathbf{S} \rightarrow \hat{\mathbf{S}}) = \sum_{t=1}^T (x_t - \tilde{x}_t)^* (x_t - \tilde{x}_t). \quad (2.29)$$

In case that the receiver has perfect knowledge of the channel state information, i.e. \mathbf{H} , then the pairwise error probability under Rayleigh fading environment can be upper bounded by [4]

$$P(\mathbf{S} \rightarrow \hat{\mathbf{S}}) = \left(\prod_{i=1}^r \lambda_i \right)^{-M_R} \cdot (\rho)^{-rM_R}, \quad (2.30)$$

where r is the rank of the error matrix \mathcal{E} , and $\lambda_i, i = 1, 2, \dots, r$ are nonzero eigenvalues of \mathcal{E} . In (2.30), $(\prod_{i=1}^r \lambda_i)^{-M_R}$ is coined as the coding gain by using certain ST codes, and rM_R which is the exponent of ρ is called the diversity gain. Since the rank of \mathcal{E} is not greater than M_T , then the maximum diversity order is $M_T M_R$.

In case of wideband systems, the fading channel is frequency selective. SF codes together with OFDM transmission are normally deployed to explore the spatial and frequency diversity. Similar to (2.26), \mathbf{S} results from jointly encoded over N OFDM tones and M_T transmit antennas. Therefore, each of the SF codeword matrix has dimension $N \times M_t$. The corresponding received signal can be expressed in a similar way as that in (3.1). However, the received signal \mathbf{Y} and the noise matrix \mathbf{W} have dimension $N \times M_R$ matrix, and \mathbf{H} represents the $M_T \times M_R$ matrix of channel frequency response. When encoding and decoding delays are permitted, STF codes with OFDM transmission can be used to explore spatial, temporal, and frequency diversity. Assuming that the STF jointly encodes over K OFDM symbols, then each of the obtained STF code has dimension $KN \times M_t$. Note that the STF code structure equivalent to stacking K SF codes together, however, all of the elements in the STF codeword matrix are jointly encoded over K , N , and M_T . The performance analysis for the SF MIMO-OFDM system and STF MIMO-OFDM system can be derived in a similar way as that in (2.30).

Note that the decoding of the ST, SF, and STF codes as shown above requires multi channel estimation at the receiver. Differential detection has gained much attention because it achieves full diversity gain without the knowledge of CSI or training symbol transmission. The key idea of the differential detection is that it uses the previous received signal, $\mathbf{Y}^{\tau-1}$, as a roughly channel estimate for the received signal at time τ in (3.1). In this way, the noise term in the differential detection has twice variance of that with coherent detection, and result in 3dB performance loss in comparison to it coherent counterpart.

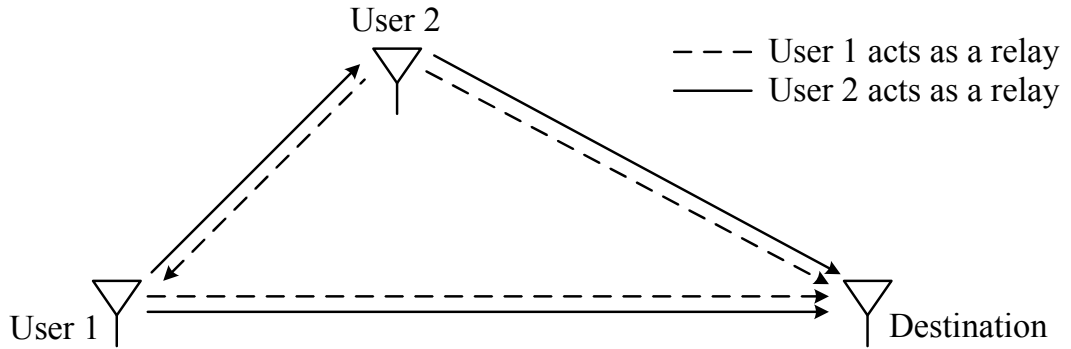


Figure 2.2: A generic two-user cooperation system.

2.5 Cooperative Diversity

Cooperative diversity or cooperative communication has recently emerged as a new class of communication paradigms that allows single-antenna terminals to achieve transmit diversity in a similar way as MIMO systems. The basic idea is that each single-antenna terminal in multi-user environment shares its antenna with other terminals in the networks, and hence form a virtual antenna array. Due to statistically independent fading among users in the networks, the inherent spatial diversity can be explored. An example of cooperative communication is shown in Figure 2.2 for a two-user cooperation system. All users transmit signals through orthogonal channels by using existing TDMA, FDMA, or CDMA schemes. Each user can be a source or a relay that overhears transmitted information of others in the network. Each relay processes such overheard information and re-transmits the overheard information to the intended destination of the source. Based on the relay processing, cooperation protocols can be separated into two classes, namely fixed relaying protocol and adaptive relaying protocol.

The fixed relaying protocol includes amplify-and-forward (AF) [19], decode-and-forward (DF) [19], and coded cooperation (CC) protocols [20]. In the AF

protocol, each relaying terminal receives a noisy signal from the source, and then amplifies and retransmits this noisy signal to the destination of the source. After that the destination combines signals from the source and all relays before jointly decoding the transmitted information. Even though the forwarded signals from all relays are noisy signals, the destination can make better decision because all received signals suffer independent fading. The DF protocol is considered as a digital version of the AF protocol by which each relay decodes the information from the source and then retransmits the decoded information to the destination. The DF protocol has been generalized to multiple-relay scenario by which all cooperating users jointly encode information by the use of distributed space-time codes. A related work on two-user cooperation system has been proposed for code division multiple access (CDMA) systems [21], [22]. In this protocol, each user uses orthogonal codes to mitigate multiple access interference. The CC protocol integrates cooperation with channel coding. Each mobile that employs the CC protocol divides data into two segments, namely N_1 and N_2 . The information segment N_1 is transmitted in the first phase by the source itself. In the second phase, the relay tries to decode the transmitted symbol by checking cyclic redundancy check (CRC) codes. If the relay successfully decodes, then the relay calculates and transmits the second code partition N_2 of the source to the destination. Otherwise, the relay sends its own second code partition to the destination or switches to non-cooperative transmission. Note that if coherent detection is performed at the destination for all of these cooperation protocols, the destination must know all inter-channel coefficients such that optimal decoding can be performed. Therefore, a mechanism to exchange the CSI information is required at the destination.

The adaptive relaying protocol [19], which includes selection relaying protocol

and incremental relaying protocol, has been proposed to avoid error propagation when the relay incorrectly decodes. In selection relaying protocol, the relay decides to detect and forward the received information from the source only when the source-relay fading channel has high instantaneous signal-to-noise ratio (SNR). However, when such source-relay channel has low SNR, users switch to a non-cooperative transmission. In case of the incremental relaying protocol, the destination only requests a second copy from the relay only if the received signal from the direct transmission is corrupted. In this way, the destination send automatic repeat request to the relay through a limited feedback signaling.

Chapter 3

Differential Modulations for MIMO systems

In this Chapter, we proposed differential modulation schemes for MIMO systems. In Section 3.1, we consider differential unitary space-time signal design for narrowband MIMO systems. In Section 3.2, we propose a differential modulation scheme for wideband MIMO systems by which fading channels are frequency-selective. Finally, Section 3.3 draws conclusions.

3.1 Differential Unitary Space-Time Signal Design for MIMO systems

In this section, we consider the design of matrix rotation based (MRB) space-time signals for narrowband MIMO systems. The proposed signal design is based on a design criterion of minimizing the union bound on BEP. Moreover, we propose to search non-integer parameters for the MRB signal scheme. The search method and computational complexity reduction are also presented. The merit of the proposed design is demonstrated by numerical calculations and performance simulations.

3.1.1 Channel Model and DUST Scheme

We consider a MIMO system with M_T transmit antennas and M_R receive antennas. The channel coefficients are assumed unknown to neither the transmitter nor the receiver. For T consecutive time intervals, the received signals are formulated in matrix form as

$$\mathbf{Y}_\tau = \sqrt{\rho} \mathbf{S}_\tau \mathbf{H}_\tau + \mathbf{W}_\tau, \quad \tau = 0, 1, \dots, \quad (3.1)$$

where τ is the time index of block transmissions, \mathbf{Y}_τ is the $T \times M_R$ received signal matrix, \mathbf{S}_τ is the $T \times M_T$ transmitted signal matrix, the $M_T \times M_R$ fading-coefficient matrix \mathbf{H}_τ and the $T \times M_R$ additive noise matrix \mathbf{W}_τ have complex Gaussian elements with $\mathcal{CN}(0, 1)$ distributed. The transmitted signal is normalized to have unit energy during one transmission period to ensure that ρ is the averaged SNR per receiver, i.e., $\mathbb{E}[\sum_{i=1}^{M_T} |s_t^i|^2] = 1$, where \mathbb{E} represents expectation operator.

In the following, we will assume square size transmitted signal matrices, i.e. $T = M_T$. The transmission process follows the fundamental differential transmitter equation [26],

$$\mathbf{S}_\tau = \begin{cases} \Phi_{z_\tau} \mathbf{S}_{\tau-1}, & \tau = 1, 2, \dots, \\ \mathbf{I}_{M_T \times M_T}, & \tau = 0. \end{cases} \quad (3.2)$$

where $\mathbf{I}_{M_T \times M_T}$ is an $M_T \times M_T$ identity matrix. $z_\tau \in \{0, 1, \dots, L-1\}$ denotes an integer index of a distinct unitary matrix signal Φ_{z_τ} drawn from a signal constellation \mathcal{V} of size $L = 2^{RM_T}$ with R represents the information rate in b/s/Hz.

We combine two consecutive received signal matrices using (3.1) and (3.2) and assume that the channel coefficients are almost constant over two consecutive blocks, i.e., $\mathbf{H}_\tau \approx \mathbf{H}_{\tau-1}$. We obtain the fundamental differential receiver equation,

$$\mathbf{Y}_\tau = \Phi_{z_\tau} \mathbf{Y}_{\tau-1} + \sqrt{2} \mathbf{W}'_\tau, \quad (3.3)$$

where $\mathbf{W}'_\tau = \frac{1}{\sqrt{2}}(\mathbf{W}_\tau - \Phi_{z_\tau} \mathbf{W}_{\tau-1})$ is an $M_T \times M_R$ additive independent noise matrix with $\mathcal{CN}(0, 1)$ distributed elements. The differential decoder performs maximum likelihood decoding and the decision rule can be expressed as [26]:

$$\hat{z}_\tau^{ML} = \arg \min_{l \in \mathbb{Z}_l} \|\mathbf{Y}_\tau - \Phi_l \mathbf{Y}_{\tau-1}\|_F, \quad (3.4)$$

where $\mathbb{Z}_l = \{0, 1, \dots, L-1\}$ and $\|\cdot\|_F$ is the Frobenius norm.

It has been shown in [71] that the exact expression of the PBEP of mistaking Φ_l for $\Phi_{l'}$ is

$$P(\Phi_l \rightarrow \Phi_{l'}) = \frac{1}{\pi} \int_0^{\frac{\pi}{2}} \prod_{m=1}^{\Delta_H} \left(1 + \frac{\gamma \lambda_m}{4 \sin^2 \theta}\right)^{-M_R} d\theta, \quad (3.5)$$

where $\gamma = \frac{\rho^2}{(1+2\rho)}$, λ_m is the m^{th} eigenvalue of the matrix $\mathbf{C}_S = (\Phi_l - \Phi_{l'}) (\Phi_l - \Phi_{l'})^\dagger$, and Δ_H is the rank of \mathbf{C}_S .

3.1.2 Design Method

The MRB Space-Time Signal Scheme

For asymptotically high SNR, the Chernoff bound of (3.5) depends on the product of non-zero eigenvalues of \mathbf{C}_s . This leads to a design criterion that aims to maximize the following diversity product [26],

$$\zeta = \frac{1}{2} \min_{l \neq l' \in \mathbb{Z}_l} |\det(\Phi_l - \Phi_{l'})|^{1/M_T}. \quad (3.6)$$

Many DUST signal constellations, such as [27]- [43] and [70]- [44], were designed based on the performance measure in (3.6). Recently in [44], the MRB space-time signal scheme was introduced particularly for communication systems with even number of transmit antennas. Assume a system with M_T transmit antennas and a unitary signal constellation of size L , a set of MRB space-time signals is defined

as [44]:

$$\mathcal{V} = \{\Phi_l(\mathbf{K}) : l = 0, 1, \dots, L-1\}, \quad (3.7)$$

where each Φ_l is a unitary matrix depending on the parameters $\mathbf{K} = \{k_{11}, \dots, k_{1M_T}; k_2\}$ whose elements are integer numbers from \mathbb{Z}_L . Specifically, denote $\mathbf{j} = \sqrt{-1}$ and $\theta_L = 2\pi/L$, then for any $l = 0, 1, \dots, L-1$, Φ_l is given by:

$$\Phi_l(\mathbf{K}) = \Lambda^l \cdot [\mathbf{I}_N \otimes \Psi(k_2\theta_L)]^l, \quad (3.8)$$

where $\Lambda = \text{diag}(e^{j\theta_L k_{11}}, \dots, e^{j\theta_L k_{1M_T}})$,

$$\Psi(\theta) = \begin{bmatrix} \cos(\theta) & \sin(\theta) \\ -\sin(\theta) & \cos(\theta) \end{bmatrix},$$

\mathbf{I}_N is the identity matrix of size $N \times N$ with $N = M_T/2$, and \otimes represents the tensor product.

Improved MRB Space-Time Signal Design

It has been argued in [71] that constellation design that achieve maximum diversity product ζ may not be appropriate, especially at medium range of SNRs. Hence it was suggested in [71] that DUST codes should be designed based on the design criterion of minimizing the union bound on BEP. Specifically, assuming that all the L space-time signals, Φ_l , are equally likely transmitted, the performance measure of BEP is approximated by the union bound,

$$BEP \leq \frac{2}{L} \sum_{l=0}^{L-2} \sum_{l'=l+1}^{L-1} P(\Phi_l \rightarrow \Phi_{l'}) \triangleq PUB, \quad (3.9)$$

where $P(\Phi_l \rightarrow \Phi_{l'})$ is specified in (3.5).

We now consider to design the MRB space-time signals using the design criterion of minimizing the union bound in (3.9). For demonstration purpose, we focus

on a constellation design method for two transmit antennas. Similar procedures can be applied to constellation design for higher number of transmit antennas. In case of $M_T = 2$, the code structure of the MRB signal scheme is

$$\Phi_l = \begin{bmatrix} e^{j\theta_L \tilde{k}_{11}} & 0 \\ 0 & e^{j\theta_L \tilde{k}_{12}} \end{bmatrix} \cdot \Psi(l\tilde{k}_2\theta_L), \quad (3.10)$$

where $l = 0, 1, \dots, L - 1$. The MRB space-time signals in (3.10) are determined by three parameters $\tilde{\mathbf{K}} = \{\tilde{k}_{11}, \tilde{k}_{12}; \tilde{k}_2\}$. Our design goal is to find a set of parameters $\tilde{\mathbf{K}}$ that minimize the *PUB* in (3.9).

Moreover, in our design, we relax the set of parameter $\tilde{\mathbf{K}}$ in (3.10) to be non-integer numbers, i.e., $\tilde{\mathbf{K}} = \{\tilde{k}_{11}, \tilde{k}_{12}; \tilde{k}_2 \mid 0 < \tilde{k}_{11}, \tilde{k}_{12}, \tilde{k}_2 < L\}$. With such extension, we increase the set of search parameters which allow us to have more chance to obtain better signals. Note that all of previous designs in [27]- [43], and [70]- [71], the set of signal parameters is confined to the set integer numbers. Actually, such requirement is not necessary in DUST modulation scheme.

Search Method

For any number of constellation size $L \geq 2$, and given values of M_T , M_R , and SNR (ρ) of interest, we perform exhaustive computer search for the best set of non-integer parameters $\tilde{\mathbf{K}}$ that minimize the *PUB*. We target constellation performances in the range of 10^{-4} to 10^{-7} which correspond to operating SNRs between 20 and 30 dB depending on L , M_T , and M_R . With symmetrical property of the full-rotation matrix $\Psi(\theta)$, we found that the summation of the best parameters \tilde{k}_{11} and \tilde{k}_{12} are approximately L in many cases of computer searching, simplifying

Table 3.1: Comparison of constellation parameters and union bounds for the MRB space-time signal design with $M_T = 2$ transmit antennas.

$[L, M_R]$	New Parameters		Original Parameters	
	$\tilde{\mathbf{K}}$	PUB	\mathbf{K}	PUB
$\begin{bmatrix} 4, 1 \\ 4, 2 \end{bmatrix}$	$\begin{bmatrix} 0.389, 3.611, 1.338 \\ 1.616, 2.384, 0.692 \end{bmatrix}$	$\begin{matrix} 5.1786e^{-4} \\ 3.5227e^{-7} \end{matrix}$	$\begin{bmatrix} 1, 1, 0 \\ 1, 1, 0 \end{bmatrix}$	$\begin{matrix} 6.4076e^{-4} \\ 6.4036e^{-7} \end{matrix}$
$\begin{bmatrix} 8, 1 \\ 8, 2 \end{bmatrix} \dagger$	$\begin{bmatrix} 2, 6, 5 \\ 2, 6, 5 \end{bmatrix}$	$\begin{matrix} 1.8647e^{-5} \\ 1.8795e^{-6} \end{matrix}$	$\begin{bmatrix} 3, 5, 2 \\ 3, 5, 2 \end{bmatrix}$	$\begin{matrix} 1.8647e^{-5} \\ 1.8795e^{-6} \end{matrix}$
$\begin{bmatrix} 16, 1 \\ 16, 2 \end{bmatrix} \dagger$	$\begin{bmatrix} 1.5, 14.5, 7.5 \\ 2, 10, 9 \end{bmatrix}$	$\begin{matrix} 6.9510e^{-5} \\ 1.3671e^{-5} \end{matrix}$	$\begin{bmatrix} 3, 9, 4 \\ 3, 9, 4 \end{bmatrix}$	$\begin{matrix} 7.7840e^{-5} \\ 1.3671e^{-5} \end{matrix}$
$\begin{bmatrix} 32, 1 \\ 32, 2 \end{bmatrix} \dagger$	$\begin{bmatrix} 4, 28, 15 \\ 9.1, 30.7, 8.2 \end{bmatrix}$	$\begin{matrix} 2.3474e^{-4} \\ 1.1025e^{-4} \end{matrix}$	$\begin{bmatrix} 3, 5, 8 \\ 3, 5, 8 \end{bmatrix}$	$\begin{matrix} 2.6699e^{-4} \\ 1.2863e^{-4} \end{matrix}$
$\begin{bmatrix} 64, 1 \\ 64, 2 \end{bmatrix} \dagger$	$\begin{bmatrix} 2.5, 51.5, 8.5 \\ 26.5, 59.5, 0.5 \end{bmatrix}$	$\begin{matrix} 7.9933e^{-4} \\ 5.4148e^{-4} \end{matrix}$	$\begin{bmatrix} 3, 21, 2 \\ 3, 21, 2 \end{bmatrix}$	$\begin{matrix} 1.1197e^{-3} \\ 1.2310e^{-3} \end{matrix}$

Note: \dagger indicates an operating SNR at 30 dB and 20 dB otherwise.

the search algorithm below is sufficient to find the best set of parameters $\tilde{\mathbf{K}}$,

- i) $0 < \tilde{k}_{11} \leq L/2$,
- ii) $(L/2 + \tilde{k}_{11}) \leq \tilde{k}_{12} < L$,
- iii) $0 < \tilde{k}_2 \leq L/2$.

For signal constellation of small size, i.e., $L = 4$, we use step size 0.001 for each parameters in $\tilde{\mathbf{K}}$. For other constellation sizes, due to the complexity of the search space, we limit our search to a searching step of 0.1.

For large signal constellation sizes, we further reduce computational complexity by applying the inequality [68],

$$\prod_{i=1}^{\Delta_H} (1 + x_i) \geq (1 + x_{gm})^{\Delta_H} \quad (3.11)$$

for $x_i > 0$ and $x_{gm} = (\prod_{i=1}^{\Delta_H} x_i)^{1/\Delta_H}$ into (3.5) to get the approximated PBEP in closed form as [71]:

$$P(\Phi_l \rightarrow \Phi_{l'}) \lesssim \frac{1}{2} \{1 - \Gamma(k, \alpha_1)\}, \quad (3.12)$$

where the expression of $\Gamma(k, \alpha_1)$ is

$$\Gamma(k, \alpha_1) = \alpha_1 \sum_{k=0}^{M_T M_R - 1} \binom{2k}{k} \left(\frac{1 - \alpha_1^2}{4}\right)^k, \quad (3.13)$$

with $\lambda_{gm} = (\Delta_P)^{1/M_T}$, $\Delta_P = \prod_{m=1}^{M_T} \lambda_m$, and $\alpha_1 = \sqrt{\frac{\gamma \lambda_{gm}}{4 + \gamma \lambda_{gm}}}$. It was shown in [71] that the approximated PBEP in (3.13) is asymptotically tight to its exact value at high SNR . Explicitly, for $M_T = 2$ and $M_R = 1$, we have

$$PUB \approx \frac{2}{L} \sum_{l=0}^{L-2} \sum_{l'=l+1}^{L-1} (0.5 - 0.75\alpha_1 + 0.25\alpha_1^3). \quad (3.14)$$

Similarly, in case of $M_T = 2$ and $M_R = 2$,

$$PUB \approx \frac{2}{L} \sum_{l=0}^{L-2} \sum_{l'=l+1}^{L-1} \Upsilon(\alpha_1), \quad (3.15)$$

where $\Upsilon(\alpha_1) = 0.5 - 1.094\alpha_1 + 1.094\alpha_1^3 - 0.656\alpha_1^5 + 0.156\alpha_1^7$.

Instead of performing numerical integrations, the approximated PUB in (3.14) and (3.15) require only algebraic computations which reduce execution times considerably.

Table 3.1 shows our parameter search results for signal constellation size $L = 4, 8, 16, 32,$ and 64 . For consistent of the predetermined operating SNRs, we chose to design the MRB signals at either 20 dB or 30 dB as indicated. To illustrate coding advantages of our design, we list $PUBs$ of the obtained codes in [44] that optimized the diversity product compare to $PUBs$ from our design. We observe that for $L = 4, 32,$ and 64 , the union bounds of the new designs are less than that of the original designs. Depending on a predetermined operating SNR, the constellation parameters can be different for system with one or two receive antennas. In case

of $L = 8$ and 16 , although the obtained parameters are different from those in [44], the union bounds of them are almost the same.

Note that, if we constraint the searching over integer parameters using the PUB in (3.9) or the approximated PUB in (3.14) or (3.15), we obtained the same $PUBs$ as those with original parameters for almost every constellation sizes. Except for constellation size $L = 64$ with $M_R = 1$, the resulting PUB is $8.6426e^{-4}$ which is better than that of original design, but it is higher than the one from non-integer searching.

3.1.3 Simulation Results

We simulated the DUST modulation schemes for two transmit and one or two receive antennas. The channel fading coefficients are assumed to be independent between antennas, but time correlated according to Jakes' model [66], in which the Doppler frequency is $f_D = 75 \text{ Hz}$ and normalized fading parameter is $f_D T_s = 0.0025$ where T_s is the sampling period.

Figures 3.1 and 3.2 show performances of the MRB signals with constellation size $L = 4$, i.e., $R = 1 \text{ b/s/Hz}$. We observe that our new codes achieve coding advantages of about $0.75 - 1 \text{ dB}$ over the codes designed in [44] at the BEP range $10^{-3} - 10^{-4}$. Moreover, we compare our signal performances to those of a code with optimum diversity sum and product in [43]; the so-called DS-DP codes. Simulation results show that the performances of the MRB codes with new parameters are close to the DS-DP code performances. Although the DS-DP code provide slightly better performance, it is a hand-crafted signal derived from Sphere Packings.

The BEP performances of constellation size $L = 32$ ($R = 2.5 \text{ b/s/Hz}$) are illustrated in Figures 3.3 and 3.4 for $M_R = 1$ and 2 , respectively. In comparison with the original parameters, our new parameters yields better performance in

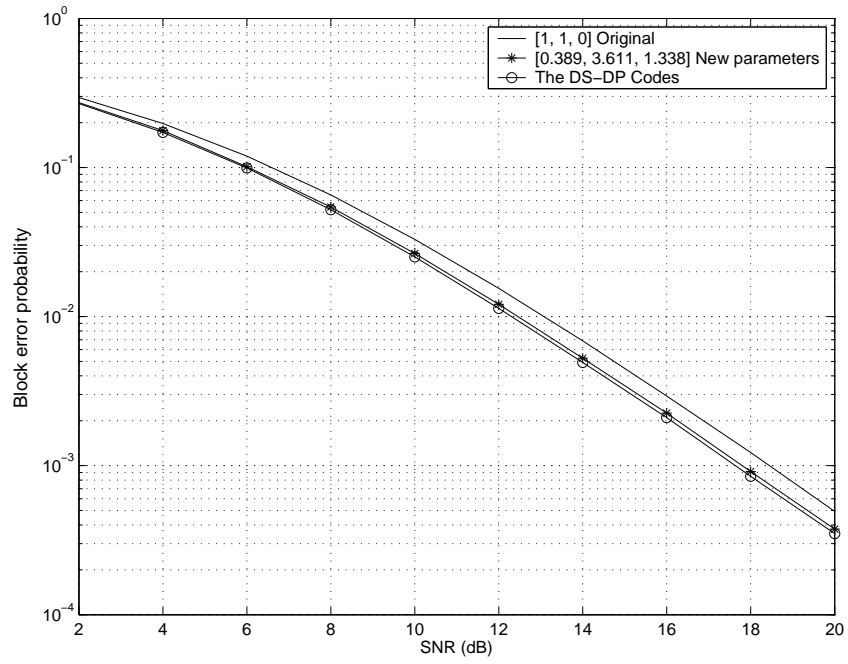


Figure 3.1: Performance for $L = 4$, $M_T = 2$, and $M_R = 1$.

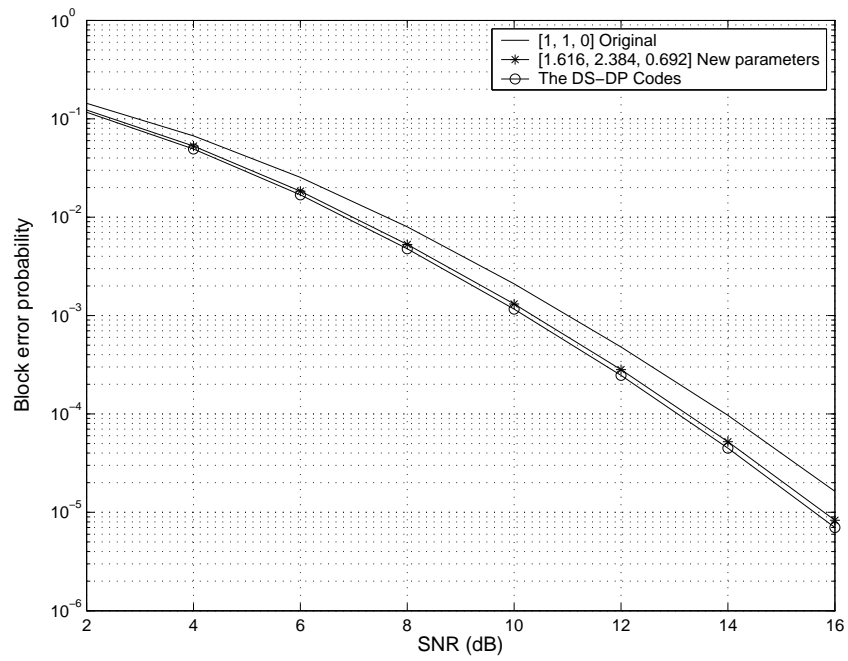


Figure 3.2: Performance for $L = 4$, $M_T = 2$, and $M_R = 2$.

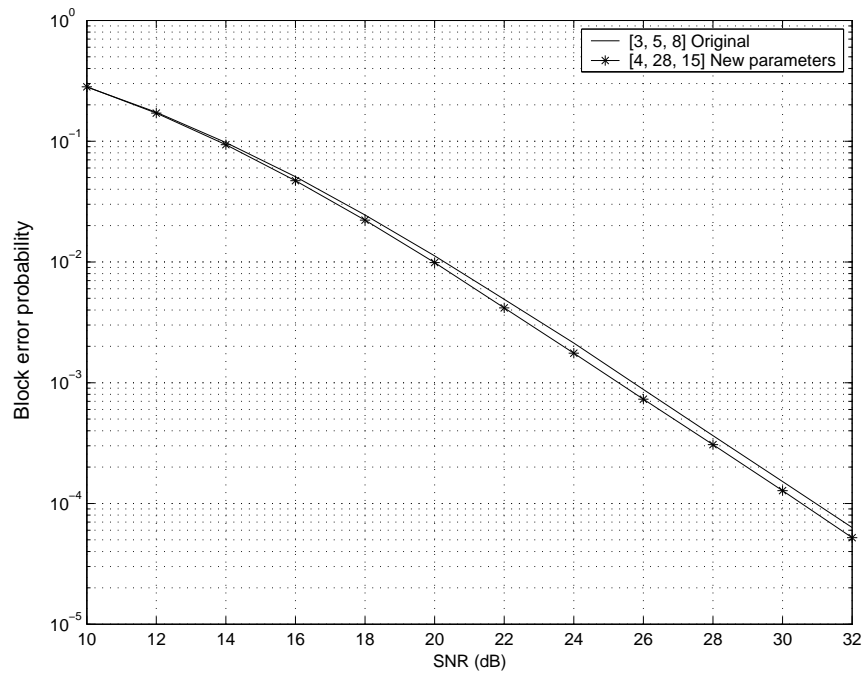


Figure 3.3: Performance for $L = 32$, $M_T = 2$, and $M_R = 1$.

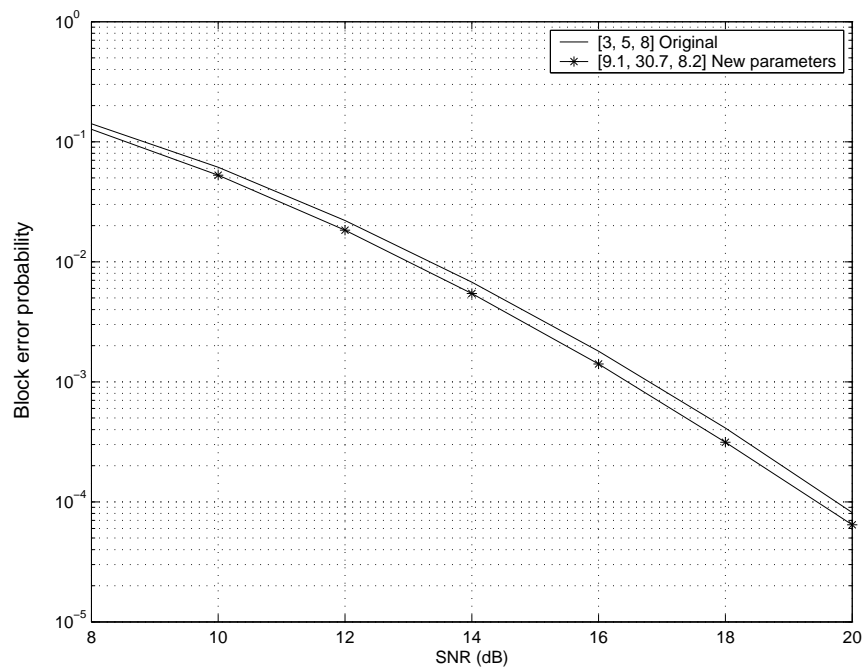


Figure 3.4: Performance for $L = 32$, $M_T = 2$, and $M_R = 2$.

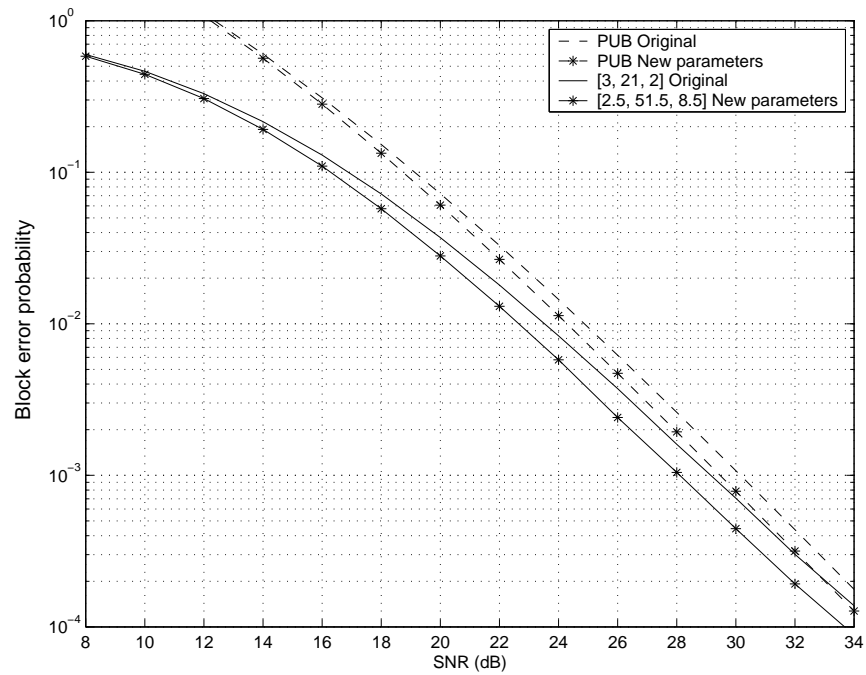


Figure 3.5: Performance for $L = 64$, $M_T = 2$, and $M_R = 1$.

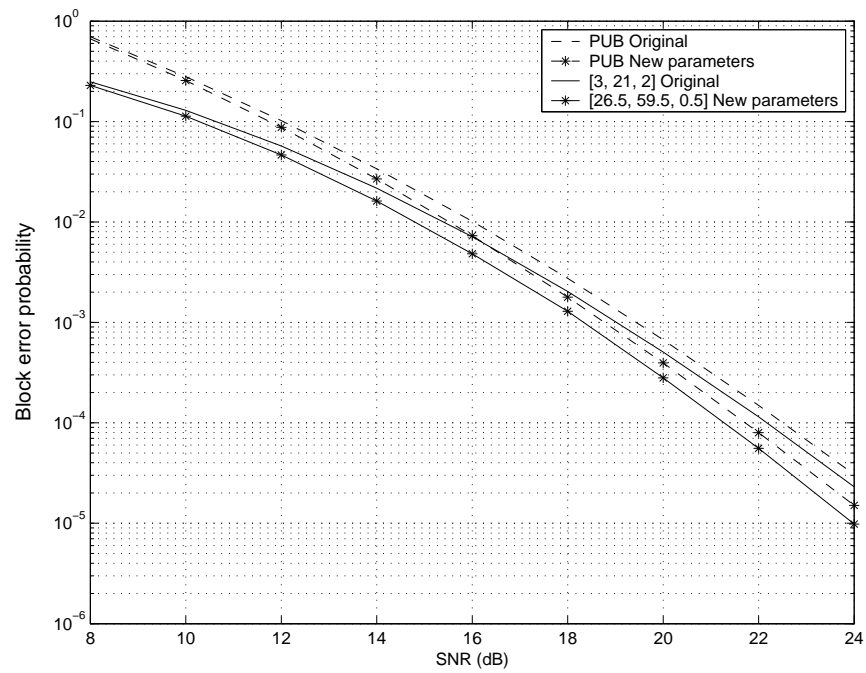


Figure 3.6: Performance for $L = 64$, $M_T = 2$, and $M_R = 2$.

both cases. This confirms the merit of the design criterion in (3.9).

For $L = 64$ or $R = 3$ b/s/Hz with $M_T = 2$, $M_R = 1$ and $M_R = 2$, the constellation performances are shown in Figures 3.5 and 3.6, respectively. We observe coding gains of 1 dB at BEP of 10^{-3} and 10^{-4} over the previous design in [44] for the single receive antenna system and the system with two receive antennas, respectively. Also in the figures, we show the tightness of the *PUB* curve, which is numerically evaluated from (3.9), to the true constellation performance. As expected, the *PUB* curve converges to the true performance at high *SNR* in both figures.

3.2 Differential Modulation for Frequency Selective MIMO-OFDM systems

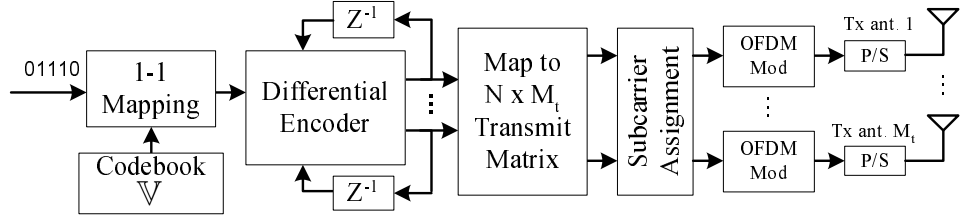
In this Section, we propose a differential modulation for wideband MIMO systems by which fading channels are frequency-selective. Differential space-time-frequency (DSTF) modulations are known as practical alternatives that are capable of exploiting the available spatial and frequency diversities without the requirement of multi-channel estimation at the receiver. However, the encoding nature of the DSTF schemes that expand several OFDM symbol periods makes the DSTF schemes susceptible to fast-changing channel conditions. We propose a differential encoding and decoding scheme for MIMO-OFDM systems that is able to differentially encode signal within each OFDM symbol period. The scheme does not only reduce encoding and decoding delay, but also relaxes the restriction on channel assumption. The successful differential decoding of the proposed scheme depends on the assumption that the fading channels keep constant over two OFDM symbol periods rather than multiple of them as required in the existing DSTF schemes.

We provide the pairwise error probability formulation, and quantify the performance criteria in terms of diversity and coding advantages. Our design criteria reveals that the existing diagonal cyclic codes can be applied to achieve full diversity. Performance simulations under various channel conditions show that our proposed scheme yields superior performance to previously proposed differential schemes.

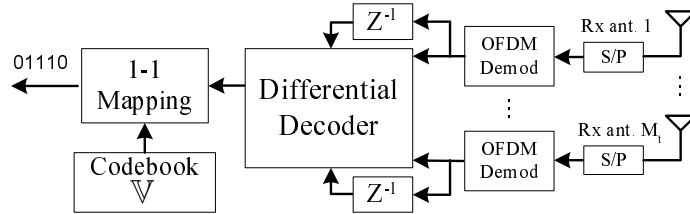
The following notations are adopted throughout this section: vectors (matrices) are denoted by boldface lower (upper) case letters; all vectors are column vectors; superscript $(\cdot)^T$ and $(\cdot)^H$ denote the transpose and conjugate transpose, respectively; $\mathcal{C}^{A \times B}$ represents the complex field of dimension $A \times B$; $\lfloor \cdot \rfloor$ represents the floor function; $\lceil \cdot \rceil$ denotes the ceiling function; $E[\cdot]$ takes the statistical expectation; $diag(\cdot)$ denotes a diagonal matrix; \mathbf{I}_M ($\mathbf{0}_M$) denotes $M \times M$ identity matrix (matrix of all zeroes); $\mathbf{1}_K$ represents the $K \times 1$ vector of all ones; for any $N \times M$ matrix \mathbf{A} we represent $det(\mathbf{A})$ as its matrix determinant and $tr(\mathbf{A})$ as its trace operator; $\mathcal{D}(\mathbf{A})$ converts each column of \mathbf{A} to a diagonal matrix and results in an $N \times NM$ matrix of a form

$$\mathcal{D}(\mathbf{A}) = \mathcal{D}([\mathbf{a}_1 \ \mathbf{a}_2 \ \cdots \ \mathbf{a}_M]) = [diag(\mathbf{a}_1) \ diag(\mathbf{a}_2) \ \cdots \ diag(\mathbf{a}_M)]; \quad (3.16)$$

\otimes denotes the matrix/vector tensor product [84]; \circ denotes the Hadamard product [84] such that for $\mathbf{A} = (a_{ij})$ and $\mathbf{B} = (b_{ij})$ are two $N \times M$ matrix, then $\mathbf{A} \circ \mathbf{B}$ is the $N \times M$ matrix whose whose $(ij)^{th}$ entry is $a_{ij}b_{ij}$; finally, $\|\mathbf{A}\|_F^2$ represents the Frobenius norm [84] of matrix \mathbf{A} which is defined as $\|\mathbf{A}\|_F^2 = tr(\mathbf{A}^H \mathbf{A}) =$



(a) Differential transmitter



(b) Differential receiver

Figure 3.7: Description of the differential MIMO-OFDM system.

$$\text{tr}(\mathbf{A}\mathbf{A}^H) = \sum_{i=1}^N \sum_{j=1}^M |a_{ij}|^2.$$

3.2.1 System Description

We consider a MIMO wireless communication system equipped with M_t transmit and M_r receive antennas. Each antenna employs an OFDM modulator with N subcarriers, as shown in Figure 3.7. The frequency-selective fading channel between transmit antenna i and receive antenna j is assumed to have L independent delay paths with arbitrary power delay profiles. The baseband equivalent channel between the i^{th} transmit antenna to the j^{th} receive antenna is modelled by a finite impulse response (FIR) filter as

$$h_{ij}^k(t) = \sum_{l=0}^{L-1} \alpha_{ij}^k(l) \delta(t - \tau_l), \quad (3.17)$$

where $\alpha_{ij}^k(l)$ is the multipath channel coefficient from the i^{th} transmit antenna to the j^{th} receive antenna at the k^{th} OFDM block, and τ_l represents the l^{th} path delay. The $\alpha_{ij}^k(l)$ is modelled as zero-mean complex Gaussian random variable with variance $E |\alpha_{ij}^k(l)|^2 = \delta_l^2$. The channel coefficients are assumed to be spatially uncorrelated for different transmit-receive link. In each transmit-receive link, the power of the L independent delay paths is normalized such that $\sum_{l=0}^{L-1} \delta_l^2 = 1$. The frequency response of the channel in (3.17) is given by

$$H_{ij}^k(f) = \sum_{l=0}^{L-1} \alpha_{ij}^k(l) e^{-j2\pi f \tau_l}. \quad (3.18)$$

At the transmitter, an information bit sequence is differentially encoded and mapped onto an $NM_t \times M_t$ transmit signal matrix

$$\mathbf{X}^k = \begin{pmatrix} x_1^k(0) & x_2^k(0) & \cdots & x_{M_t}^k(0) \\ x_1^k(1) & x_2^k(1) & \cdots & x_{M_t}^k(1) \\ \vdots & \vdots & \ddots & \vdots \\ x_1^k(N-1) & x_2^k(N-1) & \cdots & x_{M_t}^k(N-1) \end{pmatrix}, \quad (3.19)$$

where $x_i^k(n)$ is a differentially encoded data symbol to be transmitted on the n^{th} subcarrier from transmit antenna i during the k^{th} OFDM symbol period. We assume that \mathbf{X}^k is normalized to satisfy the energy constraint $E \|\mathbf{X}^k\|_F^2 = N$. We will explain details of the proposed differential encoding and decoding scheme in Section 3.2.2. In order to transmit \mathbf{X}^k , each of the i^{th} column of matrix \mathbf{X}^k is OFDM modulated using N-point IFFT and augmented by cyclic prefix. The resulting OFDM symbol is transmitted from the i^{th} transmit antenna. Note that all of the M_t OFDM symbols are transmitted simultaneously from different transmit antennas within one OFDM symbol period.

At each receive antenna, the receiver performs match filtering, cyclic prefix removing, and OFDM demodulating by N-point FFT. The received signal is a

noisy superposition of transmitted symbols from multiple transmit antennas. We model the received signal of the n^{th} subcarrier at the j^{th} receive antenna during the k^{th} OFDM symbol period as

$$y_j^k(n) = \sqrt{\rho} \sum_{i=1}^{M_t} x_i^k(n) H_{ij}^k(n) + w_j^k(n), \quad (3.20)$$

where ρ is the average signal to noise ratio per receiver, and

$$H_{ij}^k(n) = \sum_{l=0}^{L-1} \alpha_{ij}^k(l) e^{-j2\pi n \Delta f \tau_l} \quad (3.21)$$

is the subchannel gain. Here, $\Delta f = 1/T_s$ is the inter-subcarrier spacing, and T_s is the OFDM symbol period. The additive complex Gaussian noise, $w_j^k(n)$, has zero mean and unit variance, $\mathcal{CN}(0, 1)$. The additive noise is assumed to be statistically independent for different receive antennas j , subcarriers n , and OFDM symbol periods k . We observe from (3.20) that OFDM modem converts a frequency-selective fading channel into a set of parallel frequency-flat fading channels. The differential modulation scheme does not require the knowledge of channel state information at either the transmitter or the receiver. However, the subchannel gains are assumed constant over two OFDM symbol periods, i.e. $H_{ij}^k(n) \approx H_{ij}^{k-1}(n)$.

Let $\mathbf{y}_j^k = [y_j^k(0), y_j^k(1), \dots, y_j^k(N-1)]^T$ be an $N \times 1$ vector comprising the receive signal at the j^{th} received antenna during the k^{th} OFDM symbol period. We can describe \mathbf{y}_j^k as

$$\mathbf{y}_j^k = \sqrt{\rho} \mathcal{D}(\mathbf{X}^k) \mathbf{h}_j^k + \mathbf{w}_j^k, \quad j = 1, 2, \dots, M_r, \quad (3.22)$$

where $\mathcal{D}(\cdot)$ is defined in (3.16) and $\mathcal{D}(\mathbf{X}^k)$ represents an $N \times NM_t$ transmit signal matrix. The $NM_t \times 1$ channel gain vector \mathbf{h}_j^k is represented by

$$\mathbf{h}_j^k = [(\mathbf{h}_{1j}^k)^T \dots (\mathbf{h}_{M_t j}^k)^T]^T, \quad (3.23)$$

in which

$$\mathbf{h}_{ij}^k = [H_{ij}^k(0) \cdots H_{ij}^k(N-1)]^T, \quad (3.24)$$

and the noise vector has the form

$$\mathbf{w}_j^k = [w_j^k(0) w_j^k(1) \cdots w_j^k(N-1)]^T. \quad (3.25)$$

By stacking all M_r receive signal vectors together, we obtain the $NM_r \times 1$ receive signal vector

$$\mathbf{y}^k = \sqrt{\rho} (\mathbf{I}_{M_r} \otimes \mathcal{D}(\mathbf{X}^k)) \mathbf{h}^k + \mathbf{w}^k, \quad (3.26)$$

where $\mathbf{y}^k = [(\mathbf{y}_1^k)^T (\mathbf{y}_2^k)^T \cdots (\mathbf{y}_{M_r}^k)^T]^T$, $\mathbf{h}^k = [(\mathbf{h}_1^k)^T (\mathbf{h}_2^k)^T \cdots (\mathbf{h}_{M_r}^k)^T]^T$, and $\mathbf{w}^k = [(\mathbf{w}_1^k)^T (\mathbf{w}_2^k)^T \cdots (\mathbf{w}_{M_r}^k)^T]^T$, in which \mathbf{y}_j^k , \mathbf{h}_j^k , and \mathbf{w}_j^k are specified in (3.22), (3.23) and (3.25), respectively.

3.2.2 Single-Block Differential Transmit scheme

In what follows, we propose a differential encoding and decoding scheme for MIMO-OFDM systems under frequency-selective fading channels. By taking advantage of the coding strategy in [93], the proposed scheme is able to completely transmit the differentially encoded signal matrix within one OFDM symbol period. This allows us to relax the channel assumption for efficient differential decoding. Specifically, our scheme requires that the fading channels keep constant within only one OFDM block, and slowly change from one OFDM block to the next.

Before going into detail of the proposed scheme, it is worth to mention that the proposed scheme is applicable to any subcarrier selection scheme such as the subcarrier grouping method [73] or the subcarrier permutation strategy [93].

Transmit Signal Structure

We will introduce a differential encoding and decoding scheme based on a transmit scheme proposed in [93]. Specifically, for an integer Γ such that $1 \leq \Gamma \leq L$, a transmit signal matrix \mathbf{X}^k in (3.19) is partitioned into $P = \lfloor N/(\Gamma M_t) \rfloor$ submatrices as follows [93]:

$$\mathbf{X}^k = [(\mathbf{X}_1^k)^T \ (\mathbf{X}_2^k)^T \ \cdots \ (\mathbf{X}_P^k)^T \ (\mathbf{0}_{N-P\Gamma M_t})^T]^T, \quad (3.27)$$

where $\mathbf{0}_{N-P\Gamma M_t}$ denotes an $(N - P\Gamma M_t) \times M_t$ zero padding matrix to be inserted if N cannot be divided by ΓM_t . The $\Gamma M_t \times M_t$ matrix \mathbf{X}_p^k , for $p = 1, 2, \dots, P$, is modelled as

$$\mathbf{X}_p^k = \text{diag}(\mathbf{x}_{p,1}^k \ \mathbf{x}_{p,2}^k \ \cdots \ \mathbf{x}_{p,M_t}^k), \quad (3.28)$$

where $\mathbf{x}_{p,i}^k$, for $i = 1, 2, \dots, M_t$, is a $\Gamma \times 1$ vector,

$$\mathbf{x}_{p,i}^k = [s_{p,(i-1)\Gamma+1}^k \ s_{p,(i-1)\Gamma+2}^k \ \cdots \ s_{p,i\Gamma}^k]^T, \quad (3.29)$$

and all $s_{p,m}^k$, $m = 1, 2, \dots, \Gamma M_t$, are differentially encoded symbols that will be specified later.

We now specify information matrices as follows. For each p , $p = 1, 2, \dots, P$, let \mathbf{V}_p^k denote a $\Gamma M_t \times \Gamma M_t$ unitary information matrix having diagonal form as

$$\mathbf{V}_p^k = \text{diag}([v_{p,1}^k \ v_{p,2}^k \ \cdots \ v_{p,\Gamma M_t}^k]^T), \quad (3.30)$$

in which $v_{p,m}^k$, $m = 1, 2, \dots, \Gamma M_t$, is an information symbol to be transmitted over subcarrier $(p-1)\Gamma M_t + m$ during the k^{th} OFDM symbol period. We will independently design the matrix \mathbf{V}_p^k for different p . The set of all possible information matrices constitutes a constellation \mathbb{V}_p . In order to support a data rate of R b/s/Hz, \mathbb{V}_p is designed to have constellation size $\mathcal{L} = |\mathbb{V}_p| = 2^{R\Gamma M_t}$.

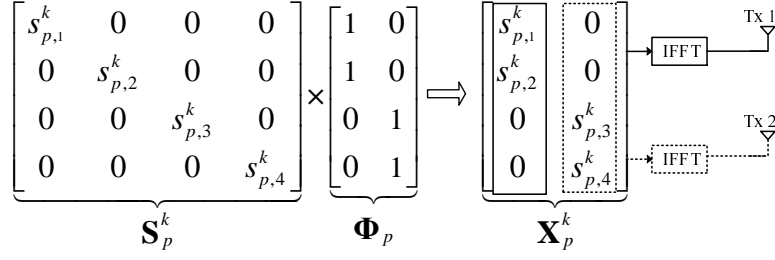


Figure 3.8: An example of a code structure for $\Gamma = 2$ and $M_t = 2$ at the p^{th} sub-matrix.

We will encode a sequence of information bits into an information matrix as specified in (3.30). The information matrix is differentially encoded, and then transformed into a SF code structure in (3.28). All of the obtained P sub-matrices are concatenated to construct the code structure in (3.27) before being transmitted over the M_t transmit antennas.

Differential Encoder and Transmission Matrix

Our proposed differential encoding scheme is composed of a concatenation of two functional blocks, namely, a differential encoder and a multiplicative mapping matrix. An example of a code structure is shown in Figure 3.8 for a case of $\Gamma = 2$ and $M_t = 2$ at the p^{th} sub-matrix.

- **Differential Encoder**

Let \mathbf{S}_p^k be a $\Gamma M_t \times \Gamma M_t$ differential encoded signal matrix to be transmitted during the k^{th} OFDM symbol period. We recursively construct \mathbf{S}_p^k from the fundamental differential equation [27], [26]

$$\mathbf{S}_p^k = \begin{cases} \mathbf{V}_p^k \mathbf{S}_p^{k-1}, & k \geq 1, \\ \mathbf{I}_{\Gamma M_t}, & k = 0, \end{cases} \quad (3.31)$$

where the differential transmission initially sends $\mathbf{S}_p^0 = \mathbf{I}_{\Gamma M_t}$ to learn the channels. The matrix \mathbf{S}_p^k is also unitary since it results from recursive mul-

tiplication of unitary information matrices. Due to the diagonal structure of \mathbf{V}_p^k , \mathbf{S}_p^k can be expressed as

$$\mathbf{S}_p^k = \text{diag}([s_{p,1}^k, s_{p,2}^k, \dots, s_{p,\Gamma M_t}^k]^T), \quad (3.32)$$

where $s_{p,m}^k$, $m = 1, 2, \dots, \Gamma M_t$, is the differentially encoded complex symbol to be transmitted at subcarrier $(p-1)\Gamma M_t + m$ during the k^{th} OFDM block. Note that, depending on how the elements of \mathbf{S}_p^k are transmitted over M_t transmit antennas, the differential schemes can be different. The DSTF schemes in [34]- [79] transmit the \mathbf{S}_p^k matrix through M_t OFDM modulators over multiple OFDM blocks. This leads to performance degradation when the fading channels do not stay constant over several OFDM blocks. In what follows, we introduce a multiplicative mapping matrix that allows us to transform \mathbf{S}_p^k into the code structure in (3.28) and completely transmit \mathbf{S}_p^k within one OFDM block. This does not only improve system performance under rapid fading environment, but also reduces encoding and decoding delay.

- **Multiplicative Mapping Matrix**

We define the $\Gamma M_t \times M_t$ multiplicative mapping matrix as [80]

$$\mathbf{\Phi}_p = [\phi_1 \ \phi_2 \ \cdots \ \phi_{M_t}], \quad (3.33)$$

in which ϕ_i is a $\Gamma M_t \times 1$ vector,

$$\phi_i = \mathbf{e}_i \otimes \mathbf{1}_\Gamma, \quad i = 1, \dots, M_t, \quad (3.34)$$

where \mathbf{e}_i is an $M_t \times 1$ unit vector whose i^{th} component is one and all others are zeroes. We post-multiply \mathbf{S}_p^k by $\mathbf{\Phi}_p$, resulting in the $\Gamma M_t \times M_t$

transmission matrix

$$\mathbf{X}_p^k = \mathbf{S}_p^k \Phi_p. \quad (3.35)$$

Consequently, the differentially encoded complex symbol $s_{p,m}^k$, as specified in (3.32), is transmitted at the $\lceil \frac{m}{\Gamma} \rceil$ transmit antenna.

Differential Decoder

According to (3.26) and (3.27), the receive signal vector corresponding to the transmit signal matrix \mathbf{X}_p^k , defined in (3.28), is given by

$$\mathbf{y}_p^k = \sqrt{\rho} (\mathbf{I}_{M_r} \otimes \mathcal{D}(\mathbf{X}_p^k)) \mathbf{h}_p^k + \mathbf{w}_p^k, \quad (3.36)$$

where $\mathcal{D}(\mathbf{X}_p^k)$ ($\mathcal{D}(\cdot)$ is a $\Gamma M_t \times \Gamma M_t M_t$ transmit matrix. The $\Gamma M_t M_t M_r \times 1$ channel vector $\mathbf{h}_p^k = [(\mathbf{h}_{p,1}^k)^T (\mathbf{h}_{p,2}^k)^T \cdots (\mathbf{h}_{p,M_r}^k)^T]^T$ comprises

$$\mathbf{h}_{p,j}^k = [(\mathbf{h}_{p,1j}^k)^T (\mathbf{h}_{p,2j}^k)^T \cdots (\mathbf{h}_{p,M_t j}^k)^T]^T, \quad (3.37)$$

where

$$\mathbf{h}_{p,ij}^k = [H_{ij}^k((p-1)\Gamma M_t) \cdots H_{ij}^k(p\Gamma M_t - 1)]^T. \quad (3.38)$$

Similarly, the receive signal vector is given by $\mathbf{y}_p^k = [(\mathbf{y}_{p,1}^k)^T (\mathbf{y}_{p,2}^k)^T \cdots (\mathbf{y}_{p,M_r}^k)^T]^T$, where $\mathbf{y}_{p,j}^k = [y_j^k((p-1)\Gamma M_t) \cdots y_j^k(p\Gamma M_t - 1)]^T$. The noise vector \mathbf{w}_p^k is in the same form as \mathbf{y}_p^k with $y_j^k(n)$ replaced by $w_j^k(n)$.

To perform differential decoding, two consecutive receive signal vectors in (3.36), i.e. \mathbf{y}_p^k and \mathbf{y}_p^{k-1} , are required to recover the information matrix at each OFDM symbol period. Since the two consecutive receive signal vectors are related through the differentially encoded signal matrix \mathbf{S}_p^k (see (3.31)), we will introduce the equivalent expression of $(\mathbf{I}_{M_r} \otimes \mathcal{D}(\mathbf{X}_p^k)) \mathbf{h}_p^k$ in terms of \mathbf{S}_p^k for subsequent differential decoding.

From (3.33) and (3.35), we can express $\mathcal{D}(\mathbf{X}_p^k)$ as

$$\mathcal{D}(\mathbf{X}_p^k) = [\text{diag}(\mathbf{S}_p^k \phi_1) \cdots \text{diag}(\mathbf{S}_p^k \phi_{M_t})]. \quad (3.39)$$

According to (3.37) and (3.39), we have

$$\mathcal{D}(\mathbf{X}_p^k) \mathbf{h}_{p,j}^k = \sum_{i=1}^{M_t} \text{diag}(\mathbf{S}_p^k \phi_i) \mathbf{h}_{p,ij}^k, \quad (3.40)$$

which can be re-written as

$$\begin{aligned} \mathcal{D}(\mathbf{X}_p^k) \mathbf{h}_{p,j}^k &= \sum_{i=1}^{M_t} (\mathbf{S}_p^k \phi_i) \circ \mathbf{h}_{p,ij}^k \\ &= \mathbf{S}_p^k \sum_{i=1}^{M_t} \phi_i \circ \mathbf{h}_{p,ij}^k \triangleq \mathbf{S}_p^k \tilde{\mathbf{h}}_{p,j}^k, \end{aligned} \quad (3.41)$$

where $\tilde{\mathbf{h}}_{p,j}^k$ in the last equality is explicitly defined. By substituting (3.38) into (3.41), we can express $\tilde{\mathbf{h}}_{p,j}^k$ as

$$\tilde{\mathbf{h}}_{p,j}^k = [(\tilde{\mathbf{h}}_{p,1j}^k)^T (\tilde{\mathbf{h}}_{p,2j}^k)^T \cdots (\tilde{\mathbf{h}}_{p,M_t j}^k)^T]^T \quad (3.42)$$

in which

$$\tilde{\mathbf{h}}_{p,ij}^k = [H_{ij}(n_{p,i}^0) H_{ij}(n_{p,i}^1) \cdots H_{ij}(n_{p,i}^{\Gamma-1})]^T, \quad (3.43)$$

where

$$n_{p,i}^\gamma = (i-1)\Gamma + (p-1)\Gamma M_t + \gamma \quad (3.44)$$

for $\gamma = 0, 1, \dots, \Gamma-1$. Denoting $\tilde{\mathbf{h}}_p^k = [(\tilde{\mathbf{h}}_{p,1}^k)^T (\tilde{\mathbf{h}}_{p,2}^k)^T \cdots (\tilde{\mathbf{h}}_{p,M_r}^k)^T]^T$ as a $\Gamma M_t M_r \times 1$ channel gain vector and using (3.41), we obtain an equivalent expression

$$(\mathbf{I}_{M_r} \otimes \mathcal{D}(\mathbf{X}_p^k)) \mathbf{h}_p^k = (\mathbf{I}_{M_r} \otimes \mathbf{S}_p^k) \tilde{\mathbf{h}}_p^k. \quad (3.45)$$

For notation convenience, let us define $\mathbf{S}_p^k \triangleq (\mathbf{I}_{M_r} \otimes \mathbf{S}_p^k)$ and $\mathbf{V}_p^k \triangleq (\mathbf{I}_{M_r} \otimes \mathbf{V}_p^k)$ such that

$$\mathbf{S}_p^k = (\mathbf{I}_{M_r} \otimes \mathbf{V}_p^k) \mathbf{S}_p^{k-1} = \mathbf{V}_p^k \mathbf{S}_p^{k-1}. \quad (3.46)$$

Hence, using (3.45) and (3.46), we can rewrite the two consecutive receive signal vectors in (3.36) as

$$\mathbf{y}_p^{k-1} = \sqrt{\rho} \mathbf{S}_p^{k-1} \tilde{\mathbf{h}}_p^{k-1} + \mathbf{w}_p^{k-1}, \quad (3.47)$$

$$\mathbf{y}_p^k = \sqrt{\rho} \mathbf{S}_p^k \tilde{\mathbf{h}}_p^k + \mathbf{w}_p^k. \quad (3.48)$$

We relate the equivalent terms of (3.47) and (3.48) through (3.46) and assume that the channel coefficients are almost constant over two consecutive OFDM blocks, i.e. $\tilde{\mathbf{h}}_p^k \approx \tilde{\mathbf{h}}_p^{k-1} \approx \tilde{\mathbf{h}}_p$, then we obtain

$$\mathbf{y}_p^k = \mathbf{V}_p^k \mathbf{y}_p^{k-1} + \sqrt{2} \tilde{\mathbf{w}}_p^k, \quad (3.49)$$

where $\tilde{\mathbf{w}}_p^k = \frac{1}{\sqrt{2}} (\mathbf{w}_p^k - \mathbf{V}_p^k \mathbf{w}_p^{k-1})$ is a noise vector whose element is $\mathcal{CN}(0, 1)$ distributed. Without acquiring channel state information, the differential decoder performs maximum likelihood decoding, and the decision rule can be stated as [26]

$$\hat{\mathbf{V}}_p^k = \arg \min_{\mathbf{V}_p^k \in \mathbb{V}_p} \|\mathbf{y}_p^k - \mathbf{V}_p^k \mathbf{y}_p^{k-1}\|_F^2 \quad (3.50)$$

$$= \arg \max_{\mathbf{V}_p^k \in \mathbb{V}_p} (\mathbf{y}_p^k)^H \mathbf{V}_p^k \mathbf{y}_p^{k-1} + (\mathbf{y}_p^{k-1})^H (\mathbf{V}_p^k)^H \mathbf{y}_p^k. \quad (3.51)$$

It is worth to mention that the detector is able to differentially decode within two OFDM symbol periods regardless of the number of transmit antennas. Therefore, our proposed scheme significantly reduces the decoding delay compared to the DSTF schemes. Note also that the proposed scheme includes the differential scheme in [73] for single antenna OFDM system as a special case.

3.2.3 Pairwise Error Probability and Design Criteria

The previous section described the proposed differential encoding and decoding scheme. In this section, we show its average pairwise error probability (PEP) and design criteria under the assumption of frequency-selective channel model in Section 3.2.1. Note that in this paper, we provide a PEP formulation based on the

results in [86] which showed the asymptotic PEP for differential detection under correlated Rayleigh fading channels. The PEP upper bound in [86] is not only asymptotically tight, but also provides a simple interpretation of the performance in terms of the eigenvalues of signal and correlation matrices.

Suppose that \mathbf{v}_p^k and $\hat{\mathbf{v}}_p^k$ are two different information matrices. With the assumption of slow fading channels, the average PEP is upper bounded by ([86], Proposition 7)

$$P\left(\mathbf{v}_p^k \rightarrow \hat{\mathbf{v}}_p^k\right) \leq \binom{2\nu - 1}{\nu} \left(\prod_{m=1}^{\nu} \beta_{p,m}\right)^{-1} \left(\frac{\rho}{2}\right)^{-\nu}, \quad (3.52)$$

where ρ represents the signal-to-noise ratio per symbol, ν is the rank and $\beta_{p,m}$'s are the non-zeros eigenvalues of the matrix

$$\mathbf{\Psi}_p \triangleq \mathbf{S}_p^{k-1} \mathbf{\Sigma}_{\tilde{\mathbf{h}}_p} (\mathbf{S}_p^{k-1})^H (\mathbf{v}_p^k - \hat{\mathbf{v}}_p^k)^H (\mathbf{v}_p^k - \hat{\mathbf{v}}_p^k), \quad (3.53)$$

in which $\mathbf{\Sigma}_{\tilde{\mathbf{h}}_p} = E[\tilde{\mathbf{h}}_p \tilde{\mathbf{h}}_p^H]$ denotes the correlation matrix of channel vector $\tilde{\mathbf{h}}_p$. Note that the PEP upper bound in (3.52) is a function of $\rho/2$, which corresponds to the 3-dB performance loss when compared to its coherent counterpart.

We will reformulate the PEP upper bound in (3.52) for the case of spatially uncorrelated MIMO channels such that we can obtain design criteria for our proposed scheme. To simplify the expression for matrix $\mathbf{\Psi}_p$ in (3.53), we evaluate the channel correlation matrix $\mathbf{\Sigma}_{\tilde{\mathbf{h}}_p}$ as follows. First, we re-write the channel frequency response in (3.21) as

$$H_{ij}^k(n) = \boldsymbol{\omega}^T(n) \mathbf{a}_{ij}^k, \quad (3.54)$$

where $\mathbf{a}_{ij}^k = [\alpha_{ij}^k(0) \ \alpha_{ij}^k(1) \ \dots \ \alpha_{ij}^k(L-1)]^T$ is an $L \times 1$ matrix of path gain coefficients, $\boldsymbol{\omega}(n) = [\omega^{n\tau_0} \ \omega^{n\tau_1} \ \dots \ \omega^{n\tau_{L-1}}]^T$, and $\omega \triangleq e^{-j2\pi\Delta f}$. According to (3.54), we

can represent $\tilde{\mathbf{h}}_{p,ij}^k$ in (3.43) as

$$\tilde{\mathbf{h}}_{p,ij}^k = \mathbf{\Omega}_{p,i} \mathbf{a}_{ij}^k, \quad (3.55)$$

where $\mathbf{\Omega}_{p,i} = [\boldsymbol{\omega}(n_{p,i}^0) \boldsymbol{\omega}(n_{p,i}^1) \cdots \boldsymbol{\omega}(n_{p,i}^{\Gamma-1})]^T \in \mathcal{C}^{\Gamma \times L}$ and $n_{p,i}^\gamma$ is defined in (3.44).

Substituting (3.55) into (3.42), we have

$$\tilde{\mathbf{h}}_{p,j}^k = \mathbf{\Omega}_p \mathbf{a}_j^k, \quad (3.56)$$

where

$$\mathbf{\Omega}_p = \text{diag}(\mathbf{\Omega}_{p,1}, \mathbf{\Omega}_{p,2}, \cdots, \mathbf{\Omega}_{p,M_t}) \in \mathcal{C}^{\Gamma M_t \times L M_t}, \quad (3.57)$$

and

$$\mathbf{a}_j^k = [(\mathbf{a}_{1j}^k)^T (\mathbf{a}_{2j}^k)^T \cdots (\mathbf{a}_{M_t j}^k)^T]^T \in \mathcal{C}^{L M_t \times 1}. \quad (3.58)$$

Based on (3.56) and the assumption that each transmit-receive link has the same power delay profile, we can calculate the correlation matrix of channel vector $\tilde{\mathbf{h}}_{p,j}^k$ as

$$\boldsymbol{\Sigma}_{\tilde{\mathbf{h}}_{p,j}} = E[\tilde{\mathbf{h}}_{p,j}^k (\tilde{\mathbf{h}}_{p,j}^k)^H] = \mathbf{\Omega}_p (\mathbf{I}_{M_t} \otimes \mathbf{\Lambda}_{\delta^2}) \mathbf{\Omega}_p^H, \quad (3.59)$$

where $\mathbf{\Lambda}_{\delta^2} = \text{diag}(\delta_0^2, \dots, \delta_{L-1}^2)$ represents an $L \times L$ diagonal matrix of power delay profile. Observe from (3.59) that $\boldsymbol{\Sigma}_{\tilde{\mathbf{h}}_{p,j}}$ is the same for all j 's. Consequently, denoting $\boldsymbol{\Sigma} \triangleq \boldsymbol{\Sigma}_{\tilde{\mathbf{h}}_{p,j}}$, we can express the correlation matrix $\boldsymbol{\Sigma}_{\tilde{\mathbf{h}}_p}$ as

$$\boldsymbol{\Sigma}_{\tilde{\mathbf{h}}_p} = \mathbf{I}_{M_r} \otimes \boldsymbol{\Sigma}. \quad (3.60)$$

Applying the property of tensor product $(\mathbf{A}_1 \otimes \mathbf{B}_1)(\mathbf{A}_2 \otimes \mathbf{B}_2)(\mathbf{A}_3 \otimes \mathbf{B}_3) = (\mathbf{A}_1 \mathbf{A}_2 \mathbf{A}_3 \otimes \mathbf{B}_1 \mathbf{B}_2 \mathbf{B}_3)$ ([84], p.251) to (3.53), we obtain

$$\boldsymbol{\Psi}_p = \mathbf{I}_{M_r} \otimes \boldsymbol{\Theta}_p, \quad (3.61)$$

in which

$$\boldsymbol{\Theta}_p = \mathbf{S}_p^{k-1} \boldsymbol{\Sigma} (\mathbf{S}_p^{k-1})^H \boldsymbol{\Delta}, \quad (3.62)$$

and $\Delta = (\mathbf{V}_p^k - \hat{\mathbf{V}}_p^k)^H (\mathbf{V}_p^k - \hat{\mathbf{V}}_p^k)$. Hence, by (3.61), the PEP in (3.52) can be expressed as

$$P(\mathbf{V}_p \rightarrow \hat{\mathbf{V}}_p) \leq \binom{2rM_r - 1}{rM_r} \left(\prod_{m=1}^r \lambda_{p,m} \right)^{-M_r} \left(\frac{\rho}{2} \right)^{-rM_r}, \quad (3.63)$$

where r is the rank and $\lambda_{p,m}$'s are the non-zero eigenvalues of the matrix Θ_p .

The PEP upper bound in (3.63) suggests two design criteria

1) Rank criterion: For any $\mathbf{V}_p^k \neq \hat{\mathbf{V}}_p^k$, design a constellation set of unitary matrices \mathbb{V}_p such that the minimum rank of Θ_p is maximized.

2) Product criterion: For any $\mathbf{V}_p^k \neq \hat{\mathbf{V}}_p^k$, design a constellation set of unitary matrices \mathbb{V}_p such that the minimum value of the product $\prod_{m=1}^r \lambda_{p,m}$ is maximized.

To quantify the maximum achievable diversity order, we substitute (3.59) into (3.62), and re-express Θ_p as

$$\Theta_p = \mathbf{S}_p^{k-1} \mathbf{\Omega}_p (\mathbf{I}_{M_t} \otimes \mathbf{\Lambda}_{\delta^2}) \mathbf{\Omega}_p^H (\mathbf{S}_p^{k-1})^H \Delta. \quad (3.64)$$

Observe from (3.64) that \mathbf{S}_p^{k-1} and \mathbf{V}_p^k are of size $\Gamma M_t \times \Gamma M_t$, the correlation matrix $\mathbf{\Omega}_p$ is of size $\Gamma M_t \times L M_t$, and $\mathbf{I}_{M_t} \otimes \mathbf{\Lambda}_{\delta^2}$ is an $L M_t \times L M_t$ diagonal matrix. Since $\Gamma \leq L$, the rank of Θ_p is at most ΓM_t . Therefore, the maximum achievable diversity gain is

$$G_d^{max} = M_r \max \left(\min_{\forall \mathbf{V}_p^k \neq \hat{\mathbf{V}}_p^k} \text{rank}(\Theta_p) \right) = \Gamma M_t M_r. \quad (3.65)$$

When the maximum diversity order is achieved, the maximum product criterion is determined by the normalized coding advantage or the so-called diversity product [26], [93]

$$\zeta = \frac{1}{2} \min_{\forall \mathbf{V}_p^k \neq \hat{\mathbf{V}}_p^k} \left| \prod_{m=1}^{\Gamma M_t} \lambda_{p,m} \right|^{\frac{1}{2\Gamma M_t}}, \quad (3.66)$$

where a larger ζ results in better performance.

In this case, we can evaluate the product of the non-zero eigenvalues of the matrix Θ_p as

$$\begin{aligned} \prod_{m=1}^{\Gamma M_t} \lambda_{p,m} &= \det \left(\mathbf{S}_p^{k-1} \mathbf{\Omega}_p (\mathbf{I}_{M_t} \otimes \mathbf{\Lambda}_{\delta^2}) \mathbf{\Omega}_p^H (\mathbf{S}_p^{k-1})^H \right) \det \left(\left(\mathbf{V}_p^k - \hat{\mathbf{V}}_p^k \right)^H \left(\mathbf{V}_p^k - \hat{\mathbf{V}}_p^k \right) \right) \\ &= \prod_{i=1}^{M_t} \det \left(\mathbf{\Omega}_{p,i} \mathbf{\Lambda}_{\delta^2} \mathbf{\Omega}_{p,i}^H \right) \prod_{m=1}^{\Gamma M_t} |v_{p,m}^k - \hat{v}_{p,m}^k|^2, \end{aligned} \quad (3.67)$$

where $\mathbf{V}_p^k - \hat{\mathbf{V}}_p^k = \text{diag}(v_{p,1}^k - \hat{v}_{p,1}^k, \dots, v_{p,\Gamma M_t}^k - \hat{v}_{p,\Gamma M_t}^k)$. In the second equality, we apply the identity $\det(\mathbf{AB}) = \det(\mathbf{BA})$ and the unitary property of matrix \mathbf{S}_p^{k-1} . Substitute (3.67) into (3.66), resulting in

$$\zeta = \left| \prod_{i=1}^{M_t} \det \left(\mathbf{\Omega}_{p,i} \mathbf{\Lambda}_{\delta^2} \mathbf{\Omega}_{p,i}^H \right) \right|^{\frac{1}{2\mathcal{M}}} \frac{1}{2} \min_{\mathbf{V}_p^k \neq \hat{\mathbf{V}}_p^k} \prod_{m=1}^{\mathcal{M}} |v_{p,m}^k - \hat{v}_{p,m}^k|^{\frac{1}{\mathcal{M}}} \quad (3.68)$$

in which $\mathcal{M} = \Gamma M_t$.

Observe from (3.68) that ζ can be maximized by designing the two terms on the right hand side separately. The first term depends only on the power delay profile, and it can be maximized by the use of proper subcarrier selection method, e.g., the subcarrier grouping method [73] or, more generally, the optimum permutation strategy proposed in [93]. The interested reader is referred to [93], section IV. B. equation 4.14 - 4.16), for more detail treatment of the subcarrier permutation method. In this work, however, we resort to random permutation strategy to enable fair performance comparison between the proposed scheme and the previously proposed scheme in [39]. The second term in (3.68) relies on the code structure. It is a challenging task to find such a good diagonal signal constellation. One method is to adopt the diagonal cyclic group code design in [26], which is well systematically designed and applicable for MIMO systems with any number of transmit antennas and any transmission rates. In particular, for a specific integer \mathcal{M} and transmission rate R such that the constellation size $\mathcal{L} = 2^{R\mathcal{M}}$.

We denote a set of parameters used to fully specify the signal constellation \mathbb{V}_p as $G_{\mathcal{M},\mathcal{L}} = (\mathcal{M}, \mathcal{L}, [u_1, u_2, \dots, u_{\mathcal{M}}])$, where $u_1, u_2, \dots, u_{\mathcal{M}}$ are chosen from a set of integer number $\mathcal{I}_L = \{0, 1, \dots, \mathcal{L} - 1\}$ that satisfies [26]

$$[u_1, u_2, \dots, u_{\mathcal{M}}] = \arg \max_{u_1, u_2, \dots, u_{\mathcal{M}} \in \mathcal{I}_L} \left(\min_{l \in \mathcal{I}_L} \left| \prod_{m=1}^{\mathcal{M}} \sin(\pi u_m l / \mathcal{L}) \right|^{\frac{1}{\mathcal{M}}} \right). \quad (3.69)$$

The sets of optimum parameters, $u_1, u_2, \dots, u_{\mathcal{M}}$, can be obtained from exhaustive computer search. Some examples of these parameters are given in [26]. Based on $G_{\mathcal{M},\mathcal{L}}$, the constellation \mathbb{V}_p are constructed from

$$\mathbf{V}_{p,l} = \text{diag} (e^{j\theta_{\mathcal{L}}u_1l}, e^{j\theta_{\mathcal{L}}u_2l}, \dots, e^{j\theta_{\mathcal{L}}u_{\mathcal{M}}l}), \quad (3.70)$$

for $l = 0, 1, \dots, \mathcal{L} - 1$, and $\theta_{\mathcal{L}} = 2\pi/\mathcal{L}$.

3.2.4 Simulation Results

In this section, we provide computer simulation results to illustrate performances of our proposed differential scheme in comparison with the previously existing schemes. We will briefly describe the simulated MIMO-OFDM system parameters, and then discuss performance results for different scenarios.

The Simulated MIMO-OFDM System Parameters

In the following simulations, each OFDM modulator utilized $N = 128$ subcarriers with the total bandwidth of 1 MHz. The corresponding OFDM symbol period was $T_s = 1/\Delta f = 128\mu s$. We added a guard interval of $20\mu s$ against intersymbol interference due to channel multipath delay spread. We used a simple two-ray and a more realistic typical urban (TU) six-ray power delay profiles. Each delay path of the two-ray profile had equal power with delay $\tau = 20\mu s$. The description of the TU channel is shown in Table I [2].

TABLE I : The typical urban (TU) six-ray power delay profile

Delay profile(μs)	0.0	0.2	0.5	1.6	2.3	5.0
Power profile	0.189	0.379	0.239	0.095	0.061	0.037

The fading channels are assumed constant within each OFDM block and slow varying from one OFDM block to another according to the Jakes' fading model [2] with f_D representing the maximum Doppler frequency in Hz . The thermal noise was complex Gaussian random variable with zero mean and variance $N_o = 1$.

We simulated the performance under different mobile environment by varying the normalized Doppler frequencies, namely, $f_D T_s = 0.0025, 0.005, 0.01, \text{ and } 0.025$ which correspond to mobile speeds of 6, 13, 26, and 65 m/s , respectively. The performance curves are demonstrated in terms of average bit error rate (BER) versus average signal energy per bit (E_b/N_o) in dB. We compare the performance of our proposed differential scheme (showed in solid lines) to that of an existing DSTF scheme in [39] (showed in dashed lines) with the same rate R . The random permutation strategy, in which the n^{th} subcarrier is moved to the \tilde{n}^{th} subcarrier, follows the Takeshita-Constello method as [78]:

$$\tilde{n} = \text{mod} \left(\frac{n(n+1)}{2}, N \right) + 1, \quad n = 1, 2, \dots, N. \quad (3.71)$$

Simulation Results

In Figure 3.9, we first investigate the effect of varying Γ to the diversity order by simulating the proposed scheme employing $M_t = 2$ and $M_r = 1$ under the TU six-ray power delay profile. For $R = 1$ b/s/Hz (omitting cyclic-prefix and guard interval), we chose $\Gamma = 1, 2, \text{ and } 3$. Their corresponding signal constellations are $G_{2,4} =$

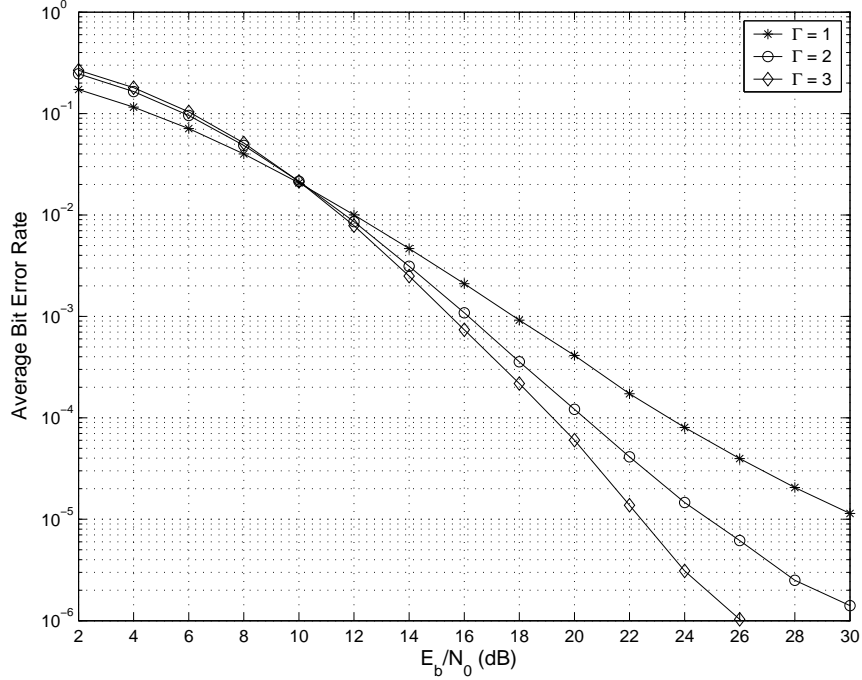


Figure 3.9: Performance for $M_t = 2$, $M_r = 1$, $R = 1$ b/s/Hz, and $\Gamma = 1, 2$, and 3 under the TU power delay profile.

$(2, 4, [1, 1])$, $G_{4,16} = (4, 16, [1, 3, 5, 7])$, and $G_{6,64} = (6, 64, [1, 9, 15, 17, 23, 25])$, respectively. In this case, the transmit matrix (3.35) is given by

$$\mathbf{X}_p^k = \begin{bmatrix} s_{p,1}^k & \dots & s_{p,\Gamma}^k & 0 & \dots & 0 \\ 0 & \dots & 0 & s_{p,\Gamma+1}^k & \dots & s_{p,\Gamma M_t}^k \end{bmatrix}^T. \quad (3.72)$$

As clearly see from the Figure, the diversity order of the proposed scheme increases with the number of jointly encoded subcarriers Γ . This observation supports our analytical analysis in (3.65) that the diversity order is proportional to the value of Γ . Hence, increasing Γ results in significant performance improvement especially in the high SNR regime.

Figures 3.10 depicts the simulation results for a system with $M_t = 2$, $M_r = 1$, and $\Gamma = 2$ in two-ray power delay profile. We chose $R = 1.5$ b/s/Hz and generated signal constellation by $G_{4,64} = (4, 64, [1, 17, 45, 53])$. It is apparent that

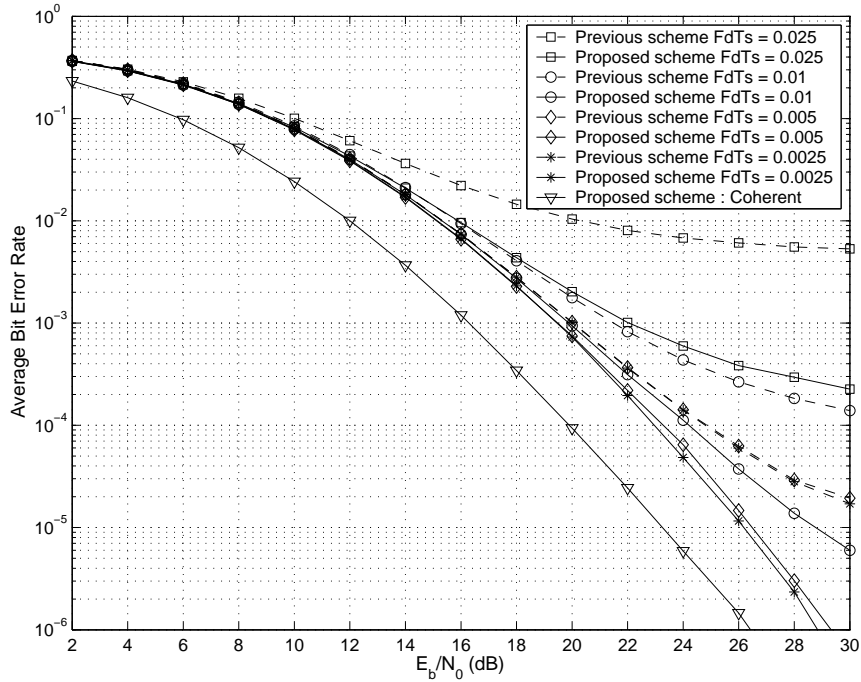


Figure 3.10: Performance for $M_t = 2$, $M_r = 1$, $\Gamma = 2$, and $R = 1.5$ b/s/Hz under the two-ray power delay profile.

the performances of our proposed scheme are superior to that of the previously proposed scheme [39] in every normalized Doppler frequency. For instance, in case of fading channels with $f_D T_s = 0.0025$ and 0.005 , our proposed scheme yields almost the same performance of $BER \approx 5 \times 10^{-5}$ at E_b/N_0 of 24 dB, which outperform those of previous scheme that achieved $BER = 1.5 \times 10^{-4}$. When fading rate increases from 0.005 to 0.01 , the performances of our proposed scheme and the previous scheme degrade to $BER = 1.22 \times 10^{-4}$ and 4.5×10^{-4} , respectively, at $E_b/N_0 = 24$ dB. Observe that the performance of the previous scheme degrades faster than that of our proposed scheme. In other words, in case of $f_D T_s = 0.0025$ and 0.005 , the proposed scheme outperforms the previous scheme about 2 dB at a BER of 10^{-4} . When the fading rate is 0.01 , our proposed scheme achieves more than 6 dB performance improvement at a BER of 10^{-4} compared to that of previous

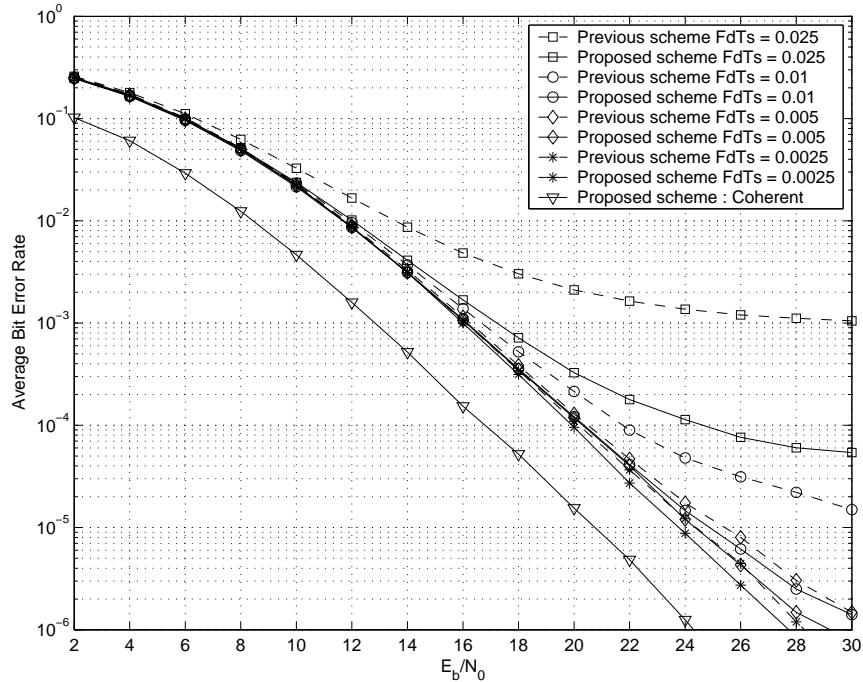


Figure 3.11: Performance for $M_t = 2$, $M_r = 1$, $\Gamma = 2$, and $R = 1$ b/s/Hz under the TU power delay profile.

scheme. For a more rapid fading at $f_D T_s = 0.025$, the previous scheme degrades even faster from $BER = 1.5 \times 10^{-4}$ to 6.81×10^{-3} and nearly reach error floor, while the performance of our propose scheme degrades from $BER \approx 5 \times 10^{-5}$ to 5.2×10^{-4} . This confirms our expectation that by coding within only one OFDM block, our propose scheme is robust to the effect of rapid channel variation. In contrast, the DSTF scheme relies on constant channel over several OFDM blocks, thereby more susceptible to rapid fading condition. Note that in all figures, we provide simulation results for coherent detections of our scheme for $f_D T_s = 0.0025$. The 3 dB performance loss due to differential detection can be observed.

The performance under the TU power delay profile is shown in Figure 3.11 for $M_t = 2$, $M_r = 1$, $\Gamma = 2$, and $R = 1$ b/s/Hz in which $G_{4,16}$ is used. Observe that under slow fade rates, i.e., $f_D T_s = 0.0025$ and 0.005 , our scheme yields slightly

better performances than those in previous scheme at E_b/N_0 of 22 dB. Significant performance difference can be observed when $f_D T_s = 0.01$. In this case, our proposed scheme achieves an average BER of 4.13×10^{-5} at $E_b/N_0 = 22$ dB, whereas the previous scheme has a BER of 9.0×10^{-5} . The performance of the proposed scheme is better than that of previous scheme about 2 dB at a BER of 10^{-4} . When $f_D T_s$ increases from 0.01 to 0.025, the BER of the previous scheme severely degrades to 1.75×10^{-3} at E_b/N_0 of 22 dB, while the BER of our proposed scheme slightly degrades to 1.92×10^{-4} .

The superior performance of our proposed scheme over the previous scheme can be obviously seen in case of $M_t = 3$ and $M_r = 1$. For $\Gamma = 2$ and $R \approx 1$ b/s/Hz (due to zero padding insertion), we generated the signal constellation by $G_{6,64}$ in which the differential encoded signal matrix has the following structure:

$$\mathbf{X}_p^k = \begin{pmatrix} s_{p,1}^k & s_{p,2}^k & 0 & 0 & 0 & 0 \\ 0 & 0 & s_{p,3}^k & s_{p,4}^k & 0 & 0 \\ 0 & 0 & 0 & 0 & s_{p,5}^k & s_{p,6}^k \end{pmatrix}^T.$$

Figures 3.12 and 3.13 show performances under the two-ray and the TU power delay profiles, respectively. Similar to the case of two transmit antennas, our scheme yields better performance and more robust to channel fading conditions than the previous scheme. In case of fast fading, e.g. $f_D T_s = 0.025$, the performance degradation is significant and high error floor can be observed in the previous scheme. In contrast, the performance of our proposed scheme slightly degrades with an acceptable error floor.

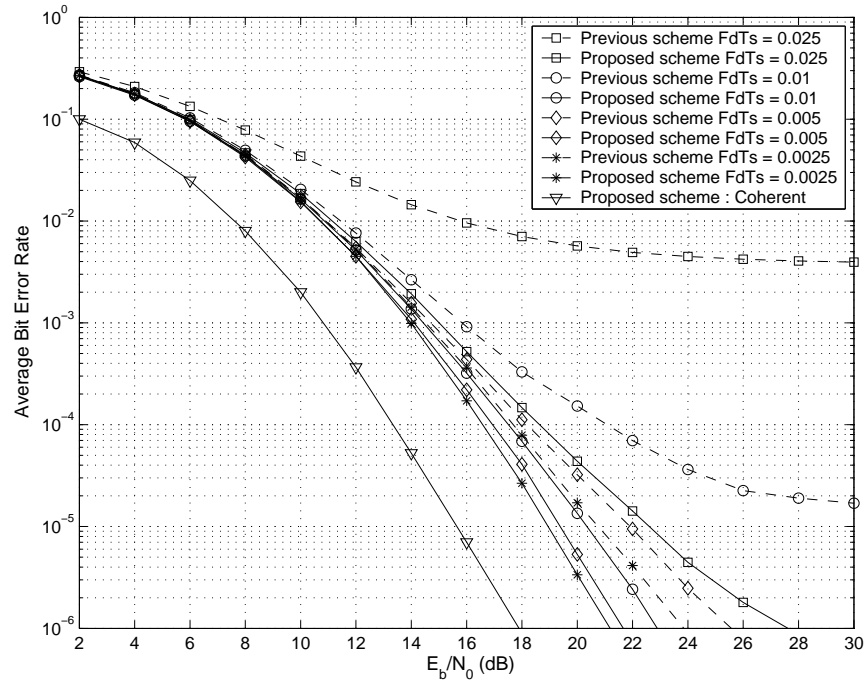


Figure 3.12: Performance for $M_t = 3$, $M_r = 1$, $\Gamma = 2$, and $R \approx 1$ b/s/Hz under the two-ray power delay profile.

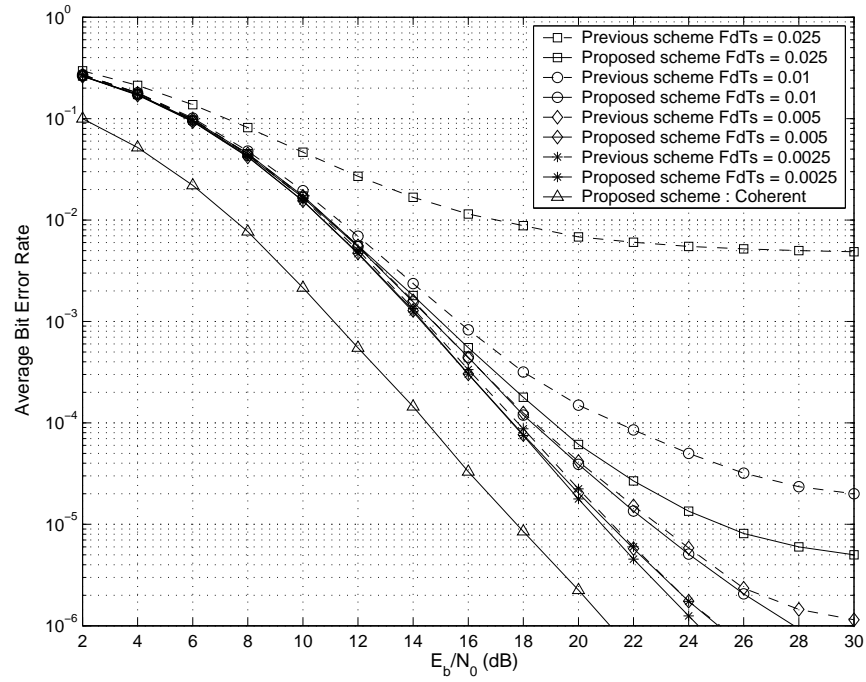


Figure 3.13: Performance for $M_t = 3$, $M_r = 1$, $\Gamma = 2$, and $R \approx 1$ b/s/Hz under the TU power delay profile.

3.3 Chapter Summary

We proposed, in this Chapter, differential modulation schemes for MIMO systems.

In the first part of the Chapter, we improved the MRB signal design for the DUST modulation system by using the design criterion of minimizing union bound on block error probability. Furthermore, we relaxed the parameter search from integers to non-integers to get better codes. By taking advantage of symmetric property of the full rotation matrix, we remarkably reduced search space for the best signal constellation. The approximated union bound was applied to further reduce computation time. Simulation results showed the performance improvement of the obtained signals, for example, about 0.75 dB for constellation size $L = 4$ and about 1 dB for $L = 64$ which support our numerical calculations.

In the second part of the Chapter, we proposed a differential scheme for MIMO-OFDM systems that can differentially encode signal within one OFDM block. The scheme allows us to relax the channel assumption to keep constant during each OFDM block and slowly change from a duration of one OFDM block to another, rather than multiple OFDM blocks as assumed in the previously existing works. We formulated the pairwise error probability and design criteria, and showed that our scheme achieves maximum diversity order by utilizing an existing diagonal cyclic codes. Comparing to the previous scheme, the proposed scheme is not only robust to the effect of rapid channel variation, but also reduces encoding and decoding delay. Simulation results showed that our proposed scheme yields better performance than those previously proposed in all of the fading conditions and different power delay profiles. In particular, for a MIMO-OFDM system with two transmit and one receive antennas under the two-ray power delay profile, the

proposed scheme outperforms the previous scheme about 2 dB in case of $f_D T_s = 0.0025$ and 0.005 at a BER of 10^{-4} . The performance improvement of more than 6 dB is observed when the fading rate is 0.01. Moreover, in case of the TU power delay profile with $f_D T_s = 0.01$, our proposed scheme achieves 2 dB performance improvement at a BER of 10^{-4} compared to the previous scheme.

Chapter 4

Differential Modulation for UWB Communication Systems

In this Chapter, we propose a differential encoding and decoding scheme for UWB systems employing MIMO multiband OFDM. In the proposed scheme, the information is jointly encoded across spatial, temporal, and frequency domains. By differentially en/decoding in the frequency domain, the proposed scheme does not rely on the assumption that the fading channel stays constant within several OFDM symbol durations. In this way, we are able to explore the available space and frequency diversities, richly inherent in UWB channels. More importantly, it allows us to incorporate the differential transmission with hopping multiband OFDM modulation so as to gain the additional diversity from time-domain spreading. In order to capture the unique multipath-rich and random-clustering properties of UWB channels, we characterize the pairwise error probability performance of the proposed scheme based on the Saleh-Valenzuela (S-V) fading model. Finally, the merit of our proposed scheme is shown through computer simulations.

The rest of the Chapter is organized as follows. Section 4.1 outlines the system description. In Section 4.2, we derive the differential encoding and decoding scheme for multiband UWB systems. The pairwise error probability is based on the S-V

fading model in Section 4.3. We show some simulation results and discussions in Section 4.4. Finally, Section 4.5 summarize the proposed scheme.

4.1 System Model

We consider a peer-to-peer multiband UWB system equipped with M_t transmit and M_r receive antennas. Within each subband, OFDM modulation with N subcarriers is used at each transmit antenna. The modulated OFDM symbols can be time-interleaved across several subbands as specified in [48].

According to the IEEE 802.15.3a standard [82], the fading channels for UWB systems are based on the S-V model for indoor channels [83]. The mathematical model of the channel impulse response from the i^{th} transmit antenna to the j^{th} receive antenna during the k^{th} OFDM block is given by [82]

$$h_{ij}^k(t) = \sum_{c=0}^C \sum_{l=0}^L \alpha_{ij}^k(c, l) \delta(t - T_c - \tau_{c,l}), \quad (4.1)$$

where $i = 1, \dots, M_t$ and $j = 1, \dots, M_r$. In each $i - j$ transmission link, $\alpha_{ij}^k(c, l)$ denotes the multipath gain coefficient of the l^{th} arrival in the c^{th} cluster at time k . The time duration T_c represents the arrival time of the c^{th} cluster, and $\tau_{c,l}$ is the delay of the l^{th} path in the c^{th} cluster relative to the cluster arrival time T_c . The cluster arrivals and the path arrivals within each cluster are modelled by Poisson process with rate Λ and λ ($\lambda > \Lambda$), respectively. The path amplitude $|\alpha_{ij}^k(c, l)|$ may follow the log-normal, Nakagami or Rayleigh distributions [82], whereas the phase $\angle \alpha_{ij}^k(c, l)$ is uniform random variable over $[0, 2\pi)$. In this paper, $|\alpha_{ij}^k(c, l)|$ is modeled as Rayleigh distribution, i.e., $\alpha_{ij}^k(c, l)$ are zero-mean complex Gaussian random variables with variances [82]

$$\Omega_{c,l} = \text{E} [|\alpha(c, l)|^2] = \Omega_{0,0} \exp \left(-\frac{T_c}{\Gamma} - \frac{\tau_{c,l}}{\gamma} \right), \quad (4.2)$$

where $\Omega_{0,0}$ is the mean energy of the first path of the first cluster, Γ is the cluster decay factor, and γ is the ray decay factor. The channel coefficients are assumed to be spatially uncorrelated and the powers of all independent delay paths are normalized such that $\sum_{c=0}^C \sum_{l=0}^L \Omega_{c,l} = 1$. The channel model parameters corresponding to different scenarios are provided in [48].

We denote $x_i^k(n)$ as a differentially encoded data symbol to be transmitted on the n^{th} subcarrier at the i^{th} transmit antenna during the k^{th} OFDM symbol period. At the receiver, after cyclic prefix removing and OFDM demodulating, the received signal at the n^{th} subcarrier at the j^{th} receive antenna during the k^{th} OFDM block is given by

$$y_j^k(n) = \sqrt{\rho} \sum_{i=1}^{M_t} x_i^k(n) H_{ij}^k(n) + w_j^k(n), \quad (4.3)$$

where ρ is the average signal to noise ratio per receiver, and

$$H_{ij}^k(n) = \sum_{c=0}^C \sum_{l=0}^L \alpha_{ij}^k(c, l) \exp[-\mathbf{j}2\pi n \Delta f (T_c + \tau_{c,l})] \quad (4.4)$$

is the subchannel gain. Here, $\Delta f = 1/T_s$ is the inter-subcarrier spacing, and T_s is the OFDM symbol period. The additive noise $w_j^k(n)$ is modeled as independent complex Gaussian random variable with zero mean and unit variance.

4.2 Differential Scheme for Multiband UWB Systems

We propose in this section a frequency-domain differential scheme for multiband UWB system. In addition, we exploit the additional diversity from band hopping inherently in multiband transmission by jointly encoding across K OFDM blocks and transmitted the K OFDM symbols on different subbands. In each OFDM block, we exploit subcarrier interleaving strategy as in [15].

4.2.1 Transmit Signal and Differential Encoding Structures

We introduce a differential multiband UWB scheme based on a transmit signal structure proposed in [52]. Particularly, \mathbf{X} is a jointly design $KN \times M_t$ space-time-frequency code structure in which it consists of stacking space-frequency signal \mathbf{X}^k , each of dimension $N \times M_t$, for K OFDM symbols. To reduce complexity of the design, we divide \mathbf{X}^k into several submatrices or groups. By introducing a fixed integer G ($1 \leq G \leq N$) as a number of jointly encoded subcarriers, \mathbf{X}^k at each OFDM symbol is partitioned into $P = \lfloor N/(GM_t) \rfloor$ submatrices as follows [52]:

$$\mathbf{X}^k = [(\mathbf{X}_1^k)^T (\mathbf{X}_2^k)^T \cdots (\mathbf{X}_P^k)^T (\mathbf{0}_{N-PGM_t})^T]^T, \quad (4.5)$$

for $k = 1, 2, \dots, K$ and T denotes the matrix transposition. The $(N - PGM_t) \times M_t$ matrix $\mathbf{0}_{N-PGM_t}$ represents a zero padding matrix to be inserted if N cannot be divided by GM_t . Each of the $GM_t \times M_t$ submatrix \mathbf{X}_p^k , for $k = 1, \dots, K$, and $p = 1, 2, \dots, P$, is modeled as

$$\mathbf{X}_p^k = \text{diag}(\mathbf{x}_{p,1}^k \ \mathbf{x}_{p,2}^k \ \cdots \ \mathbf{x}_{p,M_t}^k), \quad (4.6)$$

where $\text{diag}(\cdot)$ denotes diagonal operation that places all vectors or scalar elements at the main diagonal matrix, and $\mathbf{x}_{p,i}^k$, for $i = 1, 2, \dots, M_t$, is a $G \times 1$ vector:

$$\mathbf{x}_{p,i}^k = [s_{p,(i-1)G+1}^k \ s_{p,(i-1)G+2}^k \ \cdots \ s_{p,iG}^k]^T, \quad (4.7)$$

in which all $s_{p,m}^k$, $m = 1, 2, \dots, GM_t$, are differentially encoded symbols that will be specified later. We will differentially encode across K OFDM symbols within each group, and our desired transmit signal structure for the p^{th} group after differentially encoding is $KGM_t \times M_t$ matrix:

$$\mathbf{X}_p = [(\mathbf{X}_p^1)^T (\mathbf{X}_p^2)^T \cdots (\mathbf{X}_p^K)^T]^T, \quad (4.8)$$

where $\mathbf{1}_K$ denotes a $K \times 1$ vector of all ones, \otimes denotes the Kronecker product [84], $\Phi_p = [\phi_1 \ \phi_2 \ \cdots \ \phi_{M_t}]$ is the $GM_t \times M_t$ mapping matrix in which $\phi_i = \mathbf{e}_i \otimes \mathbf{1}_G$ is a $GM_t \times 1$ vector, and \mathbf{e}_i is an $M_t \times 1$ unit vector whose i^{th} component is one and all others are zeroes. We post-multiply \mathbf{S}_p by $\hat{\Phi}_p$, resulting in the desired $KGM_t \times M_t$ matrix

$$\mathbf{X}_p = \mathbf{S}_p \hat{\Phi}_p \quad (4.13)$$

as specified in (4.8). For better understanding the concept of the proposed scheme, we show in Figure 4.1 an example of differentially encoded signals in case of $K = 2, G = 2$, and $M_t = 2$.

4.2.2 Differentially Decoding

The received signal vector corresponding to the transmitted matrix \mathbf{X}_p is given by

$$\mathbf{y}_p = \sqrt{\rho} (\mathbf{I}_{M_r} \otimes \mathcal{D}(\mathbf{X}_p)) \mathbf{h}_p + \mathbf{w}_p, \quad (4.14)$$

where $\mathcal{D}(\mathbf{X}_p)$ denotes an operation on an $KGM_t \times M_t$ matrix \mathbf{X}_p that converts each column of \mathbf{X}_p into a diagonal matrix and results in an $KGM_t \times KGM_t M_t$ matrix, expressed by

$$\mathcal{D}(\mathbf{X}_p) = \mathcal{D}([\mathbf{x}_{p,1} \ \cdots \ \mathbf{x}_{p,M_t}]) = [\text{diag}(\mathbf{x}_{p,1}) \ \cdots \ \text{diag}(\mathbf{x}_{p,M_t})]. \quad (4.15)$$

The matrix $\mathbf{h}_p = [(\mathbf{h}_{p,1})^T \ (\mathbf{h}_{p,2})^T \ \cdots \ (\mathbf{h}_{p,M_r})^T]^T$ is a channel matrix constructed from $KGM_t M_t \times 1$ matrix:

$$\mathbf{h}_{p,j} = [(\mathbf{h}_{p,1j}^1)^T \ \cdots \ (\mathbf{h}_{p,1j}^K)^T \ \cdots \ (\mathbf{h}_{p,M_t j}^1)^T \ \cdots \ (\mathbf{h}_{p,M_t j}^K)^T], \quad (4.16)$$

where $\mathbf{h}_{p,ij}^k = [H_{ij}^k((p-1)GM_t) \ \cdots \ H_{ij}^k(pGM_t-1)]^T$ is a channel gain vector of size $GM_t \times 1$. The received signal matrix $\mathbf{y}_p = [(\mathbf{y}_{p,1})^T \ (\mathbf{y}_{p,2})^T \ \cdots \ (\mathbf{y}_{p,M_r})^T]^T$ is a

$KGM_t M_r \times 1$ matrix constructed from the $KGM_t \times 1$ receive signal vector $\mathbf{y}_{p,j} = [(\mathbf{y}_{p,j}^1)^T (\mathbf{y}_{p,j}^2)^T \cdots (\mathbf{y}_{p,j}^K)^T]^T$, in which $\mathbf{y}_{p,j}^k = [y_j^k((p-1)GM_t) \cdots y_j^k(pGM_t-1)]^T$ is a $GM_t \times 1$ matrix. The noise matrix \mathbf{w}_p is in the same form as \mathbf{y}_p with $\mathbf{y}_{p,j}$ and $\mathbf{y}_{p,j}^k$ replaced by $\mathbf{w}_{p,j}$ and $\mathbf{w}_{p,j}^k$, respectively.

By substituting (4.13) into (4.14), we can reformulate \mathbf{y}_p as

$$\mathbf{y}_p = \sqrt{\rho} \left(\mathbf{I}_{M_r} \otimes \mathcal{D}(\mathbf{S}_p \hat{\Phi}_p) \right) \mathbf{h}_p + \mathbf{w}_p. \quad (4.17)$$

To simplify (4.17), we first observe from (4.12) that $\hat{\Phi}_p$ can be re-expressed as $\hat{\Phi}_p = [\tilde{\phi}_1 \tilde{\phi}_2 \cdots \tilde{\phi}_{M_t}]$, where $\tilde{\phi}_i = \mathbf{1}_K \otimes \phi_i$. Therefore, $\mathcal{D}(\mathbf{S}_p \hat{\Phi}_p)$ can be given by

$$\mathcal{D}(\mathbf{S}_p \hat{\Phi}_p) = \left[\text{diag}(\mathbf{S}_p \tilde{\phi}_1) \cdots \text{diag}(\mathbf{S}_p \tilde{\phi}_{M_t}) \right]. \quad (4.18)$$

According to (4.16) and (4.18) for each j , we have $\mathcal{D}(\mathbf{S}_p \hat{\Phi}_p) \mathbf{h}_{p,j} = \sum_{i=1}^{M_t} \text{diag}(\mathbf{S}_p \tilde{\phi}_i) \mathbf{h}_{p,ij}$ which can be simplified to

$$\mathcal{D}(\mathbf{S}_p \hat{\Phi}_p) \mathbf{h}_{p,j} = \mathbf{S}_p \sum_{i=1}^{M_t} \tilde{\phi}_i \circ \mathbf{h}_{p,ij} \triangleq \mathbf{S}_p \tilde{\mathbf{h}}_{p,j}, \quad (4.19)$$

where the last term on the right hand side results from using the property of Hadamard product [84]. The $KG \times 1$ channel matrix $\tilde{\mathbf{h}}_{p,j}$ can be obtained by substituting (4.16) into (4.19) as $\tilde{\mathbf{h}}_{p,j} = [(\tilde{\mathbf{h}}_{p,1j}^1)^T \cdots (\tilde{\mathbf{h}}_{p,1j}^K)^T \cdots (\tilde{\mathbf{h}}_{p,M_t j}^1)^T \cdots (\tilde{\mathbf{h}}_{p,M_t j}^K)^T]^T$, where

$$\tilde{\mathbf{h}}_{p,ij}^k = [H_{ij}^k(n_{p,i}^0) H_{ij}^k(n_{p,i}^1) \cdots H_{ij}^k(n_{p,i}^{G-1})]^T \quad (4.20)$$

is of size $G \times 1$, and $n_{p,i}^g = (i-1)G + (p-1)GM_t + g$ for $g = 0, 1, \dots, G-1$. By denoting a $KGM_t M_r \times 1$ channel gain vector:

$$\tilde{\mathbf{h}}_p = [(\tilde{\mathbf{h}}_{p,1})^T (\tilde{\mathbf{h}}_{p,2})^T \cdots (\tilde{\mathbf{h}}_{p,M_r})^T]^T, \quad (4.21)$$

and using (4.19) for all j , we obtain an equivalent expression

$$(\mathbf{I}_{M_r} \otimes \mathcal{D}(\mathbf{X}_p)) \mathbf{h}_p = (\mathbf{I}_{M_r} \otimes \mathbf{S}_p) \tilde{\mathbf{h}}_p. \quad (4.22)$$

Finally, from (4.22) we can simplify (4.17) to

$$\mathbf{y}_p = \sqrt{\rho} (\mathbf{I}_{M_r} \otimes \mathbf{S}_p) \tilde{\mathbf{h}}_p + \mathbf{w}_p. \quad (4.23)$$

For notation convenience, let us define $\mathbf{S}_p \triangleq (\mathbf{I}_{M_r} \otimes \mathbf{S}_p)$ and $\mathbf{V}_p \triangleq (\mathbf{I}_{M_r} \otimes \mathbf{V}_p)$ such that

$$\mathbf{S}_p = (\mathbf{I}_{M_r} \otimes \mathbf{V}_p) \mathbf{S}_{p-1} = \mathbf{V}_p \mathbf{S}_{p-1}. \quad (4.24)$$

Accordingly, using (4.23)-(4.24) and after some manipulations, we can write the received signal as

$$\mathbf{y}_p = \mathbf{V}_p \mathbf{y}_{p-1} + \sqrt{2} \tilde{\mathbf{w}}_p, \quad (4.25)$$

where $\tilde{\mathbf{w}}_p = \frac{1}{\sqrt{2}} \mathbf{w}_p - \mathbf{V}_p \mathbf{w}_{p-1}$ is a noise vector whose each element is independent complex Gaussian random variable with zero mean and unit variance. Without acquiring channel state information, the detector follows the maximum likelihood (ML) decision rule [26]

$$\hat{\mathbf{V}}_p = \arg \min_{\mathbf{V}_p \in \mathbb{V}_p} \|\mathbf{y}_p - \mathbf{V}_p \mathbf{y}_{p-1}\|_F^2, \quad (4.26)$$

where $\|\cdot\|_F^2$ denotes the Frobinius norm [84]. Even though the decoding complexity increases exponentially with $RKGM_t$ where R is the transmission rate, the decoding complexity can be reduced to polynomial in KGM_t by lattice reduction algorithm [85].

4.3 Pairwise Error Probability

In this Section, we provide an approximate PEP formulation based on the results in [86] [87]. We first note that the channel matrix in (4.21) can be reexpressed as $\tilde{\mathbf{h}}_p = \tilde{\mathbf{h}}_{p-1} + \Delta \tilde{\mathbf{h}}_p$, where $\Delta \tilde{\mathbf{h}}_p$ represents the channel mismatch between $\tilde{\mathbf{h}}_p$ and $\tilde{\mathbf{h}}_{p-1}$. For analytical tractability, this section confines the analysis to the case

when $\Delta\tilde{\mathbf{h}}_p$ is negligible, i.e., $\tilde{\mathbf{h}}_{p-1} \approx \tilde{\mathbf{h}}_p$. Such performance formulation provides us a benchmark for subsequent performance comparisons. Later in Section 4.4, we will show from the numerical results how the channel mismatch affects the system performance.

For specific values of T_c and $\tau_{c,l}$ the PEP upper bound is given in ([86], proposition 7). The average PEP can be obtained by averaging over Poisson distributions, however, it is difficult if not possible to obtain the average PEP. In what follows, we use the approximation approach as in [87]. Suppose that \mathbf{v}_p and $\hat{\mathbf{v}}_p$ are two different information matrices, the asymptotic PEP can be approximated as

$$P_a(\mathbf{v}_p \rightarrow \hat{\mathbf{v}}_p) \approx \binom{2\nu - 1}{\nu} \left(\prod_{m=1}^{\nu} \beta_{p,m} \right)^{-1} \left(\frac{\rho}{2} \right)^{-\nu}, \quad (4.27)$$

where ρ is an average signal-to-noise ratio per symbol, ν is the rank and $\beta_{p,m}$'s are the non-zero eigenvalues of the matrix

$$\mathbf{\Psi}_p \triangleq \mathbf{S}_{p-1} \mathbf{\Sigma}_{\tilde{\mathbf{h}}_p} \mathbf{S}_{p-1}^H (\mathbf{v}_p - \hat{\mathbf{v}}_p)^H (\mathbf{v}_p - \hat{\mathbf{v}}_p), \quad (4.28)$$

in which $\mathbf{\Sigma}_{\tilde{\mathbf{h}}_p} = E[\tilde{\mathbf{h}}_p \tilde{\mathbf{h}}_p^H]$ denotes the correlation matrix of channel vector $\tilde{\mathbf{h}}_p$.

To simplify the expression for matrix $\mathbf{\Psi}_p$ in (4.28), we evaluate the channel correlation matrix $\mathbf{\Sigma}_{\tilde{\mathbf{h}}_p}$ as follows. Due to the band hopping, the K OFDM symbols in each signal matrix are sent over different subbands. With an ideal band hopping, we assume that the signal transmitted over K different frequency-bands undergo independent fading. Assuming also that the MIMO channel is spatially uncorrelated, we can find that $\mathbf{\Sigma}_{\tilde{\mathbf{h}}_p} = \mathbf{I}_{KM_r} \otimes E[\tilde{\mathbf{h}}_{p,j}^k (\tilde{\mathbf{h}}_{p,j}^k)^H]$, and it can be simplified to

$$\mathbf{\Sigma}_{\tilde{\mathbf{h}}_p} = \mathbf{I}_{KM_r} \otimes \text{diag}(\mathbf{R}_{p,1}, \dots, \mathbf{R}_{p,M_t}), \quad (4.29)$$

where $\mathbf{R}_{p,i} \triangleq E[\tilde{\mathbf{h}}_{p,ij}^k (\tilde{\mathbf{h}}_{p,ij}^k)^H]$ denotes the correlation matrix and it is the same for all j 's. From (4.20), we can see that the diagonal elements, i. e., the $(u, u)^{th}$

elements, of $\mathbf{R}_{p,i}$ are

$$R_{p,i}^{u,u} = E [|H_{ij}^k(n_{p,i}^u)|^2] = E \left[\sum_{c=0}^C \sum_{l=0}^L \Omega_{c,l} \right] = 1. \quad (4.30)$$

The off-diagonal components, i.e., the $(u, v)^{th}$ for $u \neq v$ components, of $\mathbf{R}_{p,i}$ can be expressed as

$$\begin{aligned} R_{p,i}^{u,v} &= E \left[H_{ij}^k(n_{p,i}^u) (H_{ij}^k(n_{p,i}^v))^H \right] \\ &= \sum_{c=0}^C \sum_{l=0}^L E \left[\Omega_{c,l} e^{-\mathbf{j}2\pi\Delta f(n_{p,i}^u - n_{p,i}^v)(T_c + \tau_{c,l})} \right]. \end{aligned} \quad (4.31)$$

Observing that $n_{p,i}^u - n_{p,i}^v = u - v$ and using (4.2), we can re-express (4.31) as

$$R_{p,i}^{u,v} = \Omega_{0,0} \sum_{c=0}^C \sum_{l=0}^L E \left[e^{-g(\frac{1}{\Gamma}, u, v)T_c - g(\frac{1}{\gamma}, u, v)\tau_{c,l}} \right]. \quad (4.32)$$

where $g(a, u, v) = a + \mathbf{j}2\pi(u - v)\Delta f$. According to the Poisson distribution of the multipath delays, T_c and $\tau_{c,l}$ can be modeled as summations of identically independent distributed (iid) exponential random variables with parameter Λ and λ , respectively. Therefore, averaging (4.32) over the distribution of T_c and $\tau_{c,l}$, we arrive at

$$R_{p,i}^{u,v} = \Omega_{0,0} \sum_{c=0}^C \sum_{l=0}^L \frac{\Lambda + g(\frac{1}{\Gamma}, u, v)}{g(\frac{1}{\Gamma}, u, v)} \frac{\lambda + g(\frac{1}{\gamma}, u, v)}{g(\frac{1}{\gamma}, u, v)}. \quad (4.33)$$

Since $R_{p,i}^{u,v}$ is the same for all i 's and p 's, we denote $\mathbf{R} \triangleq \mathbf{R}_{p,i}$, which allow us to further simplify (4.29) to

$$\mathbf{\Sigma}_{\tilde{\mathbf{h}}_p} = \mathbf{I}_{KM_t M_r} \otimes \mathbf{R}. \quad (4.34)$$

Substituting (4.34) into (4.28) and applying the property of tensor product $(\mathbf{A}_1 \otimes \mathbf{B}_1)(\mathbf{A}_2 \otimes \mathbf{B}_2)(\mathbf{A}_3 \otimes \mathbf{B}_3) = (\mathbf{A}_1 \mathbf{A}_2 \mathbf{A}_3 \otimes \mathbf{B}_1 \mathbf{B}_2 \mathbf{B}_3)$, we obtain

$$\mathbf{\Psi}_p = \mathbf{I}_{M_r} \otimes \mathbf{\Theta}_p, \quad (4.35)$$

in which

$$\mathbf{\Theta}_p = \mathbf{S}_{p-1}(\mathbf{I}_{KM_t} \otimes \mathbf{R})\mathbf{S}_{p-1}^H \mathbf{\Delta}, \quad (4.36)$$

and $\mathbf{\Delta} = (\mathbf{V}_p - \hat{\mathbf{V}}_p)^H (\mathbf{V}_p - \hat{\mathbf{V}}_p)$. Hence, by (4.35), the PEP in (4.27) can be expressed as

$$P_a(\mathbf{V}_p \rightarrow \hat{\mathbf{V}}_p) \approx \binom{2rM_r - 1}{rM_r} \left(\prod_{m=1}^r \lambda_{p,m} \right)^{-M_r} \left(\frac{\rho}{2} \right)^{-rM_r}. \quad (4.37)$$

where r is the rank of $\mathbf{\Theta}_p$ and $\lambda_{p,m}$'s are the non-zero eigenvalues of $\mathbf{\Theta}_p$.

To quantify the maximum diversity order which is the exponent of $\rho/2$ in (4.37), we observe from (4.36) that \mathbf{S}_{p-1} and \mathbf{V}_p are of size $GKM_t \times GKM_t$, and the correlation matrix \mathbf{R} is of size $G \times G$. Therefore, the maximum diversity gain is

$$G_d^{max} = M_r \max \left(\min_{\forall \mathbf{V}_p^k \neq \hat{\mathbf{V}}_p^k} \text{rank}(\mathbf{\Theta}_p) \right) = GKM_t M_r. \quad (4.38)$$

Note that \mathbf{R} is of full rank if G is less than the total number of multipath components $(C+1)(L+1)$. Due to the large bandwidth of UWB waveform, the received signal typically contains a significant number of resolvable multipath components. Consequently, the correlation matrix \mathbf{R} is generally of full rank. Therefore, the maximum diversity order of $GKM_t M_r$ can be achieved by using a set of proper designed codeword matrices \mathbf{V}_p .

The result in (4.38) leads to some interesting observations as follows. First, the differential multiband UWB system achieves the same diversity gain under different channel environment. This implies that the clustering property of UWB channel does not strongly affect the diversity gain of differential multiband system. On the other hand, the coding gain which is a function of $\prod_{m=1}^r \lambda_{p,m}$ is severely affected by the multipath arrival rates and decay factors through the correlation matrix \mathbf{R} . Second, by incorporating the frequency-domain differential scheme with the multiband transmission, we are able to achieve the diversity gain of $GKM_t M_r$,

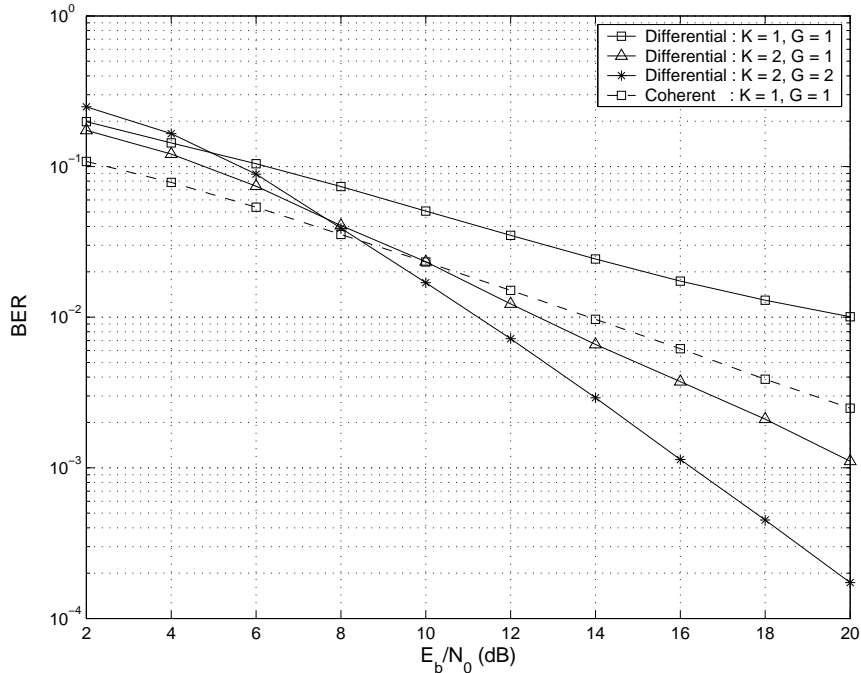


Figure 4.2: Performance under CM1, $M_t = 1$, $M_r = 1$, $R = 1$ b/s/Hz.

regardless of the channel time-correlation property. This is different from the use of differential STF coding in the conventional MIMO-OFDM systems, e.g. in [79], where the maximum achievable diversity gain is only GM_tM_r due to the requirement of almost constant channels over several OFDM blocks.

4.4 Simulation Results

We performed simulations for a multiband UWB system with $N = 128$ sub-carriers and each subband occupies bandwidth of 528 MHz. The channel model parameters followed those for CM 1 and CM 2 [82]. The data matrix \mathbf{V}_p in (4.9) were constructed by jointly coding across G , K , and M_t using existing cyclic group codes [26]. In case of repetition based coding, the codeword is given by $\mathbf{V}_p = \mathbf{I}_K \otimes \mathbf{v}_p$, where \mathbf{v}_p is a $GM_t \times GM_t$ jointly encoded diagonal matrix.

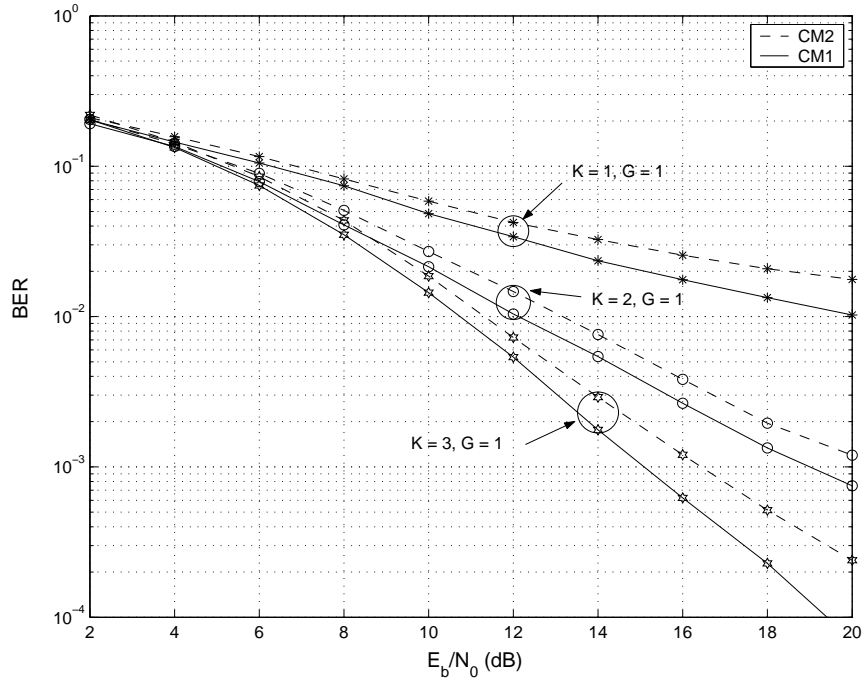


Figure 4.3: Performance under CM1 and CM2, $M_t = 1$, $M_r = 1$, $R = 1/K$ b/s/Hz.

Figure 4.2 depicts the performances of single-antenna multiband UWB system with different number of G and K . For fair comparison, the spectral efficiency is fixed at $R = 1$ b/s/Hz for all cases. The performances are simulated under CM 1. For uncoded differential system ($G = 1$ and $K = 1$), we can see that the performance loss is more than 3 dB compared to the coherent detection, and an error floor can be observed. This is due to the effect of the channel mismatch between adjacent subcarriers. By jointly encoding across two OFDM symbols ($G = 1$ and $K = 2$), the diversity gain is increased, hence resulting in significant performance improvement. As shown in Figure 4.2, the performance gain is more than 7 dB at the BER of 10^{-2} . By further jointly encoding across two subcarriers ($G = 2$ and $K = 2$), the proposed scheme obtains additional 4 dB gain at a BER of 10^{-3} . This observation is in accordance with our theoretical result in (4.37) that

the performance can be improved by increasing the number of jointly encoded subcarriers or the number of jointly encoding OFDM symbols. Moreover, at high SNR, the proposed jointly encoding differential scheme outperforms the uncoded multiband UWB system with coherent detection. We observe about 1 – 2 dB gain when $G = 1$ and $K = 2$, and about 3 – 5 dB gain when $G = 2$ and $K = 2$ at BER between $10^{-2} - 10^{-3}$.

In Figure 4.3, we compare the performance of the proposed differential scheme under CM 1 and CM 2. The information is transmitted repeatedly across $K = 1, 2$, and 3 OFDM symbols, hence the transmission rate is $1/K$ b/s/Hz. We can see that the performance of the proposed scheme under CM 1 is better than that under CM 2 for all cases. This is due to the fact that the multipath components in CM 2 are more random than that in CM 1, which implies that compared with CM 1, CM 2 results in larger channel mismatch, and hence worse performance. For each channel model, the performance improves as the number of encoded OFDM symbols increases which confirms our theoretical analysis.

Figure 4.4 depicts the performances of differential UWB-MIMO systems. The number of jointly encoded OFDM symbols is fixed at $K = 1$, and the spectral efficiency is $R = 1$ b/s/Hz for all cases. From Figure 4.4, we can observe the performance improvement as the number of antennas increases. When using two transmit and one receive antennas and encoding across one subcarrier and one OFDM symbol, the proposed scheme yields 7 dB improvement over the single antenna system. When we further jointly encode across two subcarriers, additional performance gain of about 4 dB can be observed at a BER of 10^{-3} . However, slightly error floors can still be observed when the data is encoded across multiple transmit antennas since the chance of channel mismatch is higher in this case. On

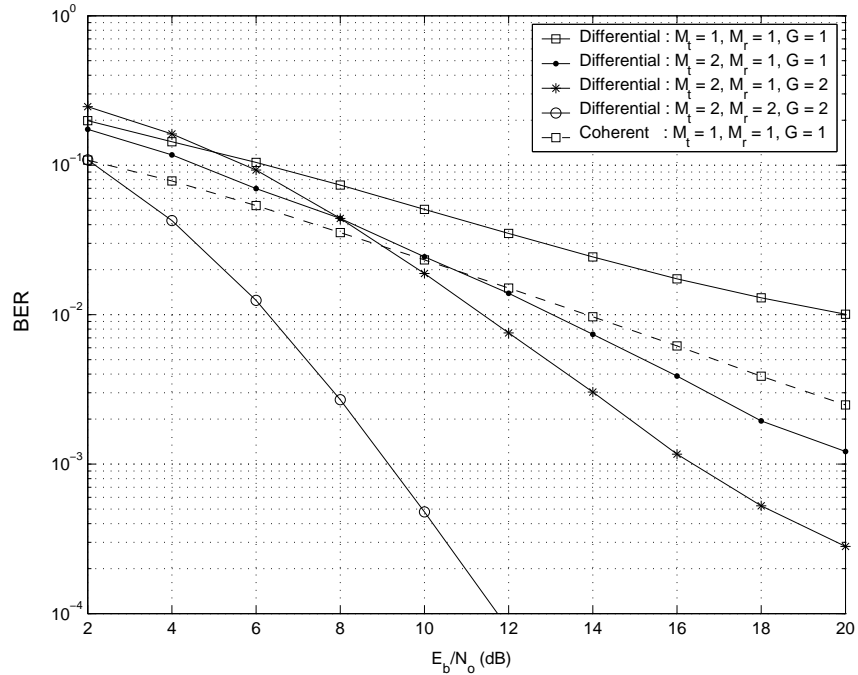


Figure 4.4: Performance comparison of the proposed differential scheme under CM1 employing SISO and MIMO processing, $K = 1$ and $R = 1$ b/s/Hz.

the other hand, increasing the number of receive antennas improves the diversity gain without the tradeoff in the channel mismatch. In particular, an additional performance gain of 6 dB is observed when two receive antennas are employed.

4.5 Chapter Summary

We propose in this Chapter a frequency-domain differential modulation scheme for multiband UWB systems. By a technique of band hopping in combination with jointly coding across spatial, temporal and frequency domains, The proposed scheme is able to explore the available spatial and multipath diversities, richly inherent in UWB environments. The analysis reveals that the proposed differential scheme achieves the same diversity advantage under different channel environ-

ments. However, the clustering behavior of UWB channels affects the performance through the coding gain. For single antenna multiband UWB system, simulation results show that the proposed differential multiband scheme yields superior performance to the conventional differential encoding scheme, particularly under very short-range line-of-sight scenario, e.g. in CM 1. We obtain about 7 dB gain at a BER of 10^{-2} when jointly encoding across one subcarrier and two OFDM symbols. Moreover, at high SNR range, the proposed jointly encoded differential scheme outperforms the uncoded coherent detection scheme of about 3 – 5 dB at BER between $10^{-2} - 10^{-3}$. In case of multiband UWB system with multiple transmit antennas, while slightly error floor occurs due to the effect of channel mismatch, additional diversity can be observed when number of transmit antennas is increased. However, increasing the number of receive antennas improves the diversity gain without tradeoff in performance due to the effect of channel mismatch.

Chapter 5

Differential Modulations for Cooperative Communications

In this Chapter, we propose differential modulation schemes for two-user cooperative communication systems. In the first part of this Chapter, Section 5.1, we consider a differential modulation for a cooperation system that employs amplify-and-forward protocol. In the second part part of this Chapter, Section 5.2, we consider a differential modulation scheme for a cooperation system with decode-and-forward protocol. Finally, Section 5.3 concludes the proposed works.

5.1 Differential Modulation for Amplify-and-Forward Cooperative Communications

In this Section, we propose a differential transmission scheme for the AF protocol in a two-user cooperative communications system. The scheme efficiently combines signals from all branches, in which only long term average of the received signals is required. As a performance benchmark, we provide an exact bit error rate (BER) formulation and its simple bounds for the optimum-combining cooperation system with differential M-ary phase shift keying (DMPSK) signal.

Based on the theoretical BER benchmark, we are able to obtain the optimum power allocation, which can be used to further improve the performance of the proposed scheme. Simulation results are shown to validate our proposed schemes and support our theoretical analysis.

5.1.1 Amplify-and-Forward Differential Cooperation Scheme

We consider a two-user cooperative communications system employing AF protocol. Each user can be a source node that sends its information to the destination, or it can be a relay node that helps transmit the other user's information. Basically, signal transmission can be separated into two phases. In Phase 1, source node transmits the information to its destination. Due to the broadcasting nature of wireless networks, this information is also received by the relay node. In Phase 2, while the source node is silent, the relay node amplifies the received signal and forwards it to the destination. In both phases, the signals of all users are transmitted through orthogonal channels by using existing schemes such as TDMA, FDMA, or CDMA [19]- [22].

In differential transmission, the information is conveyed in the difference of the phases of two consecutive symbols. Specifically, information symbols to be broadcasted by the source is given by $v_m = e^{j\phi_m}$, where $\{\phi_m\}_{m=0}^{M-1}$ is a set of M information phases. In case of DMPSK, ϕ_m can be specified as $\phi_m = 2\pi m/M$ for $m = 0, 1, \dots, M - 1$. Instead of directly transmitting the information as in coherent transmission [19], the source node differentially encodes the information symbol v_m as

$$x^\tau = v_m x^{\tau-1}, \quad (5.1)$$

where τ is the time index, and x^τ is the differentially encoded symbol to be transmitted at time τ .

In Phase 1, the source sends out the symbol x^τ with transmit power P_1 . The corresponding received signals at the destination and the relay nodes can be expressed as

$$y_{s,d}^\tau = \sqrt{P_1} h_{s,d}^\tau x^\tau + w_{s,d}^\tau, \quad (5.2)$$

and

$$y_{s,r}^\tau = \sqrt{P_1} h_{s,r}^\tau x^\tau + w_{s,r}^\tau, \quad (5.3)$$

respectively. Here, $h_{s,d}^\tau$ and $h_{s,r}^\tau$ represent the channel coefficients from the source to the destination and from the source to the relay, whereas $w_{s,d}^\tau$ and $w_{s,r}^\tau$ are additive noise.

In Phase 2, the relay amplifies the received signal and forwards it to the destination with transmit power P_2 . The received signal at the destination can be modeled as

$$y_{r,d}^\tau = \sqrt{\tilde{P}_2} h_{r,d}^\tau y_{s,r}^\tau + w_{r,d}^\tau, \quad (5.4)$$

where \tilde{P}_2 represents normalized transmit power, $h_{r,d}^\tau$ is the channel coefficient from the relay to the destination, and $w_{r,d}^\tau$ is additive noise. In Rayleigh fading environment, the channel coefficients $h_{s,d}^\tau$, $h_{s,r}^\tau$, and $h_{r,d}^\tau$ can be modeled as independent zero-mean complex Gaussian random variables with variances $\sigma_{s,d}^2$, $\sigma_{s,r}^2$, and $\sigma_{r,d}^2$, respectively. All of the fading coefficients are unknown to either the transmitter or the receiver, and they are assumed to be constant over two symbol periods. The noise $w_{s,d}^\tau$, $w_{s,r}^\tau$, and $w_{r,d}^\tau$ are modeled as independent complex Gaussian random variables with zero means and variances \mathcal{N}_0 . To ensure that the average transmit power of the relay node is P_2 , the normalized power \tilde{P}_2 is specified as

$$\tilde{P}_2 = \frac{P_2}{P_1 \sigma_{s,r}^2 + \mathcal{N}_0}, \quad (5.5)$$

where the variance $\sigma_{s,r}^2$ can be obtained from long-term average of the received

signals. The normalized power in (5.5) differs from its coherent counterpart in that the latter uses instantaneous fading amplitude, i.e. $|h_{s,r}|^2$, instead of $\sigma_{s,r}^2$.

At the destination, the received signal from the source through direct transmission in Phase 1 ($y_{s,d}^\tau$) and that from the relay in Phase 2 ($y_{r,d}^\tau$) are combined together, and then the combined output is differentially decoded. Based on the multichannel differentially coherent detection in [3], the combined signal prior to differential decoding is

$$y = a_1 (y_{s,d}^{\tau-1})^* y_{s,d}^\tau + a_2 (y_{r,d}^{\tau-1})^* y_{r,d}^\tau, \quad (5.6)$$

where the coefficients a_1 and a_2 are given by

$$a_1 = \frac{1}{\mathcal{N}_0}, \quad a_2 = \frac{P_1 \sigma_{s,r}^2 + \mathcal{N}_0}{\mathcal{N}_0 (P_1 \sigma_{s,r}^2 + P_2 \sigma_{r,d}^2 + \mathcal{N}_0)}, \quad (5.7)$$

respectively. Without acquiring CSI, the decoder use the sufficient statistics given in (5.6), and its decision rule for decoding information symbol follows

$$\hat{m} = \arg \max_{m=0,1,\dots,M-1} \text{Re} \{v_m^* y\}. \quad (5.8)$$

5.1.2 Analysis and Discussions

As shown in [89] that an ideal maximum ratio combining is obtained by using the optimum weights which are given by

$$\hat{a}_1 = \frac{1}{\mathcal{N}_0}, \quad \hat{a}_2 = \frac{P_1 \sigma_{s,r}^2 + \mathcal{N}_0}{\mathcal{N}_0 (P_1 \sigma_{s,r}^2 + P_2 |h_{r,d}|^2 + \mathcal{N}_0)}. \quad (5.9)$$

While, the exact BER formulation that is applicable for multi-channel differential scheme with arbitrary-weight combining as in (5.7) is currently not available, we provide, in this section, a BER formulation for the case of optimum combining weights as specified in (5.9). Even though, these optimum weights are not practical

for our proposed differential scheme because the instantaneous channel amplitude at the relay-destination link, i.e. $|h_{rd}|^2$, is assumed unknown to the receiver, the performance evaluation based on optimum weights (5.9) can be used as a performance benchmark for our proposed differential scheme. We will show in the next section that the performance of our proposed scheme is close to the provided BER formulation based on optimum weights in some cases which depend on channel qualities and power allocation schemes.

With the optimum weight \hat{a}_1 and \hat{a}_2 , the instantaneous SNR per bit of the optimum combiner output is [89]

$$\gamma = \gamma_1 + \gamma_2, \quad (5.10)$$

where

$$\gamma_1 = \frac{P_1 |h_{s,d}|^2}{\mathcal{N}_0}, \quad (5.11)$$

and

$$\gamma_2 = \frac{P_1 P_2 |h_{s,r}|^2 |h_{r,d}|^2}{\mathcal{N}_0 (P_1 \sigma_{s,r}^2 + P_2 |h_{r,d}|^2 + \mathcal{N}_0)}. \quad (5.12)$$

To simplify the notation, we omit the time index τ in this section for convenience in the derivation.

By using the BER expression for two-channel DMPSK in [88], the conditional BER is given by

$$P_{b|\gamma} = \frac{1}{16\pi} \int_{-\pi}^{\pi} f(\theta) \exp[-\alpha(\theta)\gamma] d\theta, \quad (5.13)$$

where

$$f(\theta) = \frac{b^2(1 - \beta^2) [3 + \cos(2\theta) - (\beta + 1/\beta) \sin \theta]}{2\alpha(\theta)}, \quad (5.14)$$

and

$$\alpha(\theta) = \frac{b^2(1 + 2\beta \sin \theta + \beta^2)}{2}. \quad (5.15)$$

Here, $\beta = a/b$ denotes a constant parameter in which a and b depends on modulation size. Specifically, $a = 10^{-3}$ and $b = \sqrt{2}$ for DBPSK modulation, and $a = \sqrt{2 - \sqrt{2}}$ and $b = \sqrt{2 + \sqrt{2}}$ for DQPSK modulation [88]. The values of a and b for larger modulation sizes can be obtained by using the result in [3].

Averaging the conditional BER over the Rayleigh fading channels, $h_{s,d}$, $h_{s,r}$, and $h_{r,d}$, results in the average BER

$$P_b = \frac{1}{16\pi} \int_{-\pi}^{\pi} f(\theta) \mathcal{M}_{\gamma_1}(\theta) \mathcal{M}_{\gamma_2}(\theta) d\theta, \quad (5.16)$$

where

$$\mathcal{M}_{\gamma_i}(\theta) = \int_{-\infty}^{+\infty} e^{-\alpha(\theta)\lambda} p_{\gamma_i}(\lambda) d\lambda, \quad (5.17)$$

denotes the MGF of the SNR γ_i for $i = 1, 2$, evaluating at $\alpha(\theta)$, and $f(\theta)$ and $\alpha(\theta)$ are specified in (5.14) and (6.16), respectively. The BER formulation in (5.16) can be further calculated as follows.

For Rayleigh fading channels, $|h_{s,d}|^2$, $|h_{s,r}|^2$, and $|h_{r,d}|^2$ are independent exponential random variables with parameter $1/\sigma_{s,d}^2$, $1/\sigma_{s,r}^2$, and $1/\sigma_{r,d}^2$, respectively. From (5.17), $\mathcal{M}_{\gamma_1}(\theta)$ can be expressed as

$$\mathcal{M}_{\gamma_1}(\theta) = \frac{1}{1 + k_{s,d}(\theta)}, \quad (5.18)$$

where

$$k_{s,d}(\theta) \triangleq \alpha(\theta) P_1 \sigma_{s,d}^2 / \mathcal{N}_0. \quad (5.19)$$

Observe that $\mathcal{M}_{\gamma_2}(\theta)$ depends on both $|h_{s,r}|^2$ and $|h_{r,d}|^2$. By averaging over $|h_{s,r}|^2$ and after some manipulations, we can express $\mathcal{M}_{\gamma_2}(\theta)$ as

$$\begin{aligned} \mathcal{M}_{\gamma_2}(\theta) &= \frac{1}{1 + k_{s,r}(\theta)} \left(1 + \frac{k_{s,r}(\theta)}{1 + k_{s,r}(\theta)} \frac{P_1 \sigma_{s,r}^2 + \mathcal{N}_0}{P_2} \right. \\ &\quad \left. \times \frac{1}{\sigma_{r,d}^2} \int_0^{\infty} \frac{\exp(-u/\sigma_{r,d}^2)}{u + R(\theta)} du \right), \end{aligned} \quad (5.20)$$

where

$$R(\theta) \triangleq \frac{P_1 \sigma_{s,r}^2 + \mathcal{N}_o}{P_2 (1 + k_{s,r}(\theta))}, \quad (5.21)$$

in which $k_{s,r}(\theta)$ is given by

$$k_{s,r}(\theta) \triangleq \alpha(\theta) P_1 \sigma_{s,r}^2 / \mathcal{N}_0, \quad (5.22)$$

Finally, by substituting (5.18) and (5.20) into (5.16), we obtain a BER expression that involves only double integration. In what follows, we can further obtain single-integral BER lower bound, single-integral BER upper bound, and their corresponding simple BER approximations that involve no integration.

The BER expression in (5.16) can be upper bounded by using the upper bound of $\mathcal{M}_{\gamma_2}(\theta)$ in (5.20). We will bound the integration term in (5.20) with a constant Z_{max} that is not a function of θ . The value of Z_{max} can be found by replacing $R(\theta)$ in the integrand with its minimum value. We can see from (5.22) and (5.21) that $R(\theta)$ reach its minimum value when $B(\theta)$ attains its maximum at $\theta = \frac{\pi}{2}$, i.e., $B(\theta) \leq \frac{-b^2(1+\beta)^2}{2}$. Accordingly, the minimum value of $R(\theta)$ is given by

$$R(\theta) \geq \frac{P_1 \sigma_{s,r}^2 + \mathcal{N}_o}{P_2} \left[1 - \frac{P_1 \sigma_{s,r}^2 b^2 (1 + \beta)^2}{2 \mathcal{N}_0} \right]^{-1} \triangleq R_{min}. \quad (5.23)$$

Substituting $R(\theta)$ in (5.20) with R_{min} , the BER upper bound is given by

$$P_b \leq \frac{1}{16\pi} \int_{-\pi}^{\pi} F(\theta) \frac{1}{[1 + k_{s,d}(\theta)][1 + k_{s,r}(\theta)]} \times \left(1 + \frac{P_1 \sigma_{s,r}^2 + 1}{P_2 \sigma_{r,d}^2} \frac{k_{s,r}(\theta)}{1 + k_{s,r}(\theta)} Z_{max} \right) d\theta, \quad (5.24)$$

in which,

$$Z_{max} = \int_0^{\infty} \exp(-u/\sigma_{r,d}^2) [u + R_{min}]^{-1} du \quad (5.25)$$

is a constant that can be easily obtained for any given values of $\sigma_{r,d}^2$ and R_{min} . The upper bound P_{ub} in (5.24) involves only single integration, and it is simpler than the exact BER provided in (5.16).

To get more insight understanding, we further simplify the BER upper bound in (5.24) as follows. For high enough SNR, we can ignore all 1's in the denominator of (5.24). This results in

$$\begin{aligned} P_b &\leq \left(1 + \frac{P_1\sigma_{s,r}^2 + 1}{P_2\sigma_{r,d}^2} Z_{max}\right) \frac{1}{16\pi} \int_{-\pi}^{\pi} \frac{f(\theta)}{k_{s,d}(\theta)k_{s,r}(\theta)} d\theta \\ &= \frac{(P_1\sigma_{s,r}^2 + 1) Z_{max} + P_2\sigma_{r,d}^2 \mathcal{N}_0^2 C(\beta, \theta)}{P_1^2 P_2 \sigma_{s,d}^2 \sigma_{s,r}^2 \sigma_{r,d}^2}, \end{aligned} \quad (5.26)$$

where

$$C(\beta, \theta) = \frac{1}{8\pi b^4} \int_{-\pi}^{\pi} \frac{(1 - \beta^2)[3 + \cos(2\theta) - (\beta + 1/\beta) \sin \theta]}{(1 + 2\beta \sin \theta + \beta^2)^3} d\theta \quad (5.27)$$

is a constant that depends on modulation size.

The BER lower bound can be obtained in a similar way as the case of the BER upper bound. We will briefly provide details of the derivations. In this case, $R(\theta)$ reaches its maximum value when $B(\theta)$ attains its minimum at $\theta = -\frac{\pi}{2}$, i.e., $B(\theta) \geq \frac{-b^2(1-\beta)^2}{2}$. Accordingly, the maximum value of $R(\theta)$ is given by

$$R(\theta) \leq \frac{P_1\sigma_{s,r}^2 + \mathcal{N}_o}{P_2} \left[1 + \frac{P_1\sigma_{s,r}^2 b^2 (1 - \beta)^2}{2\mathcal{N}_0}\right]^{-1} \triangleq R_{max}. \quad (5.28)$$

Therefore, the lower bound is given by

$$\begin{aligned} P_b &\geq \frac{1}{16\pi} \int_{-\pi}^{\pi} f(\theta) \frac{1}{[1 + k_{s,d}(\theta)][1 + k_{s,r}(\theta)]} \\ &\quad \times \left(1 + \frac{P_1\sigma_{s,r}^2 + 1}{P_2\sigma_{r,d}^2} \frac{k_{s,r}(\theta)}{1 + k_{s,r}(\theta)} Z_{min}\right) d\theta, \end{aligned} \quad (5.29)$$

in which, $Z_{min} = \int_0^{\infty} \exp(-u/\sigma_{r,d}^2) [u + R_{max}]^{-1} du$ is a constant that can be easily obtained for any given values of $\sigma_{r,d}^2$ and R_{max} . We will show in the simulation results that the lower bound is tight in high SNR region.

We further simplify the BER lower bound in (5.29) for enough high SNR by ignoring all 1's in the denominator of (5.29) expression. The resulting BER ap-

proximation of (5.29) can be expressed as

$$P_b \approx \frac{(P_1 \sigma_{s,r}^2 + 1) Z_{min} + P_2 \sigma_{r,d}^2}{P_1^2 P_2 \sigma_{s,d}^2 \sigma_{s,r}^2 \sigma_{r,d}^2} \mathcal{N}_0^2 C(\beta, \theta), \quad (5.30)$$

where $C(\beta, \theta)$ is specified in (5.27). The approximated BER in (5.30) is tight at high SNRs.

Based on the analysis in this sections, we will show in the next section that the BER expression, its upper bound and lower bound together with their simple BER approximations provide performance curves as performance benchmark of our proposed scheme. Moreover, the optimum power allocation based on this BER expressions can be used to further improve the performance of our propose scheme.

5.1.3 Simulation Results

We perform computer simulations for the two-user cooperation systems employing AF protocol with DQPSK signals. The channel fading coefficients are assumed to be independent between communication links, but time correlated according to the Jakes' model [66], in which the Doppler frequency is $f_D = 75 \text{ Hz}$ and normalized fading parameter is $f_D T_s = 0.0025$ where T_s is the sampling period. The noise variance is assumed to be unity ($\mathcal{N}_0 = 1$). We plot the performance curves in terms of average BER versus P/\mathcal{N}_0 , where P is the total transmit power. We assume that the power allocation at the source and relay nodes is fixed at $P_1 + P_2 = P$.

Figure 5.1 compares simulated performances of the proposed differential cooperative scheme to various transmission techniques, including differential direct transmission, and their coherent counterparts. For fair comparison, we simulate the direct transmission schemes with DBPSK signals. In the simulation, the channel variances at the relay link are chosen as $\sigma_{sd}^2 = \sigma_{s,r}^2 = \sigma_{r,d}^2 = 1$, and power ratios are given by $P_1 = 0.7P$ and $P_2 = 0.3P$. It is apparent that the proposed

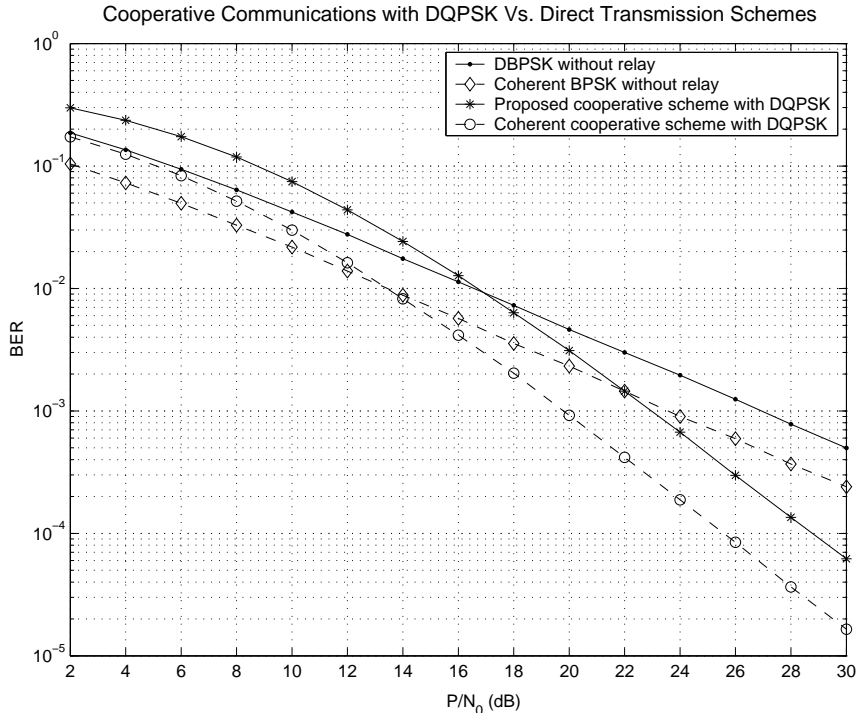


Figure 5.1: Cooperative communication system with DQPSK signals, $\sigma_{s,d}^2 = \sigma_{s,r}^2 = \sigma_{r,d}^2 = 1$, $P_1/P = 0.7$ and $P_2/P = 0.3$.

differential cooperative scheme achieves higher diversity orders than the DBPSK with direct transmission at high SNRs. We observe about 4 dB performance gain at a BER of 10^{-3} . In addition, at SNRs higher than 21 dB, the proposed differential cooperative scheme provides significant performance improvement over that of the directly transmitted BPSK with coherent detection. Therefore, the differential cooperative scheme can be a viable candidate for exploiting inherent spatial diversity over virtual antenna array in wireless networks with low complexity and simple implementation. Also in Figure 5.1, we can observe that the performance of the proposed differential cooperative scheme is 3 dB away from its coherent counterpart at high SNR region.

In Figure 5.2, we compare the performance of the proposed scheme and the optimum-combining scheme in case of equal power allocation, i.e. $P_1 = P_2 = 0.5P$.

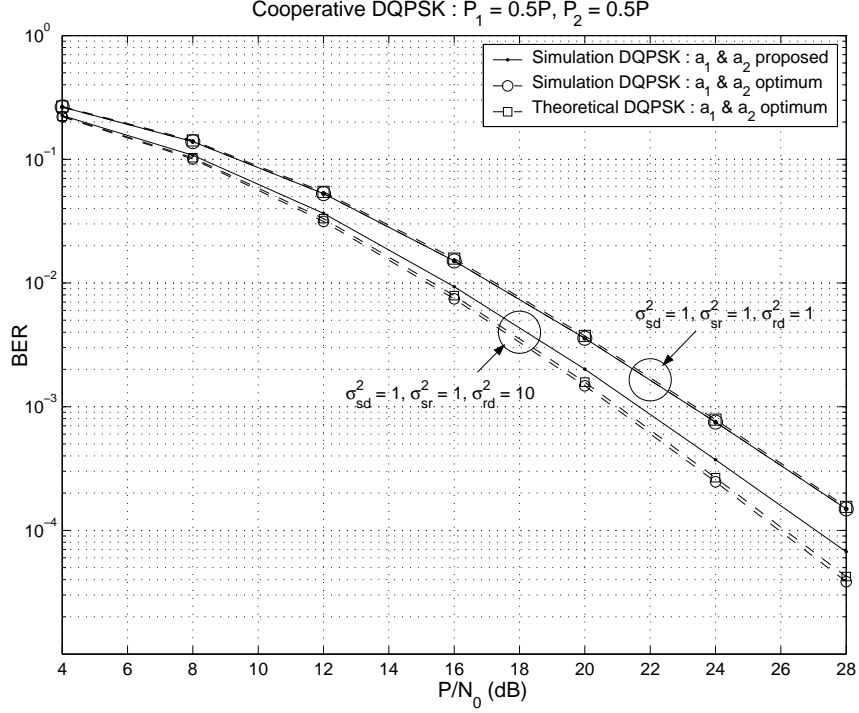


Figure 5.2: Performance comparison of the proposed scheme and that with optimum weights.

We can see that when $\sigma_{sd}^2 = \sigma_{sr}^2 = \sigma_{rd}^2 = 1$, the performance of both schemes are comparable, and both performance curves are closed to the analytical BER curve with optimum weights. When $\sigma_{sd}^2 = \sigma_{sr}^2 = 1$ and $\sigma_{rd}^2 = 10$, we observe that the performance of the proposed scheme and the optimum optimum-combining scheme are about 0.7 dB different at a BER of 10^{-3} . However, the performance curve of the optimum-combining scheme are the same as the theoretical curve with optimum weights. Hence, equal power allocation strategy does not always provide the best performance. Moreover, the results illustrate that we can use the performance curve with optimum weights as a benchmark for the performance of our proposed scheme.

We illustrate in Figure 5.3 the numerically evaluated BER with optimum weights in comparison to simulated performance of our proposed scheme. For

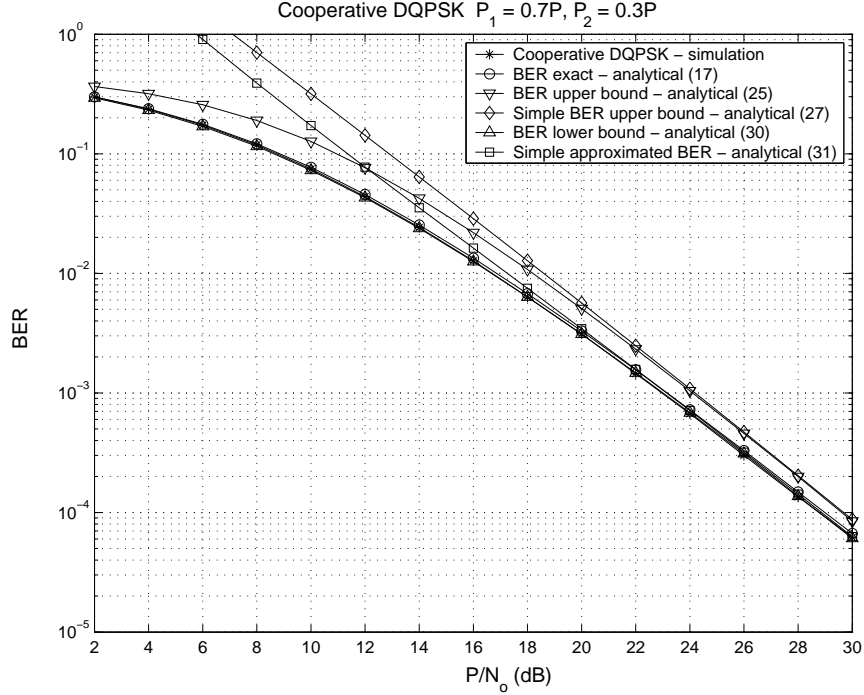


Figure 5.3: Asymptotically tight of the BER formulations with optimum weights to the simulated performance of the proposed scheme with DQPSK signals, $\sigma_{s,d}^2 = \sigma_{s,r}^2 = \sigma_{r,d}^2 = 1$.

$\sigma_{s,d}^2 = \sigma_{s,r}^2 = \sigma_{r,d}^2 = 1$, and $P_1 = 0.7P$ and $P_2 = 0.3P$, we can see that the BER expression with optimum weights in (5.16) is close to the simulated performance of the proposed scheme. The upper bound (5.24) and its simple approximation (5.26) are asymptotically parallel with the BER curve with optimum weights. The lower bound in (5.29) is asymptotically tight to the simulated performance and the BER curve using optimum weights. There is only a little bit difference at low SNRs. The simple approximated BER in (5.30) is loose at low SNRs, and it appears to be asymptotically tight at reasonable high SNR range.

We use the BER formulation with optimum weights to numerically find optimum power allocation at an SNR of 20 dB. We find that both exact BER with optimum weights and its approximated BER formulations yield the same optimum power allocation. In Figure 5.4 for a case of all channel variances are unity,

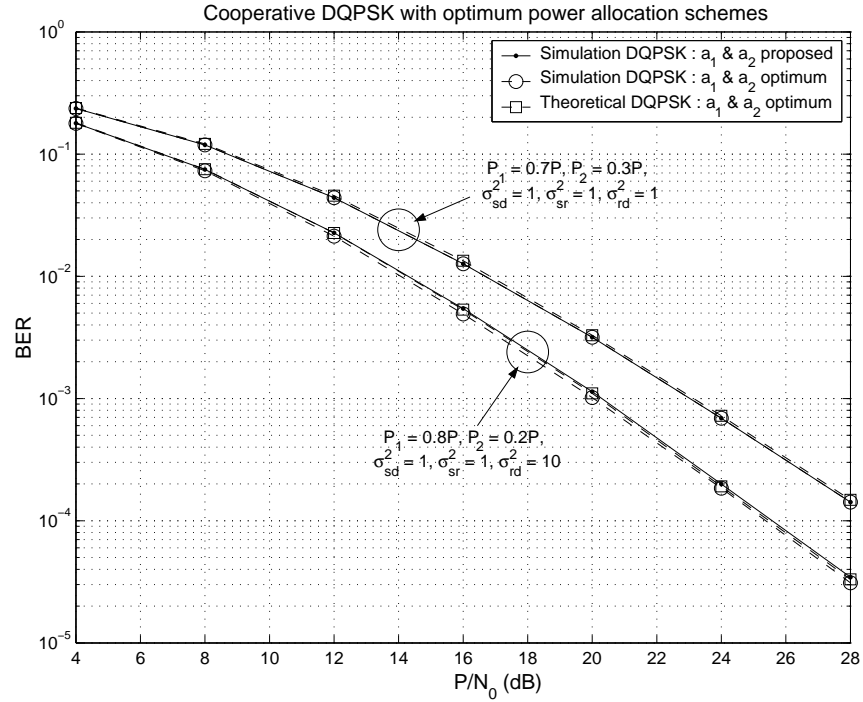


Figure 5.4: Cooperative communication system with DQPSK signals for different power allocation schemes, and different channel variances.

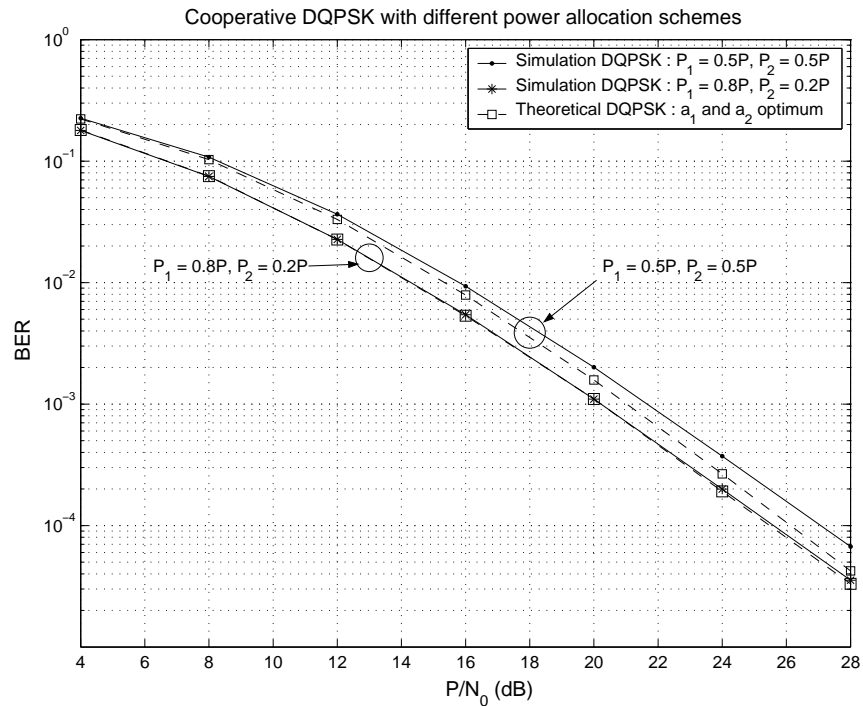


Figure 5.5: Performance comparison of optimum power allocation scheme and equal power allocation scheme, $\sigma_{s,d}^2 = \sigma_{s,r}^2 = 1$ and $\sigma_{r,d}^2 = 10$.

we show performance comparison of the simulated performance of the proposed scheme, the proposed scheme with optimum weights, and analytical BER formulation with optimum weights, there is no performance gap observed in the Figure. For a case of $\sigma_{s,d}^2 = \sigma_{s,r}^2 = 1$, and $\sigma_{r,d}^2 = 10$, the optimum powers at the source node and the relay node are $\hat{P}_1 = 0.8P$ and $\hat{P}_2 = 0.2P$, respectively. We can see in Figure 5.4 that the obtained optimum power allocation can significantly reduce the performance gap between the simulated performance of the proposed schemes and that with optimum weights. Furthermore, these two curves are close to the analytical BER curve using optimum weights. This interesting result provides a key concept in allocating power among users. Specifically, in order to balance the link qualities, lower power should be allocated to the link with larger channel variance, while higher power should be put in the link with smaller channel variance. As can be seen in Figure 5.5, with the power loading \hat{P}_1 and \hat{P}_2 , we can see the performance improvement of about 1.4 dB at a BER of 10^{-3} over the one with equal power allocation.

5.2 Differential Modulation for Decode-and-Forward Cooperative Communications

In this Section, we propose a threshold-based differential cooperative scheme employing the DF protocol. The proposed scheme not only alleviates the above-mentioned problems of synchronization and rate limitation, but also efficiently exploits the inherent spatial diversity of relay channels through the use of a pre-determined decision threshold. In particular, the relay helps forward the source symbol only if the symbol is correctly decoded. At the destination, the received

signal from the relay is combined with that from the source only if its amplitude is larger than the threshold; otherwise only the received signal from the source is used for the detection. Properly-design threshold allows the destination to make judgement whether the signal from the relay contains the information such that the signals from the source and the relay can be efficiently combined and jointly decoded. We analyze the bit error rate (BER) performance of the proposed threshold-based differential DF scheme employing differential M-ary phase shift keying (DMPSK) modulation. A tight approximate BER formulation is provided. To better understand the proposed scheme performance, we also establish BER upper bound and BER lower bound. The BER upper bound and the BER lower bound are close to the simulation results if the decision threshold and power allocation are properly designed. Based on the tight BER approximation, we jointly determine optimum decision threshold and power allocation for different scenarios. Simulation results are shown to validate our proposed schemes and support our analytical analysis.

5.2.1 Threshold-Based Decode-and-Forward Differential Cooperation Scheme

We present in this section the proposed threshold-based differential scheme for DF cooperation systems. Consider a two-user cooperation system as shown in Figure 5.6 in which signal transmission involves two transmission phases. A user who sends information directly to the destination is considered as a source node. The other user who helps forwarding the information from the source node is a relay node. In Phase 1, the source differentially encodes its information and then broadcasts the encoded symbol to the destination. Due to the broadcasting nature of the wireless networks, the relay is also able to receive the transmitted symbol from the source. In Phase 2, while the source is silent, the relay differentially

decodes the received signal from the source. If the relay correctly decodes the transmitted symbol, the relay differentially re-encodes the information, and then forwards the encoded symbol to the destination. Otherwise, the relay does not send or remains idle. In both phases, we assume that all users transmit their signals through orthogonal channels by the use of existing schemes such as TDMA, Frequency Division Multiple Access (FDMA), or Code Division Multiple Access (CDMA).

In differential modulation, the information is conveyed in the difference of the phases of two consecutive symbols. The set of information symbols to be transmitted by the source can be given by $v_m = e^{j\varphi_m}$, where $\{\phi_m\}_{m=0}^{M-1}$ is a set of M information phases. In case of differential M -ary phase shift keying (DMPSK), ϕ_m is specified as $\varphi_m = 2\pi m/M$ for $m = 0, 1, \dots, M - 1$. Instead of directly transmitting the information as in coherent transmission [19], [93], the source node differentially encodes the information symbol v_m as

$$x^\tau = v_m x^{\tau-1}, \quad (5.31)$$

where τ is the time index, and x^τ is the differentially encoded symbol to be transmitted at time τ . After differential encoding, the source sends out the symbol x^τ with transmitted power P_1 to the destination and the relay. The corresponding received signals at the destination and the relay can be expressed as

$$y_{s,d}^\tau = \sqrt{P_1} h_{s,d}^\tau x^\tau + w_{s,d}^\tau, \quad (5.32)$$

$$y_{s,r}^\tau = \sqrt{P_1} h_{s,r}^\tau x^\tau + w_{s,r}^\tau, \quad (5.33)$$

where $h_{s,d}^\tau$ and $h_{s,r}^\tau$ are fading coefficients at the source-destination link and the source-relay link, respectively, and $w_{s,d}^\tau$ and $w_{s,r}^\tau$ are additive noise. Both channel

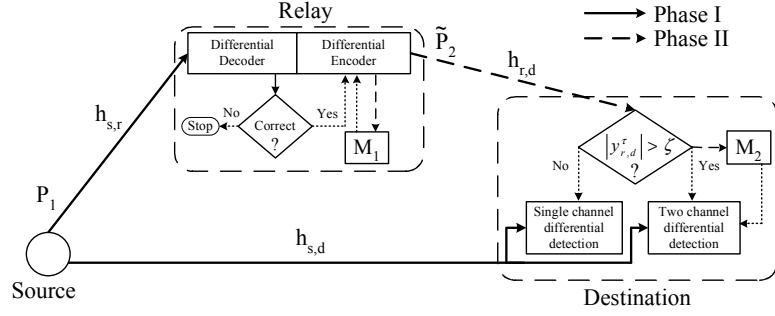


Figure 5.6: The threshold-based differential scheme for decode-and-forward cooperative communications.

coefficients $h_{s,d}^\tau$ and $h_{s,r}^\tau$ are modeled as zero-mean complex Gaussian random variables with variances $\sigma_{s,d}^2$ and $\sigma_{s,r}^2$, i.e., $\mathcal{CN}(0, \sigma_{s,d}^2)$ and $\mathcal{CN}(0, \sigma_{s,r}^2)$, respectively. Each of the additive noise terms is modeled as $\mathcal{CN}(0, \mathcal{N}_0)$ where \mathcal{N}_0 is the noise power spectral density.

In Phase 2, the relay differentially decodes the transmitted symbol from the source. Two consecutive received signals, $y_{s,r}^{\tau-1}$ and $y_{s,r}^\tau$, are required to recover the transmitted information at each symbol period. By assuming that the channel coefficient $h_{s,r}^\tau$ is almost constant over two symbol periods, the differential decoder at the relay decodes based on the decision rule: [88]

$$\hat{m} = \arg \max_{m=0,1,\dots,M-1} \text{Re} \{ (v_m y_{s,r}^{\tau-1})^* y_{s,r}^\tau \}, \quad (5.34)$$

in which the CSI is not required. In the relay-cooperation mode, the relay decides whether to forward the received information or not according to the quality of the received signal. For mathematical tractability, we assume that the relay can judge whether the decoded information is correct or not¹. If the relay incorrectly decodes the received signal, such incorrectly decoded symbol is discarded, and the

¹ Practically, this can be done at the relay by applying a simple SNR threshold on the received data. Although, it can lead to some error propagation, but for practical ranges of operating SNR, the event of error propagation can be assumed negligible.

relay does not send any information. Otherwise, the relay differentially re-encodes the correctly decoded information symbol and forward it to the destination.

In general, successful differential decoding requires that the encoder differentially encodes each information symbol with the previously transmitted symbol. For example, if the information symbols are sent every time slot, then the information symbol to be transmitted at time τ is differentially encoded with the transmitted symbol at time $\tau - 1$. In the proposed differential DF scheme, since the information symbols at the relay are transmitted only if they are correctly decoded, the transmission time of the previously transmitted symbol can be any time before the current time τ . We denote such previous transmission time as $\tau - k$, $k \geq 1$, i.e., $\tau - k$ is the latest time that the relay correctly decodes the symbol before time τ . In order to perform successful differential en/decoding, we let a memory M_1 at the relay (see Figure 5.6) store the transmitted symbol at time $\tau - k$. Note that having a memory M_1 does not increase the system complexity compared to the conventional differential system. The difference is that the memory in our proposed scheme stores the transmitted symbol at time $\tau - k$ instead of time $\tau - 1$ as does the conventional differential scheme. The differentially re-encoded signal at the relay in Phase 2 can be expressed as

$$\tilde{x}^\tau = v_m \tilde{x}^{\tau-k}, \quad (5.35)$$

where \tilde{x}^τ is the differentially encoded symbol at the relay at time τ . We can see from (5.31) and (5.35) that the differentially encoded symbols \tilde{x}^τ at the relay and x^τ at the source convey the same information symbol v_m . However, the two encoded symbols can be different since the relay differentially encodes the information symbol v_m with the symbol in the memory which may not be $x^{\tau-1}$ as used at the source. After differential re-encoding, the relay sends the symbol \tilde{x}^τ to the

destination with transmitted power P_2 , and then stores the transmitted symbol \tilde{x}^τ in the memory M_1 for subsequent differential encoding. The received signal at the destination from the relay in Phase 2 can be expressed as

$$y_{r,d}^\tau = \begin{cases} \sqrt{P_2}h_{r,d}^\tau\tilde{x}^\tau + w_{r,d}^\tau & : \text{if relay correctly decodes } (\tilde{P}_2^\tau = P_2); \\ w_{r,d}^\tau & : \text{if relay incorrectly decodes } (\tilde{P}_2^\tau = 0), \end{cases} \quad (5.36)$$

where $h_{r,d}^\tau$ is the channel coefficient from the relay to the destination and $w_{r,d}^\tau$ is an additive noise. We assume that $h_{r,d}^\tau$ is $\mathcal{CN}(0, \sigma_{r,d}^2)$ distributed, and $w_{r,d}^\tau$ is $\mathcal{CN}(0, \mathcal{N}_0)$ distributed.

The received signals at the destination comprise the received signal from the source in Phase 1 and that from the relay in Phase 2. As discussed previously, in Phase 2, the relay may forward the information or remain idle. Without knowledge of the CSI, the destination is unable to know whether the received signal from the relay contains the information or not. In order for the destination to judge whether to combine the signals from the source-destination and relay-destination links, we propose to use a decision threshold ζ at the destination node (see Figure 5.6). We consider the received signal with amplitude $|y_{r,d}^\tau|$ greater than the threshold ζ as a high-potential information bearing signal to be used for further differential detection.

Particularly, if the amplitude of the received signal from the relay is not greater than the decision threshold, i.e. $|y_{r,d}^\tau| \leq \zeta$, the destination estimates the transmitted symbol based only on the received signal from the direct link. On the other hand, if $|y_{r,d}^\tau| > \zeta$, the received signal from the source and that from the relay are combined together, and then the combined output is jointly differentially decoded. Note that in order to successfully decode, the differential detector requires the previously received signal which serves as a CSI estimate. Since the received signal

from the relay may contain the transmitted symbol or only noise, we propose to use a memory M_2 at the destination as shown in Figure 5.6 to store the previously received signal at the relay-destination link that tends to contain the information. An ideal situation is to let the memory store the received signal $y_{r,d}^\tau$ only when the signal contains the transmitted symbol; however, such information is not available since the destination does not have the knowledge of the CSI. So, to efficiently decode the received signal from the relay, we propose to let the memory M_2 stores the received signal $y_{r,d}^\tau$ whose amplitude is greater than the decision threshold. If the threshold is properly designed, then the signal in the memory M_2 corresponds to the received signal from the relay that carries the encoded symbol stored in the memory M_1 . With an assumption that the channel coefficients stay almost constant for several symbol periods, the signal in the memory M_2 serves as a channel estimate of the relay-destination link, which can then be used for efficient differential decoding at the destination. Based on the multichannel differential detection in [3], the combined signal prior to the differential decoding is

$$y = \begin{cases} a_1(y_{s,d}^{\tau-1})^* y_{s,d}^\tau + a_2(y_{r,d}^{\tau-l})^* y_{r,d}^\tau & \text{if } |y_{r,d}^\tau| > \zeta; \\ (y_{s,d}^{\tau-1})^* y_{s,d}^\tau & \text{if } |y_{r,d}^\tau| \leq \zeta, \end{cases} \quad (5.37)$$

where a_1 and a_2 are combining weight coefficients, and $\tau - l$ ($l \geq 1$) represents the time index of the latest signal in memory M_2 , i.e., $y_{r,d}^{\tau-l}$ is the most recent received signal from the relay whose amplitude is larger than the threshold. Note that different combining weights, a_1 and a_2 , result in different system performances. In Section 5.2.2, we determine the BER performance in case of $a_1 = \frac{1}{2\mathcal{N}_0}$ and $a_2 = \frac{1}{2\mathcal{N}_0}$. As we will show later, the use of such combining weights maximizes the signal-to-noise ratio (SNR) of the combiner output when the destination is able to differentially decode the signals from both source and relay. Based on

the combined signal in (5.37), the decoder at the destination jointly differentially decodes the transmitted information symbol by using the following decision rule:

$$\hat{m} = \arg \max_{m=0,1,\dots,M-1} \operatorname{Re} \{v_m^* y\}. \quad (5.38)$$

5.2.2 BER Analysis for the DF Differential scheme

In this section, we analyze the bit error rate (BER) performance for the proposed threshold-based differential DF scheme employing DMPSK modulation. We also derive an approximate BER formulation to further understand the performance of the proposed scheme. First, we classify different scenarios that lead to different instantaneous SNR's at the combiner output of the destination. Next, the probability that each scenario occurs is determined. Then, we evaluate an average BER performance by taking into account all the possible scenarios.

Classification of Different Scenarios

We classify in this subsection all different scenarios that result in different SNR's at the combiner output. Recall that if the amplitude of received signal from the relay is larger than the decision threshold ($|y_{r,d}^\tau| > \zeta$), then the destination jointly decodes the received signals from the source ($y_{s,d}^\tau$) and the relay ($y_{r,d}^\tau$). Otherwise, only the received signal $y_{s,d}^\tau$ from the source is used for differential detection. Therefore, we can classify the scenarios into two major groups, namely the scenarios that $|y_{r,d}^\tau| > \zeta$ and $|y_{r,d}^\tau| \leq \zeta$. In case that $|y_{r,d}^\tau| \leq \zeta$, the SNR can be simply determined based on the received signal from the direct link. On the other hand, if $|y_{r,d}^\tau| > \zeta$, the SNR at the combiner output depends not only on the received signals from the direct link but also on that from the relay link. According to the decision rule in (5.37), if $|y_{r,d}^\tau| > \zeta$, the performance of the differential decoder relies on the received signals from the source at the current time τ ($y_{s,d}^\tau$)

and the previous time $\tau - 1$ ($y_{s,d}^{\tau-1}$) as well as the received signal from the relay at the current time τ ($y_{r,d}^\tau$) and that stored in the memory ($y_{r,d}^{\tau-l}$). The received signals $y_{r,d}^\tau$ and $y_{r,d}^{\tau-l}$ from the relay may or may not contain the information, depending on the correctness of the decoded symbol at the relay at time τ and time $\tau - l$. If the relay decodes the symbol correctly, then the relay sends the encoded symbol with transmitted power P_2 . Thus, based on the transmitted power at the relay at time τ and time $\tau - l$, we can further classify the scenarios into four different categories, namely (a) $\tilde{P}_2^\tau = P_2$ and $\tilde{P}_2^{\tau-l} = P_2$, (b) $\tilde{P}_2^\tau = P_2$ and $\tilde{P}_2^{\tau-l} = 0$, (c) $\tilde{P}_2^\tau = 0$ and $\tilde{P}_2^{\tau-l} = P_2$, as well as (d) $\tilde{P}_2^\tau = 0$ and $\tilde{P}_2^{\tau-l} = 0$. In case that $\tilde{P}_2^\tau = P_2$ and $\tilde{P}_2^{\tau-l} = P_2$, the received signals $y_{r,d}^\tau$ and $y_{r,d}^{\tau-l}$ convey the symbols \tilde{x}^τ and $\tilde{x}^{\tau-l}$, respectively. Since the relay differentially encodes the information symbol from the source with the symbol $\tilde{x}^{\tau-k}$ in the memory M_1 , the SNR at the combiner output also depends on whether the received signal $y_{r,d}^{\tau-l}$ used for decoding corresponds to the symbol $\tilde{x}^{\tau-k}$ used for encoding. Therefore, the scenarios under $\tilde{P}_2^\tau = P_2$ and $\tilde{P}_2^{\tau-l} = P_2$ can be further separated into two cases, namely $l = k$ and $l \neq k$. All of these six possible scenarios are summarized in Figure 5.7.

In order to facilitate the BER analysis in the subsequent subsection, we define six different scenarios by Φ_i , $i = 1, 2, \dots, 6$ as follows. We let the first scenario Φ_1 be the scenario that the amplitude of the received signal is not larger than the threshold ζ , i.e.,

$$\Phi_1 \triangleq \{|y_{r,d}^\tau| \leq \zeta\}. \quad (5.39)$$

When Φ_1 occurs, the destination does not combine the received signal from the relay with that from the source. The second scenario Φ_2 is defined as the case that the amplitude of the received signal is larger than the threshold, the relay transmitted powers at both time τ and $\tau - l$ are equal to P_2 , and the received signal $y_{r,d}^{\tau-l}$ stored in memory M_2 conveys the information symbol $\tilde{x}^{\tau-k}$ stored in

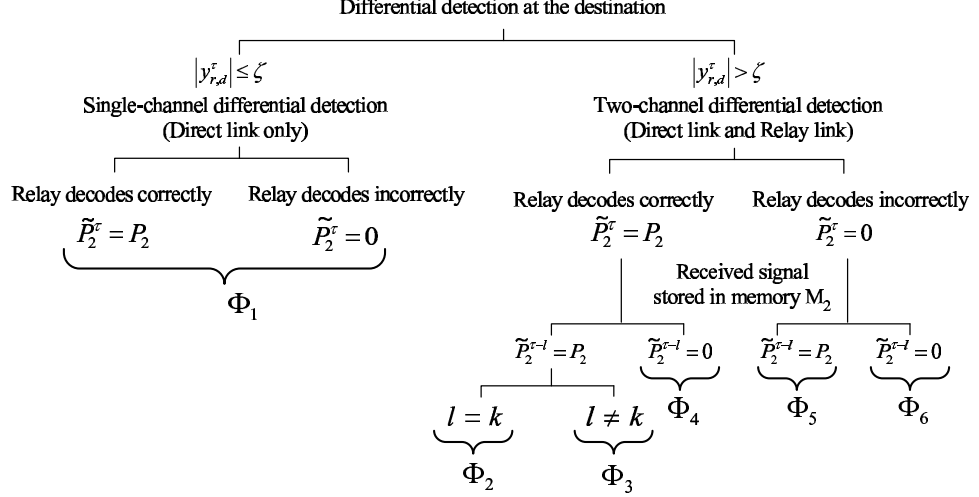


Figure 5.7: Two possible differential detection techniques at the destination; single-channel differential detection or two-channel differential detection, with six possible scenarios based on the currently received signal and the signal stored in memory M_2 .

memory M_1 . Specifically, Φ_2 can be written as

$$\Phi_2 \triangleq \left\{ |y_{r,d}^r| > \zeta, \tilde{P}_2^\tau = P_2, \tilde{P}_2^{\tau-l} = P_2, l = k \right\}. \quad (5.40)$$

The scenario Φ_3 is similar to the scenario Φ_2 excepts that the received signal $y_{r,d}^{\tau-l}$ does not contain the symbol $\tilde{x}^{\tau-k}$, i.e., $l \neq k$. We express this scenario as $\Phi_3 \triangleq \left\{ |y_{r,d}^r| > \zeta, \tilde{P}_2^\tau = P_2, \tilde{P}_2^{\tau-l} = P_2, l \neq k \right\}$. The scenarios Φ_4 to Φ_6 correspond to the scenarios that $|y_{r,d}^r| > \zeta$ and either \tilde{P}_2^τ or $\tilde{P}_2^{\tau-l}$ is zero. Under the scenario Φ_4 , the transmitted power \tilde{P}_2^τ is P_2 whereas the transmitted power $\tilde{P}_2^{\tau-l}$ is 0. We express the scenario Φ_4 as $\Phi_4 \triangleq \left\{ |y_{r,d}^r| > \zeta, \tilde{P}_2^\tau = P_2, \tilde{P}_2^{\tau-l} = 0 \right\}$. Under the scenario Φ_5 , the transmitted power \tilde{P}_2^τ is 0 whereas the transmitted power $\tilde{P}_2^{\tau-l}$ is P_2 , i.e., $\Phi_5 \triangleq \left\{ |y_{r,d}^r| > \zeta, \tilde{P}_2^\tau = 0, \tilde{P}_2^{\tau-l} = P_2 \right\}$. The scenario Φ_6 corresponds to the scenario that both \tilde{P}_2^τ and $\tilde{P}_2^{\tau-l}$ are zeros. We define the scenario Φ_6 as $\Phi_6 \triangleq \left\{ |y_{r,d}^r| > \zeta, \tilde{P}_2^\tau = 0, \tilde{P}_2^{\tau-l} = 0 \right\}$.

For subsequent performance derivation, we denote $P_{BER}^h|_{\Phi_i}$ as the conditional BER, given a scenario Φ_i and a set of channel realizations for the source-destination link, the source-relay link, and the relay-destination link. We also denote $P_r^h(\Phi_i)$ as

the chance that the scenario Φ_i occurs given a set of channel realizations. Accordingly, the conditional BER of the proposed differential DF scheme can be expressed as

$$P_{BER}^h = \sum_{i=1}^6 P_{BER}^h |_{\Phi_i} P_r^h(\Phi_i). \quad (5.41)$$

By averaging (5.41) over all channel realizations, the average BER of the proposed scheme is given by

$$P_{BER} = \sum_{i=1}^6 \mathbb{E} [P_{BER}^h |_{\Phi_i} P_r^h(\Phi_i)] = \sum_{i=1}^6 P_{BER}^{(i)}, \quad (5.42)$$

where $\mathbb{E}[\cdot]$ represents the expectation operation.

In the following subsections, we determine the chance that each scenario occurs ($P_r^h(\Phi_i)$), the conditional BER ($P_{BER}^h |_{\Phi_i}$), and finally obtain the average BER (P_{BER}) for the proposed differential DF scheme.

Probability of Occurrence

We determine in this subsection the chance that each scenario Φ_i occurs. We first note that for a specific channel realization, the amplitude of the received signal $y_{r,d}^\tau$ depends on the relay transmitted power \tilde{P}_2^τ , which in turn relies on the correctness of the decoded symbol at the relay. With DMPSK signals, the chance of incorrect decoding at the relay, and hence the chance of $\tilde{P}_2^\tau = 0$, can be obtained from the conditional symbol error rate (SER) of the transmission from the source to the relay. Based on the SER formulation for DMPSK signals in [96], we have

$$P_r^h(\tilde{P}_2^\tau = 0) = \Psi(\gamma_{s,r}^\tau) \triangleq \frac{1}{\pi} \int_0^{(M-1)\pi/M} \exp[-g(\phi)\gamma_{s,r}^\tau] d\phi, \quad (5.43)$$

where

$$\gamma_{s,r}^\tau = \frac{P_1 |h_{s,r}^\tau|^2}{\mathcal{N}_0} \quad (5.44)$$

is the instantaneous SNR per symbol at the relay due to the transmitted symbol from the source, and

$$g(\phi) = \frac{\sin^2(\pi/M)}{1 + \cos(\pi/M) \cos(\phi)}. \quad (5.45)$$

The chance that the relay forwards the symbol with transmitted power $\tilde{P}_2^\tau = P_2$ is determined by the chance of correct decoding at the relay, hence

$$P_r^h \left(\tilde{P}_2^\tau = P_2 \right) = 1 - \Psi(\gamma_{s,r}^\tau), \quad (5.46)$$

where $\Psi(\gamma_{s,r}^\tau)$ is specified in (5.43).

Consider the scenario Φ_1 in which the amplitude of the received signal $y_{r,d}^\tau$ is not greater than the decision threshold. The chance that Φ_1 occurs can be written as

$$P_r^h(\Phi_1) = P_r^h \left(|y_{r,d}^\tau| \leq \zeta \mid \tilde{P}_2^\tau = 0 \right) \Psi(\gamma_{s,r}^\tau) + P_r^h \left(|y_{r,d}^\tau| \leq \zeta \mid \tilde{P}_2^\tau = P_2 \right) [1 - \Psi(\gamma_{s,r}^\tau)]. \quad (5.47)$$

The conditional probabilities, $P_r^h(|y_{r,d}^\tau| \leq \zeta \mid \tilde{P}_2^\tau = 0)$ and $P_r^h(|y_{r,d}^\tau| \leq \zeta \mid \tilde{P}_2^\tau = P_2)$ can be obtained from the cumulative distribution function (CDF) of the random variable $|y_{r,d}^\tau|$. The received signal $y_{r,d}^\tau$ is complex Gaussian random variable with mean $\sqrt{\tilde{P}_2} h_{r,d}^\tau \tilde{x}^\tau$ and variance \mathcal{N}_0 , i.e., $y_{r,d}^\tau \sim \mathcal{CN} \left(\sqrt{\tilde{P}_2} h_{r,d}^\tau \tilde{x}^\tau, \mathcal{N}_0 \right)$. If $\tilde{P}_2^\tau = 0$ which results from incorrect decoding at the relay, the received signal $y_{r,d}^\tau$ is simply a zero-mean complex Gaussian random variable with variance \mathcal{N}_0 ($y_{r,d}^\tau \sim \mathcal{CN}(0, \mathcal{N}_0)$), and its amplitude is Rayleigh distributed. Hence, the conditional probability that $|y_{r,d}^\tau|$ is not greater than the decision threshold given that the relay does not send information can be expressed as [3]

$$P_r^h \left(|y_{r,d}^\tau| \leq \zeta \mid \tilde{P}_2^\tau = 0 \right) = 1 - \exp(-\zeta^2/\mathcal{N}_0). \quad (5.48)$$

If $\tilde{P}_2^\tau = P_2$ which corresponds to the case of correct decoding at the relay, then the received signal $y_{r,d}^\tau$ is Gaussian distributed with mean $\sqrt{\tilde{P}_2} h_{r,d}^\tau \tilde{x}^\tau$ and variance

\mathcal{N}_0 . In this case, $|y_{r,d}^\tau|^2$ can be viewed as a summation of two squared Gaussian random variables with means $m_1 = \text{Re} \{ \sqrt{P_2} h_{r,d}^\tau \tilde{x}^\tau \}$ and $m_2 = \text{Im} \{ \sqrt{P_2} h_{r,d}^\tau \tilde{x}^\tau \}$, and a common variance $\sigma^2 = \mathcal{N}_0/2$. Based on [3], $|y_{r,d}^\tau|^2$ is non-central chi-square distributed with parameter $s^2 = m_1^2 + m_2^2$, whereas $|y_{r,d}^\tau|$ is a Ricean-distributed random variable of which the probability density function (PDF) as well as the CDF can be obtained from the PDF of $|y_{r,d}^\tau|^2$ through a change of variables. In case of DMPSK signals, the parameter s can be determined as

$$s = \sqrt{P_2 |h_{r,d}^\tau \tilde{x}^\tau|^2} = \sqrt{P_2 |h_{r,d}^\tau|^2}, \quad (5.49)$$

where the second equality results from the fact that each DMPSK symbol has unit energy. From (5.49) and the results in [3], the conditional probability that $|y_{r,d}^\tau|$ is not greater than the decision threshold given that the relay sends the information with transmitted power P_2 can be written as

$$P_r^h \left(|y_{r,d}^\tau| \leq \zeta \mid \tilde{P}_2^\tau = P_2 \right) = 1 - \mathcal{M} \left(P_2 |h_{r,d}^\tau|^2, \zeta \right), \quad (5.50)$$

where

$$\mathcal{M} \left(P_2 |h_{r,d}^\tau|^2, \zeta \right) \triangleq Q_1 \left(\sqrt{\frac{P_2 |h_{r,d}^\tau|^2}{\mathcal{N}_0/2}}, \frac{\zeta}{\sqrt{\mathcal{N}_0/2}} \right), \quad (5.51)$$

in which $Q_1(\alpha, \beta)$ is the Marcum Q-function [88]:

$$Q_1(\alpha, \beta) = \int_\beta^\infty \lambda \exp \left[- \left(\frac{\lambda^2 + \alpha^2}{2} \right) \right] I_0(\alpha\lambda) d\lambda, \quad (5.52)$$

and $I_0(\cdot)$ is the zeroth-order modified Bessel function of the first kind. By substituting (5.48) and (5.50) into (5.47), we can express the chance that Φ_1 occurs as

$$P_r^h(\Phi_1) = \left(1 - e^{(-\zeta^2/\mathcal{N}_0)} \right) \Psi(\gamma_{s,r}^\tau) + \left(1 - \mathcal{M} \left(P_2 |h_{r,d}^\tau|^2, \zeta \right) \right) [1 - \Psi(\gamma_{s,r}^\tau)]. \quad (5.53)$$

The rest of the scenarios, Φ_2 to Φ_6 , are related to the situation when the amplitude of the received signal from the relay, $|y_{r,d}^\tau|$, is greater than the decision

threshold ζ . In these scenarios, both the currently received signal ($y_{r,d}^\tau$) and that stored in the memory M_2 ($y_{r,d}^{\tau-l}$) are used for differential detection at the destination. In our proposed scheme, the memory M_2 store only the received signal from the relay whose amplitude is larger than the threshold. This implies that the amplitude $|y_{r,d}^{\tau-l}|$ is larger than the threshold. Therefore, the chance that each of the scenarios Φ_2 to Φ_6 happens is conditioned on the event that $|y_{r,d}^{\tau-l}| > \zeta$. From (5.40), the chance that the scenario Φ_2 occurs is given by

$$P_r^h(\Phi_2) = P_r^h\left(|y_{r,d}^\tau| > \zeta, \tilde{P}_2^\tau = P_2, \tilde{P}_2^{\tau-l} = P_2, l = k \mid |y_{r,d}^{\tau-l}| > \zeta\right). \quad (5.54)$$

Since the events at time $\tau - l$ are independent of the events at time τ , $P_r^h(\Phi_2)$ can be written as a product of the probabilities:

$$P_r^h(\Phi_2) = P_r^h\left(|y_{r,d}^\tau| > \zeta, \tilde{P}_2^\tau = P_2\right) P_r^h\left(\tilde{P}_2^{\tau-l} = P_2, l = k \mid |y_{r,d}^{\tau-l}| > \zeta\right). \quad (5.55)$$

The first term on the right hand side of (5.55) represents the probability that the relay transmits the decoded symbol with power P_2 and the received signal from the relay is larger than the threshold. This term can be expressed as

$$P_r^h\left(|y_{r,d}^\tau| > \zeta, \tilde{P}_2^\tau = P_2\right) = P_r^h\left(|y_{r,d}^\tau| > \zeta \mid \tilde{P}_2^\tau = P_2\right) P_r^h\left(\tilde{P}_2^\tau = P_2\right). \quad (5.56)$$

In (5.56), the chance that the amplitude of the received signal from the relay is larger than the threshold given that the relay sends the information can be obtained from (5.50) as

$$P_r^h\left(|y_{r,d}^\tau| > \zeta \mid \tilde{P}_2^\tau = P_2\right) = \mathcal{M}\left(P_2|h_{r,d}^\tau|^2, \zeta\right). \quad (5.57)$$

Therefore, using the results in (5.46) and (5.57), (5.56) can be rewritten as

$$P_r^h\left(|y_{r,d}^\tau| > \zeta, \tilde{P}_2^\tau = P_2\right) = \mathcal{M}\left(P_2|h_{r,d}^\tau|^2, \zeta\right) \left(1 - \Psi(\gamma_{s,r}^\tau)\right). \quad (5.58)$$

The second term on the right hand side of (5.55) represents the chance that the relay transmits with power $\tilde{P}_2^{\tau-l} = P_2$, and the received signal $y_{r,d}^{\tau-l}$ stored in the

memory M_2 conveys the information symbol $\tilde{x}^{\tau-k}$ stored in the memory M_1 . By using the concept of conditional probability [97], we have

$$\begin{aligned}
P_r^h \left(\tilde{P}_2^{\tau-l} = P_2, l = k \mid |y_{r,d}^{\tau-l}| > \zeta \right) &= \sum_{k \geq 1} P_r^h \left(\tilde{P}_2^{\tau-k} = P_2 \mid |y_{r,d}^{\tau-k}| > \zeta \right) P_r^h \left(|y_{r,d}^{\tau-k}| > \zeta \right) \\
&\quad \times \prod_{i=1}^{k-1} P_r^h \left(|y_{r,d}^{\tau-i}| \leq \zeta \right) P_r^h \left(\tilde{P}_2^{\tau-i} = 0 \mid |y_{r,d}^{\tau-i}| \leq \zeta \right).
\end{aligned} \tag{5.59}$$

Based on (5.58), the term $P_r^h(\tilde{P}_2^{\tau-k} = P_2 \mid |y_{r,d}^{\tau-k}| > \zeta) P_r^h(|y_{r,d}^{\tau-k}| > \zeta)$ in (5.59) can be evaluated as $\mathcal{M}(P_2 | h_{r,d}^{\tau-k}|^2, \zeta) (1 - \Psi(\gamma_{s,r}^{\tau-k}))$, which can be approximated by $\mathcal{M}(P_2 | h_{r,d}^{\tau}|^2, \zeta) (1 - \Psi(\gamma_{s,r}^{\tau}))$ if the channels stay almost constant for several time slots. By applying Bayes' rule [97] and using the results in (5.43) and (5.48), we can express the product term in (5.59) as

$$\begin{aligned}
&\prod_{i=1}^{k-1} P_r^h \left(|y_{r,d}^{\tau-i}| \leq \zeta \right) P_r^h \left(\tilde{P}_2^{\tau-i} = 0 \mid |y_{r,d}^{\tau-i}| \leq \zeta \right) \\
&= \prod_{i=1}^{k-1} P_r^h \left(|y_{r,d}^{\tau-i}| \leq \zeta \mid \tilde{P}_2^{\tau-i} = 0 \right) P_r^h \left(\tilde{P}_2^{\tau-i} = 0 \right) \\
&\approx \left[(1 - e^{-\zeta^2/\mathcal{N}_0}) \Psi(\gamma_{s,r}^{\tau}) \right]^{k-1},
\end{aligned} \tag{5.60}$$

where the resulting approximation comes from approximating $P_r^h(\tilde{P}_2^{\tau-i} = 0) = \Psi(\gamma_{s,r}^{\tau-i})$ by $\Psi(\gamma_{s,r}^{\tau})$ for all i . Accordingly, we can approximate (5.59) as

$$\begin{aligned}
&P_r^h \left(\tilde{P}_2^{\tau-l} = P_2, l = k \mid |y_{r,d}^{\tau-l}| > \zeta \right) \\
&\approx \mathcal{M}(P_2 | h_{r,d}^{\tau}|^2, \zeta) (1 - \Psi(\gamma_{s,r}^{\tau})) \sum_{k \geq 1} \left[(1 - e^{-\zeta^2/\mathcal{N}_0}) \Psi(\gamma_{s,r}^{\tau}) \right]^{k-1} \\
&= \frac{\mathcal{M}(P_2 | h_{r,d}^{\tau}|^2, \zeta) (1 - \Psi(\gamma_{s,r}^{\tau}))}{(1 - e^{-\zeta^2/\mathcal{N}_0}) \Psi(\gamma_{s,r}^{\tau})}.
\end{aligned} \tag{5.61}$$

Hence, by substituting (5.58) and (5.61) into (5.55), the chance that the scenario Φ_2 happens can be approximated by

$$P_r^h(\Phi_2) \approx \frac{\mathcal{M}^2(P_2|h_{r,d}^\tau|^2, \zeta) (1 - \Psi(\gamma_{s,r}^\tau))^2}{(1 - e^{-\zeta^2/\mathcal{N}_0})\Psi(\gamma_{s,r}^\tau)}. \quad (5.62)$$

Next, we consider the scenario Φ_3 which is similar to the scenario Φ_2 except that the received signal $y_{r,d}^{\tau-l}$ stored in the memory M_2 at the destination does not convey the symbol $\tilde{x}^{\tau-k}$ stored in the memory M_2 at the relay. The chance that the scenario Φ_3 happens can be given by

$$P_r^h(\Phi_3) = P_r^h\left(|y_{r,d}^\tau| > \zeta, \tilde{P}_2^\tau = P_2, \tilde{P}_2^{\tau-l} = P_2, l \neq k \mid |y_{r,d}^{\tau-l}| > \zeta\right). \quad (5.63)$$

Observe that the scenarios Φ_2 and Φ_3 are disjoint. Thus, the chance that the scenario Φ_3 happens can be obtained from $P_r^h(\Phi_2)$ as

$$P_r^h(\Phi_3) = P_r^h(\Phi_2 \cup \Phi_3) - P_r^h(\Phi_2), \quad (5.64)$$

where $P_r^h(\Phi_2 \cup \Phi_3) = P_r^h\left(|y_{r,d}^\tau| > \zeta, \tilde{P}_2^\tau = P_2, \tilde{P}_2^{\tau-l} = P_2, \mid |y_{r,d}^{\tau-l}| > \zeta\right)$. Since the signals at time τ and time $\tau - l$ are independent, we can express $P_r^h(\Phi_2 \cup \Phi_3)$ as

$$P_r^h(\Phi_2 \cup \Phi_3) = P_r^h\left(|y_{r,d}^\tau| > \zeta, \tilde{P}_2^\tau = P_2\right) P_r^h\left(\tilde{P}_2^{\tau-l} = P_2 \mid |y_{r,d}^{\tau-l}| > \zeta\right). \quad (5.65)$$

By applying Bayes' rule, the second term on the right hand side of (5.65) is given by

$$P_r^h\left(\tilde{P}_2^{\tau-l} = P_2 \mid |y_{r,d}^{\tau-l}| > \zeta\right) = \frac{P_r^h(|y_{r,d}^{\tau-l}| > \zeta, \tilde{P}_2^{\tau-l} = P_2)}{P_r^h(|y_{r,d}^{\tau-l}| > \zeta)}. \quad (5.66)$$

The numerator on the right hand side of (5.66) is in the same form as (5.58) with τ replaced by $\tau - l$, whereas the denominator can be calculated by using the concept of total probability [97]:

$$\begin{aligned} P(|y_{r,d}^{\tau-l}| > \zeta) &= P(|y_{r,d}^{\tau-l}| > \zeta \mid \tilde{P}_2^{\tau-l} = P_2)P(\tilde{P}_2^{\tau-l} = P_2) \\ &\quad + P(|y_{r,d}^{\tau-l}| > \zeta \mid \tilde{P}_2^{\tau-l} = 0)P(\tilde{P}_2^{\tau-l} = 0). \end{aligned} \quad (5.67)$$

In (5.67), the chance that the received signal $|y_{r,d}^{\tau-l}|$ is greater than the decision threshold given that the relay does not send information can be obtained from (5.48) as

$$P_r^h \left(|y_{r,d}^{\tau-l}| > \zeta \mid \tilde{P}_2^\tau = 0 \right) = \exp(-\zeta^2/\mathcal{N}_0). \quad (5.68)$$

Substitute (5.43), (5.58) and (5.68) into (5.67) resulting in

$$\begin{aligned} P \left(|y_{r,d}^{\tau-l}| > \zeta \right) &= \mathcal{M} \left(P_2 |h_{r,d}^{\tau-l}|^2, \zeta \right) \left(1 - \Psi(\gamma_{s,r}^{\tau-l}) \right) + \exp(-\zeta^2/\mathcal{N}_0) \Psi(\gamma_{s,r}^{\tau-l}) \\ &\triangleq \Gamma(P_1 |h_{s,r}^{\tau-l}|^2, P_2 |h_{r,d}^{\tau-l}|^2). \end{aligned} \quad (5.69)$$

By assuming that the channel coefficients $h_{i,j}^{\tau-l} \approx h_{i,j}^\tau$ for any (i, j) link, then from (5.58), (5.67), and (5.69), we can determine the chance $P_r^h(\Phi_2 \cup \Phi_3)$ in (5.65) as

$$P_r^h(\Phi_2 \cup \Phi_3) = \frac{\mathcal{M}^2 \left(P_2 |h_{r,d}^\tau|^2, \zeta \right) \left(1 - \Psi(\gamma_{s,r}^\tau) \right)^2}{\Gamma(P_1 |h_{s,r}^\tau|^2, P_2 |h_{r,d}^\tau|^2)}. \quad (5.70)$$

Now the chance that the scenario Φ_3 happens can be obtained by substituting (5.62) and (5.70) into (5.64). We can express the probability $P_r^h(\Phi_3)$ as

$$\begin{aligned} P_r^h(\Phi_3) &= \mathcal{M}^2 \left(P_2 |h_{r,d}^\tau|^2, \zeta \right) \left(1 - \Psi(\gamma_{s,r}^\tau) \right)^2 \\ &\times \left(\frac{1}{\Gamma(P_1 |h_{s,r}^\tau|^2, P_2 |h_{r,d}^\tau|^2)} - \frac{1}{(1 - e^{-\zeta^2/\mathcal{N}_0}) \Psi(\gamma_{s,r}^\tau)} \right). \end{aligned} \quad (5.71)$$

Following the same steps as used to determine $P_r^h(\Phi_2 \cup \Phi_3)$, the chance that the scenario Φ_4 occurs can be expressed as

$$\begin{aligned} P_r^h(\Phi_4) &= P_r^h \left(|y_{r,d}^\tau| > \zeta, \tilde{P}_2^\tau = P_2, \tilde{P}_2^{\tau-l} = 0, |y_{r,d}^{\tau-l}| > \zeta \right) \\ &= \frac{P_r^h \left(|y_{r,d}^\tau| > \zeta, \tilde{P}_2^\tau = P_2 \right) P_r^h \left(|y_{r,d}^{\tau-l}| > \zeta, \tilde{P}_2^{\tau-l} = 0 \right)}{P_r^h \left(|y_{r,d}^{\tau-l}| > \zeta \right)}. \end{aligned} \quad (5.72)$$

By substituting (5.58) and (5.69) into (5.72), we arrive at

$$P_r^h(\Phi_4) = \frac{\mathcal{M} \left(P_2 |h_{r,d}^\tau|^2, \zeta \right) \exp(-\zeta^2/\mathcal{N}_0) \Psi(\gamma_{s,r}^\tau) \left(1 - \Psi(\gamma_{s,r}^\tau) \right)}{\Gamma(P_1 |h_{s,r}^\tau|^2, P_2 |h_{r,d}^\tau|^2)}. \quad (5.73)$$

Similarly, the chances that the scenario Φ_5 happen can be determined as

$$\begin{aligned} P_r^h(\Phi_5) &= P_r^h \left(|y_{r,d}^\tau| > \zeta, \tilde{P}_2^\tau = 0, \tilde{P}_2^{\tau-l} = P_2, ||y_{r,d}^{\tau-l}| > \zeta \right) \\ &= \frac{P_r^h(|y_{r,d}^\tau| > \zeta, \tilde{P}_2^\tau = 0) P_r^h(|y_{r,d}^{\tau-l}| > \zeta, \tilde{P}_2^{\tau-l} = P_2)}{P_r^h(|y_{r,d}^{\tau-l}| > \zeta)}. \end{aligned} \quad (5.74)$$

With an assumption that the channels at time τ and time $\tau - l$ are the same, we can see from (5.72) and (5.74) that the chances that the scenarios Φ_4 and Φ_5 happen are equal. Therefore, $P_r^h(\Phi_5)$ can be expressed in the same form as (5.73). Lastly, the chance that the scenario Φ_6 occurs can be determined as

$$\begin{aligned} P_r^h(\Phi_6) &= P_r^h \left(|y_{r,d}^\tau| > \zeta, \tilde{P}_2^\tau = 0, \tilde{P}_2^{\tau-l} = 0, ||y_{r,d}^{\tau-l}| > \zeta \right) \\ &= \frac{P_r^h(|y_{r,d}^\tau| > \zeta, \tilde{P}_2^\tau = 0) P_r^h(|y_{r,d}^{\tau-l}| > \zeta, \tilde{P}_2^{\tau-l} = 0)}{P_r^h(|y_{r,d}^{\tau-l}| > \zeta)}. \end{aligned} \quad (5.75)$$

Substituting (5.43) and (5.68) into (5.75), we have

$$P_r^h(\Phi_6) = \frac{\exp(-2\zeta^2/\mathcal{N}_0)\Psi(\gamma_{s,r}^\tau)}{\Gamma(P_1|h_{s,r}^\tau|^2, P_2|h_{r,d}^\tau|^2)}. \quad (5.76)$$

Average BER analysis

In this subsection, we provide the conditional BER given that each scenario Φ_i for $i = 1, 2, \dots, 6$ happens. From the resulting conditional BER together with the chance that each scenario occurs as derived in the previous subsection, we then provide the average BER formulation for the proposed differential DF scheme.

- **Conditional BER of each scenario**

When the scenario Φ_1 occurs, the destination estimates the transmitted symbol v_m from the source by using only the received signal $y_{s,d}^\tau$ from the source. Based on the conditional BER formulation of DMPSK with single channel reception [88], the conditional BER for the scenario Φ_1 is

$$P_{BER}^h|_{\Phi_1} = \Omega_1(\gamma_1) \triangleq \frac{1}{4\pi} \int_{-\pi}^{\pi} f_1(\theta) \exp[-\alpha(\theta)\gamma_1] d\theta, \quad (5.77)$$

where γ_i represents the instantaneous SNR given that the scenario Φ_i occurs, and

$$f_1(\theta) = \frac{1 - \beta^2}{1 + 2\beta \sin \theta + \beta^2}, \quad (5.78)$$

$$\alpha(\theta) = \frac{b^2}{2 \log_2 M} (1 + 2\beta \sin \theta + \beta^2), \quad (5.79)$$

in which M is the constellation size. In case of the scenario Φ_1 , the instantaneous SNR γ_1 is specified as $\gamma_1 = P_1 |h_{s,d}^\tau|^2 / \mathcal{N}_0$ [88]. In (5.78) and (5.79), the parameter $\beta = a/b$ is a constant whose value depends on constellation size. For example, $a = 10^{-3}$ and $b = \sqrt{2}$ for DBPSK modulation, and $a = \sqrt{2 - \sqrt{2}}$ and $b = \sqrt{2 + \sqrt{2}}$ for DQPSK modulation [88]. The values of a and b for larger constellation sizes can be obtained by using the result in [3].

The scenarios Φ_2 to Φ_6 correspond to the case that the destination combines the received signal $y_{s,d}^\tau$ from the source and $y_{r,d}^\tau$ from the relay. The conditional BER for these scenarios depends on the combining weight coefficients a_1 and a_2 (see (5.37)). Under the scenario Φ_2 , the received signals from the source and the relay can be expressed as

$$y_{s,d}^\tau = v_m y_{s,d}^{\tau-1} + \tilde{w}_{s,d}^\tau, \quad (5.80)$$

$$y_{r,d}^\tau = v_m y_{r,d}^{\tau-l} + \tilde{w}_{r,d}^\tau, \quad (5.81)$$

where $\tilde{w}_{s,d}^\tau$ and $\tilde{w}_{r,d}^\tau$ are the additive noise terms, and each of them is zero-mean Gaussian distributed with variance $2\mathcal{N}_0$. Since the noise terms of the received signals from both direct link and relay link have the same mean and variance, the SNR of the combiner output under the scenario Φ_2 can

be maximized by choosing the weighting coefficients $a_1 = a_2 = \frac{1}{2\mathcal{N}_0}$. Such weighting coefficients lead to an optimum two-branch differential detection with equal gain combining. With weighting coefficients $a_1 = a_2 = \frac{1}{2\mathcal{N}_0}$, the conditional BER can be determined by using the conditional BER formulation for DMPSK with multi-channel reception [88]. Thus, we can express $P_{BER}^h|_{\Phi_2}$ as

$$P_{BER}^h|_{\Phi_2} = \Omega_2(\gamma_2) \triangleq \frac{1}{16\pi} \int_{-\pi}^{\pi} f_2(\theta) \exp[-\alpha(\theta)\gamma_2] d\theta, \quad (5.82)$$

where

$$f_2(\theta) = \frac{b^2(1 - \beta^2)[3 + \cos(2\theta) - (\beta + \frac{1}{\beta})\sin(\theta)]}{2\alpha(\theta)}, \quad (5.83)$$

and $\alpha(\theta)$ is specified in (5.79). The instantaneous SNR γ_2 is given by

$$\gamma_2 = \frac{P_1|h_{s,d}^\tau|^2}{\mathcal{N}_0} + \frac{P_2|h_{r,d}^\tau|^2}{\mathcal{N}_0}. \quad (5.84)$$

For the remaining scenarios, namely Φ_3 to Φ_6 , the destination also combines the received signal from the source and that from the relay. However, the use of the two-channel differential detection for these four cases are not guaranteed to be optimum since either the received signals $y_{r,d}^\tau$ or $y_{r,d}^{\tau-l}$ from the relay contain only noise. Up to now, the conditional BER formulation for DMPSK with arbitrary-weighted combining has not been available in the literature. For analytical tractability of the analysis, we resort to an approximate BER, in which the signal from the relay is considered as noise when Φ_3 to Φ_6 occur. As we will show in the succeeding section, the analytical BER obtained from this approximation is very close to the simulation results. The approximate conditional BER for the scenarios Φ_i , $i = 3, \dots, 6$, are $P_{BER}^h|_{\Phi_i} \approx \Omega_2(\gamma_i)$, where

$$\gamma_i = \frac{P_1|h_{s,d}^\tau|^2}{\mathcal{N}_0 + \mathcal{N}_i/(P_1|h_{s,d}^\tau|^2/\mathcal{N}_0)}, \quad (5.85)$$

in which \mathcal{N}_i represents the noise power that comes from the relay link given that the scenario Φ_i occurs. The noise power \mathcal{N}_i depends on the received signal from the relay at the current time τ ($y_{r,d}^\tau$) and that stored in the memory ($y_{r,d}^{\tau-l}$). Under the scenario Φ_3 , \mathcal{N}_3 is given by $(P_2|h_{r,d}|^2 + \mathcal{N}_0)^2/\mathcal{N}_0$. Under the scenarios Φ_4 and Φ_5 , the relay does not send the information at either time τ or time $\tau-l$. These two scenarios result in the same noise power such that $\mathcal{N}_4 = \mathcal{N}_5 = P_2|h_{r,d}|^2 + \mathcal{N}_0$. The last scenario, i.e., Φ_6 , corresponds to the case when both $y_{r,d}^\tau$ and $y_{r,d}^{\tau-l}$ does not contain any information symbol. The noise power \mathcal{N}_6 is equal to the noise variance \mathcal{N}_0 .

- **Average BER**

In what follows, we determine the average BER $P_{BER}^{(i)} \triangleq \text{E} [P_{BER}^h |_{\Phi_i} P_r^h(\Phi_i)]$ for each scenario. Assuming that the channels of different transmit-receive links are independent, the average BER for the scenario Φ_1 can be obtained by using (5.53) and (5.77) such that

$$P_{BER}^{(1)} = \text{E} \left[\Omega_1 \left(\frac{P_1 |h_{s,d}^\tau|^2}{\mathcal{N}_0} \right) \right] \text{E} \left[\left(1 - e^{-\zeta^2/\mathcal{N}_0} \right) \Psi \left(\frac{P_1 |h_{s,r}^\tau|^2}{\mathcal{N}_0} \right) + \left(1 - \mathcal{M}(P_2 |h_{r,d}^\tau|^2, \zeta) \right) \left(1 - \Psi \left(\frac{P_1 |h_{s,r}^\tau|^2}{\mathcal{N}_0} \right) \right) \right] \quad (5.86)$$

Averaging over the Rayleigh fading channels $h_{s,d}^\tau$, $h_{s,r}^\tau$, and $h_{r,d}^\tau$, the average BER under the scenario Φ_1 is given by

$$P_{BER}^{(1)} = F_1 \left(1 + \frac{\alpha(\theta) P_1 \sigma_{s,d}^2}{\mathcal{N}_0} \right) \left[\left(1 - e^{-\zeta^2/\mathcal{N}_0} \right) G \left(1 + \frac{g(\phi) P_1 \sigma_{s,r}^2}{\mathcal{N}_0} \right) + \left(1 - \frac{1}{\sigma_{r,d}^2} \int_0^\infty \mathcal{M}(P_2 q, \zeta) e^{-q/\sigma_{r,d}^2} dq \right) \left(1 - G \left(1 + \frac{g(\phi) P_1 \sigma_{s,r}^2}{\mathcal{N}_0} \right) \right) \right], \quad (5.87)$$

where $g(\phi)$ and $f_1(\theta)$ are specified in (5.45) and (5.78), respectively, and

$$G(c(\phi)) = \frac{1}{\pi} \int_0^{(M-1)\pi/M} \frac{1}{c(\phi)} d\phi, \quad (5.88)$$

$$F_1(c(\theta)) = \frac{1}{4\pi} \int_{-\pi}^{\pi} \frac{f_1(\theta)}{c(\theta)} d\theta, \quad (5.89)$$

in which $c(\theta)$ is an arbitrary function of θ . According to (5.62) and (5.82), the average BER under the scenario Φ_2 can be approximated as

$$P_{BER}^{(2)} \approx \mathbb{E} \left[\Omega_2 \left(\frac{P_1 |h_{s,d}^\tau|^2}{\mathcal{N}_0} + \frac{P_2 |h_{r,d}^\tau|^2}{\mathcal{N}_0} \right) \cdot \frac{\mathcal{M}^2(P_2 |h_{r,d}^\tau|^2, \zeta) \left(1 - \Psi \left(\frac{P_1 |h_{s,r}^\tau|^2}{\mathcal{N}_0} \right) \right)^2}{1 - (1 - e^{-\zeta^2/\mathcal{N}_0}) \Psi \left(\frac{P_1 |h_{s,r}^\tau|^2}{\mathcal{N}_0} \right)} \right]. \quad (5.90)$$

By averaging over the channel realization, we have

$$P_{BER}^{(2)} \approx \frac{1}{\sigma_{r,d}^2} \int_0^\infty s_2(q) \mathcal{M}^2(P_2 q, \zeta) e^{-\frac{q}{\sigma_{r,d}^2}} dz \\ \times \frac{1}{\sigma_{s,r}^2} \int_0^\infty \frac{\left(1 - \Psi \left(\frac{P_1 u}{\mathcal{N}_0} \right) \right)^2}{1 - (1 - e^{-\zeta^2/\mathcal{N}_0}) \Psi \left(\frac{P_1 u}{\mathcal{N}_0} \right)} e^{-\frac{u}{\sigma_{s,r}^2}} du, \quad (5.91)$$

where

$$s_2(q) = \frac{1}{16\pi} \int_{-\pi}^{\pi} \frac{f_2(\theta)}{1 + \frac{\alpha(\theta) P_1 \sigma_{s,d}^2}{\mathcal{N}_0}} e^{-\alpha(\theta) \frac{P_2 q}{\mathcal{N}_0}} d\theta. \quad (5.92)$$

The average BER under the scenario Φ_3 can be approximated as $P_{BER}^{(3)} \approx \mathbb{E}[\Omega_2(\gamma_3)$

$(P_r^h(\Phi_2 \cup \Phi_3) - P_r^h(\Phi_2))]$. From (5.62), (5.70), and (5.85), we can approximate the average BER under the scenario Φ_3 as

$$P_{BER}^{(3)} \approx \mathbb{E} \left[\Omega_2 \left(\frac{P_1 |h_{s,d}^\tau|^2}{\mathcal{N}_0 + \frac{(P_2 |h_{r,d}^\tau|^2 + \mathcal{N}_0)^2}{P_1 |h_{s,d}^\tau|^2}} \right) \mathcal{M}^2(P_2 |h_{r,d}^\tau|^2, \zeta) \left(1 - \Psi \left(\frac{P_1 |h_{s,r}^\tau|^2}{\mathcal{N}_0} \right) \right)^2 \right. \\ \left. \times \left(\frac{1}{\Gamma(P_1 |h_{s,r}^\tau|^2, P_2 |h_{r,d}^\tau|^2)} - \frac{1}{1 - (1 - e^{-\zeta^2/\mathcal{N}_0}) \Psi \left(\frac{P_1 |h_{s,r}^\tau|^2}{\mathcal{N}_0} \right)} \right) \right]. \quad (5.93)$$

Average over all channel coefficients, resulting in

$$P_{BER}^{(3)} \approx \frac{1}{\sigma_{s,r}^2} \int_0^\infty \left[\frac{1}{4\pi} \int_{-\pi}^\pi f_2(\theta) s_3(u, \theta) d\theta \right] e^{-u/\sigma_{s,r}^2} du, \quad (5.94)$$

where

$$\begin{aligned} s_3(u, \theta) = & \frac{1}{\sigma_{s,d}^2 \sigma_{r,d}^2} \int_0^\infty \int_0^\infty \exp \left(-\frac{\alpha(\theta) P_1 z}{\mathcal{N}_0 + \frac{(P_2 q + \mathcal{N}_0)^2}{P_1 z}} - \frac{z}{\sigma_{s,d}^2} - \frac{q}{\sigma_{r,d}^2} \right) \left(1 - \Psi \left(\frac{P_1 u}{\mathcal{N}_0} \right) \right)^2 \\ & \times \mathcal{M}^2(P_2 q, \zeta) \left(\frac{1}{\Gamma(P_1 u, P_2 q)} - \frac{1}{1 - (1 - e^{-\zeta^2/\mathcal{N}_0}) \Psi \left(\frac{P_1 u}{\mathcal{N}_0} \right)} \right) dq dz. \end{aligned} \quad (5.95)$$

Under the scenario Φ_4 , the approximate BER can be expressed as

$$\begin{aligned} P_{BER}^{(4)} \approx & \mathbb{E} \left[\Omega_2 \left(\frac{P_1 |h_{s,d}^\tau|^2}{\mathcal{N}_0 + \frac{P_2 |h_{r,d}^\tau|^2 + \mathcal{N}_0}{P_1 |h_{s,d}^\tau|^2 / \mathcal{N}_0}} \right) \exp(-\zeta^2/\mathcal{N}_0) \mathcal{M}(P_2 |h_{r,d}^\tau|^2, \zeta) \right. \\ & \left. \times \frac{\Psi \left(\frac{P_1 |h_{s,r}^\tau|^2}{\mathcal{N}_0} \right) \left(1 - \Psi \left(\frac{P_1 |h_{s,r}^\tau|^2}{\mathcal{N}_0} \right) \right)}{\Gamma(P_1 |h_{s,r}^\tau|^2, P_2 |h_{r,d}^\tau|^2)} \right]. \end{aligned} \quad (5.96)$$

By averaging over all channel coefficients, we obtain

$$P_{BER}^{(4)} \approx \frac{1}{\sigma_{s,r}^2} \int_0^\infty \left[\frac{1}{4\pi} \int_{-\pi}^\pi f_2(\theta) s_4(u, \theta) d\theta \right] e^{-u/\sigma_{s,r}^2} du, \quad (5.97)$$

where

$$\begin{aligned} s_4(u, \theta) = & \frac{1}{\sigma_{s,d}^2 \sigma_{r,d}^2} \int_0^\infty \int_0^\infty \exp \left(-\frac{\alpha(\theta) P_1 z}{\mathcal{N}_0 + \frac{P_2 q + \mathcal{N}_0}{P_1 z / \mathcal{N}_0}} - \frac{\zeta^2}{\mathcal{N}_0} - \frac{z}{\sigma_{s,d}^2} - \frac{q}{\sigma_{r,d}^2} \right) \\ & \times \mathcal{M}(P_2 q, \zeta) \frac{\Psi \left(\frac{P_1 u}{\mathcal{N}_0} \right) \left(1 - \Psi \left(\frac{P_1 u}{\mathcal{N}_0} \right) \right)}{\Gamma(P_1 u, P_2 q)} dq dz. \end{aligned} \quad (5.98)$$

Based on the chance that the scenario Φ_5 occurs and the conditional bit error probability $P_{BER}^h|_{\Phi_5}$, we can see that the approximate BER under the scenario Φ_5 is the same as that under the scenario Φ_4 , and hence $P_{BER}^{(5)}$ can

be expressed as in (5.96). From (5.76) and (5.85), the average BER under the scenario Φ_6 can be approximate as

$$P_{BER}^{(6)} \approx \mathbb{E} \left[\Omega_2 \left(\frac{P_1 |h_{s,d}^\tau|^2}{\mathcal{N}_0 + \mathcal{N}_0 / (P_1 |h_{s,d}^\tau|^2 / \mathcal{N}_0)} \right) \frac{\exp(-2\zeta^2 / \mathcal{N}_0) \Psi \left(\frac{P_1 |h_{s,r}^\tau|^2}{\mathcal{N}_0} \right)^2}{\Gamma(P_1 |h_{s,r}^\tau|^2, P_2 |h_{r,d}^\tau|^2)} \right]. \quad (5.99)$$

By averaging over all channel coefficients, we have

$$P_{BER}^{(6)} \approx \exp(-2\zeta^2 / \mathcal{N}_0) \left[\frac{1}{16\pi} \int_{-\pi}^{\pi} f_2(\theta) s_6(\theta) d\theta \right] \\ \times \frac{1}{\sigma_{s,r}^2} \frac{1}{\sigma_{r,d}^2} \int_0^\infty \int_0^\infty \frac{\Psi^2(P_1 u / \mathcal{N}_0)}{\Gamma(P_1 u, P_2 q)} \exp\left(-\frac{u}{\sigma_{s,r}^2} - \frac{q}{\sigma_{r,d}^2}\right) dq du, \quad (5.100)$$

where

$$s_6(\theta) = \frac{1}{\sigma_{s,d}^2} \int_0^\infty \exp\left(-\frac{\alpha(\theta) P_1 z}{\mathcal{N}_0 + \mathcal{N}_0 / (P_1 z / \mathcal{N}_0)} - \frac{z}{\sigma_{s,d}^2}\right) dz. \quad (5.101)$$

To this end, we have completed the derivation of the average BER for all possible scenarios. Finally, the average BER, P_{BER} , can be determined by summing together the average BER $P_{BER}^{(i)}$ for $i = 1, 2, \dots, 6$:

$$P_{BER} = P_{BER}^{(1)} + P_{BER}^{(2)} + P_{BER}^{(3)} + 2P_{BER}^{(4)} + P_{BER}^{(6)}, \quad (5.102)$$

in which $P_{BER}^{(i)}$ are specified in (5.87), (5.91), (5.94), (5.97), and (5.100).

5.2.3 BER Upper Bound and BER Lower Bound

We provide in this section BER upper bound and BER lower bound of the proposed threshold-based differential DF scheme. Then, we show through simulation results that when the power allocation and the decision threshold are properly designed, the BER upper bound and the BER lower bound are close to the simulated BER.

To obtain a BER upper bound, we first note that the conditional BER for each case, $P_{BER}^h|_{\Phi_i}$, is at most $1/2$. In addition, if the threshold is properly designed, then the chance that the scenarios Φ_3 to Φ_6 happen are small compared to the chance that the scenarios Φ_1 and Φ_2 happens. Therefore, the BER of the proposed DF cooperative scheme can be obtained by bounding the conditional BER $P_{BER}^h|_{\Phi_3}$, $P_{BER}^h|_{\Phi_4}$, $P_{BER}^h|_{\Phi_5}$, and $P_{BER}^h|_{\Phi_6}$ by $1/2$. The resulting BER upper bound can be expressed as

$$P_{BER} \leq P_{BER}^{(1)} + P_{BER}^{(2)} + \frac{1}{2}\{P_r^h(\Phi_3) + P_r^h(\Phi_4) + P_r^h(\Phi_5) + P_r^h(\Phi_6)\}, \quad (5.103)$$

where $P_{BER}^{(1)}$ and $P_{BER}^{(2)}$ are determined in (5.87) and (5.91), and $P_r^h(\Phi_i)$, $i = 3, 4, 5$, and 6 , are given in (5.63), (5.73), (5.74), and (5.76), respectively.

Next, we determine a BER lower bound as follows. Since the exact expressions of the chances that the scenarios Φ_2 and Φ_3 occur involve the approximation that the channel coefficients are constant for several symbol periods, and the BER formulation given that the scenario Φ_3 happens is currently unavailable, it is hard to obtain the exact BER of $P_{BER}^{(2)}$ and $P_{BER}^{(3)}$. As we will show later in this section, if the power ratio and the threshold are properly designed, the chance that the scenario Φ_3 occurs tends to be small compared to the chance that the scenario Φ_2 occurs. In addition, the conditional BER under the scenario Φ_3 ($P_{BER}^h|_{\Phi_3}$) is larger than that under the scenario Φ_2 ($P_{BER}^h|_{\Phi_2}$). Therefore, the BER lower bound of the proposed scheme can be obtained by bounding the conditional BER $P_{BER}^h|_{\Phi_3}$ with $P_{BER}^h|_{\Phi_2}$. In this way, the BER under the scenarios Φ_2 and Φ_3 can be lower bounded as

$$P_{BER}^{(2)} + P_{BER}^{(3)} \geq E[P_{BER}^h|_{\Phi_2} P_r^h(\Phi_2 \cup \Phi_3)], \quad (5.104)$$

where $P_r^h(\Phi_2 \cup \Phi_3)$, which is evaluated in (5.70), is the chance that the scenarios Φ_2 and Φ_3 occur. According to (5.62) and (5.82), the average BER in (5.104) can

be expressed as

$$P_{BER}^{(2)} + P_{BER}^{(3)} \geq \mathbb{E} \left[\Omega_2 \left(\frac{P_1 |h_{s,d}^\tau|^2}{\mathcal{N}_0} + \frac{P_2 |h_{r,d}^\tau|^2}{\mathcal{N}_0} \right) \frac{\mathcal{M}^2(P_2 |h_{r,d}^\tau|^2, \zeta) \left(1 - \Psi \left(\frac{P_1 |h_{s,r}^\tau|^2}{\mathcal{N}_0} \right) \right)^2}{\Gamma(P_1 |h_{s,r}^\tau|^2, P_2 |h_{r,d}^\tau|^2)} \right]. \quad (5.105)$$

By averaging over the channel realization, we obtain

$$\begin{aligned} P_{BER}^{(2)} + P_{BER}^{(3)} &\geq \frac{1}{\sigma_{s,r}^2} \int_0^\infty \left[\frac{1}{16\pi} \int_{-\pi}^\pi \frac{f_2(\theta) s(u, \theta)}{1 + \alpha(\theta) \frac{P_1 \sigma_{s,d}^2}{\mathcal{N}_0}} d\theta \right] \exp(-u/\sigma_{s,r}^2) du. \\ &\triangleq \text{LB}\{P_{BER}^{(2)} + P_{BER}^{(3)}\} \end{aligned} \quad (5.106)$$

where

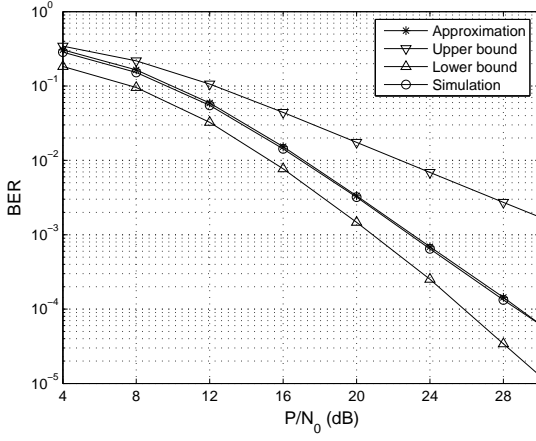
$$s(u, \theta) = \frac{1}{\sigma_{r,d}^2} \int_0^\infty \frac{\mathcal{M}^2(P_2 q, \zeta) \left(1 - \Psi \left(\frac{P_1 u}{\mathcal{N}_0} \right) \right)^2}{\Gamma(P_1 u, P_2 q)} \exp\left(-\frac{\alpha(\theta) P_2 q}{\mathcal{N}_0} - \frac{q}{\sigma_{r,d}^2}\right) dq. \quad (5.107)$$

Since the exact BER formulations under the scenarios 4, 5, and 6 are currently unavailable, and the chances that these three scenarios happen are small at high SNR, we further lower bound the BER $P_{BER}^{(4)}$, $P_{BER}^{(5)}$, and $P_{BER}^{(6)}$ by 0. As a result, the BER of the proposed differential DF scheme can be lower bounded by

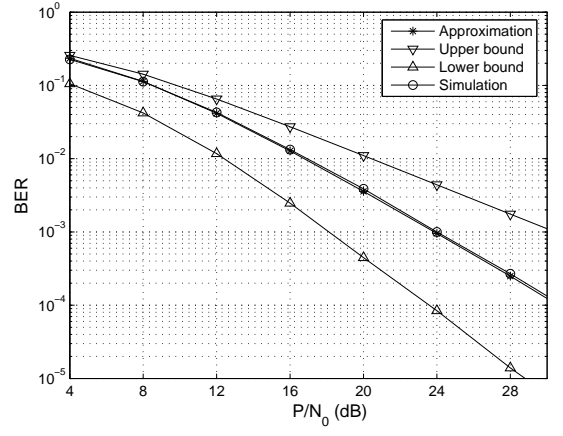
$$P_{BER} \geq P_{BER}^{(1)} + \text{LB}\{P_{BER}^{(2)} + P_{BER}^{(3)}\}, \quad (5.108)$$

where $P_{BER}^{(1)}$ is determined in (5.87).

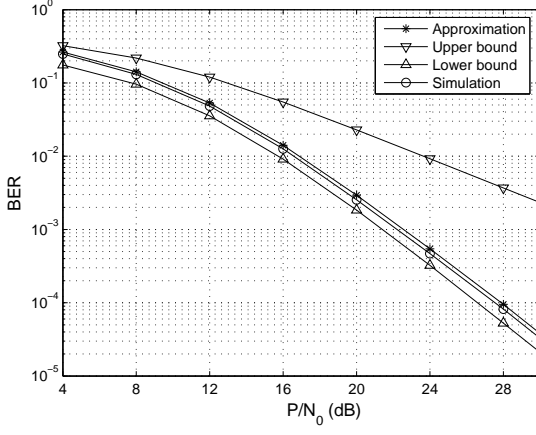
In Figure 5.8, we compare the BER approximation (5.102), the BER upper bound (5.103), and the BER lower bound (5.108) with the simulated performance in case of DQPSK modulation. In Figures 5.8(a)-5.8(c), we consider the differential DF cooperation system with $\sigma_{s,d}^2 = \sigma_{s,r}^2 = \sigma_{r,d}^2 = 1$, i.e., all the channel links have the same qualities. From the figures, we can see that the approximate BER closely matches with the simulated BER, and both the approximate BER and the simulated BER lie between the BER upper bound and the BER lower



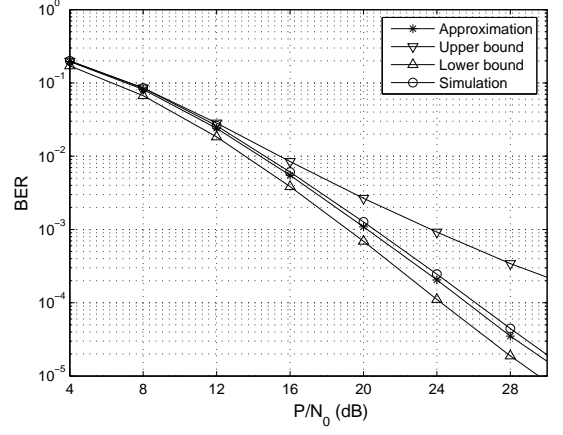
(a) $P_1 = 0.5P, P_2 = 0.5P, \zeta = 1, \sigma_{r,d}^2 = 1.$



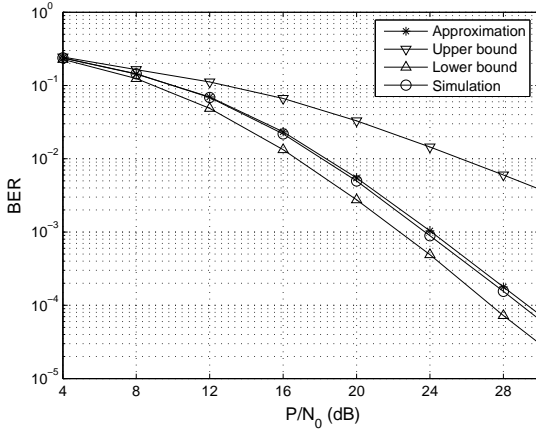
(d) $P_1 = 0.5P, P_2 = 0.5P, \zeta = 1, \sigma_{r,d}^2 = 10.$



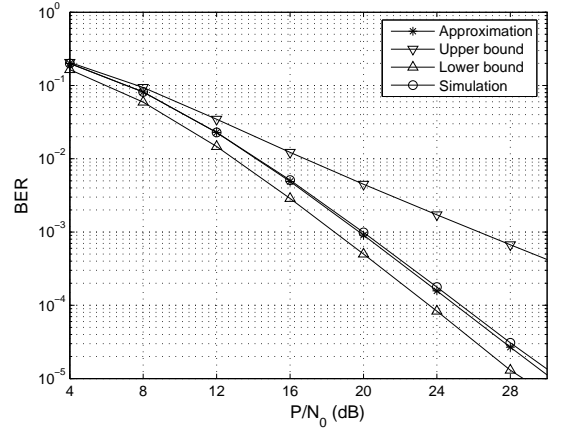
(b) $P_1 = 0.8P, P_2 = 0.2P, \zeta = 1, \sigma_{r,d}^2 = 1.$



(e) $P_1 = 0.5P, P_2 = 0.5P, \zeta = 2, \sigma_{r,d}^2 = 10.$



(c) $P_1 = 0.8P, P_2 = 0.2P, \zeta = 2, \sigma_{r,d}^2 = 1.$



(f) $P_1 = 0.8P, P_2 = 0.2P, \zeta = 2, \sigma_{r,d}^2 = 10.$

Figure 5.8: DQPSK: BER performance versus P/\mathcal{N}_0 : $\sigma_{s,d}^2 = 1, \sigma_{s,r}^2 = 1.$

bound. Moreover, the system performance depends on the power allocation and the threshold. By choosing proper power allocation and threshold, not only the BER performance improves, but also the lower bound is closer to the simulated performance. For example, considering a system with threshold of $\zeta = 1$ and total transmit power $P_1 + P_2 = P$ where P_1 and P_2 are transmitted power of the source and the relay, respectively. By changing the power allocation from $P_1/P = 0.5$ to $P_1/P = 0.8$ the BER performance is improved by 1 dB at a BER of 10^{-4} , while the performance gap between the simulated BER and the BER lower bound is reduced by 2 dB at the same BER. This result follows the fact that when the threshold ζ is appropriately chosen, the scenarios Φ_3 to Φ_6 occur with much smaller probability than the scenarios Φ_1 and Φ_2 . Even though the BER under each of the scenarios Φ_3 to Φ_6 is larger than that under the scenarios Φ_1 or Φ_2 , the average BER $P_{BER}^{(i)}$, $i = 3, \dots, 6$ are smaller. The BER P_{BER} is dominated by the BER under scenarios Φ_1 and Φ_2 . Therefore, the performance gaps between the bounds and the approximate BER is small if the threshold is properly designed.

We have the same observation in Figures 5.8(d)-5.8(f) for a system with $\sigma_{s,d}^2 = 1$, $\sigma_{s,r}^2 = 1$, and $\sigma_{r,d}^2 = 10$. At a threshold of $\zeta = 1$, the performance can be improved by allocating more power at the source and less power at the relay. This is in agreement with the results in [93] which illustrate that the channel link between source and relay and the channel link between relay and destination should be balanced in order to achieve a performance diversity of two. Interestingly, by choosing a proper threshold, the performance can be significantly improved, regardless of the power allocation. For instance, increasing the threshold from 1 to 2, the performance of the proposed scheme with equal power allocation improves 4 dB at a BER of 10^{-4} . At the threshold of $\zeta = 2$, by changing the power allocation

from $P_1/P = 0.5$ to $P_1/P = 0.8$, the system performance is further improved by only 0.5 dB at the same BER. This implies that the effect of the threshold dominates; the performance does not severely depend on the power allocation after the threshold is properly designed.

Another observation obtained from Figure 5.8 is that the threshold depends on the channel link qualities. To be specific, the threshold should be increased as the link quality between the relay and the destination increases. For example, under the scenario $\sigma_{s,d}^2 = \sigma_{s,r}^2 = 1$, the threshold $\zeta = 1$ results in superior performance in case of $\sigma_{r,d}^2 = 1$ while the threshold $\zeta = 2$ leads to better performance in case of $\sigma_{r,d}^2 = 10$. This observation can be explained as follows. When the link quality between the relay and the destination is good, i.e., the channel variance is high, the received signal from the relay tends to have large energy if it carries the information. As a result, by increasing the threshold from 1 to 2, we reduce the chance that the received signal whose amplitude is larger than the threshold contains no information. Thus, with threshold of 2, the received signals from the relay and the destination are efficiently combined, and hence resulting in better performance.

5.2.4 Optimum Decision Threshold and Power Allocation

As we observe in simulation results in the previous section, the choice of power allocation and threshold ζ affect the performance a lot; we determine in this section an optimum decision threshold and an optimum power allocation for the proposed differential DF cooperation system based on the tight BER approximation in (5.102). To simplify the notation, let us denote $r = P_1/P$ as the power ratio of the transmitted power at the source (P_1) over the total power (P). For a fixed total transmitted power $P_1 + P_2 = P$, we are going to jointly optimize

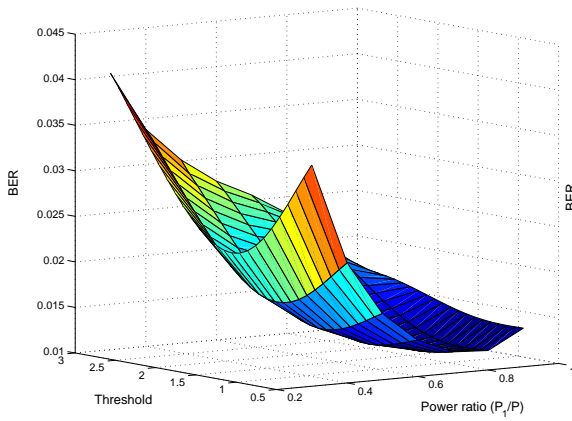
the threshold ζ and the power ratio r such that the tight BER approximation in (5.102) is minimized. The optimization problem can be formulated as

$$\min_{\zeta, r} P_{BER}(\zeta, r), \quad (5.109)$$

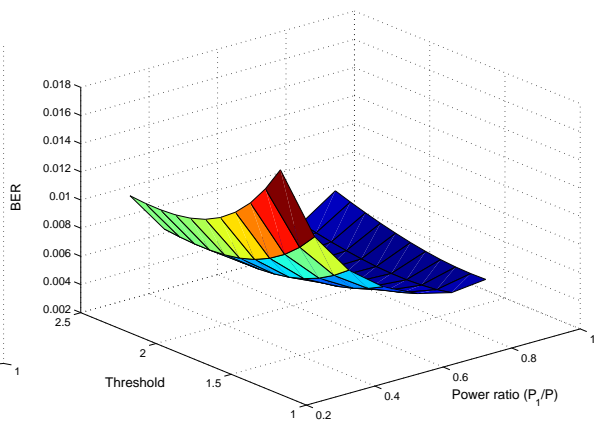
where $P_{BER}(\zeta, r)$ represents the BER approximation with $P_1 = rP$ and $P_2 = (1 - r)P$.

Figure 5.9 shows the BER performance of the proposed scheme with DQPSK signals as a function of power allocation and threshold. In Figures 5.9(a)-5.9(c), we consider the case when the channel variances of all communication links are equal, i.e., $\sigma_{s,d}^2 = \sigma_{s,r}^2 = \sigma_{r,d}^2 = 1$. The BER approximation is plotted in Figure 5.9(a) and its cross sections are shown in Figure 5.9(b) and 5.9(c) together with the simulated BER curves. Based on the approximate BER in Figure 5.9(a), the jointly optimum power allocation and decision threshold are $r = 0.7$ and $\zeta = 1$. Figure 5.9(b) compares the cross sectional curve of the approximate BER with $r = 0.7$ with the simulated BER. We can see that the approximate BER is close to the simulated BER. Furthermore, the proposed scheme with any threshold less than 1.5 yields almost the same BER performance, and the performance significantly degrades as the threshold increases more than 1.5. This is because as the threshold increases, the chances that the scenarios Φ_4 to Φ_6 occur increases, and hence the average BER is dominated by the BER under these scenarios. Figure 5.9(c) depicts the approximate and simulated BER curves as functions of power allocation in case of the decision threshold $\zeta = 1$. We can obviously see that the power ratio of $r = 0.7$ results in the optimum performance.

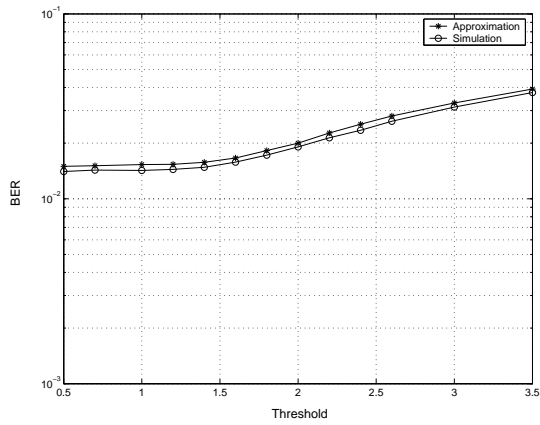
In Figures 5.9(d)-5.9(f), we consider the case of channel variances $\sigma_{s,d}^2 = 1$, $\sigma_{s,r}^2 = 1$, $\sigma_{r,d}^2 = 10$. Figure 5.9(d) depicts the BER of the proposed scheme as a function of the power allocation r and the decision threshold ζ . In this scenario,



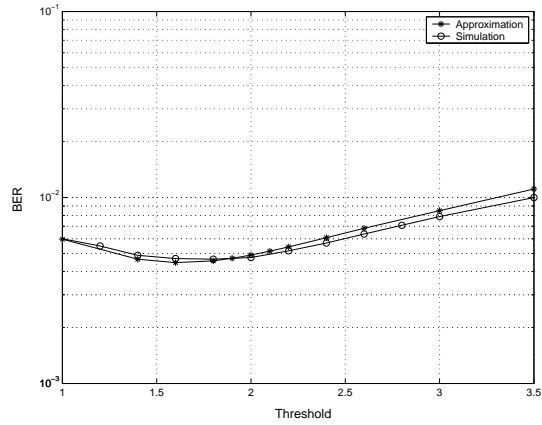
(a) Jointly optimum ζ and r .



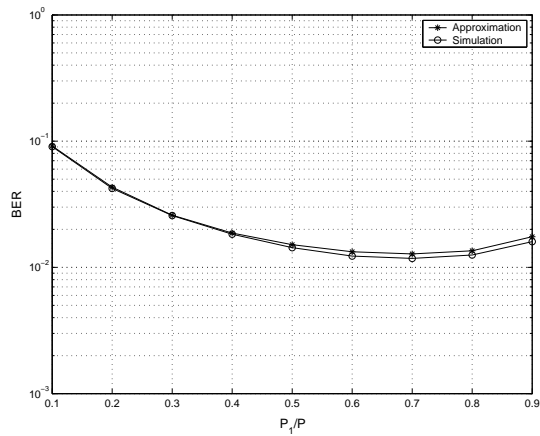
(d) Jointly optimum ζ and r .



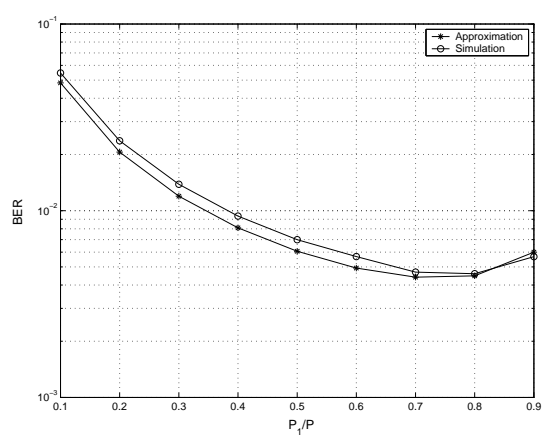
(b) Vary ζ , $P_1 = 0.7P$ and $P_2 = 0.3P$.



(e) Vary ζ , $P_1 = 0.8P$ and $P_2 = 0.2P$.



(c) Vary r , $\zeta = 1$.



(f) Vary r , $\zeta = 1.7$.

Figure 5.9: DQPSK: Performance comparison of theoretical BER curves and simulated curves.

(a)-(c) $\sigma_{s,d}^2 = \sigma_{s,r}^2 = \sigma_{r,d}^2 = 1$. (d)-(f) $\sigma_{s,d}^2 = 1$, $\sigma_{s,r}^2 = 1$, $\sigma_{r,d}^2 = 10$.

we can see that the jointly optimum power allocation and decision threshold are $r = 0.8$ and $\zeta = 1.7$. Figure 5.9(e) shows a cross sectional curve of the approximate BER in Figure 5.9(d) at $r = 0.8$ together with the simulated BER performance of the cooperation system with the same power allocation. We can see that the approximate BER closely matches to the simulated BER for every threshold value. According to both the simulated BER and the approximate BER, the optimum threshold for this case is about 1.7. We show in Figure 5.9(f) a comparison of the approximate BER and the simulated BER with decision threshold $\zeta = 1.7$ under different power allocation. Clearly, the approximate BER follows the same trend as the simulated BER, and the optimum power allocation is $r = 0.8$ for the differential DF system with decision threshold $\zeta = 1.7$.

5.2.5 Simulation Results

We consider a two-user cooperation system employing the DF protocol. The channel fading coefficients are modeled according to the Jakes' model [66] with the Doppler frequency $f_D = 75 \text{ Hz}$ and normalized fading parameter $f_D T_s = 0.0025$ where T_s is the sampling period. The noise variance is $\mathcal{N}_0 = 1$. The DQPSK modulation is used in all simulations. We plot the BER performance curves as functions of P/\mathcal{N}_0 , where P is the total transmitted power. We assume that the power allocation at the source node and relay node are fixed at $P_1 + P_2 = P$.

Figure 5.10 compares the performance of the proposed threshold-based differential DF scheme to that of the differential DF scheme without threshold at the destination and that of the differential DF scheme that the relay always forwards the decoded symbols to the destination. We consider the system with power allocation $P_1 = 0.5P$, $P_2 = 0.5P$, and channel variances $\sigma_{s,d}^2 = 1$, $\sigma_{s,r}^2 = 1$, and $\sigma_{r,d}^2 = 10$. We can see that the proposed differential DF scheme outperforms the other two

schemes. The reason is that a decoding error at the relay tends to result in an error at the destination. Hence, the performance of the differential DF scheme in which all the decoded symbols at the relay are forwarded is worse than that of the proposed scheme. In particular, the performance degradation of 11 dB can be observed at a BER of 10^{-3} . Adding a threshold at the destination can reduce the chance that the incorrectly decoded signal from the relay is combined to the signal from the source. Therefore, the proposed scheme yields superior performance to the differential DF scheme without threshold. As shown in Figure 5.10, the proposed scheme yields about 4 dB gain at a BER of 10^{-3} compared to the scheme without threshold. We also show the performance of coherent DF scheme in which the relay forwards only the correctly decoded symbols. Such scheme is the coherent counterpart of both the proposed differential DF scheme and the differential DF scheme without threshold. The proposed scheme shows 5 dB performance gap in comparison to its coherent counterpart, but the differential scheme without a decision threshold losses about 9 dB in comparison to its coherent counterpart at a BER of 10^{-3} .

Figures 5.11(a) and 5.11(b) illustrate the BER performances of the proposed scheme with different thresholds. In Figure 5.11(a), the power allocation is $P_1 = 0.7P$ and $P_2 = 0.3P$, and the channel variances are $\sigma_{s,d}^2 = \sigma_{s,r}^2 = \sigma_{r,d}^2 = 1$. We can see that the proposed scheme achieves the performance diversity of two at high SNR for any threshold. However, the performance degrades as the threshold increases. Figure 5.11(b) shows the BER performance in case of power allocation $P_1 = 0.7P$ and $P_2 = 0.3P$, and channel variances $\sigma_{s,d}^2 = 1$, $\sigma_{s,r}^2 = 1$, and $\sigma_{r,d}^2 = 10$. Obviously, different thresholds result in different BER performances. The threshold of $\zeta = 1.7$ provides the best performance in this scenario. Furthermore, if the threshold is too

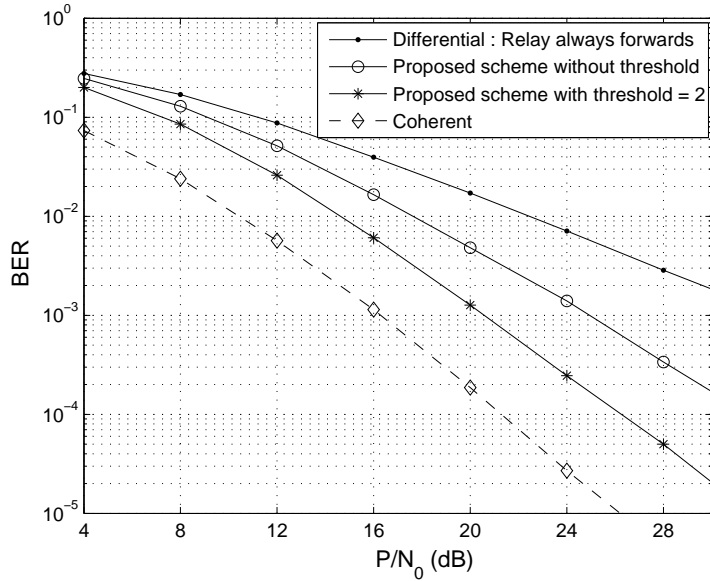


Figure 5.10: DQPSK with or without CRC at relay node, and with or without threshold at destination node, $P_1 = P_2 = 0.5P$, $\sigma_{s,d}^2 = 1$, $\sigma_{s,r}^2 = 1$, $\sigma_{r,d}^2 = 10$.

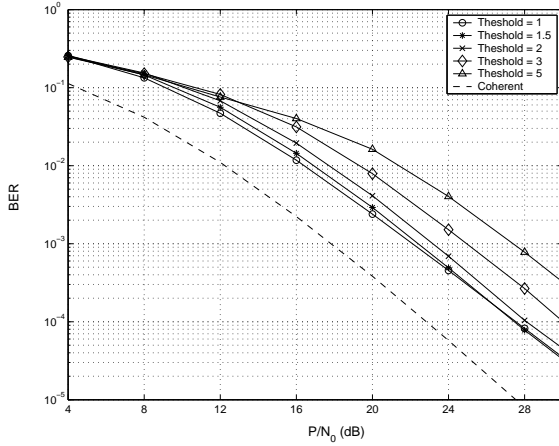
small, e.g. $\zeta = 1$, not only the BER performance degrades but also the diversity order is less than two. This is because when the threshold is small, the destination tends to combine the signals from both the relay and the destination. As a result, the incorrect decoding at the relay leads to significant performance degradation at the destination.

In Figures 5.12(a) and 5.12(b), we study the effect of power allocation on the BER performance for the proposed scheme with a fixed threshold. In Figure 5.12(a), we consider the cooperation system with channel variances $\sigma_{s,d}^2 = \sigma_{s,r}^2 = \sigma_{r,d}^2 = 1$ and a threshold $\zeta = 2$. We can see that the power ratios $r = P_1/P = 0.5, 0.6$, and 0.7 yield almost the same performances. When the power ratio increases to $r = 0.9$, the performance degradation is about 2 dB at BER of 10^{-4} compared to the equal power allocation scheme. This is due to the fact that at $r = 0.9$, small power is allocated at the relay. Consequently, even though the received signal from the relay carries an information, there is high

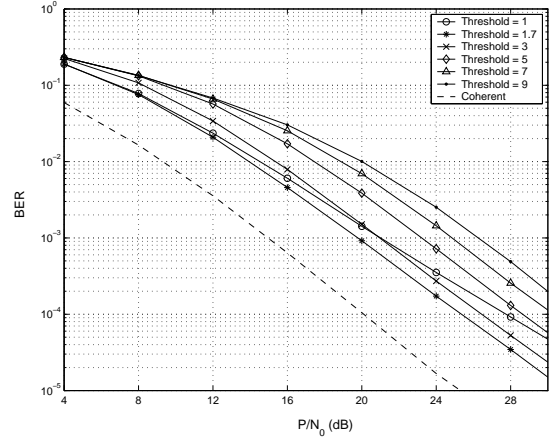
chance that its amplitude is smaller than the threshold, and hence the detection is based only on the received signal from the direct link. Figure 5.12(b) depicts the performance in case of channel variances $\sigma_{s,d}^2 = 1$, $\sigma_{s,r}^2 = 1$, and $\sigma_{r,d}^2 = 10$, and a threshold $\zeta = 1$. We can see that the performance improves as the power ratio increases from $r = 0.5$ to $r = 0.9$. The reason is that the relay-destination link is of high quality while the threshold is small. With only small power at the relay, the amplitude of the received signal from the relay can be larger than the threshold. Therefore, by allocating more power at the source, we not only increase the chance of correct decoding at the relay, but also increase the SNR of the MRC output. Based on the numerical results in 5.9(d), the optimum power ratio for this scenario is $r = 0.9$ at the SNR of $P/N_0 = 16$ dB. Clearly, the simulation results in Figure 5.12(b) agree with the numerical results at the SNR of 16 dB. Moreover, Figure 5.12(b) illustrates that the power ratio of $r = 0.9$ results in optimum performance for the entire SNR range. At the threshold $\zeta = 1$, the proposed scheme with optimum power allocation achieves about 5 dB improvement over that with equal power allocation at a BER of 10^{-4} .

Figures 5.13(a) and 5.13(b) compare the performances of the proposed differential DF scheme with different power allocation and decision threshold. We consider the case of $\sigma_{s,d}^2 = \sigma_{s,r}^2 = \sigma_{r,d}^2 = 1$ in Figure 5.13(a), and the case of $\sigma_{s,d}^2 = \sigma_{s,r}^2 = 1$, and $\sigma_{r,d}^2 = 10$ in Figure 5.13(b). From both figures, it is clear that the proposed scheme with jointly optimum power allocation and optimum threshold yield the best performance over the entire SNR range. In case of equal link qualities, i.e., $\sigma_{s,d}^2 = \sigma_{s,r}^2 = \sigma_{r,d}^2 = 1$, optimum power allocation and optimum threshold yields 2 dB performance improvement at a BER of 10^{-4} compared to the scheme with equal power allocation and without threshold. In addition, if the power allocation

is optimum, the scheme without threshold yields almost the same performance as that with optimum threshold. When the quality of the relay-destination link is very good, e.g. $\sigma_{r,d}^2 = 10$, the use of optimum threshold is more important than the use of optimum power allocation at high SNR. Specifically, by properly choosing the threshold, the proposed differential DF scheme achieves almost the same performance for any power allocation at high SNR. As we can see from Figure 5.13(b), in case of equal power allocation, using the optimum threshold leads to more than 5 dB improvement gain over the scheme without threshold at a BER of 10^{-4} . With optimum threshold, the performance difference between the proposed scheme with optimum power allocation and that with equal power allocation is only about 0.5 dB at a BER of 10^{-4} .

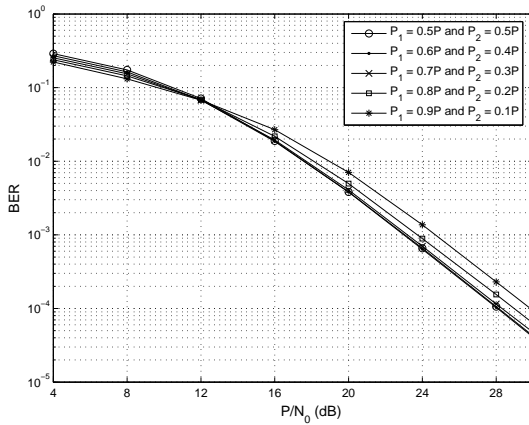


(a) $r = 0.7, \sigma_{s,d}^2 = \sigma_{s,r}^2 = \sigma_{r,d}^2 = 1.$

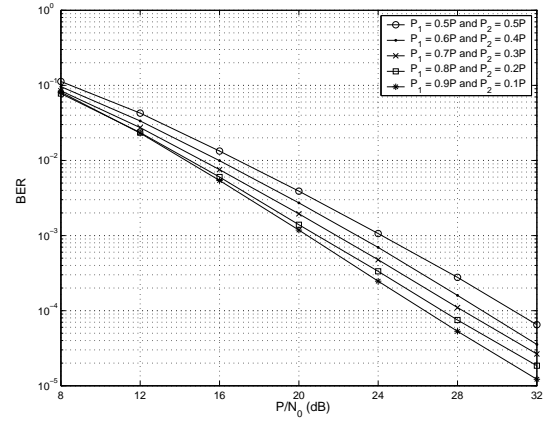


(b) $r = 0.8, \sigma_{s,d}^2 = \sigma_{s,r}^2 = 1, \sigma_{r,d}^2 = 10.$

Figure 5.11: DQPSK: Different thresholds with fixed power allocation.

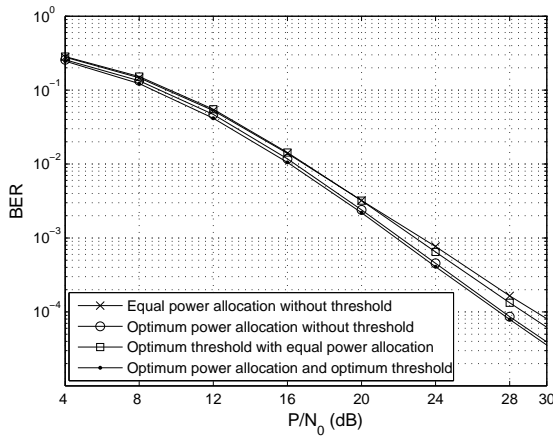


(a) $\zeta = 2, \sigma_{s,d}^2 = \sigma_{s,r}^2 = \sigma_{r,d}^2 = 1.$

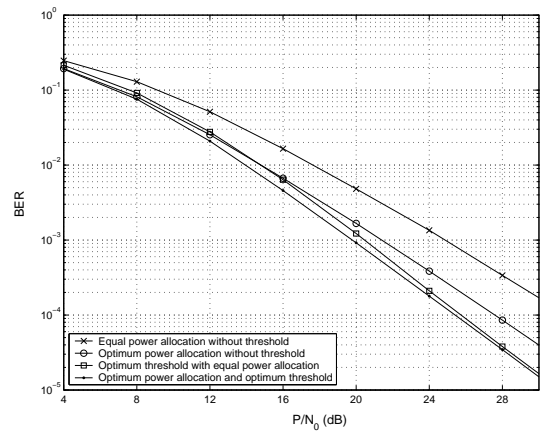


(b) $\zeta = 1, \sigma_{s,d}^2 = \sigma_{s,r}^2 = 1, \sigma_{r,d}^2 = 10.$

Figure 5.12: DQPSK: Different power allocations with fixed threshold.



(a) $\sigma_{s,d}^2 = \sigma_{s,r}^2 = \sigma_{r,d}^2 = 1.$



(b) $\sigma_{s,d}^2 = \sigma_{s,r}^2 = 1, \sigma_{r,d}^2 = 10.$

Figure 5.13: DQPSK: Different power allocations and different thresholds.

5.3 Chapter Summary

We proposed, in this Chapter, differential modulation schemes for two-user cooperative communication systems.

In the first part of the Chapter, we proposed a differential scheme for amplify-and-forward protocol in cooperative communications systems. The proposed scheme with DQPSK signals provided 4 dB performance improvement at a BER of 10^{-3} over that of DBPSK direct transmission scheme. In comparison to the coherent detection without relay, the proposed scheme provided a practical alternative with lower complexity and simpler implementation. In addition, simulation results showed that the performance of the proposed scheme was superior to that of direct transmission with coherent detection at SNRs higher than 21 dB. This is due to the fact that the cooperative communications provide more diversity gain than the direct transmission schemes. While the BER analysis of the proposed scheme is not available currently, we provided the exact BER expression based on optimum combining weights, and it is considered as a performance benchmark for our proposed scheme. By using the obtained optimum power allocation based on the provided BER expression, the proposed scheme is able to achieve comparable performance to the scheme with optimum weights in any channel variances of all links. Moreover, the performance with optimum power strategy outperforms that from equal power scheme of about 1.4 dB at a BER of 10^{-3} .

In the second part of the Chapter, we proposed a threshold-based differential decode-and-forward scheme for cooperative communication systems. By allowing the relay forward only the correctly decoded symbols and introducing a decision threshold at the destination node, the proposed scheme efficiently combines the signals from the direct and the relay links. We provided BER analysis of the

proposed scheme with DMPSK modulation by categorizing six different scenarios that lead to different instantaneous SNR's at the combiner output of the destination. A tight BER approximation is also provided. Based on the tight BER approximation, we determine the optimum decision threshold and power allocation numerically. Both theoretical and simulation results revealed that the optimum threshold and optimum power allocation rely on the qualities of the channel links. When the quality of the relay-destination link is much larger than the other links, i.e., $\sigma_{s,d}^2 = \sigma_{s,r}^2 = 1$ and $\sigma_{r,d}^2 = 10$, then the decision threshold is more important than the power allocation at high SNR. For instance, in case of DQPSK signals with equal power allocation, using the optimum threshold resulted in more than 5 dB improvement gain over the scheme without threshold at a BER of 10^{-4} . By further using the optimum power allocation, the performance improvement is about 0.5 dB at the same BER. Simulation results also showed that the proposed scheme with DQPSK signals provides 11 dB performance improvement at a BER of 10^{-3} over the differential DF scheme that the relay always forwards the decoded symbols.

Chapter 6

Differential Modulations for Multi-Node Cooperative Communications

In this Chapter, we propose differential modulation schemes for multi-node cooperative communication systems. In the first part of this Chapter, Section 6.1, we consider a differential modulation for a cooperation system that employs amplify-and-forward protocol. In the second part part of this Chapter, Section 6.2, we consider a differential modulation scheme for a cooperation system with decode-and-forward protocol. Finally, Section 6.3 conclusions are given.

6.1 Differential Modulation for Multi-Node Amplify-and-Forward Cooperative Communications

In this Section, we propose a differential scheme for multi-node amplify-and-forward cooperative communications. In the proposed scheme, the destination requires only long-term average of the received signals to efficiently combines signals from all communications links. As a performance benchmark, we provide an exact BER formulation of the optimum-combining cooperation system using dif-

ferential M-ary phase shift keying (DMPSK) signals. In order to obtain analytical result for optimum power allocation scheme which is not available in [99] even for a two-user scenario, we provide BER upper bounds and simple BER approximations. Based on the tight BER approximation, closed-form optimum power allocation is evaluated, and then used to further improve the performance of the proposed scheme. Simulation results are shown to validate our proposed schemes and support our theoretical analysis.

The rest of this Section is organized as follows. Section 6.1.1 outlines the differential scheme for multi-node cooperative communications. In Section 6.1.2, we provide BER formulation of the proposed scheme based on the optimum combining. Also in this section, we provide BER upper bound and BER lower bound together with their simple approximations. Optimum power allocation of the proposed scheme is investigated in Section 6.1.3. We show some simulation results in Section 6.1.4. Finally, Section 6.3 summarizes the proposed scheme.

6.1.1 Multi-Node AF Differential Scheme

We consider a multi-node cooperative wireless network with a source and N relays, as shown in Figure 6.1. Each node in the network can be a source that sends information to its destination, or it can be a relay that helps transmit information of others. We consider a cooperation strategy based on amplify-and-forward protocol [19] in which each relay amplifies the received signal from the source and then forwards it to the destination. Specifically, for a cooperation system with a source and N relays, signal transmissions of the considered cooperation system comprise $N + 1$ phases. In Phase 1, the source node transmits information to its intended destination. Due to the broadcasting nature of the wireless network, the information is also received by the relays. In Phases 2 to $N + 1$, each relay

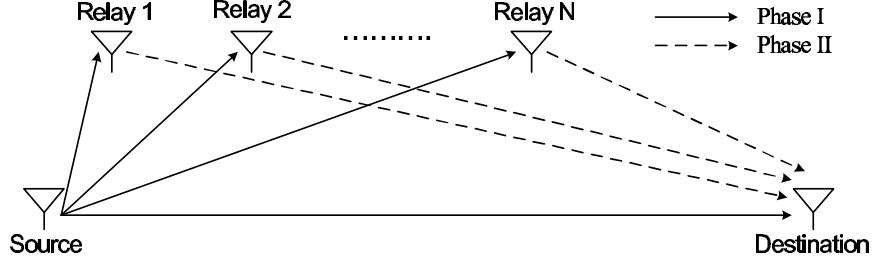


Figure 6.1: Multi-node differential AF scheme.

amplifies the received signal and forward it to the destination. In all phases, we assume that all signals are transmitted through orthogonal channels by the use of existing schemes such as TDMA, FDMA [19], or CDMA [21]- [22].

Suppose the DMPSK modulation is used, i.e., the information is conveyed in the phase difference between two consecutive symbols. The modulated information at the source in Phase 1 can be described as $v_m = e^{j\phi_m}$, where $\phi_m = 2\pi m/M$ for $m = 0, 1, \dots, M - 1$, and M is the constellation size. The source differentially encodes the information symbol v_m as

$$x^\tau = v_m x^{\tau-1}, \quad (6.1)$$

where τ is the time index, and x^τ is the differentially encoded symbol to be transmitted at time τ . Then the source transmits x^τ with transmitted power P_s to the destination and the relays. The corresponding received signals at the destination and the i^{th} relay, $i = 1, 2, \dots, N$, can be expressed as

$$y_{s,d}^\tau = \sqrt{P_s} h_{s,d}^\tau x^\tau + w_{s,d}^\tau, \quad (6.2)$$

and

$$y_{s,r_i}^\tau = \sqrt{P_s} h_{s,r_i}^\tau x^\tau + w_{s,r_i}^\tau. \quad (6.3)$$

where $h_{s,d}^\tau$ and h_{s,r_i}^τ represent channel coefficients from the source to the destination and from the source to the i^{th} relay, respectively. The terms $w_{s,d}^\tau$ and w_{s,r_i}^τ are

additive white Gaussian noise at the destination and the i^{th} relay, respectively.

In Phases 2 to $N + 1$, each relay amplifies the received signal in (6.63) and forwards it to the destination with transmit power P_i . Accordingly, the received signal at the destination from the i^{th} relay is given by

$$y_{r_i,d}^\tau = \frac{\sqrt{P_i}}{\sqrt{P_s \sigma_{s,r_i}^2 + \mathcal{N}_0}} h_{r_i,d}^\tau y_{s,r_i}^\tau + w_{r_i,d}^\tau, \quad (6.4)$$

where $h_{r_i,d}^\tau$ is the channel coefficient from the i^{th} relay to the destination, and $w_{r_i,d}^\tau$ is additive noise at the destination. Consider the case of independent Rayleigh fading channels, then the channel coefficients $h_{s,d}^\tau$, h_{s,r_i}^τ , and $h_{r_i,d}^\tau$ are modeled as independent zero-mean complex Gaussian random variables with variances $\sigma_{s,d}^2$, σ_{s,r_i}^2 , and $\sigma_{r_i,d}^2$, respectively. All the noise terms $w_{s,d}^\tau$, w_{s,r_i}^τ , and $w_{r_i,d}^\tau$ are modeled as independent complex Gaussian random variables, each with zero mean and variance \mathcal{N}_0 . The scheme does not require the instantaneous channel state information at either the relays or the destination. Observe from (6.4) that the transmitted power at the relay is normalized by $P_s \sigma_{s,r_i}^2 + \mathcal{N}_0$, which implies that only the channel variance between the source and relay i , σ_{s,r_i}^2 , is required at relay i . In practice, such information can be obtained through long term averaging of the received signal from the source to the i^{th} relay.

At the destination, the received signal from the source and the relays are combined and then used to estimate the transmitted information. All channel coefficients $h_{s,d}^\tau$, h_{s,r_i}^τ , and $h_{r_i,d}^\tau$ are unknown to either the relays or the destination, but they are assumed almost constant over two symbol periods such that the destination can use the received signal in the previous time slot as channel estimate. Based on the received signals from the direct link ($y_{s,d}^\tau$) in Phase 1 and that from all of the relay links ($y_{r_i,d}^\tau$) in Phases 2 to $N + 1$, the combined signal at the destination

can be written as

$$y = a_s (y_{s,d}^{\tau-1})^* y_{s,d}^\tau + \sum_{i=1}^N a_i (y_{r_i,d}^{\tau-1})^* y_{r_i,d}^\tau, \quad (6.5)$$

where a_s and a_i are combining weights. To maximize the SNR of the combiner output, the combining weights can be determined as

$$a_s = \frac{1}{\mathcal{N}_0}, \quad (6.6)$$

$$a_i = \frac{P_s \sigma_{s,r_i}^2 + \mathcal{N}_0}{\mathcal{N}_0 (P_s \sigma_{s,r_i}^2 + P_i \sigma_{r_i,d}^2 + \mathcal{N}_0)}. \quad (6.7)$$

Here, the channel variances between the relays and the destination, $\sigma_{r_i,d}^2$, and channel variances between the source and the relays, σ_{s,r_i}^2 , are assumed available at the destination. The channel variances $\sigma_{r_i,d}^2$ can be obtained through long term averaging of the received signals at the destination, whereas the channel variances σ_{s,r_i}^2 can be forwarded from the relays to the destination over reliable channel links. Without acquiring perfect channel state information, the combined signal (6.5) is differentially decoded by using the detection rule

$$\hat{m} = \arg \max_{m=0,1,\dots,M-1} \text{Re} \{v_m^* y\}. \quad (6.8)$$

6.1.2 BER Performance Analysis for the Multi-Node AF Differential Scheme

We provide in this section BER performance analysis based on optimum combining weights in [89], and it will be considered as BER performance benchmark for the proposed scheme.

From (6.5), the optimum combining weights can be determined as

$$\hat{a}_s = \frac{1}{\mathcal{N}_0}, \quad (6.9)$$

and

$$\hat{a}_i = \frac{P_s \sigma_{s,r_i}^2 + \mathcal{N}_0}{\mathcal{N}_0 (P_s \sigma_{s,r_i}^2 + P_i |h_{r_i,d}^\tau|^2 + \mathcal{N}_0)}. \quad (6.10)$$

Note that the optimum combining weights (6.10) requires the knowledge of instantaneous channel information which is not available in the proposed scheme. However, the BER analysis based on these combining weights is used as BER performance benchmark of our proposed scheme. We will show an interesting observation in Section 6.1.4 that the BER performance of our proposed scheme yields very close to the BER performance benchmark when optimum power allocation is applied.

Using the optimum combining weights \hat{a}_s and \hat{a}_i , an instantaneous SNR at the combiner output is given by

$$\gamma = \gamma_s + \sum_{i=1}^N \gamma_i, \quad (6.11)$$

where

$$\gamma_s = \frac{P_s |h_{s,d}^\tau|^2}{\mathcal{N}_0}, \quad (6.12)$$

and

$$\gamma_i = \frac{P_s P_i |h_{s,r_i}^\tau|^2 |h_{r_i,d}^\tau|^2}{\mathcal{N}_0 (P_s \sigma_{s,r_i}^2 + P_i |h_{r_i,d}^\tau|^2 + \mathcal{N}_0)}. \quad (6.13)$$

For a given SNR γ in (6.11), the conditional BER expression for L -channel diversity receptions can be expressed as [88]

$$P_{b|\gamma} = \frac{1}{2^{2L}\pi} \int_{-\pi}^{\pi} f(\theta) \exp[-\alpha(\theta)\gamma] d\theta, \quad (6.14)$$

where

$$f(\theta) = \frac{b^2}{2\alpha(\theta)} \sum_{l=1}^L \binom{2L-1}{L-1} [(\beta^{-l+1} - \beta^{l+1}) \cos((l-1)(\theta + \frac{\pi}{2})) - (\beta^{-l+2} - \beta^l) \cos((l)(\theta + \frac{\pi}{2}))], \quad (6.15)$$

and

$$\alpha(\theta) = \frac{b^2(1 + 2\beta \sin \theta + \beta^2)}{2 \log_2 M}. \quad (6.16)$$

Here, $L = N + 1$, and $\beta = a/b$ in which $a = 10^{-3}$ and $b = \sqrt{2}$ for DBPSK modulation, and $a = \sqrt{2 - \sqrt{2}}$ and $b = \sqrt{2 - \sqrt{2}}$ for DQPSK modulation [88]. For higher constellation sizes, β can be obtained from the results in [3]. Averaging the conditional BER (6.14) over the Rayleigh fading channels by using the moment generating function (MGF) method. The exponential function of the summation of the instantaneous SNR in (6.14) can be written in product form of the MGF of each instantaneous SNR. Specifically, the average BER can expressed as

$$P_b = \frac{1}{2^{2(N+1)}\pi} \int_{-\pi}^{\pi} f(\theta) \mathcal{M}_{\gamma_s}(\theta) \prod_{i=1}^N \mathcal{M}_{\gamma_i}(\theta) d\theta, \quad (6.17)$$

where $\mathcal{M}_{\gamma_\mu}(\theta) = \int_{-\infty}^{+\infty} e^{-\alpha(\theta)\lambda} p_{\gamma_\mu}(\lambda) d\lambda$ represents of the MGF of the instantaneous SNR γ_μ for $\mu \in \{s, 1, \dots, N\}$. In (6.17), $\mathcal{M}_{\gamma_s}(\theta)$ is obtained through an integration over an exponential random variable $|h_{s,d}|^2$ such that

$$\mathcal{M}_{\gamma_s}(\theta) = \frac{1}{1 + k_{s,d}(\theta)}, \quad (6.18)$$

in which

$$k_{s,d}(\theta) \triangleq \alpha(\theta) P_s \sigma_{s,d}^2 / \mathcal{N}_0. \quad (6.19)$$

The MGF $\mathcal{M}_{\gamma_i}(\theta)$ in (6.17) can be obtained through integrations over two exponential random variables $|h_{s,r_i}|^2$ and $|h_{r_i,d}|^2$. By first averaging over $|h_{s,r_i}|^2$ and then averaging over $|h_{r_i,d}|^2$, we have

$$\mathcal{M}_{\gamma_i}(\theta) = \frac{1}{\sigma_{r_i,d}^2} \int_0^\infty \Omega_i(\theta) \exp\left(-\frac{u}{\sigma_{r_i,d}^2}\right) du, \quad (6.20)$$

where

$$\Omega_i(\theta) = \frac{\mathcal{N}_0 (P_i u + P_s \sigma_{s,r_i}^2 + \mathcal{N}_0)}{\mathcal{N}_0 (P_i u + P_s \sigma_{s,r_i}^2 + \mathcal{N}_0) + \alpha(\theta) P_s P_i \sigma_{s,r_i}^2 u}. \quad (6.21)$$

By denoting

$$k_{s,r_i}(\theta) \triangleq \alpha(\theta) P_s \sigma_{s,r_i}^2 / \mathcal{N}_0, \quad (6.22)$$

and $\hat{k}_{s,r_i}(\theta) \triangleq P_i(1 + k_{s,r_i}(\theta))$, we can rewrite $\Omega_i(\theta)$ in (6.21) as

$$\begin{aligned} \Omega_i(\theta) &= \frac{P_i u + P_s \sigma_{s,r_i}^2 + \mathcal{N}_0}{\hat{k}_{s,r_i}(\theta) u + P_s \sigma_{s,r_i}^2 + \mathcal{N}_0} \\ &= \frac{1}{1 + k_{s,r_i}(\theta)} + \frac{1 - 1/[1 + k_{s,r_i}(\theta)]}{1 + \hat{k}_{s,r_i}(\theta) u / (P_s \sigma_{s,r_i}^2 + \mathcal{N}_0)}. \end{aligned} \quad (6.23)$$

Substituting (6.23) into (6.20), we have

$$\mathcal{M}_{\gamma_i}(\theta) = \frac{1}{1 + k_{s,r_i}(\theta)} \left(1 + \frac{k_{s,r_i}(\theta)}{1 + k_{s,r_i}(\theta)} \frac{P_s \sigma_{s,r_i}^2 + \mathcal{N}_0}{P_i} \frac{1}{\sigma_{r_i,d}^2} Z_i(\theta) \right), \quad (6.24)$$

where

$$Z_i(\theta) = \int_0^\infty \frac{\exp(-u/\sigma_{r_i,d}^2)}{u + R_i(\theta)} du, \quad (6.25)$$

and

$$R_i(\theta) \triangleq \frac{P_s \sigma_{s,r_i}^2 + \mathcal{N}_0}{P_i [1 + k_{s,r_i}(\theta)]}, \quad (6.26)$$

in which $k_{s,r_i}(\theta)$ is specified in (6.22). By applying the results from [100] (p. 358 equation 3.352.4 and p. 934 equation 8.212.1), we can express (6.25) in a simple formulation with finite-limit integration as

$$Z_i(\theta) = -e^{\hat{R}_i(\theta)} \left[\mathcal{E} + \ln \hat{R}_i(\theta) + \int_0^{\hat{R}_i(\theta)} \frac{\exp(-t) - 1}{t} dt \right], \quad (6.27)$$

in which $\mathcal{E} = 0.57721566490\dots$ represents the Euler's constant [100], and $\hat{R}_i(\theta) = \frac{R_i(\theta)}{\sigma_{r_i,d}^2}$. Finally, by substituting (6.18) and (6.24) into (6.17), the average BER formulation of the proposed multi-node differential AF scheme can be expressed as

$$P_b = \frac{1}{2^{2(N+1)} \pi} \int_{-\pi}^{\pi} \frac{f(\theta)}{1 + k_{s,d}(\theta)} \prod_{i=1}^N \frac{1}{1 + k_{s,r_i}(\theta)} \left(1 + \frac{k_{s,r_i}(\theta) Z_i(\theta)}{1 + k_{s,r_i}(\theta)} \frac{P_s \sigma_{s,r_i}^2 + \mathcal{N}_0}{P_i \sigma_{r_i,d}^2} \right) d\theta. \quad (6.28)$$

Observe that the BER formulation in (6.28) involves double integration. Although (6.28) can be calculated numerically, it is difficult to get insights. In the sequel, we provide a single-integral BER upper bound, a simple BER upper bound that involves no integration, and two tight BER approximations.

We first determine the BER upper bound and its simple expression as follows. From (6.24), we can see that the BER upper bound can be obtained by bounding $R_i(\theta)$ in the denominator of the integrand of $\mathcal{M}_{\gamma_i}(\theta)$. By substituting θ in (6.16) with $\pi/2$, $\alpha(\theta)$ can be upper bounded by $\alpha(\theta) \leq (b^2(1 + \beta)^2)/2$. Then, $R_i(\theta)$ is lower bounded by

$$R_i(\theta) \geq \frac{P_s \sigma_{s,r_i}^2 + \mathcal{N}_0}{P_i} \left[1 + \frac{P_s \sigma_{s,r_i}^2 b^2 (1 + \beta)^2}{2 \mathcal{N}_0} \right]^{-1} \triangleq R_{i,min}. \quad (6.29)$$

Substituting $R_i(\theta) = R_{i,min}$ into (6.25) results in an upper bound on $Z_i(\theta)$, i.e., $Z_i(\theta) \leq Z_{i,max}$ where

$$\begin{aligned} Z_{i,max} &= \int_0^\infty \frac{\exp(-u/\sigma_{r_i,d}^2)}{u + R_{i,min}} du \\ &= -e^{\hat{R}_{i,min}} \left[\mathcal{E} + \ln \hat{R}_{i,min} + \int_0^{\hat{R}_{i,min}} \frac{\exp(-t) - 1}{t} dt \right], \end{aligned} \quad (6.30)$$

in which $\hat{R}_{i,min} = R_{i,min}/\sigma_{r_i,d}^2$. The simple expression with finite integral in the second equality of (6.30) is obtained in a similar way as that in (6.27) where \mathcal{E} represents the Euler's constant. For a specific channel variance $\sigma_{r_i,d}^2$, the term $Z_{i,max}$ can be simply calculated. By bounding $Z_i(\theta)$ in (6.28) with $Z_{i,max}$, we obtain the BER upper bound

$$P_b \leq \frac{1}{2^{2(N+1)}\pi} \int_{-\pi}^{\pi} \frac{f(\theta)}{1 + k_{s,d}(\theta)} \prod_{i=1}^N \frac{1}{1 + k_{s,r_i}(\theta)} \left(1 + \frac{k_{s,r_i}(\theta) Z_{i,max} P_s \sigma_{s,r_i}^2 + \mathcal{N}_0}{1 + k_{s,r_i}(\theta) P_i \sigma_{r_i,d}^2} \right) d\theta. \quad (6.31)$$

We further simplify the BER upper bound (6.31) to get more insights on the achievable diversity order and simpler BER evaluation. For high enough SNR, all

1's in the denominator of (6.31) can be discarded. After some manipulations, the simple BER upper bound can be expressed as

$$P_b \leq \frac{C(\beta, N) \mathcal{N}_0^{N+1}}{P_s \sigma_{s,d}^2} \cdot \prod_{i=1}^N \frac{P_i \sigma_{r_i,d}^2 + (P_s \sigma_{s,r_i}^2 + \mathcal{N}_0) Z_{i,max}}{P_s P_i \sigma_{s,r_i}^2 \sigma_{r_i,d}^2}, \quad (6.32)$$

where

$$C(\beta, N) = \frac{1}{2^{2(N+1)} \pi} \int_{-\pi}^{\pi} \frac{f(\theta)}{\alpha^{N+1}(\theta)} d\theta \quad (6.33)$$

is a constant that depends on modulation size and number of relays, and $f(\theta)$ and $\alpha(\theta)$ are specified in (6.15) and (6.16), respectively. The BER upper bound in (6.32) reveals that when N relays are available in the network, the diversity order of $N + 1$ can be obtained.

In what follows, we determine two BER approximations in which one of them is an asymptotically tight simple BER approximation. We first note that $\alpha(\theta)$ in (6.16) can be lower bounded by $\alpha(\theta) \geq \alpha(-\pi/2) = (b^2(1 - \beta)^2)/2$. Accordingly, $R_i(\theta)$ can be upper bounded by

$$R_i(\theta) \leq \frac{P_s \sigma_{s,r_i}^2 + \mathcal{N}_0}{P_i} \left[1 + \frac{P_s \sigma_{s,r_i}^2 b^2 (1 - \beta)^2}{2 \mathcal{N}_0} \right]^{-1} \triangleq R_{i,max}. \quad (6.34)$$

By substituting $R_i(\theta) = R_{i,max}$ into (6.25), we get a lower bound on $Z_i(\theta)$, denoted by $Z_{i,min}$:

$$\begin{aligned} Z_{i,min} &= \int_0^{\infty} \frac{\exp(-u/\sigma_{r_i,d}^2)}{[u + R_{i,max}]} du \\ &= -e^{\hat{R}_{i,max}} \left[\mathcal{E} + \ln \hat{R}_{i,max} + \int_0^{\hat{R}_{i,max}} \frac{\exp(-t) - 1}{t} dt \right], \end{aligned} \quad (6.35)$$

in which $\hat{R}_{i,max} = R_{i,max}/\sigma_{r_i,d}^2$ and \mathcal{E} is the Euler's constant. Then, replacing $Z_i(\theta)$ in (6.28) with $Z_{i,min}$, we obtain a BER approximation

$$P_b \gtrsim \frac{1}{2^{2(N+1)} \pi} \int_{-\pi}^{\pi} \frac{f(\theta)}{1 + k_{s,d}(\theta)} \prod_{i=1}^N \frac{1}{1 + k_{s,r_i}(\theta)} \left(1 + \frac{k_{s,r_i}(\theta) Z_{i,min} P_s \sigma_{s,r_i}^2 + \mathcal{N}_0}{1 + k_{s,r_i}(\theta) P_i \sigma_{r_i,d}^2} \right) d\theta. \quad (6.36)$$

Furthermore, by ignoring all 1's in the denominator of (6.36), we get a simpler BER approximation

$$P_b \approx \frac{C(\beta, N) \mathcal{N}_0^{N+1}}{P_s \sigma_{s,d}^2} \cdot \prod_{i=1}^N \frac{P_i \sigma_{r_i,d}^2 + (P_s \sigma_{s,r_i}^2 + \mathcal{N}_0) Z_{i,min}}{P_s P_i \sigma_{s,r_i}^2 \sigma_{r_i,d}^2}, \quad (6.37)$$

where $C(\beta, N)$ and $Z_{i,min}$ are specified in (6.33) and (6.35), respectively. We can see from the exponent of the noise term in (6.37) that the obtained diversity order is $N+1$. We will show in the simulation results that these two BER approximations are tight at high SNR region.

6.1.3 Optimum Power Allocation for Multi-Node AF Differential Scheme

We determine in this section the optimum power allocation of the proposed multi-node differential AF scheme based on the tight simple BER approximation (6.37). Moreover, we further simplify the BER approximation in order to obtain analytical solution of power allocation among users.

Our primary goal is to minimize the BER in (6.37) under a constraint of a fixed total transmitted power, $P = P_s + \sum_{i=1}^N P_i$. The optimization problem can be formulated as

$$\begin{aligned} \arg \min_{P_s, \{P_i\}_{i=1}^N} & \left\{ \frac{C(\beta, N) \mathcal{N}_0^{N+1}}{P_s \sigma_{s,d}^2} \prod_{i=1}^N \frac{P_i \sigma_{r_i,d}^2 + (P_s \sigma_{s,r_i}^2 + \mathcal{N}_0) Z_{i,min}}{P_s P_i \sigma_{s,r_i}^2 \sigma_{r_i,d}^2} \right\}, \\ & \text{subject to } P_s + \sum_{i=1}^N P_i \leq P, P_i \geq 0, \forall i, \end{aligned} \quad (6.38)$$

where $Z_{i,min}$ is specified in (6.35). In order to obtain a simple optimum power allocation, we further approximate $Z_{i,min}$ as follows. At high enough SNR, $R_{i,max}$ in (6.34) can be further simplified to

$$\begin{aligned} R_{i,max} &= \frac{P_s \sigma_{s,r_i}^2 + \mathcal{N}_0}{P_i (1 + b^2 (1 - \beta)^2 P_s \sigma_{s,r_i}^2 / (2\mathcal{N}_0))} \\ &\approx \frac{2\mathcal{N}_0}{b^2 (1 - \beta)^2 P_i}. \end{aligned} \quad (6.39)$$

Substituting (6.39) into (6.35), $Z_{i,min}$ can be approximated as

$$\begin{aligned} Z_{i,min} &\approx \int_0^\infty \frac{\exp(-u/\sigma_{r_i,d}^2)}{u + 2\mathcal{N}_0/(b^2(1-\beta)^2P_i)} du \\ &= \int_0^\infty \frac{\exp(-u/\sigma_{r_i,d}^2)}{u + 2\mathcal{N}_0/(b^2(1-\beta)^2P_s c_i)} du, \end{aligned} \quad (6.40)$$

where

$$c_i = P_i/P_s, \quad (6.41)$$

in which P_s and P_i are the transmitted powers at the source and the relay i , respectively. By denoting $\hat{B}_{c_i} = 2\mathcal{N}_0/(b^2(1-\beta)^2P_s c_i)$ and using the results in (6.27), (6.40) can be reexpressed as

$$Z_{i,min} \approx -e^{B_{c_i}} \left[\mathcal{E} + \ln B_{c_i} + \int_0^{B_{c_i}} \frac{\exp(-t) - 1}{t} dt \right], \quad (6.42)$$

where

$$B_{c_i} = \frac{\hat{B}_{c_i}}{\sigma_{r_i,d}^2} = \frac{2\mathcal{N}_0}{b^2(1-\beta)^2\sigma_{r_i,d}^2 P_s c_i}. \quad (6.43)$$

Note that the integration term in the right hand side of (6.42) is small compared to the other terms inside the bracket, so it can be neglected without significant effect to the resulted power allocation. So in what follows, we are going to determine optimum power allocations based on the approximate $Z_{i,min}$:

$$Z_{i,min} \approx -e^{B_{c_i}} (\mathcal{E} + \ln B_{c_i}) \triangleq \hat{Z}_{i,min}. \quad (6.44)$$

As will be shown through numerical evaluation, the obtained optimum power allocation based on $\hat{Z}_{i,min}$ in (6.44) yields almost the same performance to that with exact $Z_{i,min}$ as specified in (6.35).

By applying $\hat{Z}_{i,min}$ in (6.44) into the optimization problem (6.38), and removing

some constant terms, the optimization problem is simplified to

$$\begin{aligned} \arg \min_{P_s, \{P_i\}_{i=1}^N} & \left\{ \frac{1}{P_s^{N+1}} \prod_{i=1}^N \frac{P_i \sigma_{r_i,d}^2 - P_s \sigma_{s,r_i}^2 e^{B_{c_i}} (\mathcal{E} + \ln B_{c_i})}{P_i} \right\}, \\ \text{subject to } & P_s + \sum_{i=1}^N P_i \leq P, \quad P_i \geq 0, \quad \forall i. \end{aligned} \quad (6.45)$$

Using the Lagrangian method, we let

$$\mathcal{L} = \frac{1}{P_s^{N+1}} \prod_{i=1}^N \frac{P_i \sigma_{r_i,d}^2 - P_s \sigma_{s,r_i}^2 e^{B_{c_i}} (\mathcal{E} + \ln B_{c_i})}{P_i} + \hat{\lambda} (P_s + \sum_{i=1}^N P_i - P) \quad (6.46)$$

Taking logarithm of (6.46) and substituting c_i from (6.41), we obtain

$$\begin{aligned} \mathcal{G} = & - (N+1) \ln P_s + \lambda (\mathbf{c}^T \mathbf{1} - P/P_s) - \sum_{i=1}^N \ln c_i \\ & + \sum_{i=1}^N \ln (c_i \sigma_{r_i,d}^2 - \sigma_{s,r_i}^2 e^{B_{c_i}} (\mathcal{E} + \ln B_{c_i})), \end{aligned} \quad (6.47)$$

in which $\mathbf{c} = [1, c_1, \dots, c_N]^T$ is an $N \times 1$ vector, and $\mathbf{1}$ is denoted as an $N \times 1$ vector containing all ones as its elements. By differentiating (6.59) with respect to c_i and equate the obtained result to zero, we have

$$\frac{\partial \mathcal{G}}{\partial c_i} = \lambda - \frac{1}{c_i} + \frac{\sigma_{r_i,d}^2 + \sigma_{s,r_i}^2 \left[\frac{B_{c_i} e^{B_{c_i}}}{c_i} (\mathcal{E} + \ln B_{c_i}) + \frac{e^{B_{c_i}}}{c_i} \right]}{c_i \sigma_{r_i,d}^2 - \sigma_{s,r_i}^2 e^{B_{c_i}} (\mathcal{E} + \ln B_{c_i})} = 0. \quad (6.48)$$

Next differentiating (6.59) with respect to P_s , we have

$$\frac{\partial \mathcal{G}}{\partial P_s} = -\frac{(N+1)}{P_s} + \lambda \frac{P}{P_s^2} + \sum_{i=1}^N \frac{\sigma_{s,r_i}^2 \frac{e^{B_{c_i}}}{P_s} \left[\frac{B_{c_i}}{P_s} (\mathcal{E} + \ln B_{c_i}) + 1 \right]}{c_i \sigma_{r_i,d}^2 - \sigma_{s,r_i}^2 e^{B_{c_i}} (\mathcal{E} + \ln B_{c_i})} = 0. \quad (6.49)$$

From (6.49), we can find that

$$\lambda = (N+1) \frac{P_s}{P} - \frac{1}{P} \sum_{i=1}^N \frac{\sigma_{s,r_i}^2 \Upsilon e^{B_{c_i}} (\mathcal{E} + \ln B_{c_i} + \frac{1}{B_{c_i}})}{c_i [c_i \sigma_{r_i,d}^2 - \sigma_{s,r_i}^2 e^{B_{c_i}} (\mathcal{E} + \ln B_{c_i})]}, \quad (6.50)$$

in which we denote $\Upsilon \triangleq (2\mathcal{N}_0)/(b^2(1-\beta^2)\sigma_{r_i,d}^2)$. Observe from (6.40) that B_{c_i} can be re-expressed as $B_{c_i} = (2\mathcal{N}_0)/(b^2(1-\beta)^2\sigma_{r_i,d}^2 P q c_i)$ where $q \triangleq P_s/P$ for $q \in (0, 1)$.

Then, substituting (6.50) into (6.48), we have

$$(N+1)q - \frac{1}{c_i} + \frac{\sigma_{r_i,d}^2 + \sigma_{s,r_i}^2 \left[\frac{\Upsilon}{Pq c_i^2} e^{B_{c_i}} (\mathcal{E} + \ln B_{c_i}) + \frac{e^{B_{c_i}}}{c_i} \right]}{c_i \sigma_{r_i,d}^2 - \sigma_{s,r_i}^2 e^{B_{c_i}} (\mathcal{E} + \ln B_{c_i})} - Q(c_i, q) = 0, \quad (6.51)$$

in which $Q(c_i, q) \triangleq \frac{1}{P} \sum_{i=1}^N \frac{\sigma_{s,r_i}^2 \Upsilon e^{B_{c_i}} (\mathcal{E} + \ln B_{c_i} + \frac{1}{B_{c_i}})}{c_i [c_i \sigma_{r_i,d}^2 - \sigma_{s,r_i}^2 e^{B_{c_i}} (\mathcal{E} + \ln B_{c_i})]}$. Given a specific q , we can find the corresponding c_i , denoted by $c_i(q)$ that satisfies (6.51). The optimum power allocation can then be obtained by finding $q = \hat{q}$ that satisfies

$$1 + \sum_{i=1}^N c_i(\hat{q}) - \frac{1}{\hat{q}} = 0. \quad (6.52)$$

The resulting optimum power allocation for the source (a_s) is

$$a_s = \hat{q}, \quad (6.53)$$

and that for each relay i (a_i) is

$$a_i = \hat{q} c_i(\hat{q}), \quad i = 1, 2, \dots, N. \quad (6.54)$$

Optimum power allocation for single-relay systems

For single relay systems, the optimization problem (6.51) and (6.52) is reduced to finding q such that

$$(N+1)q - \frac{1}{c_1} + \frac{\sigma_{r_1,d}^2 + \sigma_{s,r_1}^2 \Upsilon e^{B_{c_1}} \left[\frac{1}{Pq} (\mathcal{E} + \ln B_{c_1}) + \frac{1}{B_{c_1}} \right]}{c_1^2 [c_1 \sigma_{r_1,d}^2 - \sigma_{s,r_1}^2 e^{B_{c_1}} (\mathcal{E} + \ln B_{c_1})]} - \frac{1}{P} \frac{\sigma_{s,r_1}^2 \Upsilon e^{B_{c_1}} (\mathcal{E} + \ln B_{c_1} + \frac{1}{B_{c_1}})}{c_1 [c_1 \sigma_{r_1,d}^2 - \sigma_{s,r_1}^2 e^{B_{c_1}} (\mathcal{E} + \ln B_{c_1})]} = 0,$$

and $1 + c_1(q) - \frac{1}{q} = 0,$ (6.55)

which can be simply solved by any single dimensional search techniques. In this way, the complexity of the optimization problem can be greatly reduced, while the resulting optimum power allocation are close to that from exhaustive search in [99]. For example, Tables 6.1 and 6.2 show optimum power allocation based

on the exhaustive numerical search [99] and that from solving the low-complexity optimization problem (6.55), respectively. The optimization is determined at reasonable high SNR region, e.g. 20 or 30 dB. For illustration purpose, we consider a cooperation system using DBPSK or DQPSK modulation. In the Tables, we represent different channel qualities as $[\sigma_{s,d}^2, \sigma_{s,r_i}^2, \sigma_{r_i,d}^2]$ which corresponds to channel variances of source-destination link, source-relay link, relay-destination link, respectively. We can see that in both DBPSK and DQPSK modulations and at any relay location, the obtained optimum power allocation based on the closed-form formulation are very close to that from the numerical search results. We observe about 1 – 2% different between the numerical results and analytical results.

Optimum power allocation for multi-relay systems

For multi-relay systems, (6.51) and (6.52) can be used to find the optimum power allocation. Nevertheless, the optimization based on (6.51) and (6.52) involves $N + 1$ dimensional search because $Q(c_i, q)$ in (6.51) contains power allocation of each relay inside the summation. To reduce complexity of the search space, we remove the summation inside $Q(c_i, q)$ such that the approximate $Q(c_i, q)$ depends only on the c_i of interest. Therefore, an optimum power allocation can be approximately obtained by finding q such that

$$(N + 1)q - \frac{1}{c_i} + \frac{\sigma_{r_i,d}^2 + \sigma_{s,r_i}^2 \Upsilon e^{B_{c_i}} \left[\frac{1}{Pq} (\mathcal{E} + \ln B_{c_i}) + \frac{1}{B_{c_i}} \right]}{c_i^2 [c_i \sigma_{r_i,d}^2 - \sigma_{s,r_i}^2 e^{B_{c_i}} (\mathcal{E} + \ln B_{c_i})]} - \frac{1}{P} \frac{\sigma_{s,r_i}^2 \Upsilon e^{B_{c_i}} (\mathcal{E} + \ln B_{c_i} + \frac{1}{B_{c_i}})}{c_i [c_i \sigma_{r_i,d}^2 - \sigma_{s,r_i}^2 e^{B_{c_i}} (\mathcal{E} + \ln B_{c_i})]} = 0,$$

$$\text{and } 1 + \sum_{i=1}^N c_i(q) - \frac{1}{q} = 0, \forall i, i = 1, \dots, N. \quad (6.56)$$

From (6.56), the optimum power allocation that involves $(N+1)$ dimensional search is reduced to single dimensional search over the parameter q , $q \in (0, 1)$.

Table 6.1: Optimum power allocation for cooperation system with one relay based on exhaustive numerical search.

$[\sigma_{s,d}^2, \sigma_{s,r_i}^2, \sigma_{r_i,d}^2]$	DBPSK	DQPSK
	$[a_s, a_1]$	$[a_s, a_1]$
$[1, 1, 1]$	$[0.66, 0.34]$	$[0.70, 0.30]$
$[1, 10, 1]$	$[0.54, 0.46]$	$[0.54, 0.46]$
$[1, 1, 10]$	$[0.80, 0.20]$	$[0.80, 0.20]$

Table 6.2: optimum power allocation for cooperation system with one relay based on approximate closed-form formulation.

$[\sigma_{s,d}^2, \sigma_{s,r_i}^2, \sigma_{r_i,d}^2]$	DBPSK	DQPSK
	$[a_s, a_1]$	$[a_s, a_1]$
$[1, 1, 1]$	$[0.66, 0.34]$	$[0.69, 0.31]$
$[1, 10, 1]$	$[0.54, 0.46]$	$[0.54, 0.46]$
$[1, 1, 10]$	$[0.79, 0.21]$	$[0.78, 0.22]$

In Table 6.3, we summarize the numerical search results based on the multi-dimensional search of the optimization problem (6.38) under different channel variances. We compare the obtained results to those from approximate one-dimensional search (6.56) as shown in Table 6.4. In the Table we represent different channel qualities as $[\sigma_{s,d}^2, \sigma_{s,r_i}^2, \sigma_{r_i,d}^2]$ which corresponds to the set of channel variances of source-relay link, source-relay link, and relay-destination link, respectively. With the optimization in (6.56), the searching time for optimum power allocation reduces dramatically, while the obtained power allocation is very close to that from exact multi-dimensional search.

In addition, we can see from the obtained numerical results in both tables that, for any channel link qualities, more power should be allocated to the source in both types of modulation techniques. When the channel link qualities between

Table 6.3: Optimum power allocation for cooperation system with two relays based on exhaustive search.

$[\sigma_{s,d}^2, \sigma_{s,r_i}^2, \sigma_{r_i,d}^2]$	DBPSK	DQPSK
	$[a_s, a_1, a_2]$	$[a_s, a_1, a_2]$
$[1, 1, 1]$	$[0.46, 0.33, 0.21]$	$[0.48, 0.33, 0.19]$
$[1, 10, 1]$	$[0.44, 0.28, 0.28]$	$[0.40, 0.30, 0.30]$
$[1, 1, 10]$	$[0.65, 0.21, 0.14]$	$[0.66, 0.21, 0.13]$

Table 6.4: Optimum power allocation for cooperation system with two relays based on approximate formulation (6.55).

$[\sigma_{s,d}^2, \sigma_{s,r_i}^2, \sigma_{r_i,d}^2]$	DBPSK	DQPSK
	$[a_s, a_1, a_2]$	$[a_s, a_1, a_2]$
$[1, 1, 1]$	$[0.49, 0.2574, 0.2574]$	$[0.50, 0.25, 0.25]$
$[1, 10, 1]$	$[0.47, 0.265, 0.265]$	$[0.39, 0.31, 0.30]$
$[1, 1, 10]$	$[0.65, 0.1738, 0.1738]$	$[0.67, 0.1625, 0.1625]$

the source and the relays are good, i.e. $[\sigma_{s,d}^2, \sigma_{s,r_i}^2, \sigma_{r_i,d}^2] = [1, 10, 1]$ in this case, the system replicates the multiple transmitted antenna system. Therefore, almost equal powers should be allocated to the source and the relays. However, more power should be allocated to the source such that the transmit information can reach the relays, and the remaining power is allocated to the relays. The results also show that if there are two relays in the networks, almost the same amount of power as the source should be allocated to the first relay, and the rest amount of power is allocated to the second relay. In case of $[\sigma_{s,d}^2, \sigma_{s,r_i}^2, \sigma_{r_i,d}^2] = [1, 1, 10]$ which indicates that the channel qualities between the relays and the destination are good. When comparing to the case $[\sigma_{s,d}^2, \sigma_{s,r_i}^2, \sigma_{r_i,d}^2] = [1, 1, 1]$, higher power should be allocated at the source, while less powers should be put at the relays. The reason is that the channel quality at the source-destination link is lower than

that of the relay-destination links, so more power is required at the source to balance the qualities of all possible links such that the system can provide reliable communications.

To obtain some insight on the optimum power allocation at the source and the relays. Let the power allocation at the source as $a_s = P_s/P$, the power allocation at each relay as $a_i = P_i/P$, and the $N \times 1$ power allocation vector as $\mathbf{a} = [a_s, a_1, a_2, \dots, a_N]^T$. We define

$$\Psi_P = \frac{2N_0}{b^2(1-\beta)^2\sigma_{r_i,d}^2 P}, \quad (6.57)$$

such that

$$B_{c_i} = \frac{2N_0}{b^2(1-\beta)^2\sigma_{r_i,d}^2 P_s c_i} = \frac{\Psi_P}{a_i}. \quad (6.58)$$

By formulating the Lagrangian expression in a similar way as in (6.46). After removing some constant terms, and taking logarithm of the simplified Lagrangian expression, we have

$$\hat{\mathcal{G}} = -\ln a_s + \lambda(\mathbf{a}^T \mathbf{1} - 1) + \sum_{i=1}^N \ln \left[\frac{\sigma_{r_i,d}^2}{a_s} + \frac{\sigma_{s,r_i}^2}{a_i} e^{\frac{\Psi_P}{a_i}} (-\mathcal{E} - \ln \Psi_P + \ln a_i) \right], \quad (6.59)$$

We differentiate (6.59) with respect to a_s and a_i such that

$$\frac{\partial \mathcal{G}}{\partial a_s} = \frac{\partial \mathcal{G}}{\partial a_i}, \quad (6.60)$$

After some manipulations, we have

$$\begin{aligned} & \frac{1}{a_s} \left[1 + \sum_{j=1}^N \frac{\sigma_{r_j,d}^2}{\sigma_{r_j,d}^2 + \frac{a_s}{a_j} \sigma_{s,r_j}^2 \exp(\Psi_P/a_j) (-\mathcal{E} - \ln \Psi_P + \ln a_j)} \right] \\ &= \frac{1}{a_i} \left[\frac{\sigma_{s,r_i}^2 e^{\frac{\Psi_P}{a_i}} \left[-1 + (-\mathcal{E} - \ln \Psi_P + \ln a_i) \left(1 + \frac{\Psi_P}{a_i} \right) \right]}{\frac{a_i}{a_s} \sigma_{r_i,d}^2 + \sigma_{s,r_i}^2 \exp(\Psi_P/a_j) (-\mathcal{E} - \ln \Psi_P + \ln a_i)} \right]. \end{aligned} \quad (6.61)$$

In (6.61), we can see that at high SNR region, the expression $\exp(\Psi_P/a_j)(-\mathcal{E} - \ln \Psi_P + \ln a_j)$ is positive. Therefore, the term in the bracket on the right hand side of (6.61) is greater than one. However, the term in the bracket on the right hand side is less than one. This is because the nominator is far less than the denominator. Consequently, for any channel variance and any modulation method, the optimum power allocation is such that $a_s > a_i$ for all i which confirms the obtained results showed in Tables 6.1, 6.2, 6.3, and 6.4.

6.1.4 Simulation Results

We simulate the multi-node differential amplify-and-forward cooperation systems with DBPSK or DQPSK modulation. We consider two scenarios in which there are two or three relays ($N = 2$, or 3) in the network. The channel coefficients follow the Jakes' model [66] with Doppler frequency $f_D = 75 \text{ Hz}$ and normalized fading parameter $f_D T_s = 0.0025$ where T_s is the sampling period. The noise variance is assumed to be unity ($\mathcal{N}_0 = 1$). The average BER curves are plotted as functions of P/\mathcal{N}_0 .

We illustrate in Figure 6.2 the performance of the cooperation system with two relays. DBPSK signaling is used. The simulation is performed under equal channel variances, i.e. $[1, 1, 1]$, and equal power allocation strategy (i.e. $P_s = P_1 = P_2 = P/3$). We can see that the exact theoretical BER curve well matches to the simulated BER performance. In addition, the BER upper bound, the simple BER upper bound, and the simple BER approximations are tight to the simulated curve at high SNR. The BER curve for coherent detection is also showed in the figure; we observe a performance gap of about 4 dB between the proposed scheme and the coherent detection scheme at a BER of 10^{-3} .

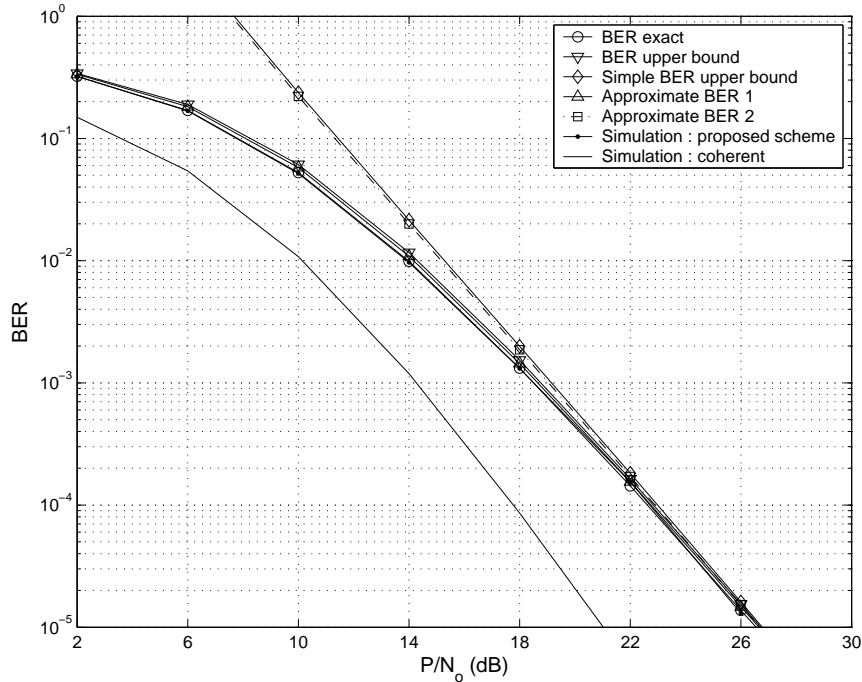


Figure 6.2: DBPSK : Two relays, equal power allocation strategy, and $\sigma_{s,d}^2 = \sigma_{s,r_i}^2 = \sigma_{r_i,d}^2 = 1$.

Figure 6.3 shows BER performance of the proposed scheme in case of DQPSK modulation. The simulation scenario follows the same setup as that for Figure 6.2. We observe that the exact BER, the two BER approximations are tight to the simulated BER curves over the entire SNR range. On the other hand, the BER upper bound and the simple BER upper bound are asymptotically parallel to the simulated BER curve. Comparing to the coherent detection, the performance gap between the proposed scheme and its coherent counterpart is about 4 dB at a BER of 10^{-3} .

We illustrate in Figure 6.4 BER performance of the proposed scheme with DQPSK modulation when using different number of relays (N). In the simulation, we consider two possible number of relays, namely $N = 2$ and $N = 3$. The simulation scenario is the same as that of Figure 6.2. It is apparent that the proposed differential cooperative scheme achieves higher diversity orders as N increases. At

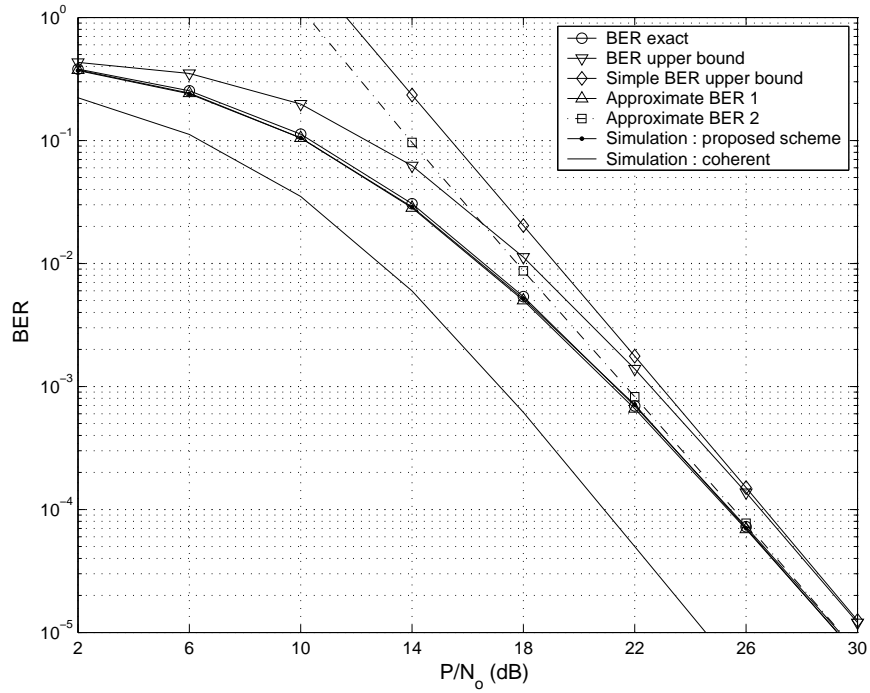


Figure 6.3: DQPSK : Two relays, equal power allocation strategy, and $\sigma_{s,d}^2 = \sigma_{s,r_i}^2 = \sigma_{r_i,d}^2 = 1$.

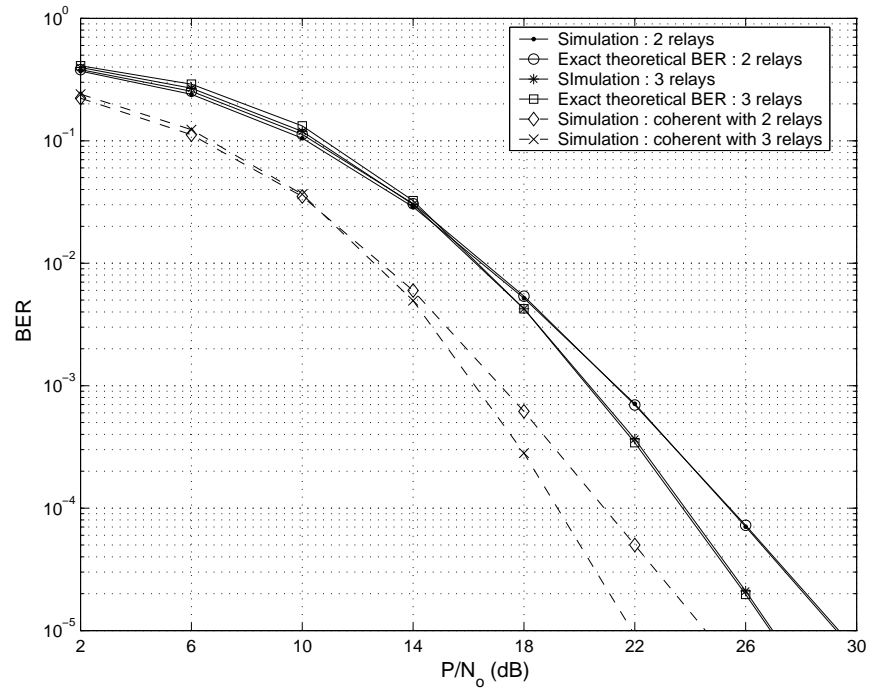


Figure 6.4: DQPSK : Two and three relays, equal power allocation strategy, and $\sigma_{s,d}^2 = \sigma_{s,r_i}^2 = \sigma_{r_i,d}^2 = 1$.

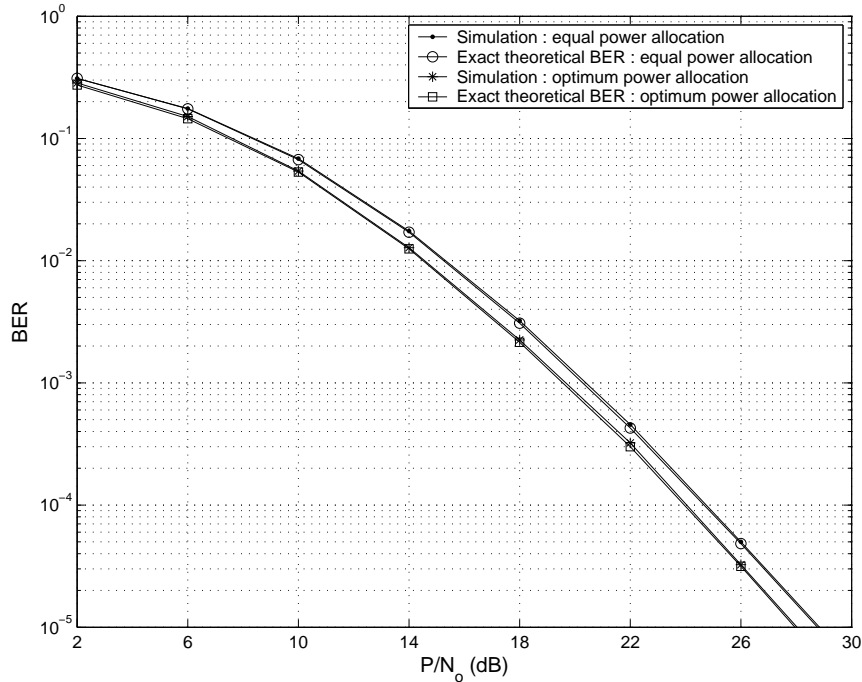


Figure 6.5: DQPSK : Two relays, optimum power allocation strategy, and $\sigma_{s,d}^2 = 1$, $\sigma_{s,r_i}^2 = 10$, $\sigma_{r_i,d}^2 = 1$.

a BER of 10^{-3} , we observe about 1.7 – 2 dB gain as N increases from 2 to 3. Also in the figure, the exact theoretical BER curves are tight to the simulated curves. In addition, the performance curves of our proposed scheme are about 4 dB away from that of coherent detection.

Figure 6.5 shows the BER performance of the proposed scheme with optimum power allocation strategy in comparison to that of equal power allocation. We consider a DQPSK modulation system a case when there are two relays in the network. The channel variances are $[1, 10, 1]$, and the optimum power allocation is $[0.39, 0.31, 0.30]$ (from Table 6.4). The simulated curves show that when all relays are close to the source, i.e. $\sigma_{s,r_i}^2 = 10$, the proposed scheme with optimum power allocation yields about 0.6 dB gain at a BER of 10^{-3} over the proposed scheme with equal power allocation. Also in the figure, the exact theoretical BER curves are provided for both power allocation schemes, and they closely match to the

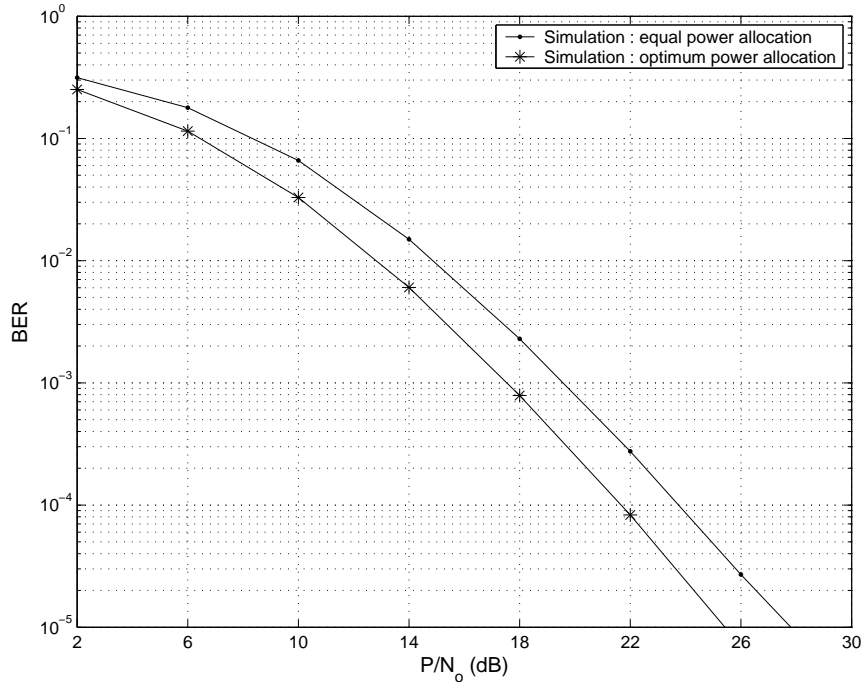


Figure 6.6: DQPSK : Two relays, optimum power allocation strategy, and $\sigma_{s,d}^2 = \sigma_{s,r_i}^2 = 1$, and $\sigma_{r_i,d}^2 = 10$.

simulated performances.

In Figure 6.6, we consider the BER performance with optimum power allocation strategy for DQPSK modulation system with two relays in the network. The channel variances are $[1, 1, 10]$, and the optimum power allocation for this case is $[0.67, 0.1625, 0.1625]$ (from Table 6.4). We observe that the performance with optimum power allocation is about 2 dB superior to that with equal power allocation at a BER of 10^{-3} .

6.2 Differential Modulation for Multi-Node Decode-and-Forward Cooperative Communications

In this Section, we consider a multi-node differential modulation scheme for decode-and-forward cooperative communications. By utilizing a decision threshold

at each relay-destination link and combining only the received signal whose amplitude is larger than the threshold, the proposed scheme enables efficient combining at the destination. The BER performance of the proposed scheme is analyzed for differential M-ary phase shift keying signals. We provide an approximate BER formulation of the proposed scheme, and then derive a tractable BER lower bound to provide more insights. Based on the obtained BER lower bound, we jointly optimize the power allocation and decision thresholds to further enhance the system performance.

The rest of this Section is organized as follows. Section 6.2.1 explains system description and signal models of the proposed scheme. An approximate BER analysis together with its low-complexity BER lower bound are derived in Section 6.2.2. In Section 6.2.3, we formulate an optimization problem to determine joint optimum power and optimum threshold. Discussion on the obtained numerical results are provided. Performance simulation results are shown and discussed in Section 6.2.4. Section 6.3 summarizes the proposed work.

6.2.1 Signal Models for the Multi-Node DF Differential Scheme

We consider a differential modulation scheme for multi-node decode-and-forward cooperative communications, coined as DiffDF as shown in Figure 6.7. With a source and N cooperative relays, signal transmissions of the DiffDF scheme comprises $N + 1$ phases. Suppose the DMPSK modulation is used, then in Phase 1, the source differentially encodes the information v_m at time τ as $x^\tau = v_m x^{\tau-1}$, where $v_m = e^{j\varphi_m}$ in which $\varphi_m = 2\pi m/M$ for $m = 0, 1, \dots, M - 1$, and M is the constellation size. The symbol x^τ is transmitted with transmit power P_s to the destination. Because of the broadcasting advantage in wireless networks, the in-

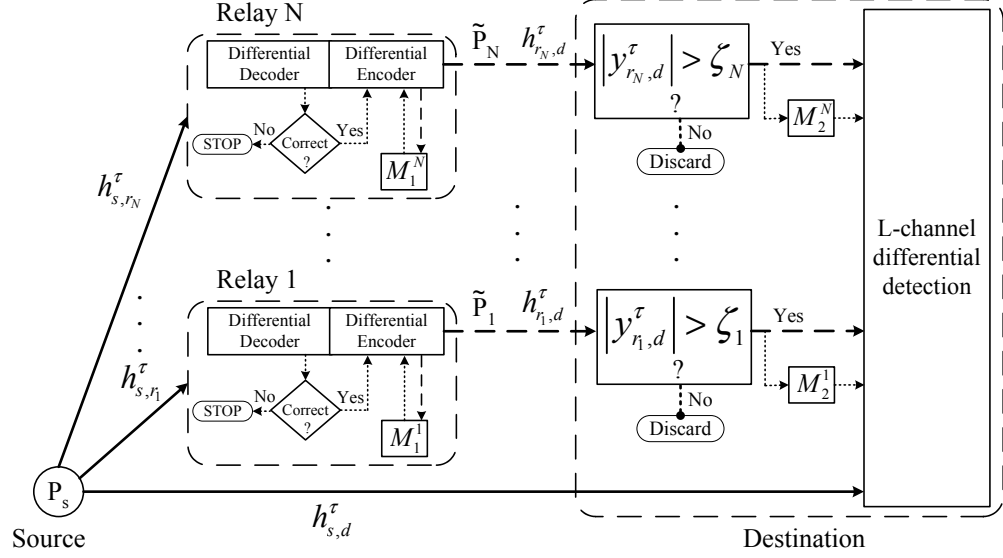


Figure 6.7: System descriptions of the multi-node differential DF scheme.

formation can also be received by each relay. The corresponding received signals at the destination and the i^{th} relay can be expressed as

$$y_{s,d}^\tau = \sqrt{P_s} h_{s,d}^\tau x^\tau + \eta_{s,d}^\tau, \quad (6.62)$$

and

$$y_{s,r_i}^\tau = \sqrt{P_s} h_{s,r_i}^\tau x^\tau + \eta_{s,r_i}^\tau, i = 1, 2, \dots, N, \quad (6.63)$$

where $h_{s,d}^\tau$ and h_{s,r_i}^τ represent channel coefficients from the source to the destination and to the i^{th} relay, respectively, and $\eta_{s,d}^\tau$ and η_{s,r_i}^τ are the additive noise terms.

From the received signal in (6.63), each relay differentially decodes by: [88]

$$\hat{m} = \arg \max_{m=0,1,\dots,M-1} \text{Re}\{(v_m y_{s,r_i}^{\tau-1})^* y_{s,r_i}^\tau\}. \quad (6.64)$$

In Phases 2 to $N+1$, if each relay incorrectly decodes, such incorrectly decoded symbol is discarded. Otherwise, the relay differentially re-encodes the information symbol as $\tilde{x}^\tau = v_m \tilde{x}^{\tau-k}$, and forwards \tilde{x}^τ to the destination with transmitted power $\tilde{P}_i = P_i$. Furthermore, \tilde{x}^τ is stored in the memory M_1^i for subsequent differential encoding. Note that the time index $\tau - k$ in $\tilde{x}^{\tau-k}$ can be any time before time τ

depending on the decoding result in the previous time. The received signal at the destination in Phases 2 to $N + 1$ can be expressed as

$$y_{r_i,d}^\tau = \begin{cases} \sqrt{P_i} h_{r_i,d}^\tau \tilde{x}^\tau + \eta_{r_i,d}^\tau, & \text{if relay correctly decodes } (\tilde{P}_i = P_i); \\ \eta_{r_i,d}^\tau, & \text{Otherwise } (\tilde{P}_i = 0), \end{cases} \quad (6.65)$$

where $i = 1, 2, \dots, N$, $h_{r_i,d}^\tau$ denotes the channel coefficient between the i^{th} relay and the destination, and $\eta_{r_i,d}^\tau$ represents an additive noise. In this paper, $h_{s,d}^\tau$, h_{s,r_i}^τ , and $h_{r_i,d}^\tau$ are modeled as zero means complex Gaussian random variables with variances $\sigma_{s,d}^2$, σ_{s,r_i}^2 , and $\sigma_{r_i,d}^2$, respectively. All additive noise $\eta_{s,d}^\tau$, η_{s,r_i}^τ , and $\eta_{r_i,d}^\tau$ are modeled as zero means complex Gaussian random variables with variances \mathcal{N}_0 .

Since the perfect knowledge of CSI is not available, the destination does not know whether the received signal from the i^{th} relay contains the information. For each i^{th} relay-destination link, a decision threshold ζ_i is used at the destination to make decision on the value of $|y_{r_i,d}^\tau|$ whether to combine such signal. Specifically, if $|y_{r_i,d}^\tau| \leq \zeta_i$ for all i , the destination estimates the transmitted symbol based only on the received signal from the direct link. However, if $|y_{r_i,d}^\tau| > \zeta_i$ for any i , the received signal from the source and that from the i^{th} relay are combined for jointly decoding. The combined signal at the destination is

$$y = w_s^{DF} (y_{s,d}^{\tau-1})^* y_{s,d}^\tau + \sum_{i=1}^N w_i^{DF} I_{\zeta_i}[|y_{r_i,d}^\tau|] (y_{r_i,d}^{\tau-l})^* y_{r_i,d}^\tau. \quad (6.66)$$

where w_s^{DF} and w_i^{DF} are combining weights, and $y_{r_i,d}^{\tau-l}$ ($l \geq 1$) in memory M_2^i is the most recent received signal from the i^{th} relay by which $|y_{r_i,d}^{\tau-l}| > \zeta_i$. In (6.66), we denotes $I_{\zeta_i}[|y_{r_i,d}^\tau|]$ as an indicator function such that $I_{\zeta_i}[|y_{r_i,d}^\tau|] = 1$ if $|y_{r_i,d}^\tau| > \zeta_i$; otherwise, $I_{\zeta_i}[|y_{r_i,d}^\tau|] = 0$. Using (6.66), the destination jointly differentially decodes the transmitted information by

$$\hat{m} = \arg \max_{m=0,1,\dots,M-1} \text{Re} \{v_m^* y\}. \quad (6.67)$$

Note that using different combining weights (w_s^{DF} and w_i^{DF}) results in different system performances. In this paper, we use $w_s^{DF} = w_i^{DF} = 1/(2\mathcal{N}_0)$ in order to maximize the signal-to-noise ratio (SNR) at the combiner output.

6.2.2 Approximate BER formulation

To obtain BER analysis for the proposed scheme. We first specify different SNR scenarios and determine the probability of occurrence of each scenario. After that, the approximate BER expression and a BER lower bound are provided.

- Definition of different SNR scenarios** Different combined SNR results from the comparison between the received signal ($y_{r_i,d}^\tau$) and the threshold (ζ_i) as well as the signals stored in memory M_1^i and M_2^i . In this way, each relay-destination link encounters six possible SNR scenarios and each of these SNR scenarios is defined as follows. Denote an integer number s_j^i as a SNR scenario of the link between the i^{th} relay and the destination for a given network state j , i.e. $s_j^i \in \{1, 2, 3, 4, 5, 6\}$. The parameter s_j^i is used to specify the SNR scenario $\Phi_{s_j^i}^i$ for $i = 1, 2, \dots, N$ which represents a set of joint events as follows. When $s_j^i = 1$, $\Phi_1^i \triangleq \{|y_{r_i,d}^\tau| \leq \zeta_i\}$ is defined as a joint event that received signals from all relay links are not greater than the thresholds. $\Phi_2^i \triangleq \{|y_{r_i,d}^\tau| > \zeta_i, \tilde{P}_i^\tau = P_i, \tilde{P}_i^{\tau-l} = P_i, l = k\}$ represents a joint event including $|y_{r_i,d}^\tau| > \zeta_i$, the relay correctly decodes at time τ and $\tau - 1$, and the information symbols at time k and l are the same. The rest scenarios are $\Phi_3^i \triangleq \{|y_{r_i,d}^\tau| > \zeta_i, \tilde{P}_i^\tau = P_i, \tilde{P}_i^{\tau-l} = P_i, l \neq k\}$, $\Phi_4^i \triangleq \{|y_{r_i,d}^\tau| > \zeta_i, \tilde{P}_i^\tau = P_i, \tilde{P}_i^{\tau-l} = 0\}$, $\Phi_5^i \triangleq \{|y_{r_i,d}^\tau| > \zeta_i, \tilde{P}_i^\tau = 0, \tilde{P}_i^{\tau-l} = P_i\}$, and $\Phi_6^i \triangleq \{|y_{r_i,d}^\tau| > \zeta_i, \tilde{P}_i^\tau = 0, \tilde{P}_i^{\tau-l} = 0\}$. They are interpreted in a similar way as that of Φ_2^i .

- Probability of occurrence for each SNR scenario** We determine in what

follows the probability of occurrence of each $\Phi_{s_j^i}^i$, denoted as $P_r^{h,DF}(\Phi_{s_j^i}^i)$, for $s_j^i = 1, 2, \dots, 6$. We first find that the probability that the i^{th} relay forwards information with transmit power $\tilde{P}_i = 0$ due to incorrect decoding is related to the symbol error rate of DMPSK signals as [96]

$$\Psi(\gamma_{s,r_i}^{DF}) = \frac{1}{\pi} \int_0^{(M-1)\pi/M} \exp[-g(\phi)\gamma_{s,r_i}^{DF}] d\phi, \quad (6.68)$$

where $\gamma_{s,r_i}^{DF} = P_s |h_{s,r_i}^\tau|^2 / \mathcal{N}_0$ represents an instantaneous SNR at the i^{th} relay, and $g(\phi) = \frac{\sin^2(\pi/M)}{1 + \cos(\pi/M) \cos(\phi)}$. Accordingly, the probability of correct decoding at the i^{th} relay (or probability of forwarding with transmit power $\tilde{P}_i = P_i$) is $1 - \Psi(\gamma_{s,r_i}^{DF})$.

The chance that Φ_1^i occurs is determined by the weighted sum of conditional probabilities given that $\tilde{P}_i = P_i$ or 0. We have

$$\begin{aligned} P_r^{h,DF}(\Phi_1^i) &= P_r^{h,DF}(|y_{r_i,d}^\tau| \leq \zeta_i \mid \tilde{P}_i^\tau = 0) \Psi(\gamma_{s,r_i}^\tau) \\ &\quad + P_r^{h,DF}(|y_{r_i,d}^\tau| \leq \zeta_i \mid \tilde{P}_i^\tau = P_i) [1 - \Psi(\gamma_{s,r_i}^\tau)] \\ &= (1 - \exp(-\zeta_i^2 / \mathcal{N}_0)) \Psi(\gamma_{s,r_i}^\tau) \\ &\quad + (1 - \mathcal{M}(P_i |h_{r_i,d}^\tau|^2, \zeta_i)) [1 - \Psi(\gamma_{s,r_i}^\tau)], \end{aligned} \quad (6.69)$$

where the second equality is obtained by substituting $P_r^{h,DF}(|y_{r_i,d}^\tau| \leq \zeta_i \mid \tilde{P}_i^\tau = 0) = 1 - \exp(-\zeta_i^2 / \mathcal{N}_0)$, which is related to the cumulative distribution function (CDF) of the Rayleigh-distributed random variable. However, $P_r^{h,DF}(|y_{r_i,d}^\tau| \leq \zeta_i \mid \tilde{P}_i^\tau = P_i)$ is related to the CDF of Rician-distributed random variable such that $P_r^{h,DF}(|y_{r_i,d}^\tau| \leq \zeta_i \mid \tilde{P}_i^\tau = P_i) = 1 - \mathcal{M}(P_i |h_{r_i,d}^\tau|^2, \zeta_i)$, where

$$\mathcal{M}(P_i |h_{r_i,d}^\tau|^2, \zeta_i) \triangleq Q_1(\sqrt{P_i |h_{r_i,d}^\tau|^2 / (\mathcal{N}_0/2)}, \zeta_i / \sqrt{\mathcal{N}_0/2}), \quad (6.70)$$

in which $Q_1(\alpha, \beta)$ is the Marcum Q-function [88].

The chance that each of the scenarios Φ_2 to Φ_6 happens will be conditioned on the event that $|y_{r_i,d}^{\tau-l}| > \zeta_i$. Using the definition in Section 6.2.2) and

noting that the events at time $\tau - l$ and time τ are independent, the chance that Φ_2^i occurs is given by

$$P_r^{h,DF}(\Phi_2^i) = P_r^{h,DF} \left(|y_{r_i,d}^\tau| > \zeta_i, \tilde{P}_i^\tau = P_i \right) \\ \times P_r^{h,DF} \left(\tilde{P}_i^{\tau-l} = P_i, l = k \mid |y_{r_i,d}^{\tau-l}| > \zeta_i \right). \quad (6.71)$$

From the result in (6.68) and the fact that $P_r^{h,DF}(|y_{r_i,d}^\tau| > \zeta_i \mid \tilde{P}_i^\tau = P_i) = \mathcal{M}(P_i|h_{r_i,d}^\tau|^2, \zeta_i)$, the first term in (6.71) can be obtained as $P_r^{h,DF}(|y_{r_i,d}^\tau| > \zeta_i, \tilde{P}_i^\tau = P_i) = \mathcal{M}(P_i|h_{r_i,d}^\tau|^2, \zeta_i)(1 - \Psi(\gamma_{s,r_i}^\tau))$. Using the concept of conditional probability and applying Bayes' rule [97], the second term in (6.71) can be approximated by $P_r^{h,DF}(\tilde{P}_i^{\tau-l} = P_i, l = k \mid |y_{r_i,d}^{\tau-l}| > \zeta_i) \approx \frac{\mathcal{M}(P_i|h_{r_i,d}^{\tau-l}|^2, \zeta_i)(1 - \Psi(\gamma_{s,r_i}^{\tau-l}))}{1 - (1 - e^{-\zeta_i^2/\mathcal{N}_0})\Psi(\gamma_{s,r_i}^{\tau-l})}$. Therefore, (6.72) can be simplified to

$$P_r^{h,DF}(\Phi_2^i) \approx \frac{\mathcal{M}^2(P_i|h_{r_i,d}^\tau|^2, \zeta_i)(1 - \Psi(\gamma_{s,r_i}^\tau))^2}{1 - (1 - e^{-\zeta_i^2/\mathcal{N}_0})\Psi(\gamma_{s,r_i}^\tau)}. \quad (6.72)$$

Next, the chance that the scenario Φ_3^i happens can be obtained through an expression that related to $P_r^{h,DF}(\Phi_2^i)$ as

$$P_r^{h,DF}(\Phi_3^i) = P_r^{h,DF}(\Phi_2^i \cup \Phi_3^i) - P_r^{h,DF}(\Phi_2^i), \quad (6.73)$$

where

$$P_r^{h,DF}(\Phi_2^i \cup \Phi_3^i) \triangleq P_r^{h,DF}(|y_{r_i,d}^\tau| > \zeta_i, \tilde{P}_i^\tau = P_i, \tilde{P}_i^{\tau-l} = P_i, |y_{r_i,d}^{\tau-l}| > \zeta_i). \quad (6.74)$$

Applying Bayes' rule, (6.74) can be expressed as

$$P_r^{h,DF}(\Phi_2^i \cup \Phi_3^i) = P_r^{h,DF}(|y_{r_i,d}^\tau| > \zeta_i, \tilde{P}_i^\tau = P_i) \\ \times \frac{P_r^{h,DF}(|y_{r_i,d}^{\tau-l}| > \zeta_i, \tilde{P}_i^{\tau-l} = P_i)}{P_r^{h,DF}(|y_{r_i,d}^{\tau-l}| > \zeta_i)}, \quad (6.75)$$

From the concept of total probability [97], we have

$$P(|y_{r_i,d}^{\tau-l}| > \zeta_i) = \mathcal{M}(P_i|h_{s,r_i}^{\tau-l}|^2, \zeta_i)(1 - \Psi(\gamma_{s,r_i}^{\tau-l})) + e^{-\frac{\zeta_i^2}{\mathcal{N}_0}} \Psi(\gamma_{s,r_i}^{\tau-l}) \\ \triangleq \Gamma(P_s|h_{s,r_i}^{\tau-l}|^2, P_i|h_{r_i,d}^{\tau-l}|^2). \quad (6.76)$$

Finally, substituting (6.72) and (6.75)-(6.76) into (6.73) results in

$$P_r^{h,DF}(\Phi_3^i) = \mathcal{M}^2(P_i|h_{r_i,d}^\tau|^2, \zeta_i) \left(\Gamma^{-1}(P_s|h_{s,r_i}^\tau|^2, P_i|h_{r_i,d}^\tau|^2) - (1 - (1 - e^{-\zeta_i^2/\mathcal{N}_0})\Psi(\gamma_{s,r_i}^\tau))^{-1} \right) (1 - \Psi(\gamma_{s,r_i}^\tau))^2. \quad (6.77)$$

Following the same steps as used to determine $P_r^{h,DF}(\Phi_2^i \cup \Phi_3^i)$, the chance that Φ_4^i occurs can be expressed as

$$P_r^{h,DF}(\Phi_4^i) = \frac{\mathcal{M}(P_i|h_{r_i,d}^\tau|^2, \zeta_i) e^{\left(\frac{-\zeta_i^2}{\mathcal{N}_0}\right)} \Psi(\gamma_{s,r_i}^\tau) (1 - \Psi(\gamma_{s,r_i}^\tau))}{\Gamma(P_s|h_{s,r_i}^\tau|^2, P_i|h_{r_i,d}^\tau|^2)}. \quad (6.78)$$

With an assumption that the channels at time τ and time $\tau-l$ are almost the same, after some manipulations, we can find that $P_r^{h,DF}(\Phi_5^i) = P_r^{h,DF}(\Phi_4^i)$.

Lastly, the chance that the scenario Φ_6^i occurs can be determined as

$$\begin{aligned} P_r^{h,DF}(\Phi_6^i) &= \frac{P_r^{h,DF}(|y_{r_i,d}^\tau| > \zeta_i, \tilde{P}_i^\tau = 0) P_r^{h,DF}(|y_{r_i,d}^{\tau-l}| > \zeta_i, \tilde{P}_i^{\tau-l} = 0)}{P_r^{h,DF}(|y_{r_i,d}^{\tau-l}| > \zeta_i)} \\ &= e^{\frac{-2\zeta_i^2}{\mathcal{N}_0}} \Psi(\gamma_{s,r_i}^\tau) (\Gamma^{-1}(P_s|h_{s,r_i}^\tau|^2, P_i|h_{r_i,d}^\tau|^2)). \end{aligned} \quad (6.79)$$

• Approximate BER Expression

We know from the previous section that each relay contributes six possible SNR scenarios at the destination. For a network with N relays, there are totally 6^N numbers of network states. We denote $S_j \triangleq [s_j^1 \ s_j^2 \ \dots \ s_j^N]$ as an $1 \times N$ matrix of a network state j , where $s_j^i \in \{1, 2, \dots, 6\}$. Accordingly, the average BER can be expressed as

$$P_b^{DF} = E \left[P_b^{h,DF} \right] = \sum_{j=1}^{6^N} E \left[\left(P_b^{h,DF} |_{S_j} \right) \prod_{i=1}^N P_r^{h,DF}(\Phi_{s_j^i}^i) \right], \quad (6.80)$$

where $P_r^{h,DF}(\Phi_{s_j^i}^i)$ for each s_j^i is specified in (6.69)-(6.79), $P_b^{h,DF} |_{S_j}$ represents a conditional BER for a given S_j , and $E[\cdot]$ denotes the expectation operator.

Since it is difficult to find a closed-form solution for the BER in (6.80), we further simplify (6.80) by separating a set of all possible network states, denoted

by \mathbb{S} , into two disjoint subsets as $\mathbb{S} = \mathbb{S}^{1,2} \cup (\mathbb{S}^{1,2})^c$, where $\mathbb{S}^{1,2}$ denotes all possible of network states that every element in the network state S_j is either one or two, and $(\mathbb{S}^{1,2})^c$ denotes the remaining possible network states. Note that the cardinality of $\mathbb{S}^{1,2}$ and $(\mathbb{S}^{1,2})^c$ are $|\mathbb{S}^{1,2}| = 2^N$ and $|(\mathbb{S}^{1,2})^c| = 6^N - 2^N$, respectively. In this way, we can express the average BER (6.80) as

$$\begin{aligned} P_b^{DF} &= \sum_{j=1}^{2^N} E \left[\left(P_b^{h,DF} |_{S_j \in \mathbb{S}^{1,2}} \right) \prod_{i=1}^N P_r^{h,DF}(s_j^i) \right] \\ &\quad + \sum_{j=1}^{6^N - 2^N} E \left[\left(P_b^{h,DF} |_{S_j \in (\mathbb{S}^{1,2})^c} \right) \prod_{i=1}^N P_r^{h,DF}(s_j^i) \right], \\ &\triangleq P_{b,1}^{DF} + P_{b,2}^{DF}. \end{aligned} \quad (6.81)$$

The first term in the right hand side of (6.81), $P_{b,1}^{DF}$, results from the cases where every element in the network state S_j is either one or two; the second term, $P_{b,2}^{DF}$, results from the remaining cases. These two terms can be determined as follows.

First, for notational convenience, let us denote $L(S_j)$ as the number of combining branches. By definition, we can express $L(S_j)$ as

$$L(S_j) = \sum_{i=1}^N \hat{L}(s_j^i) + 1, \quad (6.82)$$

where $\hat{L}(s_j^i) = 0$ when $s_j^i = 1$, and $\hat{L}(s_j^i) = 1$ otherwise. Note that the addition of 1 in (6.82) corresponds to the contribution of signal from the direct link.

Next, consider the case that every element in the network state S_j is either one or two, the conditional BER $P_b^{h,DF} |_{S_j \in \mathbb{S}^{1,2}}$ can be obtained from the the multi-branch differential detection of DMPSK signals as [88]:

$$P_b^{h,DF} |_{S_j \in \mathbb{S}^{1,2}} = \frac{1}{2^{2L(S_j)} \pi} \int_{-\pi}^{\pi} f(\theta, \beta, L(S_j)) \exp \left[-\alpha(\theta) \gamma_{S_j \in \mathbb{S}^{1,2}}^{DF} \right] d\theta \triangleq \Lambda(\gamma_{S_j \in \mathbb{S}^{1,2}}^{DF}), \quad (6.83)$$

in which $f(\theta, \beta, L(S_j))$ and $\alpha(\theta)$ are specified in (6.15) and (6.16), respectively. The term $\gamma_{S_j \in \mathbb{S}^{1,2}}^{DF}$ is the SNR at the combined output, which is given by

$$\gamma_{S_j \in \mathbb{S}^{1,2}}^{DF} = \frac{P_s |h_{s,d}^\tau|^2}{\mathcal{N}_0} + \sum_{i=1}^N \frac{(s_j^i - 1) P_i |h_{r_i,d}^\tau|^2}{\mathcal{N}_0}, \quad s_j^i \in \{1, 2\}, \quad \forall i. \quad (6.84)$$

Then, the conditional BER $P_b^{h,DF} |_{S_j \in (\mathbb{S}^{1,2})^c}$ for the remaining cases can be found as follows. Since up to now the conditional BER formulation for DMPSK with arbitrary-weighted combining has not been available in the literature, $P_b^{h,DF} |_{S_j \in (\mathbb{S}^{1,2})^c}$ cannot be exactly determined. For analytical tractability of the analysis, we resort to an approximate BER, in which the signal from the relay i is considered as noise when any scenario from Φ_3^i to Φ_6^i occurs. As we will show in the succeeding section, the analytical BER obtained from this approximation is close to the simulation results. The conditional BER for these cases can be approximated as $P_b^{h,DF} |_{S_j \in (\mathbb{S}^{1,2})^c} \approx \Lambda(\gamma_{S_j \in (\mathbb{S}^{1,2})^c}^{DF})$, where

$$\gamma_{S_j \in (\mathbb{S}^{1,2})^c}^{DF} = \frac{P_s |h_{s,d}^\tau|^2 + \sum_{i=1}^N I_2[s_j^i] P_i |h_{r_i,d}^\tau|^2}{\mathcal{N}_0 + \hat{\mathcal{N}}_0}, \quad s_j^i \in \{1, 2, \dots, 6\}, \quad \forall i, \quad (6.85)$$

in which $\hat{\mathcal{N}}_0 \triangleq (\sum_{i=1}^N (1 - I_2[s_j^i]) \mathcal{N}_{s_j^i}) / (P_s |h_{s,d}^\tau|^2 / \mathcal{N}_0 + \sum_{i=1}^N I_2[s_j^i] P_i |h_{r_i,d}^\tau|^2 / \mathcal{N}_0)$, and $\mathcal{N}_{s_j^i}$ depends on s_j^i as follows: $\mathcal{N}_{s_j^i} = (P_i |h_{r_i,d}^\tau|^2 + \mathcal{N}_0)^2 / \mathcal{N}_0$ when $s_j^i = 2$, $\mathcal{N}_{s_j^i} = P_i |h_{r_i,d}^\tau|^2 + \mathcal{N}_0$ when $s_j^i = 3, 4, 5$, and $\mathcal{N}_{s_j^i} = \mathcal{N}_0$ when $s_j^i = 6$. In (6.85), $I_2[s_j^i]$ is defined as an indicator function based on the occurrence of s_j^i such that $I_2[s_j^i] = 1$ when $s_j^i = 2$, and $I_2[s_j^i] = 0$ when $s_j^i = 1, 3, 4, 5, 6$.

From the above results, $P_{b,2}^{DF}$ in (6.81) can be approximated as

$$P_{b,2}^{DF} \approx \sum_{j=1}^{6^N - 2^N} \frac{1}{4^{L(S_j)} \pi} \int_{-\pi}^{\pi} f(\theta, \beta, L(S_j)) E \left[e^{\left(-\alpha(\theta) \gamma_{S_j \in (\mathbb{S}^{1,2})^c}^{DF} \right)} \prod_{i=1}^N P_r^{h,DF}(s_j^i) \right] d\theta, \quad (6.86)$$

where

$$\begin{aligned}
& E \left[e^{\left(-\alpha(\theta) \gamma_{S_j \in (\mathbb{S}^{1,2})^c}^{DF} \right)} \prod_{i=1}^N P_r^{h,DF}(s_j^i) \right] \\
&= \underbrace{\int \cdots \int}_{2N+1 \text{ folds}} \exp \left(-\alpha(\theta) \gamma_{S_j \in (\mathbb{S}^{1,2})^c}^{DF} \right) \\
&\quad \times \prod_{i=1}^N P_r^{h,DF}(s_j^i) f(\varepsilon_1) f(\varepsilon_2) \cdots f(\varepsilon_{2N+1}) d\varepsilon_1 d\varepsilon_2 \cdots d\varepsilon_{2N+1}, \quad (6.87)
\end{aligned}$$

in which $\gamma_{S_j \in (\mathbb{S}^{1,2})^c}^{DF}$ is given in (6.85), and $\prod_{i=1}^N P_r^{h,DF}(s_j^i)$ is calculated by using (6.69)-(6.79). We can see from (6.86) that the evaluation of $P_{b,2}^{DF}$ involves at most $(2N+2)$ -fold integration. Although $P_{b,2}^{DF}$ can be numerically determined, the calculation time is prohibitively long even for a cooperation system with small number of relays.

Now we determine $P_{b,1}^{DF}$ in (6.81) as follows. The term $\prod_{i=1}^N P_r^{h,DF}(s_j^i)$ is a product of probabilities of occurrence of scenarios 1 and 2, and it can be expressed as

$$\prod_{i=1}^N P_r^{h,DF}(s_j^i) = \prod_{i=1}^N \left[(2 - s_j^i) P_r^{h,DF}(\Phi_1^i) + (s_j^i - 1) P_r^{h,DF}(\Phi_2^i) \right], \quad (6.88)$$

Substitute (6.83), (6.84), and (6.88) into the expression of $P_{b,1}^{DF}$ in (6.81), and then average over all CSIs, resulting in

$$P_{b,1}^{DF} \approx \sum_{j=1}^{2^N} \left(\frac{1}{2^{2L(S_j)\pi}} \right) \int_{-\pi}^{\pi} \left(\frac{f(\theta, \beta, L(S_j))}{1 + \alpha(\theta) P_s \sigma_{s,d}^2 / \mathcal{N}_0} \right) \prod_{i=1}^N \left[(2 - s_j^i) X + (s_j^i - 1) Y \right] d\theta, \quad (6.89)$$

where we denote $X \triangleq E [P_r^{h,DF}(\Phi_1^i)]$ which can be determined as

$$\begin{aligned}
X &= (1 - e^{-\zeta_i^2 / \mathcal{N}_0}) G \left(1 + \frac{g(\phi) P_s \sigma_{s,r_i}^2}{\mathcal{N}_0} \right) \\
&\quad + (1 - \int_0^\infty \frac{\mathcal{M}(P_i q, \zeta_i)}{\sigma_{r_i,d}^2} e^{-q/\sigma_{r_i,d}^2} dq) \left(1 - G \left(1 + \frac{g(\phi) P_s \sigma_{s,r_i}^2}{\mathcal{N}_0} \right) \right), \quad (6.90)
\end{aligned}$$

in which $G(c(\phi)) \triangleq \frac{1}{\pi} \int_0^{(M-1)\pi/M} [c(\phi)]^{-1} d\phi$, and

$Y \triangleq E [\exp(-\alpha(\theta)P_i|h_{r_i,d}^\tau|^2/\mathcal{N}_0) \cdot P_r^{h,DF}(\Phi_2^i)]$ which can be approximated as

$$Y \approx \frac{1}{\sigma_{s,r_i}^2 \sigma_{r_i,d}^2} \int_0^\infty \int_0^\infty \frac{\mathcal{M}^2(P_i q, \zeta_i) (1 - \Psi(P_s u / \mathcal{N}_0))^2}{1 - (1 - e^{-\zeta_i^2 / \mathcal{N}_0}) \Psi(P_s u / \mathcal{N}_0)} \times e^{-(\alpha(\theta) \frac{P_i}{\mathcal{N}_0} + \frac{1}{\sigma_{r_i,d}^2})q} e^{-u/\sigma_{s,r_i}^2} dq du. \quad (6.91)$$

Substituting (6.86) and (6.89) into (6.81), we finally obtain the average BER of the multi-node DiffDF scheme.

To get more insightful understanding, we further determine a BER lower bound of the multi-node DiffDF scheme as follows. Since the exact BER formulations under the scenarios Φ_4^i , Φ_5^i , and Φ_6^i are currently unavailable, and the chances that these three scenarios happen are small at high SNR, we lower bound the BER from these scenarios by zero. Also, we lower bound the BER under the scenario Φ_3^i by that under Φ_2^i ; this allows us to express the lower bound in terms of $P_r^h(\Phi_2^i \cup \Phi_3^i)$ (instead of $P_r^h(\Phi_3^i)$ or $P_r^h(\Phi_2^i)$) which can be obtain without any approximation. In this way, the BER of multi-node DiffDF scheme can be lower bounded by

$$P_b^{lb,DF} \approx \sum_{j=1}^{2^N} \left(\frac{1}{2^{2L(S_j)} \pi} \right) \int_{-\pi}^{\pi} \left(\frac{f(\theta, \beta, L(S_j))}{1 + \alpha(\theta) P_s \sigma_{s,d}^2 / \mathcal{N}_0} \right) \prod_{i=1}^N \left[(2 - s_j^i) X + (s_j^i - 1) \hat{Y} \right] d\theta, \quad (6.92)$$

where X is given in (6.90) and

$$\begin{aligned} \hat{Y} &\triangleq E [\exp(-\alpha(\theta)P_i|h_{r_i,d}^\tau|^2/\mathcal{N}_0) \cdot P_r^{h,DF}(\Phi_2^i \cup \Phi_3^i)] \\ &= \frac{1}{\sigma_{s,r_i}^2} \int_0^\infty s(u, \theta) e^{-u/\sigma_{s,r_i}^2} du, \end{aligned} \quad (6.93)$$

in which

$$s(u, \theta) \triangleq \int_0^\infty \frac{\mathcal{M}^2(P_i q, \zeta_i) (1 - \Psi(P_s u / \mathcal{N}_0))^2}{\sigma_{r_i,d}^2 \Gamma(P_s u, P_i q)} e^{-(\alpha(\theta) \frac{P_i}{\mathcal{N}_0} + \frac{1}{\sigma_{r_i,d}^2})q} dq. \quad (6.94)$$

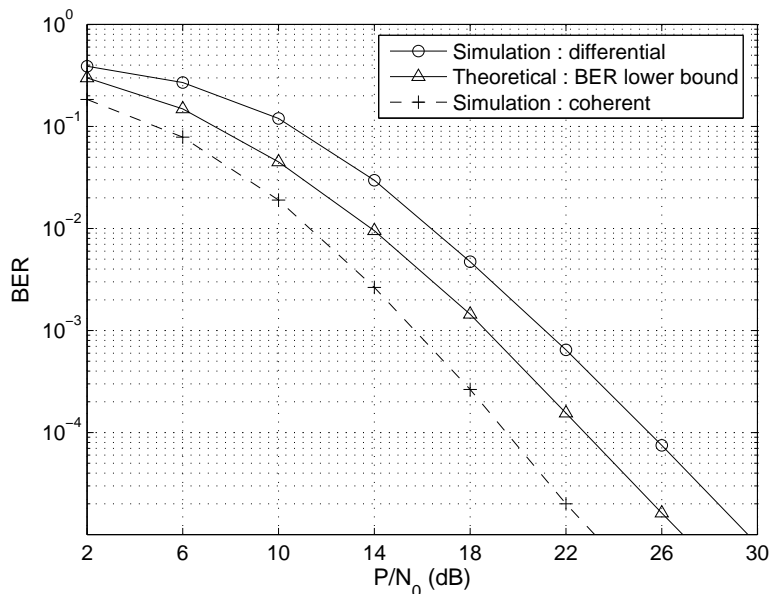


Figure 6.8: DQPSK: equal power allocation, $\sigma_{s,d}^2 = \sigma_{s,r_i}^2 = \sigma_{r_i,d}^2 = 1$, and $\zeta = 1$

We will show through numerical evaluation that the BER lower bound (6.92) is very close to the simulated performance under some simulation scenarios.

Figure 6.8 compares the performance of the BER lower bound with the simulated performance. We consider a DQPSK cooperation system with two relays. All relays are allocated with equal power. The decision threshold is set at $\zeta = 1$ and all channel variances are $\sigma_{s,d}^2 = \sigma_{s,r_i}^2 = \sigma_{r_i,d}^2 = 1$ for all i . From Figure 6.8, we observe a performance gap of about 2 dB between the BER lower bound and the simulated performance. The BER lower bound yields the same diversity order as that from the simulated performance even though there is a performance gap between these two curves. Under this simulation setup, the performance of the DiffDF scheme is 5 dB away from the performance with coherent detection at a BER of 10^{-3} . An interest-

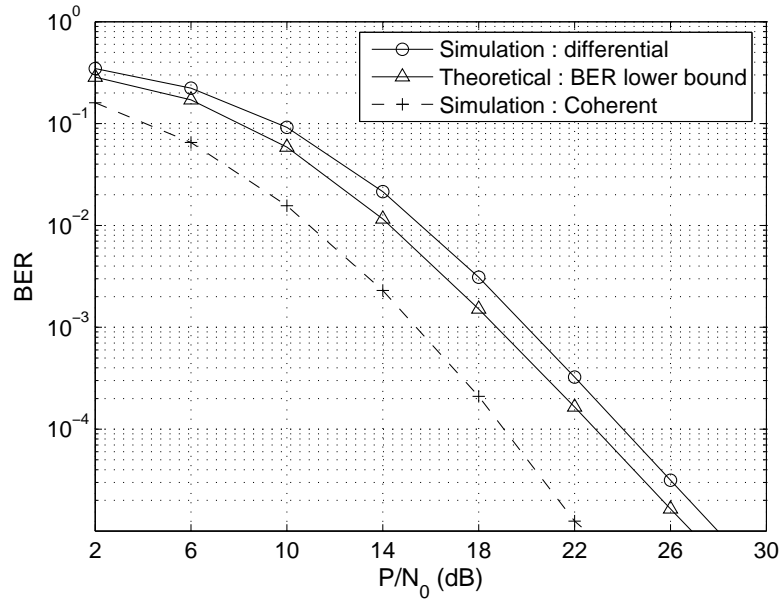


Figure 6.9: DQPSK: optimum power allocation, $\sigma_{s,d}^2 = \sigma_{s,r_i}^2 = \sigma_{r_i,d}^2 = 1$, and $\zeta = 1$

ing observation is that when the transmit powers are optimally allocated ($P_s = 0.6P, P_i = 0.2P$) with a fixed threshold at $\zeta = 1$ as shown in Figure 6.9, the performance gap between the simulated performance and the BER lower bound is reduced to about 1 dB at a BER of 10^{-3} . In addition, the performance of the DiffDF scheme is closer to the performance of coherent detection scheme. Based on the two figure, we can see that the performance gap between the differential detection and coherent detection is a bit far from the 3 dB gap that we would expect from the conventional differential detection and its coherent counterpart. The reason is that the power allocation in our proposed scheme is not optimum. Hence, the chances that the SNR scenarios $\Phi_3^i - \Phi_6^i$ occur are high which degrades the performance. However, the performance of the BER lower bound is about 3 dB away from the performance with coherent detection because the chances that $\Phi_3^i - \Phi_6^i$ occur

are discarded.

6.2.3 Optimizing Power Allocation and Thresholds

We determine in this section the performance improvement by jointly optimizing power allocation and thresholds based on the BER lower bound (6.92). Specifically, for a fixed total power $P = P_s + \sum_{i=1}^N P_i$, we jointly optimize the threshold ζ_i , power allocation $a_s = P_s/P$ at the source and $a_i = P_i/P$ at relay i such that the BER lower bound (6.92) is minimized:

$$(\{\hat{\zeta}_i\}_{i=1}^N, \hat{a}_s, \{\hat{a}_i\}_{i=1}^N) = \arg \min_{\{\zeta_i\}_{i=1}^N, a_s, \{a_i\}_{i=1}^N} P_b^{lb,DF}(\{\zeta_i\}_{i=1}^N, a_s, \{a_i\}_{i=1}^N), \quad (6.95)$$

where $P_b^{lb,DF}(\{\zeta_i\}_{i=1}^N, a_s, \{a_i\}_{i=1}^N)$ results from substituting $P_s = a_s P$ and $P_i = a_i P$ into (6.92). However, joint optimization in (6.95) involves $2N + 1$ dimensional search, including $N + 1$ power allocation ratios and N decision thresholds. To make the optimization problem tractable and to get some insight on the optimum power allocation and the optimum threshold value, each relay is assumed to be allocated with the same transmit power, and the decision thresholds are assumed the same at the destination. In this way, the source is allocated with power $a_s = P_s/P$ and each relay is equally allocated with power $(P - a_s P)/N$. Hence, the search space of this optimization problem involves only two dimensional search, namely a_s and ζ . The optimization problem (6.95) is simplified to

$$(\zeta^*, a_s^*) = \arg \min_{\zeta, a_s} P_b^{lb,DF}(\zeta, a_s, \{a_i\}_{i=1}^N), \quad (6.96)$$

where $P_b^{lb,DF}(\zeta, a_s, \{a_i\}_{i=1}^N)$ results from substituting $\zeta_i = \zeta$, $P_s = a_s P$, and $P_i = (1 - a_s)P/N$ into (6.92).

Table 6.5 summarizes the obtained power allocation and thresholds based on the optimization problem (6.96). As a demonstration purpose, we consider DBPSK or

Table 6.5: Optimum power allocation and thresholds for a cooperation system with two relays.

$[\sigma_{s,d}^2, \sigma_{s,r_i}^2, \sigma_{r_i,d}^2]$	DBPSK	DQPSK
	$[a_s, a_1, a_2, \zeta]$	$[a_s, a_1, a_2, \zeta]$
$[1, 1, 1]$	$[0.50, 0.25, 0.25, 0.4]$	$[0.52, 0.24, 0.24, 0.4]$
$[1, 10, 1]$	$[0.44, 0.28, 0.28, 0.4]$	$[0.40, 0.30, 0.30, 0.4]$
$[1, 1, 10]$	$[0.68, 0.16, 0.16, 1.6]$	$[0.70, 0.15, 0.15, 1.8]$

DQPSK cooperation systems with two relays. Different channel variances are used to investigate power allocation and thresholds for different cooperation network setups. Particularly, larger channel variance between two nodes implies closer distance between them. The obtained numerical results are given in Table 6.5. Even though the obtained power allocation is sub-optimum, their values provide some insightful information on how much power should be allocated to improve system performance. In particular, higher power should be allocated at the source in order to maintain link reliability. In addition, higher threshold should be used when the channel variance is high. For example, if all the channel links are of the same quality, about half of the transmit power should be allocated at the source, while the optimum threshold is 0.4. On the other hand, if the channel link between each relay and destination is very good, then the optimum power allocation at the source increases to about 70% of the transmit power, and the optimum threshold increases to 1.6 for DBPSK and 1.8 for DQPSK.

6.2.4 Simulation Results

We simulate DBPSK and DQPSK cooperation systems with two or three relays. The channel coefficients follow the Jakes' model [2] with Doppler frequency $f_D = 75 \text{ Hz}$ and normalized fading parameter $f_D T_s = 0.0025$ where T_s is the sampling period. The noise variance is set at $\mathcal{N}_0 = 1$. For fair comparison, the performance curves are plotted as functions of P/\mathcal{N}_0 .

Figure 6.10 shows the effect of using different number of relays on the performance of the DQPSK DiffDF scheme. Each node has equal power allocation, and the threshold at destination is fixed at $\zeta = 1$. The channel variances are $\sigma_{s,d}^2 = \sigma_{s,r_i}^2 = \sigma_{r_i,d}^2 = 1$ for all i . The simulation results show that the diversity order increases with the number of relays. We observe about 3.5 dB performance improvement at a BER of 10^{-4} when the number of relays increases from one to two relays. An additional 2 dB gain at the same BER is obtained when the system increases to three relays. We also observe a performance gap of about 5.5 dB at a BER of 10^{-3} between the DiffDF scheme and its coherent counterpart for a cooperation system with three relays.

Figure 6.11 shows the effect of using different thresholds on the performance of the proposed scheme. We consider a DBPSK cooperation system with three relays. Equal power allocation is used. The channel variances are $\sigma_{s,d}^2 = \sigma_{s,r_i}^2 = 1$, and $\sigma_{r_i,d}^2 = 10$ for all i . Clearly, different thresholds result in different performance. Specifically, the proposed scheme with $\zeta = 2$ provides the best performance under this simulation scenario. When $\zeta = 1$, not only BER deteriorates but also the diversity order reduces. Hence, the decision threshold must be appropriately chosen such that the DiffDF scheme yields good performance. Comparing the simulated performance when $\zeta = 2$ with the coherent cooperative scheme without threshold,

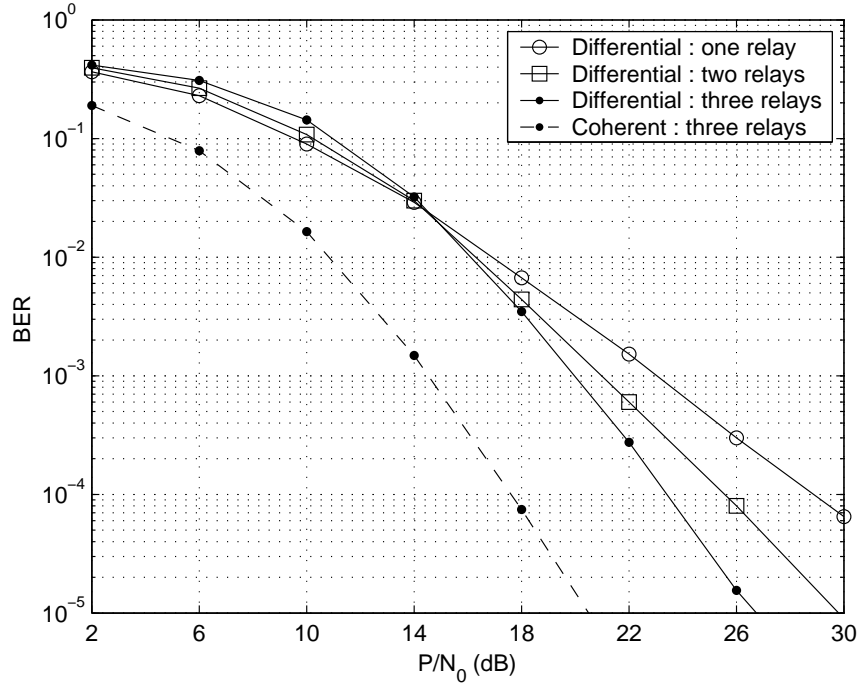


Figure 6.10: DQPSK : different number of relays, equal power allocation, threshold = 1, and $\sigma_{s,d}^2 = \sigma_{s,r_i}^2 = \sigma_{r_i,d}^2 = 1$.

we observe about 6 dB performance gap between the two performance curves at a BER of 10^{-3} . Such large performance gap is observed because the DiffDF scheme does not know exactly the CSIs or the transmit power at each relay whether it is 0 or P_i . Hence, it results in lower coding gain and degrades the performance.

We show in Figure 6.12 the performance improvement when the appropriate power allocation and decision thresholds are chosen. We consider a DQPSK cooperation system with two relays. The channel variances are $\sigma_{s,d}^2 = \sigma_{s,r_i}^2 = 1$, and $\sigma_{r_i,d}^2 = 10$ for all i . In this scenario, the optimum power allocation is $a_s = 0.70$, $a_1 = 0.15$, and $a_2 = 0.15$, and the optimum threshold is $\zeta = 1.8$. We can see that the performance curve with optimum values of power allocation and threshold significantly improves from that with equal power allocation and an arbitrary decision threshold ($\zeta = 1$ in this case). A performance gain of 4–5 dB is observed at a BER of $10^{-3} - 10^{-4}$. Also in Figure 6.12, we compare the performance of

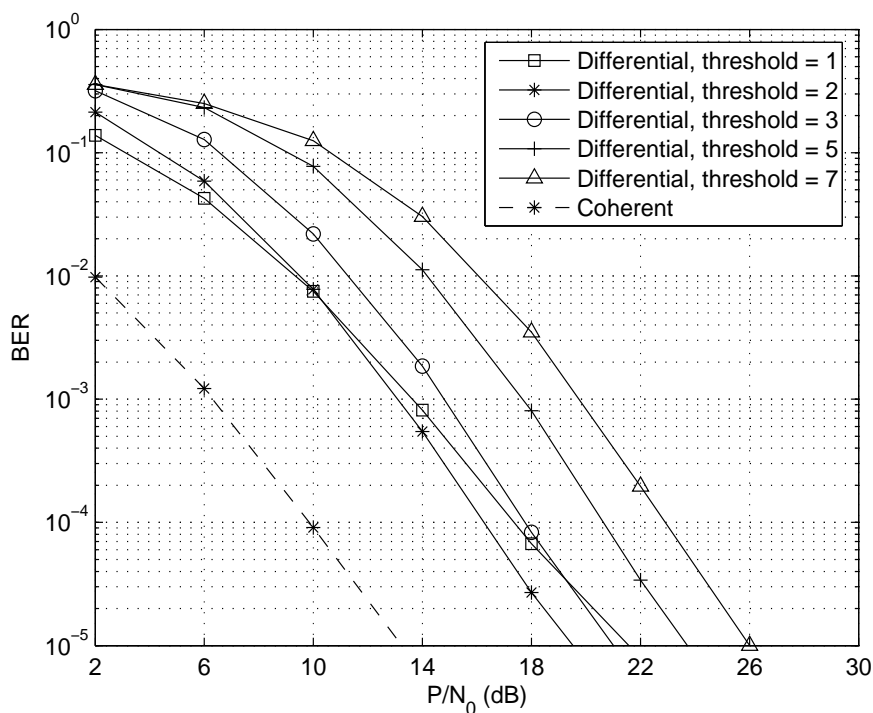


Figure 6.11: DBPSK : three relays, fixed power allocation but different thresholds, and $\sigma_{s,d}^2 = \sigma_{s,r_i}^2 = 1$, and $\sigma_{r_i,d}^2 = 10$.

optimum power allocation and optimum threshold with that of optimum power allocation ($a_s = 0.8$, $a_1 = 0.1$, and $a_2 = 0.1$) but an arbitrary threshold ($\zeta = 1$). We can see that jointly optimization power allocation and threshold leads to about 1 dB to 2.5 dB at BER between 10^{-3} and 10^{-5} , compared with optimum power allocation but arbitrary threshold. Note that the performance of the DiffDF scheme with optimum power allocation and optimum threshold is 5 dB away from that of coherent detection.

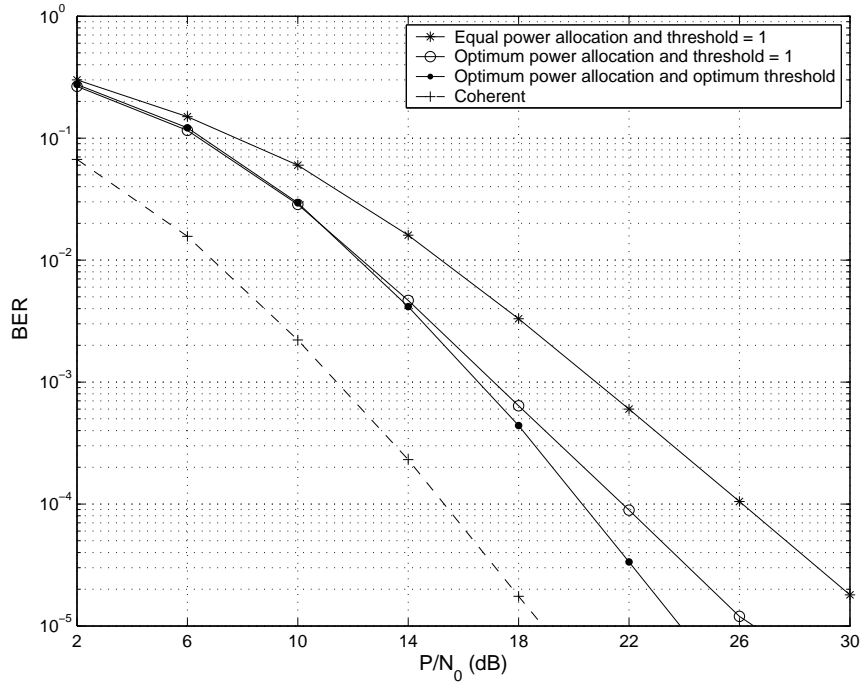


Figure 6.12: DQPSK : two relays, different power allocation and thresholds, and $\sigma_{s,d}^2 = \sigma_{s,r_i}^2 = 1, \sigma_{r_i,d}^2 = 10$.

6.3 Chapter Summary

We proposed in this chapter differential modulation schemes for multi-node cooperative communication systems.

In the first part of the chapter, we considered a multi-node differential scheme for a cooperation system with amplify-and-forward protocol. We provide as performance benchmark an exact BER expression for DMPSK modulation based on optimum combining weights. It is shown to closely match to the simulated performance. BER upper bounds and BER approximations are provided; they are tight to the simulated performance, especially in high SNR region. Based on the simple BER upper bound and the BER approximation, we can find that the diversity order of the proposed scheme is $N + 1$ when N is the number of relays and it is confirmed by the simulation results. We observe about 1.7 – 2 dB gain at a BER

of 10^{-3} when N increases from 2 to 3. The BER approximation is further simplified in order to obtain analytical result for optimum power allocation scheme. Based on the simple BER approximation, a closed-form power allocation scheme is obtained for single-relay case. An approximate power allocation scheme is provided for multi-relay scenario. Both the numerical evaluation and the analytical result show that more power should be allocated to the source in order to achieve better performance. When all relays are close to the source, the proposed scheme obtains about 0.6 dB gain over that with equal power allocation at a BER of 10^{-3} . When all relays are close to the destination, the performance with optimum power allocation scheme achieves about 2 dB improvement over that with equal power allocation scheme.

In the second part of the chapter, we considered a differential scheme for multi-node decode-and-forward cooperative communications in which each of N cooperative relays forwards only correctly decoded symbol to the destination. For each relay-destination link, a decision threshold is used at the destination for efficient signal combining. An approximate BER analysis for differential M-ary phase shift keying (DMPSK) is provided, and a low-complexity BER lower bound is derived. The BER lower bound is very close to the simulated performance under some scenarios. While jointly optimizing power allocation and thresholds based on the BER lower bound introduces $2N + 1$ dimensional searching, the search space is reduced by assuming that the same power is used at each relay and the same threshold is used at the destination. Numerical results revealed that more power should be allocated at the source to maintain link reliability and the rest of power is allocated to each relay. In addition, higher threshold should be used when all relays are close to the destination. Simulation results showed that the diversity

gain of the proposed scheme increases with the number of relays. Under a DBPSK cooperation system, the proposed scheme with different thresholds leads to performance improvement up to 6 dB at a BER of 10^{-4} . In case of DQPSK cooperation system, the proposed scheme with joint optimum power allocation and optimum threshold achieved about 4 – 5 dB gain over that with equal power allocation and a unit threshold at a BER of $10^{-3} - 10^{-4}$.

Chapter 7

Device Lifetime Maximization in Cooperative Communications

In this Chapter, we propose to increase the device lifetime by exploiting the cooperation diversity and taking both location and energy advantages in the wireless networks. The framework is based on the decode-and-forward (DF) cooperation protocol which is well suitable for wireless LAN or cellular settings; nevertheless, other cooperation protocols such as amplify-and-forward protocol can be similarly employed as well. We formulate an optimization problem with an objective to maximize the minimum device lifetime under bit-error-rate (BER) constraint. First, we consider the network with cooperative nodes in which each node can act as a source that transmits its information or a relay that helps forward the source information. We determine which nodes should cooperate and how much power to allocate for cooperative transmission. To solve the formulated problem which is NP hard, we first deduce an analytical solution for a two-node cooperative wireless network to obtain some insights. Based on the two-node solution, we then develop a fast suboptimal algorithm to reduce the complexity of the formulated problem. Furthermore, we propose to improve the device lifetime by deploying additional cooperative relays over a network with energy depleting nodes. We determine which

locations to place the relays and how much power to cooperate. An efficient suboptimal algorithm is also developed to reduce complexity of the formulated problem. Simulation results show that the proposed cooperative network achieves 2 times longer lifetime than that of the non-cooperative network. In addition, deploying one cooperative relay in a proper location can improve up to 3 times longer lifetime than that of the non-cooperative wireless network.

The rest of the Chapter is organized as follows. Section 7.1 outlines system model for non-cooperative network and cooperative wireless network. In Section 7.1.1, first we formulate an optimization problem to maximize the minimum device lifetime. Then, an analytical solution is provided for a two-node cooperative network. Finally, a suboptimal algorithm is developed for a multi-node scenario. In Section 7.2.1, we further improve the device lifetime by deploying relays in the wireless network. The relay locations and power allocations are determined based on the proposed algorithm. Simulation results and discussions are shown in Section 7.4. Finally, Section 7.5 summarizes the proposed work.

7.1 System Model

Consider a wireless network with N randomly deployed cooperative nodes as shown in Figure 7.1. Each node knows its next node in the predetermined route by which its information can be delivered to the destination node. The destination node can be a base station or an access point in case of wireless LANs, or a piconet coordinator in case of wireless PANs, or a data gathering unit in case of wireless sensor networks. In this section, we first describe a system model of the non-cooperative wireless network. Then, we present a system model of the cooperative wireless network employing the DF protocol.

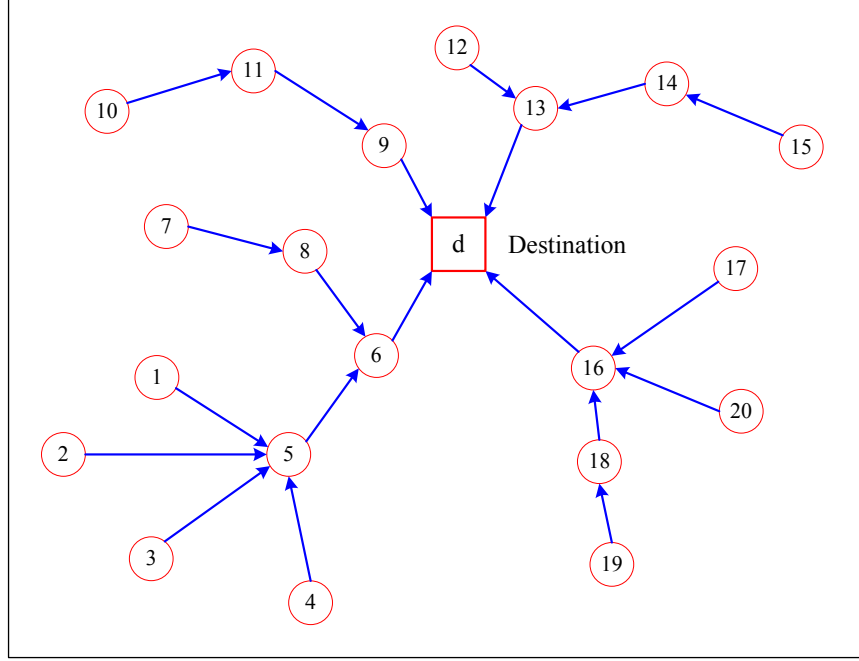


Figure 7.1: An example of non-cooperative wireless network with a destination (denoted by d).

7.1.1 Non-Cooperative Wireless Network

In a non-cooperative wireless network, each source node only transmits its own information to the destination node through a predetermined route. Figure 7.1 shows an example of a wireless network with several randomly deployed nodes. Suppose there are N nodes in the network, and let x_j denote the symbol to be transmitted from node j to its next node, denoted as n_j , in its predetermined route. The symbol x_j can be the information of node j itself, or it can be the information of other nodes that node j routes through the destination. The received signal at n_j due to the transmitted information from node j can be expressed as

$$y_{jn_j} = \sqrt{P_{jj}}h_{jn_j}x_j + w_{jn_j}, \quad (7.1)$$

where P_{jj} is the transmit power of node j , h_{jn_j} is the fading coefficient from node j to n_j , and w_{jn_j} is an additive noise. The channel coefficient h_{jn_j} is modeled as a complex Gaussian random variable with zero mean and variance $\sigma_{jn_j}^2$, i.e.,

$\mathcal{CN}(0, \sigma_{jn_j}^2)$, and the noise w_{jn_j} is $\mathcal{CN}(0, N_0)$ distributed. The channel variance $\sigma_{jn_j}^2$ is modeled as

$$\sigma_{jn_j}^2 = \eta D_{jn_j}^{-\alpha}, \quad (7.2)$$

where D_{jn_j} denotes distance between node j and n_j , α is the propagation loss factor, and η is a constant whose value depends on the propagation environment. Based on the received signal model in (7.1) and the BER formulation in [93], the average BER performance for the non-cooperative node with binary phase shift keying (BPSK) signals is upper bounded by

$$\text{BER}_j \leq \frac{N_0}{4P_{jj}\sigma_{jn_j}^2}. \quad (7.3)$$

Let the performance requirement of node j be $\text{BER}_j \leq \varepsilon$, where ε denotes the maximum allowable BER, which is assumed the same for every node. Accordingly, the optimal transmit power for non-cooperative node can be obtained from (7.3) as

$$P_{jj} = \frac{N_0}{4\varepsilon\sigma_{jn_j}^2}. \quad (7.4)$$

We denote E_j as the initial battery of node j , and denote P_s as the amount of processing power (i.e. power used for encoding information, collecting data, and etc.) at the source node. Let λ_{lj} ($l = 1, 2, \dots, N$ and $l \neq j$) be the data rate that node l sends information to node j , and λ_{jj} be the data rate that node j sends information to its next node, n_j . Then, the total power that node j uses to send the information to its next node n_j is $\lambda_{jj}P_s + \sum_{l=1}^N \lambda_{lj}P_{jj}$, where $\lambda_{jj}P_s$ is the total processing power at node j , $\lambda_{jj}P_{jj}$ represents the power that node j sends its own formation, and $\sum_{l=1, l \neq j}^N \lambda_{lj}P_{jj}$ corresponds to the power that node j routes information of other nodes. Accordingly, the device lifetime of node j can be determined as

$$T_j = \frac{E_j}{\lambda_{jj}P_s + P_{jj} \sum_{l=1}^N \lambda_{lj}} = \frac{4\varepsilon\sigma_{jn_j}^2 E_j}{(4\varepsilon\sigma_{jn_j}^2 \lambda_{jj}P_s + N_0 \sum_{l=1}^N \lambda_{lj})}. \quad (7.5)$$

From (7.5), we can see that the lifetime of each node relies on both the initial energy and the geographical location of the node. Clearly, the node whose energy is small and location is far away from its next node tends to have small device lifetime. In the following subsection, we introduce the use of cooperative communications to extend the device lifetime.

7.1.2 Cooperative Wireless Network Employing the DF Protocol

We consider a wireless network where all nodes can transmit cooperatively, i.e., each node can be a source node that transmits its information or a relay node that helps the source node. The cooperation protocol is based on DF protocol which comprises 2 transmission phases. In Phase 1, the source node sends the information to its next node on the route. In Phase 2, the relaying node decodes the information it receives from the source and helps forward the correctly decoded information. In both phases, the source and the relays transmit signals through orthogonal channels by using TDMA, FDMA, or CDMA schemes.

For subsequent evaluation, we define a power allocation matrix \mathbf{P} as an $N \times N$ matrix with the following properties:

1. Each element $P_{ij} \geq 0$, $i = 1, 2, \dots, N$ and $j = 1, 2, \dots, N$.
2. P_{jj} represents the power that node j uses to transmit its own information to its next node n_j and the relays.
3. P_{ij} represents the power that node i helps forward information of node j , information of other nodes, to the next node n_j .

Assuming that all nodes have the information to be transmitted, we have $P_{jj} > 0$. Figure 7.2 (a) illustrates a cooperative network with $N = 4$ nodes. Each solid line

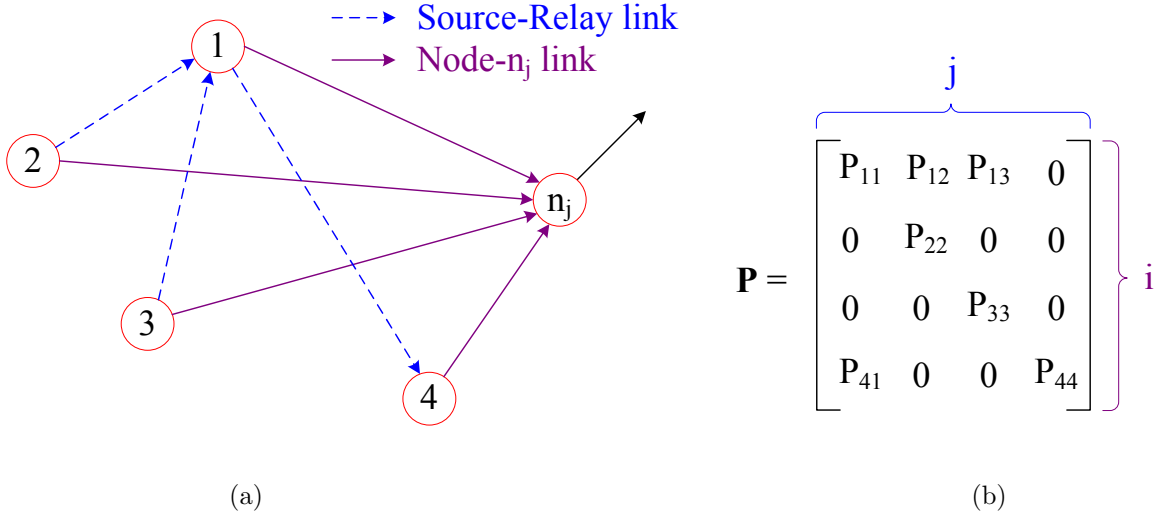


Figure 7.2: The proposed cooperative wireless network: (a) A cooperative wireless network with 4 nodes. (b) The corresponding power allocation matrix.

represents the transmission link from the source node to its next node, and each dash line represents the link from the source to the relay. Figure 7.2 (b) shows the power allocation matrix \mathbf{P} that corresponds to the cooperative wireless network in Figure 7.2 (a). All non-zero diagonal elements of matrix \mathbf{P} represent the transmit powers at the source nodes. From Figure 7.2 (a), node 1 helps relay information of node 2 and 3 to their intended destination. Therefore, the first row of the power allocation matrix \mathbf{P} contains non-zero values of P_{12} and P_{13} which represent powers that node 1 helps node 2 and node 3, respectively. Similarly, since node 4 helps forward information of node 1, the last row of matrix \mathbf{P} contains non-zero element of P_{41} .

Suppose sensor j acts as a source (or helped node) and node i acts as a relay (or helping node). When node j sends its information in Phase 1, the received signal at the destination can be described in the same form as that in (7.1), while the received signal at the helping node i is given by

$$y_{ji} = \sqrt{P_{jj}}h_{ji}x_j + w_{ji}, \quad (7.6)$$

where h_{ji} is the channel coefficient from node j to node i , and w_{ji} is additive noise. The channel h_{ji} is modeled as $\mathcal{CN}(0, \sigma_{ji}^2)$ distributed, and the noise w_{ji} is modeled as $\mathcal{CN}(0, N_0)$ distributed. Similar to (7.2), the channel variance σ_{ji}^2 is formulated as $\sigma_{ji}^2 = kD_{ji}^{-\alpha}$, where D_{ji} is the distance between node j and node i . In Phase 2, the relay forwards the information of node j to next node n_j only if the symbol is correctly decoded [93]. The received signal at the next node n_j in Phase 2 is modeled as [93]

$$y_{in_j} = \sqrt{\tilde{P}_{ij}} h_{in_j} x_j + w_{in_j}, \quad (7.7)$$

where $\tilde{P}_{ij} = P_{ij}$ if the relay decodes the symbol correctly, otherwise $\tilde{P}_{ij} = 0$. The channel coefficient h_{in_i} and the noise w_{in_i} are $\mathcal{CN}(0, \sigma_{in_i}^2)$ and $\mathcal{CN}(0, N_0)$ distributed, respectively. At the destination, the directly received signal from the source in Phase 1, and that from the relay in Phase 2 are combined using the maximum ratio combining (MRC). Assume that the energy of the transmitted symbol x_j has unit energy, then the instantaneous SNR at the MRC output of node n_j is

$$\gamma_{n_j} = \frac{P_{jj}|h_{jn_j}|^2 + \tilde{P}_{ij}|h_{in_j}|^2}{N_0}. \quad (7.8)$$

If BPSK modulation is used, the conditional BER of the cooperative transmission is given by [109]:

$$\text{BER}^h(\gamma_{n_j}) = \frac{1}{\pi} \int_0^{\pi/2} \exp\left(-\frac{\gamma_{n_j}}{\sin^2 \theta}\right) d(\theta), \quad (7.9)$$

where γ_{n_j} is specified in (7.8). Similar to (7.9), we can find that the chance of incorrectly decoding at the relay is $\text{BER}^h(P_{jj}|h_{ji}|^2/N_0)$, and the chance of correctly decoding at the relay is $1 - \text{BER}^h(P_{jj}|h_{ji}|^2/N_0)$. By taking into account the result of decoding at the relay, the conditional BER can be written as $\text{BER}^h(P_{jj}|h_{jn_j}|^2/N_0 + P_{ij}|h_{in_j}|^2/N_0)(1 - \text{BER}^h(P_{jj}|h_{ji}|^2/N_0)) + \text{BER}^h(P_{jj}|h_{jn_j}|^2/N_0)\text{BER}^h(P_{jj}|h_{ji}|^2/N_0)$. Averaging the conditional BER expression over all Rayleigh fading channels, the

average BER in case of BPSK modulation is [93]

$$\begin{aligned} \text{BER}_j = & F\left(1 + \frac{P_{jj}\sigma_{jn_j}^2}{N_0 \sin^2 \theta}\right) \cdot F\left(1 + \frac{P_{jj}\sigma_{ji}^2}{N_0 \sin^2 \theta}\right) \\ & + F\left(\left(1 + \frac{P_{jj}\sigma_{jn_j}^2}{N_0 \sin^2 \theta}\right) \left(1 + \frac{P_{ij}\sigma_{in_j}^2}{N_0 \sin^2 \theta}\right)\right) \cdot \left[1 - F\left(1 + \frac{P_{jj}\sigma_{ji}^2}{N_0 \sin^2 \theta}\right)\right], \end{aligned} \quad (7.10)$$

where $F(x(\theta)) = \frac{1}{\pi} \int_0^{\pi/2} [x(\theta)]^{-1} d\theta$. The first term on the right hand side of (7.10) corresponds to the case of incorrectly decoding at the relay, and the second term corresponds to the case of correctly decoding at the relay. By assuming that all channel links are available, i.e., $\sigma_{jn_j}^2 \neq 0$ and $\sigma_{ji}^2 \neq 0$, the BER upper bound of the closed form BER expression in (7.10) can be obtained by removing the negative term and all one's in (7.10). The resulting BER upper bound is given by [93]

$$\text{BER}_j \leq N_0^2 \frac{A^2 P_{ij} \sigma_{in_j}^2 + B P_{jj} \sigma_{ji}^2}{P_{jj}^2 P_{ij} \sigma_{jn_j}^2 \sigma_{ji}^2 \sigma_{in_j}^2}, \quad (7.11)$$

where $A = F(\sin^{-2} \theta) = 0.25$ and $B = F(\sin^{-4} \theta) = 0.1875$. We can see from (7.11) that cooperative transmission leads to a performance diversity of two. The BER upper bound in (7.11) gives some insight understanding that when the source and the relay transmit cooperatively, the total transmitted power required at the source and the relay is less than that requires for non-cooperative transmission to yield the same BER performance. Therefore, by properly allocating the transmitted power at the source (P_{jj}) and the transmitted power at the relay (P_{ij}), the lifetime of the source can be significantly increased whereas the lifetime of the relay is slightly decreased. Note that, for multi-hop relay networks, the signal model in [94] can also be applied to the proposed framework in a similar way.

7.2 Lifetime Maximization by Cooperative Node Employment

In this section, we consider a cooperative wireless network with randomly distributed nodes, each employing the DF cooperation protocol. We aim to maximize the minimum device lifetime over all nodes in the network. First, we formulate the lifetime maximization problem. Then, an analytical solution is provided for a network with two nodes. Finally, based on the solution for the two-node network, a fast suboptimal algorithm is developed to solve the problem with multiple nodes.

7.2.1 Problem Formulation

As shown in the previous section, the cooperative scheme increases the diversity gain and hence significantly improves the system performance. This implies that the cooperative scheme requires less power to achieve the same performance as the non-cooperative scheme, and thus can be used to improve the device lifetime. Note that different nodes can have different remaining energy, and different nodes can have different effects on performance improvement depending on their locations. So the nodes with energy advantages or location advantages can help the depleting nodes. The questions are which node should help which node, and how much power to help in order to efficiently increase the device lifetime. To answer these questions, we formulate the problem as follows.

In cooperative wireless network, the overall transmit power of each node is a summation of the power that the node transmits its own information and the power that the node cooperatively helps forward information of other nodes to their next nodes. Let P_r be the processing power at each relay node, i.e. the power that the relay uses in decoding and forwarding the information. From the power allocation

matrix \mathbf{P} as defined in Section 7.1.1, the overall transmit power of the cooperating node i is $P_{ii} \sum_{l=1}^N \lambda_{li} + \sum_{j=1, j \neq i}^N P_{ij} (\sum_{l=1}^N \lambda_{lj})$, and the overall processing power of node i is $\lambda_{ii} P_s + \sum_{j=1, j \neq i}^N P_r \text{sgn}(P_{ij}) (\sum_{l=1}^N \lambda_{lj})$ where $\text{sgn}(P_{ij})$ is the sign function that returns 1 if $P_{ij} > 0$, and 0 otherwise. Hence, the lifetime of the cooperating node i can be expressed as

$$T_i(\mathbf{P}) = \frac{E_i}{\lambda_{ii} P_s + P_{ii} \sum_{l=1}^N \lambda_{li} + \sum_{j=1, j \neq i}^N (P_r \text{sgn}(P_{ij}) + P_{ij}) (\sum_{l=1}^N \lambda_{lj})}, \quad (7.12)$$

where E_i is the initial battery energy of node i . Obviously, the lifetime of node i reduces if node i helps transmit information of other nodes. On the other hand, the more the power P_{ij} that node i helps node j , the longer the lifetime of node j . Therefore, it is crucial to properly design the power allocation matrix \mathbf{P} such that the minimum device lifetime is maximized.

With an objective to maximize the minimum device lifetime under the constraint that each node satisfies its BER requirement, the problem can be formulated as

$$\begin{aligned} & \max_{\mathbf{P}} \min_i T_i(\mathbf{P}) & (7.13) \\ \text{s.t.} & \begin{cases} \text{Performance: } \text{BER}_i \leq \varepsilon, \forall i; \\ \text{Power: } 0 < P_{ii} \leq P_{\max}, \forall i; \\ \text{Power: } 0 \leq P_{ij} \leq P_{\max}, \forall j \neq i, \end{cases} \end{aligned}$$

where ε denotes the required BER to maintain the quality of service of each transmission link. The first constraint is to satisfy the BER performance requirement in which the BER is given by (7.10), the second constraint is to guarantee that each node has information to transmit and the transmit power is no greater than P_{\max} , the third constraint is to ensure that all the allocated powers are non-negative and no greater than P_{\max} . Due to the assignment and combinatorial nature, the formulated problem is NP hard [110].

7.2.2 Analytical Solution for a Two-Node Wireless Network

To get some insightful understanding on the formulated problem, we provide in this section a closed-form analytical solution at high SNR scenario for a wireless network with $N = 2$ nodes, each transmitting its information directly to the destination d .

In this two-node network, there are three possible transmission strategies, namely, 1) each node transmits non-cooperatively, 2) one node helps forward information of the other by the use cooperation protocol, and 3) both nodes help forward information of each other by using the DF cooperation protocol. In the sequel, we will maximize the minimum device lifetime for each strategy. The optimum power allocation is the one that maximize the minimum device lifetime over all possible strategies. Without loss of generality, we assume that the transmit power required for non-cooperative transmission in each link is less than P_{\max} .

Non-cooperative transmission among nodes

Based on the discussion in Section 7.1.1, the optimum power allocation for non-cooperative case is

$$P_{jj} = \frac{N_0}{4\varepsilon\sigma_{jd}^2} \quad (7.14)$$

for $j = 1, 2$, and $P_{ij} = 0$ for $i \neq j$. Substituting (7.14) into (7.5), the optimum device lifetime in case of non-cooperative transmission can be determined as

$$T_{non-coop}^* = \min \left[\frac{4\varepsilon\sigma_{1d}^2 E_1}{4\varepsilon\sigma_{1d}^2 \lambda_{11} (P_s + N_0)}, \frac{4\varepsilon\sigma_{2d}^2 E_2}{4\varepsilon\sigma_{2d}^2 \lambda_{22} (P_s + N_0)} \right]. \quad (7.15)$$

Cooperative transmission when one node helps the other node

Without loss of generality, we will provide the solution for the case when node i helps relay the information of node j to the destination. In this scenario, the

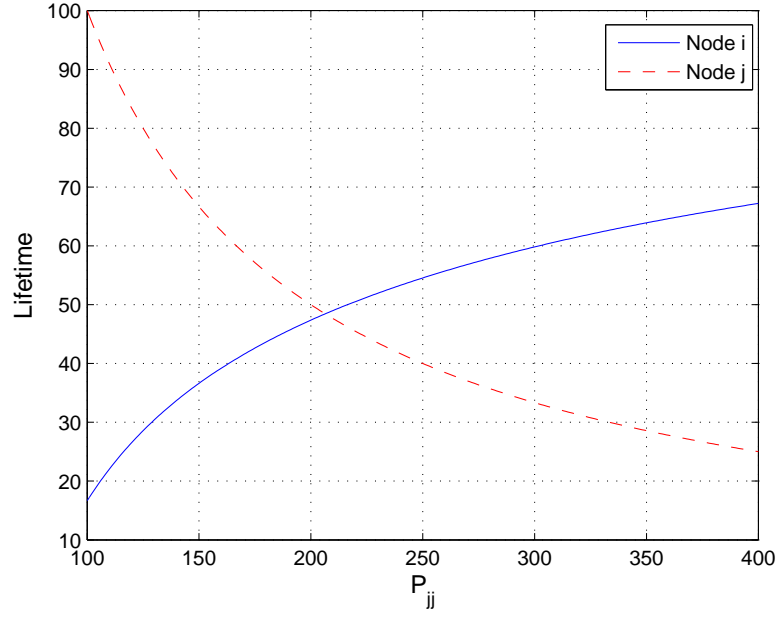


Figure 7.3: Lifetimes of the two cooperative nodes as functions of the transmit power of the helped node (P_{22}).

lifetimes of node i and node j are given by

$$T_i = \frac{E_i}{\lambda_{ii}(P_s + P_{ii}) + \lambda_{jj}(P_r + P_{ij})} \quad (7.16)$$

and

$$T_j = \frac{E_j}{\lambda_{jj}(P_s + P_{jj})}. \quad (7.17)$$

Based on (7.16) and (7.17), appropriately choosing the powers of P_{ii} , P_{ij} , and P_{jj} can maximize the minimum device lifetime while performances of both nodes satisfy the specified BER requirements.

In order for node i to satisfy the BER requirement ε , the optimum transmit power of node i (P_{ii}) can be obtained by using the formulation in (7.14). According to the BER upper bound in (7.11), the optimum power P_{jj} that node j transmits its own information, and power P_{ij} that node i helps forward information of node j must satisfy

$$\frac{N_0^2 A^2 P_{ij} \sigma_{id}^2 + N_0^2 B P_{jj} \sigma_{ji}^2}{P_{jj}^2 P_{ij} \sigma_{jd}^2 \sigma_{ji}^2 \sigma_{ii}^2} = \varepsilon. \quad (7.18)$$

From (7.18), we can express P_{ij} in term of P_{jj} as

$$P_{ij} = \frac{P_{jj}}{C_{ij}P_{jj}^2 - D_{ij}} \triangleq f(P_{jj}), \quad (7.19)$$

where

$$C_{ij} = \frac{\varepsilon\sigma_{id}^2\sigma_{jd}^2}{BN_0^2} \quad (7.20)$$

and

$$D_{ij} = \frac{A^2\sigma_{id}^2}{B\sigma_{ji}^2}. \quad (7.21)$$

By substituting P_{ij} from (7.19) and P_{ii} from (7.14) into (7.16), we have

$$T_i = \frac{E_i}{\lambda_{ii}(P_s + \frac{N_0}{4\varepsilon\sigma_{id}^2}) + \lambda_{jj}(P_r + f(P_{jj}))}. \quad (7.22)$$

We can see that both T_i in (7.22) and T_j in (7.17) are functions of P_{jj} . Therefore, the optimization problem in (7.13) is simplified to

$$T_{i-helps-j}^* = \max_{P_{jj}} \left[\min \left(\frac{E_i}{\lambda_{ii}(P_s + \frac{N_0}{4\varepsilon\sigma_{id}^2}) + \lambda_{jj}(P_r + f(P_{jj}))}, \frac{E_j}{\lambda_{jj}(P_s + P_{jj})} \right) \right]. \quad (7.23)$$

Since the lifetime T_i increases with the power P_{jj} while the lifetime T_j decreases with P_{jj} , the minimum device lifetime is maximized when $T_i = T_j$. As an illustrated example, Figure 7.3 plots the lifetimes T_i and T_j as functions of P_{jj} for a specific set of parameters. For unconstraint optimization of (7.23), we can see from Figure 7.3 that the optimal power P_{jj} in (7.23) is the one that results in $T_i = T_j$. Therefore, the optimal solution to (7.23) can be obtained by finding P_{jj} such that

$$\frac{E_i}{\lambda_{ii}(P_s + \frac{N_0}{4\varepsilon\sigma_{id}^2}) + \lambda_{jj}(P_r + f(P_{jj}))} = \frac{E_j}{\lambda_{jj}(P_s + P_{jj})}. \quad (7.24)$$

By using (7.19)-(7.21) and (7.23)-(7.24), the optimum device lifetime in case of node i helps node j is given by

$$T_{i-helps-j}^* = \frac{E_j}{\lambda_{jj}(P_s + P_{jj}^*)}, \quad (7.25)$$

where P_{jj}^* is the solution to

$$C_{ij}E_i\lambda_{jj}P_{jj}^3 + KC_{ij}P_{jj}^2 - (D_{ij}\lambda_{jj}E_i + \lambda_{jj}E_j)P_{jj} - \Upsilon D_{ij} = 0, \quad (7.26)$$

in which $\Upsilon = E_i\lambda_{jj}P_s - E_j\lambda_{ii}P_s - \lambda_{jj}E_jP_r + (\lambda_{ii}N_0E_j)/(4\varepsilon\sigma_{id}^2)$. Accordingly, we can find that $P_{ij}^* = f(P_{jj}^*)$ through the relation in (7.19).

If the resulting P_{ij}^* is not larger than P_{\max} , then (7.25) is the optimum device lifetime for this scenario. Otherwise, let $P_{ij}^* = P_{\max}$ and find P_{jj}^* to satisfy the BER requirement in (7.18). After some manipulations, we have

$$P_{jj}^* = \frac{-Q_1 + \sqrt{Q_1^2 + Q_2Q_3P_{\max}^2}}{Q_2P_{\max}}, \quad (7.27)$$

where $Q_1 = B\sigma_{ji}^2N_o^2$, $Q_2 = 2\varepsilon\sigma_{id}^2\sigma_{ji}^2\sigma_{jd}^2$, and $Q_3 = 2A^2\sigma_{id}^2N_o^2$. Therefore, the lifetime of node i and node j are

$$T_i^* = \frac{E_i}{\lambda_{ii}(P_s + P_{ii}) + \lambda_{jj}(P_r + P_{\max})} \quad (7.28)$$

and

$$T_j^* = \frac{E_j}{\lambda_{jj}(P_s + P_{jj}^*)}, \quad (7.29)$$

respectively, and the optimum device lifetime when $P_{ij}^* > P_{\max}$ is the minimum between T_i^* and T_j^* . Hence, the optimum device lifetime when node i helps node j can be obtained as

$$T_{i\text{-helps-}j}^* = \begin{cases} \frac{E_j}{\lambda_{jj}(P_s + P_{jj}^*)}, & P_{ij}^* \leq P_{\max}; \\ \min\{T_i^*, T_j^*\}, & P_{ij}^* > P_{\max}, \end{cases} \quad (7.30)$$

where P_{jj}^* , T_i^* , and T_j^* are specified in (7.40), (7.28), and (7.29), respectively.

Cooperative transmission when both nodes help each other

When both nodes help each other, the lifetime of node i , $i = 1$ and 2 , is given by (7.16). Similar to the previous case, we first consider the formulated problem without maximum power constraint, then we find solution by taking into account the maximum power constraints.

Under this cooperation strategy, the power that node i helps node j (P_{ij}) can be obtained in the same way as in (7.19). Hence, the lifetime of node i can be expressed as

$$T_i = \frac{E_i}{\lambda_{ii}(P_s + P_{ii}) + \lambda_{jj}(P_r + \frac{P_{jj}}{C_{ij}P_{jj}^2 - D_{ij}})}, \quad (7.31)$$

where C_{ij} and D_{ij} are specified in (7.20) and (7.21), respectively. Recall that without maximum power constraint, the necessary condition to maximize the device lifetime of the two-node wireless network is $T_i = T_j$, and observe from (7.31) that both lifetime T_i and lifetime T_j are in terms of the powers P_{ii} and P_{jj} . Therefore, the optimum device lifetime can be obtained by finding P_{ii}^* and P_{jj}^* that maximizes T_i under the condition: $T_i = T_j$. From (7.31), the optimum device lifetime when both users help each other is

$$\begin{aligned} T_{both-help}^* &= \frac{E_i}{\lambda_{ii}(P_s + P_{ii}^*) + \lambda_{jj}(P_r + \frac{P_{jj}^*}{C_{ij}(P_{jj}^*)^2 - D_{ij}})} \\ &= \frac{E_j}{\lambda_{jj}(P_s + P_{jj}^*) + \lambda_{ii}(P_r + \frac{P_{ii}^*}{C_{ji}(P_{ii}^*)^2 - D_{ji}})}, \end{aligned} \quad (7.32)$$

where P_{ii}^* and P_{jj}^* are the solutions to the following optimization problem:

$$\begin{aligned} &\arg \max_{P_{ii}, P_{jj}} \frac{E_i}{\lambda_{ii}(P_s + P_{ii}) + \lambda_{jj}(P_r + \frac{P_{jj}}{C_{ij}P_{jj}^2 - D_{ij}})} \\ \text{s.t.} &\begin{cases} \frac{[(\lambda_{ii}P_s + \lambda_{jj}P_r + \lambda_{ii}P_{ii})(C_{ij}P_{jj}^2 - D_{ij}) + \lambda_{jj}P_{jj}](C_{ji}P_{ii}^2 - D_{ji})}{[(\lambda_{jj}P_s + \lambda_{ii}P_r + \lambda_{jj}P_{jj})(C_{ji}P_{ii}^2 - D_{ji}) + \lambda_{ii}P_{ii}](C_{ij}P_{jj}^2 - D_{ij})} = \frac{E_i}{E_j}, \\ P_{jj} > \sqrt{\frac{D_{ij}}{C_{ij}}}, \quad \forall j \neq i. \end{cases} \end{aligned} \quad (7.33)$$

In (7.33), the first constraint is to ensure that $T_i = T_j$, and the second constraint is to guarantee that $P_{ij} = \frac{P_{jj}}{C_{ij}P_{jj}^2 - D_{ij}} > 0$.

If $P_{ij}^* \leq P_{\max}$ and $P_{ji}^* \leq P_{\max}$, then the solution to (7.32) is the optimum device lifetime for this case. Otherwise, the optimization problem can be separated into two subproblems. Firstly, we let $P_{ij}^* = P_{\max}$ and find P_{jj}^* from (7.27). Substituting the obtained P_{jj}^* into (7.31), we can see that both the obtained T_i and T_j are functions of P_{ii} . Therefore, the optimal device lifetime for this subproblem is to

maximize $\min\{T_i, T_j\}$ over P_{ii} . Secondly, we let $P_{ji}^* = P_{\max}$ and find P_{ii}^* from (7.27), then T_i and T_j obtained by using (7.31) are function of P_{jj} . The optimal device lifetime for the second subproblem is to maximize $\min\{T_i, T_j\}$ over P_{jj} . Finally, the optimum solutions from two subproblems are compared, and the optimum device lifetime when $P_{ij}^* > P_{\max}$ or $P_{ji}^* > P_{\max}$ is the maximum among these two solutions. Therefore, the optimum device lifetime when both nodes help each other is given by

$$T_{both-help}^* = \begin{cases} \frac{E_i}{\lambda_{ii}(P_s + P_{ii}^*) + \lambda_{jj}(P_r + \frac{P_{jj}^*}{C_{ij}(P_{jj}^*)^{2-D_{ij}}})}, & P_{ij}^* \text{ and } P_{ji}^* \leq P_{\max}, \\ \max(\mathcal{T}), & P_{ij}^* \text{ or } P_{ji}^* > P_{\max}, \end{cases} \quad (7.34)$$

where $\mathcal{T} \triangleq \max_{P_{ii}} \min\{T_i(ii), T_j(ii)\}, \max_{P_{jj}} \min\{T_i(jj), T_j(jj)\}$, P_{ii}^* and P_{jj}^* are solutions to (7.33), and T_i , and T_j are specified in (7.31).

Finally the optimal device lifetime, denoted as T_D^* , for the two-node wireless network can be obtained from (7.15), (7.25), and (7.34) by

$$T_D^* = \max \{T_{non-coop}^*, T_{1-helps-2}^*, T_{2-helps-1}^*, T_{both-help}^*\}. \quad (7.35)$$

In (7.35), we obtain the optimum device lifetime for the two-node wireless network by comparing the maximum lifetime of four possible cooperation strategies. However, as the number of nodes increases, although the optimal solution can be obtained through full search, it is computationally expensive. To overcome the complexity issue, we propose in the subsequent subsection a suboptimal greedy algorithm to determine the power allocation and the corresponding device lifetime.

7.2.3 Suboptimal Algorithm for Multi-Node Wireless Network

The basic idea of the proposed greedy suboptimal algorithm is to find a node to be helped and its helping node step by step. In each step, the node to be helped

is the one who has minimum lifetime, and has not been helped by others. The helping node in each step is the one who maximizes the minimum device lifetime after it helps the selected helped node. In this way, the minimum device lifetime can be increased step by step. The iteration stops if the device lifetime cannot be significantly improved or all nodes in the network have been helped. Note that the proposed greedy suboptimal approach can be applied to any multi-node cooperation strategy. In what follows, we first maximize the minimum device lifetime for a given pair of helped and helping nodes, and then describe our proposed algorithm in details.

For a specific pair of helped and helping nodes, their transmit powers and the corresponding lifetime can be determined in a similar way to the two-node network as discussed in the previous subsection. Specifically, consider a two-node cooperation strategy, then the optimum device lifetime when node i helps node j can be obtained by solving

$$T_{i\text{-helps-}j}^* = \max_{P_{jj}} \left[\min \left(\frac{E_i}{\Psi_i + (P_r + f(P_{jj})) \sum_{l=1}^N \lambda_{lj}}, \frac{E_j}{\Psi_j + P_{jj} \sum_{l=1}^N \lambda_{lj}} \right) \right] \quad (7.36)$$

where

$$\Psi_i = \lambda_{ii} P_s + P_{ii} \sum_{l=1}^N \lambda_{li} + \sum_{k=1, k \neq i, j}^N (P_r \text{sgn}(P_{ik}) + P_{ik}) (\sum_{l=1}^N \lambda_{lk}), \quad (7.37)$$

and

$$\Psi_j = \lambda_{jj} P_s + \sum_{k=1, k \neq j}^N (P_r \text{sgn}(P_{jk}) + P_{jk}) (\sum_{l=1}^N \lambda_{lk}), \quad (7.38)$$

in which Ψ_i and Ψ_j are constants that do not depend on P_{jj} . Using the equality $T_i = T_j$, after some manipulations, we can determine $T_{i\text{-helps-}j}^*$ as

$$T_{i\text{-helps-}j}^* = \frac{E_j}{\Psi_j + P_{jj}^* \sum_{l=1}^N \lambda_{lj}}, \quad (7.39)$$

where P_{jj}^* is the solution to

$$C_{ij} E_i \sum_{l=1}^N \lambda_{lj} P_{jj}^3 + G C_{ij} P_{jj}^2 - (D_{ij} E_i + E_j) (\sum_{l=1}^N \lambda_{lj}) P_{jj} - G D_{ij} = 0, \quad (7.40)$$

in which $G = E_i\Psi_j - E_j\Psi_i - E_jP_r\Sigma_{l=1}^N\lambda_{lj}$, and Ψ_i and Ψ_j are specified in (7.37) and (7.38), respectively. If the resulting $P_{ij}^* = f(P_{jj}^*)$ is larger than P_{\max} then the same calculation steps as in the previous subsection can be used to determine $T_{i\text{-helps-}j}^*$. This solution is used to determine the device lifetime in each step of our proposed algorithm as follows.

Initially, the power allocation matrix \mathbf{P} is assigned as a diagonal matrix with its diagonal component P_{jj} follows (7.14), i.e., the initial scheme is the non-cooperative transmission scheme. The corresponding lifetime of node j is $T_j = E_j/(\lambda_{jj}P_s + P_{jj}\Sigma_{l=1}^N\lambda_{lj})$. Construct a helped list which is a list of all possible nodes to be helped: $H_{list} = \{1, 2, \dots, N\}$. First, the algorithm finds the helped node from the helped list by choosing the node who has minimum lifetime, i.e., the helped node \hat{j} is given by

$$\hat{j} = \arg \min_{j \in H_{list}} T_j. \quad (7.41)$$

Second, the algorithm finds a node to help node \hat{j} by choosing among all nodes i , $i = 1, 2, \dots, N$ and $i \neq \hat{j}$. For each possible helping node i , the algorithm uses (7.36) to find power allocation for the helping node i and the helped node \hat{j} . Then, the algorithm determines $T_D^*(i)$ as the minimum lifetime among nodes in the networks after node i helps node \hat{j} . The obtained $T_D^*(i)$ from all possible helping nodes are compared, and then the algorithm selects node $\hat{i} = \arg \max_i T_D^*(i)$ to help node \hat{j} . Next, the algorithm updates the power allocation matrix \mathbf{P} and updates the helped list by removing node \hat{j} from the helped list. Then, the algorithm goes back to the first step. This iteration is continued until all nodes have been helped, i.e., the helped list is empty, or the device lifetime cannot be significantly increased. The resulting \mathbf{P} is the power allocation matrix which gives answer to the questions which node should help which node and how much power to cooperate. The detailed algorithm is shown in Table 7.1.

The proposed algorithm is suboptimal and it is based on the cooperation strategy with only one relay ($K = 1$). However, the proposed algorithm significantly improves the device lifetime, as will be shown by simulation results in Section 7.4. Additionally, the complexity of the proposed algorithm only increases quadratically with the number of nodes. Note that the performance of the proposed algorithm can be further improved by exploiting the cooperation strategy with more than one relay; nevertheless, such performance improvement comes with the price of higher complexity. Note also that all of the necessary computations can be performed offline. Once the algorithm is executed, the nodes follow the determined power allocation and cooperation strategy. Since the proposed algorithm allocates power based on the average channel realizations, the algorithm needs to be updated only when the network topology changes considerably, and the additional overhead for the cooperation assignment is required only at the beginning of the transmission. Furthermore, it is clear from (7.36) that the helped node and helping node should be close to each other. Taking into consideration this observation, we can further reduce the complexity of the proposed algorithm to find the helping node for each helped node by only searching over the nodes that are close to the helped node. In this way, only the local information is needed to compute the power allocation matrix. Although this leads to performance degradation, the performance loss is insignificant, as will be shown by computer simulations in Section 7.4.

Table 7.1: Suboptimal algorithm for maximizing the minimum device lifetime of wireless network with multiple cooperative nodes

<p>Initialization: $P_{jj} = \frac{N_0}{4\varepsilon_j \delta_{jj}^2}$, $T_j = E_j / \lambda_{jj}(P_s + P_{jj})$, $T_D^* = \min[T_j]$, and $H_{list} = \{1, 2, \dots, N\}$.</p>
<p>Iteration:</p> <ol style="list-style-type: none"> 1) Select the helped node with the minimum lifetime from the helped list: $\hat{j} = \arg \min_{j \in H_{list}} T_j$, where $T_j = E_j / (\lambda_{jj} P_s + P_{jj} \sum_{l=1}^N \lambda_{lj})$. 2) Select the helping node from $\phi_{\hat{j}} = \{1, 2, \dots, N\} - \{\hat{j}\}$. <ul style="list-style-type: none"> • For each $i \in \phi_{\hat{j}}$, solve (7.23) for T_i and $T_{\hat{j}}$, and then find the corresponding minimum device lifetime $T_D^*(i)$. • Select \hat{i} that results in maximum of minimum device lifetime, $\hat{i} = \arg \max_{i \in \phi_{\hat{j}}} T_D^*(i)$, as the helping node. 3) Update power allocation matrix \mathbf{P} and helped list H_{list}. Go to 1).
<p>End If the helped list is empty: $H_{list} = \emptyset$, or the device lifetime cannot be significantly increased. return \mathbf{P}.</p>

7.3 Lifetime Maximization by Cooperative Relay Deployment

In this section, we improve the device lifetime by exploiting the cooperation diversity through the deployment of relays in energy depleting networks. The relays do not have information to be transmitted; however, they are able to help forward information of the nodes. With the help from the relays, the nodes can exploit cooperation diversity to improve their lifetimes. As a result, the relay deployment reduces the need to change battery of each node which in turn helps reduce maintenance cost. In addition, the relay deployment does not require any modification of the nodes. The additional implementation cost is only the cost of the relay installation. By using a proper number of relays and placing the relays in appropriate locations, the device lifetime can be greatly increased while the overall cost is minimized. In the sequel, we determine locations of relays in the network

with an objective to maximize the minimum device lifetime.

We consider a wireless network with N randomly-located nodes and a destination. The nodes are denoted as nodes $1, 2, \dots, N$, and the relays are represented by R_1, R_2, \dots, R_K . Since there is no cooperation among the nodes, the power allocation matrix \mathbf{P} as defined in Section 7.1.1 is an $N \times N$ diagonal matrix whose diagonal element, P_{jj} , represents the power that node j transmits the information to its next node. We assume that all nodes have information to transmit, i.e., $P_{jj} > 0$ for all j . The lifetime of node j is given by

$$T_j(\mathbf{P}) = \frac{E_j}{\lambda_{jj}P_s + P_{jj}\sum_{l=1}^N \lambda_{lj}}. \quad (7.42)$$

We also define in this section a $K \times N$ relay power allocation matrix $\hat{\mathbf{P}}$ whose $(i, j)^{th}$ element, \hat{P}_{ij} , represents the power that the relay R_i helps the node j . We assume that each relay does not have its own information to transmit; it only helps transmit information of other nodes. By denoting E_{R_i} as the initial energy of relay R_i , the lifetime of relay R_i can be written as

$$T_{R_i}(\hat{\mathbf{P}}) = \frac{E_{R_i}}{\sum_{j=1}^N (P_r \text{sgn}(\hat{P}_{ij}) + \hat{P}_{ij})(\sum_{l=1}^N \lambda_{lj})}. \quad (7.43)$$

As an example, a wireless network with four nodes and two relays is depicted in Figure 7.4 (a). In the figure, the solid line represents a link from a node (source j or relay) to the next node n_j , and the dashed line represents a link from a source to a relay. Figure 7.4 (b) shows the power allocation matrix \mathbf{P} and the relay power allocation matrix $\hat{\mathbf{P}}$ which correspond to the wireless network in Figure 7.4 (a). Since all four nodes transmit their information to n_j , all diagonal elements of the matrix \mathbf{P} are non-zeros. As shown in Figure 7.4 (a) by solid lines with square (“□”) and circle (“○”), relay R_1 helps transmit information of node 1 and node 2, respectively. Therefore, \hat{P}_{11} and \hat{P}_{12} are non-zero elements in the first

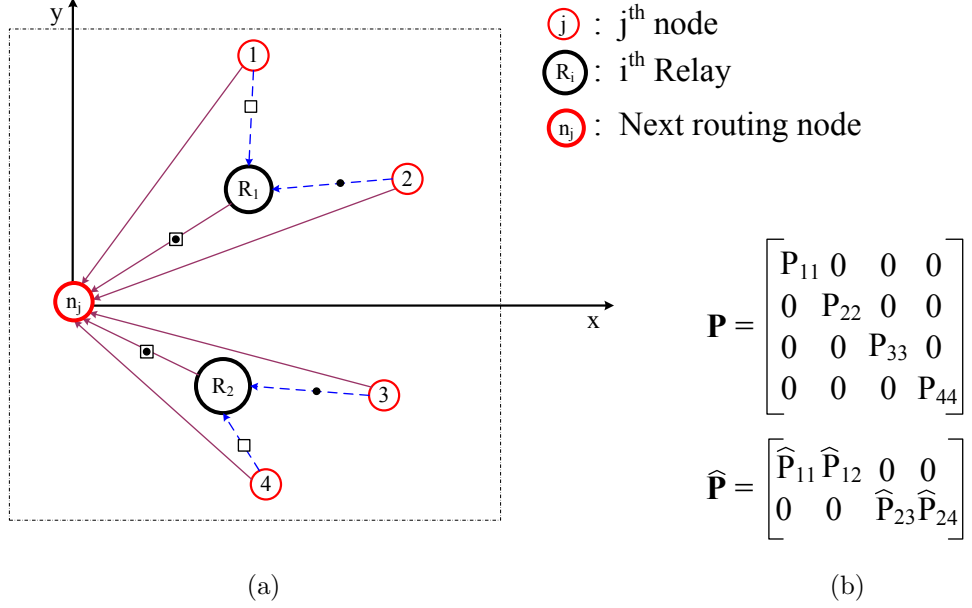


Figure 7.4: Cooperative wireless network with relay deployment: (a) One cluster with 4 nodes, 2 relays, and 1 destination. (b) The corresponding power allocation matrices (\mathbf{P}) and ($\hat{\mathbf{P}}$) for the nodes and the relays, respectively.

row of the matrix \hat{P} . Similarly, relay R_2 helps transmit information of node 3 and node 4 to the destination; \hat{P}_{23} and \hat{P}_{24} are non-zero elements in the second row of \hat{P} .

We denote x_j and y_j as the locations of node j on the x-axis and the y-axis, respectively, and denote a location vector of node j as $\bar{\mathbf{D}}_j = [x_j \ y_j]^T$. Accordingly, the channel variance between node j and its next node n_j is given by $\sigma_{jn_j}^2 = \eta \|\bar{\mathbf{D}}_j - \bar{\mathbf{D}}_{n_j}\|^{-\alpha}$ where $\|\cdot\|$ denotes the Frobenius norm [84]. The locations of the relays are specified by a $2 \times K$ matrix $\mathbf{D}_R = [\bar{\mathbf{D}}_{R_1} \ \bar{\mathbf{D}}_{R_2} \ \cdots \ \bar{\mathbf{D}}_{R_K}]$ in which the i^{th} column indicates the location of relay R_i , i.e., $\bar{\mathbf{D}}_{R_i} = [x_{R_i} \ y_{R_i}]^T$ is the location vector of relay R_i . Then, the channel variance between relay R_i and node n_j can be given by $\sigma_{R_i, n_j}^2 = \eta \|\bar{\mathbf{D}}_{R_i} - \bar{\mathbf{D}}_{n_j}\|^{-\alpha}$, and the channel variance between node j and relay R_i is $\sigma_{j, R_i}^2 = \eta \|\bar{\mathbf{D}}_j - \bar{\mathbf{D}}_{R_i}\|^{-\alpha}$. If node j is helped by relay R_i , then the BER performance of node j is of the form similar to (7.10) with P_{ij} and σ_{ji}^2

replaced by \hat{P}_{ij} and σ_{j,R_i}^2 , respectively.

Our objective is to determine the matrices \mathbf{D}_R , \mathbf{P} , and $\hat{\mathbf{P}}$ such that the minimum device lifetime is maximized. We formulated the optimization problem as

$$\max_{\mathbf{D}_R, \mathbf{P}, \hat{\mathbf{P}}} \min_{i,j} \{T_j(\mathbf{P}), T_{R_i}(\hat{\mathbf{P}})\} \quad (7.44)$$

$$\text{s.t.} \begin{cases} \text{Performance: } \text{BER}_j \leq \varepsilon, \forall j; \\ \text{Power: } 0 < P_{ii} \leq P_{\max}, P_{ij} = 0 \forall i, j \neq i; \\ \text{Power: } 0 \leq \hat{P}_{ij} \leq P_{\max}, \forall i, j. \end{cases}$$

In (7.44), the first constraint is to satisfy the BER requirement. The second constraint is to guarantee that all nodes transmit their information with powers no greater than P_{\max} and there is no cooperation among nodes. The third constraint is to ensure that the powers that the relays help the nodes are non-negative and no greater than P_{\max} . Due to the assignment and combinatorial nature of the formulated problem, the problem in (7.44) is NP hard [110]. Since it is computationally expensive to obtain the optimal solution to (7.44), we propose in what follows a fast suboptimal algorithm.

The basic idea of the proposed algorithm is to add one relay at a time into the network. Each time the location of the added relay is chosen as the one, among all possible locations, that results in maximum of the minimum device lifetime. The algorithm stops when the device lifetime improvement is insignificant after adding another relay or when the maximum number of relays is reached. In the sequel, we first describe the algorithm to determine the device lifetime in each step, and then we describe the proposed algorithm in details. To maximize the minimum device lifetime when the number of relays and their locations are given, we use greedy suboptimal algorithm as follows. Initially, all nodes are sorted in ascending order according to their non-cooperative lifetimes, as specified in (7.5), and then listed

Table 7.2: Suboptimal algorithm to determine device lifetime when relay locations are fixed

<p>Initialization: $P_{jj} = \frac{N_0}{4\varepsilon_j\sigma_{jj}^2}$, $T_j = \frac{E_j}{\lambda_{jj}(P_s+P_{jj})}$, $T_D^* = \min[T_j]$, Sort N nodes by their lifetimes in ascending order and list in H_{list}.</p>
<p>Iteration:</p> <ol style="list-style-type: none"> 1) Select the first node in the H_{list} as the helped node. 2) Select the helping relay $R_{\hat{i}}$ from the set of K relays. <ul style="list-style-type: none"> • For each i, use the heuristic algorithm to maximize the minimum device lifetime, $T_D^*(i)$. • Select $R_{\hat{i}}$ that results in maximum of minimum device lifetime to help the node \hat{j}. 3) Update $P_{\hat{j}\hat{j}}$ in \mathbf{P} and update $\hat{P}_{\hat{i}\hat{j}}$ in $\hat{\mathbf{P}}$. Set $\hat{P}_{i\hat{j}} = 0$ for all $i \neq \hat{i}$ and set $T_D^* = T_D^*(\hat{i})$. Remove node \hat{j} from the helped list H_{list}. Go to 1).
<p>End: If the helped list is empty: $H_{list} = \emptyset$, or the device lifetime cannot be significantly increased. Return \mathbf{P}, $\hat{\mathbf{P}}$, T_D^*.</p>

in a helped list H_{list} . In each iteration, first, select the first node in the helped list as the one to be helped. Second, determine the minimum device lifetime after all of the relay R_i 's ($i = 1, 2, \dots, K$) help the selected node, and then choose the relay $R_{\hat{i}}$ where \hat{i} is the relay that maximizes the minimum device lifetime to help the selected node. Next, update the power allocation matrices \mathbf{P} and $\hat{\mathbf{P}}$, remove the selected first step. The iteration continues until all nodes have been helped and the helped list is empty or until the device lifetime improvement is insignificant.

The proposed algorithm for finding the relay locations are as follows. We denote K_{\max} as the maximum number of relays and denote Φ_D as the set of all possible relay locations. Initially, the number of relays is set to zero. In each iteration, the number of relay is increased by one, and the optimum relay location $\hat{\mathbf{D}}$ is determined using one of the heuristic search methods (e.g., local search or simulated annealing) together with the algorithm in Table 7.2. The location $\hat{\mathbf{D}}$ that results in maximum of the minimum device lifetime is selected as the relay location.

Table 7.3: Algorithm to determine relay locations

Initialization: $q = 0$
Iteration:
1) Increase number of relays: $q = q+1$
2) For each location $\mathbf{D}_l \in \Phi_D$. Set $\mathbf{D}_{R_q} = \mathbf{D}_l$. Find T_D^* , \mathbf{P} and $\hat{\mathbf{P}}$ using the algorithm in Table 7.2 Denote the obtained results by $T_D^*(l)$, $\mathbf{P}(l)$ and $\hat{\mathbf{P}}(l)$
3) Find the relay location R_q : $\mathbf{D}_{R_q} = \mathbf{D}_{l^*}$, where $l^* = \arg \max_l T_D^*(l)$
4) Update \mathbf{P} , $\hat{\mathbf{P}}$, and T_D^* . Go to 1).
End: If the device lifetime improvement is insignificant, or $q = K_{\max}$. Return \mathbf{P} , $\hat{\mathbf{P}}$, T_D^* .

Then, the device lifetime is updated. Finally, the algorithm goes back to the first step. The algorithm stops if the device lifetime improvement is insignificant or the number of relays reaches K_{\max} . The detailed algorithm is presented in Table 7.3. Note that the proposed algorithm allows at most one relay to help each node. Although it is suboptimal, simulation results in Section 7.4 shows that the proposed algorithm significantly improves the device lifetime. In addition, all of the required computations can be performed offline.

7.4 Simulation Results and Discussions

In all simulations, BPSK modulation is used in the system, the propagation loss factor is $\alpha = 3$, $\eta = 1$, and the BER requirement of each node is $\varepsilon = 10^{-3}$. The processing power of each node (P_s) is set at 25% of transmit power of the node whose location is at (10m, 0). The processing power of each relay (P_r) is set at 50% of P_s . All node have equal initial battery energy of $E_j = 10^5$. The noise variance is set at $N_o = 10^{-2}$. Unless stated otherwise, the nodes are randomly distributed based on uniform distribution over the considered area, and the destination is located in the center. Each node sends information to the destination via a route

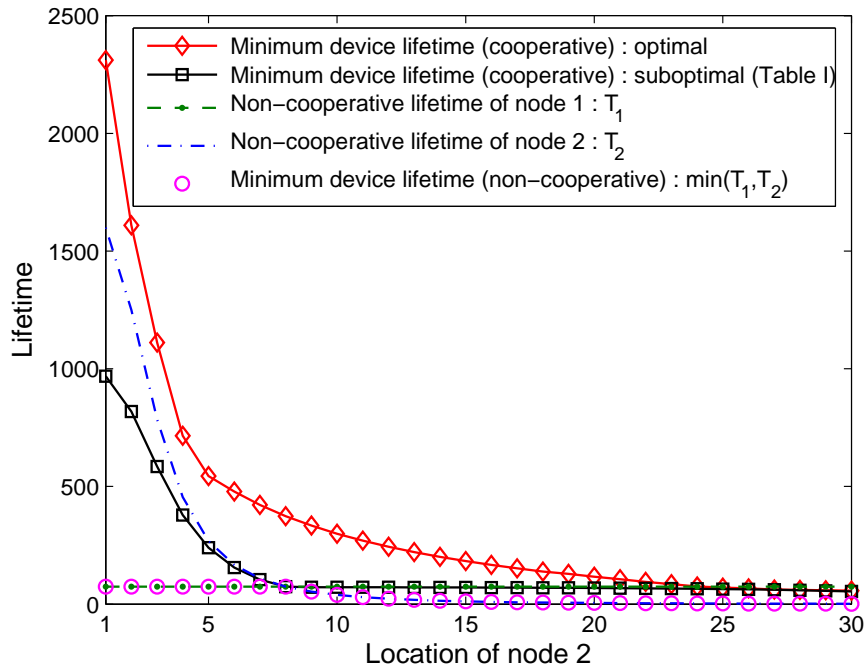


Figure 7.5: Lifetimes of nodes in the two-node wireless network.

that is determined using Dijkstra’s shortest path algorithm.

In Figure 7.5, we consider a two-node wireless network where the destination is located at coordinate $(0, 0)$. Node 1 is fixed at coordinate $(0, 8\text{m})$. The location of node 2 varies from $(0, 1)$ to $(0, 30\text{m})$. Consider non-cooperative transmission, the lifetime of node 1 has a constant value because its location is fixed. The lifetime of node 2 decreases as it moves far away from the destination. We can see that the minimum device lifetime of non-cooperative scheme is determined by the lifetime of the node who is located farther from the destination as shown by a curve with circle (“o”). Under cooperative transmission, the minimum device lifetime is significantly increased, especially when node 2 is located close to the destination. The reason is that when node 2 is close to the destination, it requires small transmit power to reach the destination. After node 2 helps node 1, the transmit power of

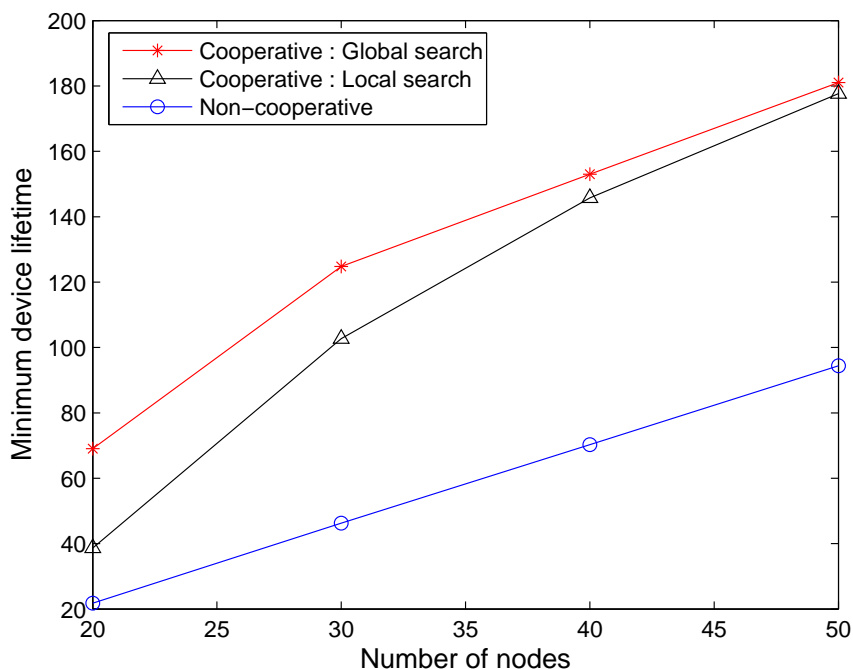


Figure 7.6: Device lifetime with different number of randomly-located nodes.

node 2 slightly increases, while the transmit power of node 1 greatly reduces due to the cooperation diversity. With the proposed suboptimal approach (Table 7.1), the minimum device lifetime is improved to almost the same as the lifetime of the node who is closer to the destination as shown by a curve with rectangular (“□”). By using the optimal power allocation obtained in Section 7.2.1, the minimum device lifetime can be further increased (see a curve with diamond “◇”) since both nodes take advantage of the cooperation diversity while using smaller amount of their transmit powers.

Figure 7.6 depicts the minimum device lifetimes according to different number of multiple cooperative nodes. The number of randomly-located nodes vary from 20 to 50 over an area of size $100m \times 100m$. In the simulation, we normalize the transmission rate to be the same for all network sizes. We compare the minimum device lifetime of (1) the non-cooperative scheme, (2) the cooperative scheme in

which the helping node for each source node is chosen among all nodes, and (3) the cooperative scheme in which the helping node is chosen among the nodes whose distances from the source node is less than 20 meters. From the figure, we can see that the minimum device lifetime of the cooperative network is higher than that of the non-cooperative network for all network sizes. For example, the cooperative network improves the minimum device lifetime by 2 times longer than that of non-cooperative network when there are 50 nodes in the network. Moreover, the cooperative scheme with local search yields close performance to that with global search, especially when the node density is high. This confirms our expectation that the helping node is the one that is located close to the helped node. Note that the minimum device lifetime of both non-cooperative and cooperative schemes increase with number of nodes because the chance of getting help by a node with good location and high energy increases as the number of node increases.

Figure 7.7 shows the minimum device lifetime of a wireless network with cooperative relay deployment. We consider a case when there are 20 randomly-located nodes and a relay with initial energy of $E_{R_i} = 10^6$ in area of $100m \times 100m$. In the figure, a node with circle (“o”) represents a randomly-located node, and a node with rectangular (“□”) shows the location of the destination. In the simulation, we vary the relay location in a grid area of $100m \times 100m$. The x-axis and the y-axis represents the relay location at coordinate (x, y) , and the z-axis represents the corresponding minimum device lifetime. The minimum device lifetime of non-cooperative network is the same for all possible relay locations, and it is shown by a point with (“◇”). The minimum device lifetime of cooperative network, on the other hand, is gradually improved when the relay moves closer to the destination. Specifically, when the relay is far away from the destination the minimum device

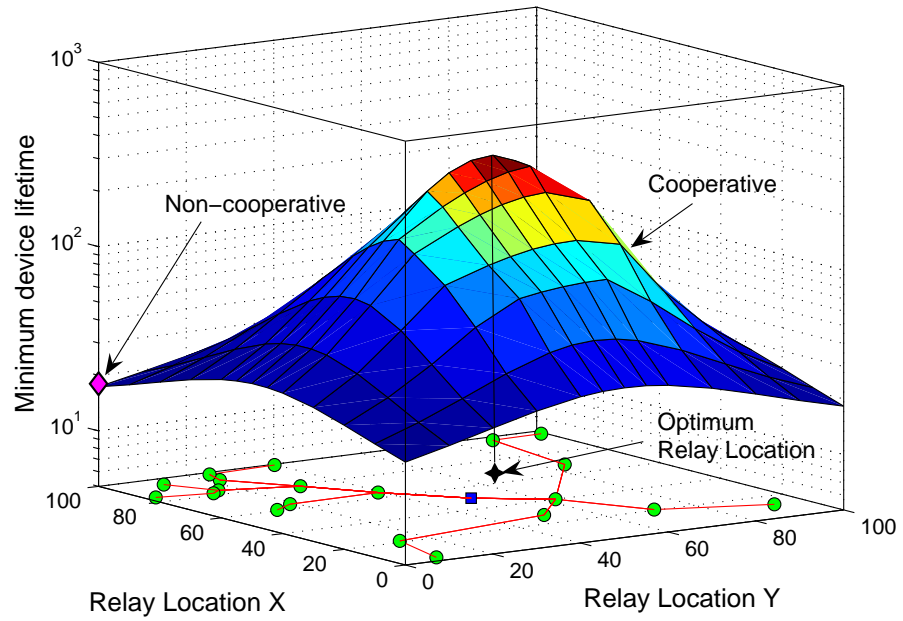


Figure 7.7: Device lifetime for a wireless network with a cooperative relay deployment.

lifetime of the cooperative network is the same as that of non-cooperative network. In addition, the minimum device lifetime can be further improved up to 12 times longer if the relay is located close to the center of the area. This is because the node that is nearest to the destination tends to drain out its battery first, and its lifetime can be greatly improved by placing the relay close to the destination.

Figure 7.8, shows the minimum device lifetime according to different number of cooperative relays. We consider a wireless network with 20 randomly-located nodes in an area of $100m \times 100m$. The initial energy of each relay is 10^5 . The minimum device lifetime of the cooperative network with one randomly-added cooperative relay is about 2 times longer than that of the non-cooperative network, as shown by a curve with cross (“×”). If the relay is placed at the optimum location, the minimum device lifetime of the cooperative network can be improved to 3 times longer than that of non-cooperative network. Furthermore, when two to four relays are added into the network, the minimum device lifetime can be further increased

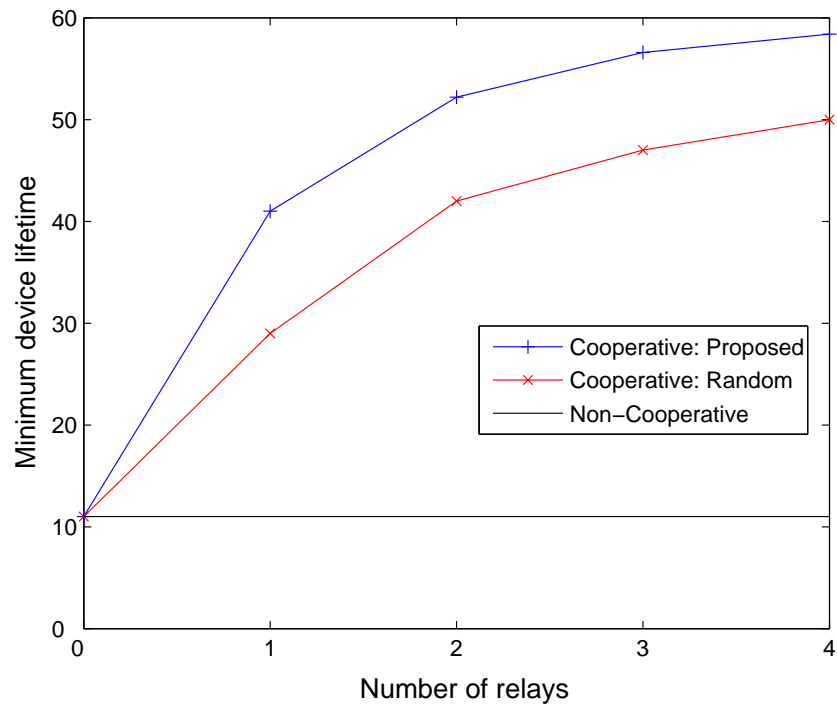


Figure 7.8: Device lifetime of the proposed cooperative wireless network where different number of cooperative relays are deployed.

in both optimum relay location case and random relay location case. However, the minimum device lifetime is almost saturated when more than two relays are deployed in the network.

7.5 Chapter Summary

We propose, in this Chapter, the lifetime maximization by cooperative-node employment and relay deployment in wireless network. By introducing cooperation protocol among nodes, both energy and location advantages are explored, such that the device lifetime is improved. First, decode-and-forward cooperation protocol is employed among nodes. With an objective to maximize the minimum device lifetime, we determine which nodes should cooperate and how much power

to allocate for cooperation. An analytical solution for a two-user wireless network is provided. In case of multiple-node scenario, it turns out that the formulated problem is NP hard. A suboptimal algorithm is developed to reduce the complexity of the formulated problem. By using the proposed suboptimal algorithm, simulation results show that the minimum device lifetime of the two-user cooperative network can be increased to almost the same as the lifetime of the node that is closer to the destination. When there are 50 randomly located nodes in the network, the minimum device lifetime of cooperative network increases 2 times compared with that of the non-cooperative network. Furthermore, we propose to improve the device lifetime by adding cooperative relays into the networks. An optimization problem is formulated to determine the power allocation as well as the relay locations. By optimally placing a cooperative relay with energy 10 times higher than energy of the nodes, the cooperative device lifetime increases 3 times over that for the non-cooperative networks. Furthermore, when energy of relays are equal to energy of the nodes, the proposed algorithm shows that only a few cooperative relays are required in order to improve the device lifetime until saturation.

Chapter 8

Conclusions and Future Research

8.1 Conclusions

In this dissertation, we propose various differential modulation schemes for space-time/cooperative communication systems. The primary goal of the proposed schemes is to reduce receiver complexity by omitting channel estimations as required by their coherent counterparts. In addition, the proposed schemes are able to explore all available diversities such as spatial, time, and/or frequency diversities.

We first consider, for narrowband MIMO systems, the matrix rotation based (MRB) signal design for the differential unitary space-time modulation system. In this work, the signal design criterion is based on minimizing union bound on block error probability. Furthermore, we relax the parameter search from integers to non-integers to get better codes. By taking advantage of symmetric property of the full rotation matrix, we remarkably reduce search space for the best signal constellation. The approximated union bound was applied to further reduce computation time. Simulation results show the performance improvement of the obtained signals, for example, about 0.75 dB for constellation size $L = 4$ and about

1 dB for $L = 64$ which support our numerical calculations. Interestingly, the obtained signal parameters for constellation size $L = 4$ provides almost the same performance as that from optimum codes.

We then propose, for wideband MIMO systems, a differential scheme for MIMO-OFDM systems that can differentially encode signal within one OFDM block. The proposed scheme relaxes the channel assumption to keep constant during each OFDM block and slowly change from a duration of one OFDM block to another, rather than multiple OFDM blocks as assumed in the previously existing works. We formulated the pairwise error probability and design criteria, and showed that our scheme achieves maximum diversity order by utilizing an existing diagonal cyclic codes. Comparing to the previous scheme, the proposed scheme is not only robust to the effect of rapid channel variation, but also reduces encoding and decoding delay. Simulation results showed that our proposed scheme yields better performance than those previously proposed in all of the fading conditions and different power delay profiles. In particular, for a MIMO-OFDM system with two transmit and one receive antennas under the two-ray power delay profile, the proposed scheme outperforms the previous scheme about 2 dB in case of $f_D T_s = 0.0025$ and 0.005 at a BER of 10^{-4} . The performance improvement of more than 6 dB is observed when the fading rate is 0.01. Moreover, in case of the TU power delay profile with $f_D T_s = 0.01$, our proposed scheme achieves 2 dB performance improvement at a BER of 10^{-4} compared to the previous scheme.

We also present in this thesis the frequency-domain differential scheme for multiband UWB systems. By a technique of band hopping in combination with jointly coding across spatial, temporal and frequency domains, The proposed scheme is able to explore the available spatial and multipath diversities, richly

inherent in UWB environments. The analysis reveals that the proposed differential scheme achieves the same diversity advantage under different channel environments. However, the clustering behavior of UWB channels affects the performance through the coding gain. For single antenna multiband UWB system, simulation results show that the proposed differential multiband scheme yields superior performance to the conventional differential encoding scheme, particularly under very short-range line-of-sight scenario, e.g. in CM 1. We obtain about 7 dB gain at a BER of 10^{-2} when jointly encoding across one subcarrier and two OFDM symbols. Moreover, at high SNR range, the proposed jointly encoded differential scheme outperforms the uncoded coherent detection scheme of about 3 – 5 dB at BER between $10^{-2} - 10^{-3}$. In case of multiband UWB system with multiple transmit antennas, while slightly error floor occurs due to the effect of channel mismatch, additional diversity can be observed when number of transmit antennas is increased. However, increasing the number of receive antennas improves the diversity gain without tradeoff in performance due to the effect of channel mismatch.

Although the differential schemes for MIMO systems show promising performance improvement, the deployment of multi-antenna terminals in some applications such as cellular networks or ad-hoc networks may be difficult since the mobile terminals are practically small. We next propose differential modulation schemes for cooperative communications. In these propose schemes, each single-antenna equipped terminal in the networks is allowed to share its antenna with others to obtain MIMO-like diversity while provide low complexity implementation. We first consider a differential scheme for amplify-and-forward protocol in a two-user cooperative communications systems. The proposed scheme with differ-

ential quadrature phase shift keying (DQPSK) signals provided 4 dB performance improvement at a BER of 10^{-3} over that of differential quadrature phase shift keying (DBPSK) direct transmission scheme. In comparison to the coherent detection without relay, the proposed scheme provided a practical alternative with lower complexity and simpler implementation. In addition, simulation results showed that the performance of the proposed scheme was superior to that of direct transmission with coherent detection at SNRs higher than 21 dB. This is due to the fact that the cooperative communications provide more diversity gain than the direct transmission schemes. While the BER analysis of the proposed scheme is not available currently, we provided the exact BER expression for differential M-ary phase shift keying (DMPSK) modulation based on optimum combining weights, and it is considered as a performance benchmark for our proposed scheme. By using the obtained optimum power allocation based on the provided BER expression, the proposed scheme is able to achieve comparable performance to the scheme with optimum weights in any channel variances of all links. Moreover, the performance with optimum power strategy outperforms that from equal power scheme of about 1.4 dB at a BER of 10^{-3} .

We further develop a threshold-based decode-and-forward differential scheme for two-user cooperation systems. By allowing the relay forward only the correctly decoded symbols and introducing a decision threshold at the destination node, the proposed scheme efficiently combines the signals from the direct and the relay links. We provide BER analysis of the proposed scheme with DMPSK modulation by categorizing six different scenarios that lead to different instantaneous SNR's at the combiner output of the destination. A tight BER approximation is also provided. Based on the tight BER approximation, we determine the optimum de-

cision threshold and power allocation numerically. Both theoretical and simulation results reveal that the optimum threshold and optimum power allocation rely on the qualities of the channel links. When the quality of the relay-destination link is much larger than the other links, i.e., $\sigma_{s,d}^2 = \sigma_{s,r}^2 = 1$ and $\sigma_{r,d}^2 = 10$, then the decision threshold is more important than the power allocation at high SNR. For instance, in case of DQPSK signals with equal power allocation, using the optimum threshold results in more than 5 dB improvement gain over the scheme without threshold at a BER of 10^{-4} . By further using the optimum power allocation, the performance improvement is about 0.5 dB at the same BER. Simulation results also show that the proposed scheme with DQPSK signals provides 11 dB performance improvement at a BER of 10^{-3} over the differential DF scheme that the relay always forwards the decoded symbols.

We next propose a multi-node amplify-and-forward differential scheme for cooperative communications. We provide as performance benchmark an exact BER expression for DMPSK modulation based on optimum combining weights. It is shown to closely match to the simulated performance. BER upper bounds and BER approximations are provided; they are tight to the simulated performance, especially in high SNR region. Based on the simple BER upper bound and the BER approximation, we can find that the diversity order of the proposed scheme is $N + 1$ when N is the number of relays and it is confirmed by the simulation results. We observe about 1.7 – 2 dB gain at a BER of 10^{-3} when N increases from 2 to 3. The BER approximation is further simplified in order to obtain analytical result for optimum power allocation scheme. Based on the simple BER approximation, a closed-form power allocation scheme is obtained for single-relay case. An approximate power allocation scheme is provided for multi-relay scenario. Both the

numerical evaluation and the analytical result show that more power should be allocated to the source in order to achieve better performance. When all relays are close to the source, the proposed scheme obtains about 0.6 dB gain over that with equal power allocation at a BER of 10^{-3} . When all relays are close to the destination, the performance with optimum power allocation scheme achieves about 2 dB improvement over that with equal power allocation scheme.

We then consider a differential scheme for multi-node decode-and-forward cooperative communications in which each of N cooperative relays forwards only correctly decoded symbol to the destination. For each relay-destination link, a decision threshold is used at the destination for efficient signal combining. An approximate BER analysis for DMPSK is provided, and a low-complexity BER lower bound is derived. The BER lower bound is very close to the simulated performance under some scenarios. While jointly optimizing power allocation and thresholds based on the BER lower bound introduces $2N + 1$ dimensional searching, the search space is reduced by assuming that the same power is used at each relay and the same threshold is used at the destination. Numerical results reveal that more power should be allocated at the source to maintain link reliability and the rest of power is allocated to each relay. In addition, higher threshold should be used when all relays are close to the destination. Simulation results show that the diversity gain of the proposed scheme increases with the number of relays. Under a DBPSK cooperation system, the proposed scheme with different thresholds leads to performance improvement up to 6 dB at a BER of 10^{-4} . In case of DQPSK cooperation system, the proposed scheme with joint optimum power allocation and optimum threshold achieves about 4 – 5 dB gain over that with equal power allocation and a unit threshold at a BER of $10^{-3} - 10^{-4}$.

Under physical layer perspective, cooperative communications shows significant performance improvement over a system with direct transmission. We investigate, in network layer, energy saving by exploiting cooperative diversity in cooperative wireless networks. Specifically, we consider the lifetime maximization by cooperative-node employment and relay deployment in wireless network. By introducing cooperation protocol among nodes, both energy and location advantages are explored, such that the device lifetime is improved. First, decode-and-forward cooperation protocol is employed among nodes. With an aim to maximize the minimum device lifetime, we determine which nodes should cooperate and how much power to allocate for cooperation. An analytical solution for a two-user wireless network is provided. In case of multiple-node scenario, it turns out that the formulated problem is NP hard. A suboptimal algorithm is developed to reduce the complexity of the formulated problem. By using the proposed suboptimal algorithm, simulation results show that the minimum device lifetime of the two-user cooperative network can be increased to almost the same as the lifetime of the node that is closer to the destination. When there are 50 randomly located nodes in the network, the minimum device lifetime of cooperative network increases 2 times compared with that of the non-cooperative network. Furthermore, we propose to improve the device lifetime by adding cooperative relays into the networks. An optimization problem is formulated to determine the power allocation as well as the relay locations. By optimally placing a cooperative relay with energy 10 times higher than energy of the nodes, the device lifetime increases 3 times over that from the non-cooperative networks. Furthermore, when energy of relays are equal to energy of the nodes, the proposed algorithm shows that only a few cooperative relays are required in order to improve the device lifetime until saturation.

8.2 Future Research

There are a wide range of future research areas that are deserved further investigation. In what follows, we present some interesting future works that require immediate attention.

Since all of the differential modulation schemes that we proposed are based on the differential detection using two consecutive receive symbols, it is worthy to consider multiple-symbol differential detection (MSDD). The MSDD technique provides coding gain improvement and enhances the performance to very closed to the performance of its coherent counterpart.

In the current differential schemes for MIMO-OFDM and MIMO-UWB systems, the performance degradation due to various kinds of interference has not been investigated. The inter-symbol interference can occur when the delay spread is longer than the length of the cyclic prefix. If several devices employing MIMO-OFDM or MIMO-UWB systems simultaneously operate in the vicinity by using the same frequency band, multiple access interference may cause performance degradation. In addition, if some part of frequency band of the MIMO-UWB devices overlap with the operating frequency of a narrowband device, the narrowband interference should also be taken into account.

In the cooperative communication paradigm, it is challenging and very important to find an exact BER expression or an SER expression for the AF differential and the DF differential schemes based on arbitrary combining weights. Furthermore, the effect of channel temporal correlation on system performance of these schemes is an interesting issue to be further investigated.

In addition, a relay selection strategy of the cooperative differential modulation scheme is also a valuable issue to be considered. The relay selection provides

simple implementation because only one RF chain is required. In addition, the relay selection also guarantees to provide the same diversity order as the MRC combining technique. However, those advantages tradeoff with achieving lower coding gain in comparison to that from MRC combining.

Another aspect is to employ distributed differential space time codes among all relays. In this case, after all relays receive signal from the source, various classes of available unitary space-time codes can be used at the relays to formulate MIMO-like transmission. This setup can also be extended to a scenario that there are several cluster of nodes, and each cluster is implemented with distributed differential space time codes.

Since the proposed differential multi-node cooperative communications focuses on a simple multi-node topology. It is interesting and more complete to consider a more general multi-node scenarios. Specifically, by considering a scenario that all relays combines receives signal from all previous relays and the source.

In the current work on the differential DF cooperative scheme, we assume that the relay can make judgement on the correctness of the decoded symbol. However, in a real application, this capability may not be practicable. It is interesting to investigate the possibility of deploying a threshold at each relay to make decision on the received signal. If the obtained BER formulation is mathematically tractable, optimum threshold for each relay can be further determined to improve performance of the proposed scheme.

For the lifetime maximization in cooperative systems, the current work focuses on improving device lifetime of each user and the framework is a centralize scheme. The provided algorithms are built on top of an existing routing algorithm, and hence each transmitter know the next hop. It is interesting to find the lifetime

improvement in cooperative routing problem. In addition, a more general model of distributed implementation is worthwhile to be investigated.

BIBLIOGRAPHY

- [1] T. S. Rappaport, *Wireless Communications: Principles and Practice*. Prentice Hall PTR, 2nd edition, 2002.
- [2] G. Stuber, *Principle of Mobile Communications*, 2nd Ed. Kluwer Academic Publishers, 2001.
- [3] J. G. Proakis, *Digital Communications*. New York, NY: McGraw-Hill, 4th ed., 2000.
- [4] V. Tarokh, N. Seshadri, and A. R. Calderbank, "Space-time codes for high data rate wireless communication: Performance criterion and code construction," *IEEE Trans. Inform. Theory*, vol. 44, pp. 744-765, Mar. 1998.
- [5] I. E. Telatar, "Capacity of multi-antenna gaussian channels," *European Trans. on Telecommunications*, 585-595, Nov. 1999.
- [6] S. Alamouti, "A simple transmit diversity technique for wireless communications," *IEEE J. Select. Areas Commun.*, vol. 16, no. 8, pp. 1451-1458, Mar. 1998.
- [7] V. Tarokh, H. Jafarkhani, and A. R. Calderbank, "Space-time block codes from orthogonal designs," *IEEE Trans. Inform. Theory*, vol. 45, no. 5, pp. 1456-1467, Mar. 1999.

- [8] S. Siwamogsatham, M. P. Fitz, and J. Grim, "A new view of performance analysis of transmit diversity schemes in correlated Rayleigh fading," *IEEE Trans. Inform. Theory*, vol. 48, pp. 950-956, Apr. 2002.
- [9] W. Su, Z. Safar, and K. J. R. Liu, "Space-time signal design for time-correlated Rayleigh fading channels," *IEEE Intl. Conf. on Commun.*, vol. 5, pp. 3175-3179, May 2003.
- [10] D. Agrawal, V. Tarokh, A. F. Naguib, and N. Seshadri, "Space-time coded OFDM for high data rate wireless communication over wideband channels," *IEEE Vehicular Tech. Conf.*, vol. 3, pp. 2232-2236, 1998.
- [11] B. Lu and X. Wang, "Space-time code design in OFDM systems," *IEEE Global Telecommun. Conf.*, vol. 2, no. 3, pp. 1000-1004, Nov.-Dec. 27-1, 2000.
- [12] K. Lee and D. Williams, "A space-frequency transmitter diversity technique for OFDM systems," *IEEE Global Telecommun. Conf.*, vol. 3, pp. 1473-1477, Dec. 2000.
- [13] H. Bolcskei and A. J. Paulraj, "Space-frequency coded broadband OFDM systems," *IEEE Wireless Commun. and Networking Conf.*, vol. 1, pp. 1-6, Sep. 2000.
- [14] Y. Gong and K. B. Lataief, "An efficient space-frequency coded wideband OFDM system for wireless communications," *IEEE Global Telecommun. Conf.*, San Antonio, USA, Nov. 2001.
- [15] W. Su, Z. Safar, M. Olfat, K. J. R. Liu, "Obtaining full-diversity space-frequency codes from space-time codes via mapping," *IEEE Transactions*

- on Signal Processing (Special Issue on MIMO Wireless Systems)*, vol. 51, no. 11, pp. 2905-2916, Nov. 2003.
- [16] Y. Gong and K. B. Lataief, "Space-frequency-time coded OFDM for broadband wireless communications," *IEEE Global Telecommun. Conf.*, San Antonio, USA, Nov. 2001.
- [17] A. F. Molisch, M. Z. Win, and J. H. Winters, "Space-time-frequency coding for MIMO-OFDM systems," *IEEE Commun. Letters*, vol. 6, pp. 370-372, Sept. 2002.
- [18] W. Su, Z. Safar, and K. J. R. Liu, "Towards maximum achievable diversity in space, time and frequency: performance analysis and code design," *IEEE Trans. on Wireless Commun.*, to appear.
- [19] J. N. Laneman, D. N. C. Tse, and G. W. Wornell, "Cooperative diversity in wireless networks: efficient protocols and outage behavior," *IEEE Trans. Inform. Theory*, vol. 50, no. 12, pp. 3062-3080, Dec. 2004.
- [20] T. E. Hunter and A. Nosratinia, "Cooperative diversity through coding," in *Proc. IEEE Intl. Symp. Inform. Theory, (ISIT)*, Laussane, Switzerland, p. 220, Jul. 2002.
- [21] A. Sendonaris, E. Erkip, and B. Aazhang, "User cooperation diversity, Part I: system description," *IEEE Trans. on Commun.*, vol. 51, no. 11, pp. 1927-1938, Nov. 2003.
- [22] A. Sendonaris, E. Erkip, and B. Aazhang, "User cooperation diversity, Part II: implementation aspects and performance analysis," *IEEE Trans. on Commun.*, vol. 51, no. 11, pp. 1939-1948, Nov. 2003.

- [23] W. Su, A. K. Sadek, and K. J. R. Liu, "SER performance analysis and optimum power allocation for decode-and-forward cooperation protocol in wireless networks," in *Proc. IEEE WCNC*, New Orleans, LA, Mar. 2005.
- [24] EIA/TIA IS-54, Cellular system dual-mode mobile stationbase station compatibility standard.
- [25] B. M. Hochwald and T. L. Marzetta, "Unitary space-time modulation for multiple-antenna communication in Rayleigh flat-fading," *IEEE Trans. on Information Theory*, pp. 543-564, Mar. 2000.
- [26] B. M. Hochwald and W. Sweldens, "Differential unitary space-time modulation," *IEEE Trans. Commun.*, vol. 48, pp. 2041-2052, Dec. 2000.
- [27] B. L. Hughes, "Differential space-time modulation," *IEEE Trans. Inform. Theory*, vol. 46, pp. 2567-2578, Nov. 2000.
- [28] V. Tarokh and H. Jafarkhani, "A differential detection scheme for transmit diversity," *IEEE J. Select. Areas Commun.*, vol. 18, pp. 1169-1174, Jul. 2000.
- [29] H. Jafarkhani and V. Tarokh, "Multiple transmit antenna differential detection from generalized orthogonal designs," *IEEE Trans. on Information Theory*, pp. 2626-2631, Sept. 2001.
- [30] G. Ganesan and P. Stoica, "Differential detection based on space-time block codes," *Wireless Personal Commun.*, Kluwer Academic Publishers, vol. 21, pp. 163-180, 2002.
- [31] G. Ganesan and P. Stoica, "Differential modulation using space-time block codes," *IEEE Signal Processing Letters*, pp. 57-60, 2002.

- [32] Z. Chen, G. Zhu, J. Shen, and Y. Liu, "Differential space-time block codes from amicable orthogonal designs," *IEEE Wireless Communications and Networking Conference (WCNC)*, pp. 768772, Mar. 2003.
- [33] M. Tao and R. S. Cheng, "Differential space-time block codes," *IEEE Globecom*, pp. 1098-1102, Nov. 2001.
- [34] S. N. Diggavi, N. Al-Dhahir, A. Stamoulis, and A. R. Calderbank, "Differential space-time coding for frequency-selective channels," *IEEE Commun. Letters*, , vol. 6, pp. 253-255, Jun. 2002.
- [35] H. Li, "Differential space-time modulation with maximum spatio-spectral diversity," *IEEE Intl. Conf. on Commun.*, vol. 4, pp. 2588-2592, May 2003.
- [36] H. Li, "Differential space-time-frequency modulation over frequency-selective fading channels," *IEEE Commun. Letters*, vol. 7, pp. 349-351, Aug. 2003.
- [37] H. Li, "Differential space-time modulation with full spatio-spectral diversity and arbitrary number of transmit antennas in ISI channels," *IEEE Intl. Conf. on Acoustics, Speech, and Signal Processing*, vol. 4, pp. 37-40, Apr. 2003.
- [38] J. Wang and K. Yao, "Differential unitary space-time-frequency coding for MIMO OFDM systems," *Conf. Record of the Thirty-Sixth Asilomar Conf. on Signals, Systems and Computers*, vol. 2, pp. 1867-1871, Nov. 3-6, 2002.
- [39] Q. Ma, C. Tepedelenlioğlu, and Z. Liu, "Differential space-time-frequency coded OFDM with maximum diversity," *Conf. on Information Sciences and Systems, The Johns Hopkins University*, Mar. 12-14, 2003.

- [40] Q. Ma, C. Tepedelenlioğlu, and Z. Liu, “Full diversity block diagonal codes for differential space-time-frequency coded OFDM,” *IEEE Global Telecommun. Conf.*, vol. 2, pp. 868-872, Dec. 1-5, 2003.
- [41] Q. Ma, C. Tepedelenlioğlu, and Z. Liu, “Differential space-time-frequency coded OFDM with maximum multipath diversity,” *Submitted to IEEE Trans. Wireless Commun.*, 2003.
- [42] A. Shokrollahi, B. Hassibi, B. M. Hochwald, and W. Sweldens, “Representation theory for high-rate multiple-antenna code design”, *IEEE Trans. Inform. Theory*, vol. 47, pp. 2335-2367, Sep. 2001.
- [43] X.-B. Liang and X.-G. Xia, “Unitary signal constellations for differential space-time modulation with two transmit antennas: parametric codes, optimal designs, and bounds”, *IEEE Trans. Inform. Theory*, vol. 48, no. 8, pp. 2291-2322, Aug. 2002.
- [44] C. Shan, A. Nallanathan, and P. Y. Kam, “Signal constellation for differential unitary space-time modulation with multiple transmit antennas”, *Vehicular Technology Conference, the 57th IEEE Semiannual*, vol. 1, pp. 713-716, Apr. 2003.
- [45] J. Wang, M. K. Simon, and K. Yao, “On the optimum design of differential unitary space-time modulation”, *to appear in IEEE Trans. Commun.*
- [46] M. K. Byun and B. G. Lee, “New bounds of pairwise error probability for space-time codes in Rayleigh fading channels”, *IEEE Proc. WCNC 2002*, pp. 89-93. Mar. 2002.

- [47] H. Bölcskei and M. Borgmann, "Code design for non-coherent MIMO-OFDM systems," *Allerton Conf. on Commun., Control, and Comput., Monticello, IL*, pp. 237-246, Oct. 2002.
- [48] A. Batra, "Multi-band OFDM Physical Layer Proposal for IEEE P802.15 Task Group 3a," www.multibandofdm.org, Mar. 2004.
- [49] M. Ho, V. S. Somayazulu, J. Foerster, and S. Roy, "A differential detector for an ultra-wideband communications system," *IEEE Vehicular Technology Conf.*, vol. 4, no. 9, pp. 1896 - 1900, May. 2002.
- [50] G. Durisi and S. Benedetto, "Performance of coherent and noncoherent receivers for UWB communications," *IEEE International Conf. on Commun...*, vol. 6, no. 9, pp. 3429 - 3433, Jun. 2004.
- [51] M-O Wessman, A. Svensson, and E. Agrell, "Frequency diversity performance of coded multiband-OFDM systems on IEEE UWB channels," *IEEE Vehicular Technology Conf.*, Sep. 2004.
- [52] W. P. Siriwongpairat, W. Su, M. Olfat, and K. J. R. Liu "Space-time-frequency coded multiband UWB communication systems," *IEEE Wireless Commun. and Networking Conf.*, to appear.
- [53] M. O. Hasna and M.-S. Alouini, "Performance analysis of two-hop relayed transmissions over Rayleigh fading channels," in *Proc. IEEE Vehicular Tech. Conf. (VTC)*, vol. 4, pp. 1992-1996, Nov. 2003.
- [54] D. Chen and J. N. Laneman, "Noncoherent demodulation for cooperative diversity in wireless systems," *IEEE Global Comm. Conf. (GLOBECOM)*, Dallas, TX, pp. 31-35, Nov. 2004.

- [55] M. C. Valenti and B. Zhao, "Distributed turbo codes: Towards the capacity of the relay channel," *IEEE Vehicular Tech. Conf.*, vol. 1, pp. 322-326, Oct. 2003.
- [56] Anders Host-Madsen, "Upper and lower bounds for channel capacity of asynchronous cooperative diversity networks," *IEEE Trans. on Inform. Theory*, vol. 50, pp. 3062-3080, Dec. 2004.
- [57] J. Luo, R. S. Blum, L. J. Greenstein, L. J. Cimini, and A. M. Haimovich, "New approaches for cooperative use of multiple antennas in ad hoc wireless networks," *IEEE Vehicular Technology Conf.*, vol. 4, pp. 2769-2773, Sep. 2004.
- [58] H. Zhu, T. Himsoon, W. P. Siriwongpairat, and K. J. R. Liu, "Energy-efficient cooperative transmission over multiuser OFDM networks: who helps whom and how to cooperate," *IEEE WCNC*, vol. 2, pp. 1030-1035, Mar. 2005.
- [59] A. Bletsas, A. Lippman, and D. P. Reed, "A simple distributed method for relay selection in cooperative diversity wireless networks based on reciprocity and channel measurements," *IEEE Vehicular Technology Conf.*, vol. 3, pp. 1484-1488, May 2005.
- [60] M. Dianati, X. Ling, S. Naik, and X. Shen, "Performance analysis of the node cooperative ARQ scheme for wireless Ad-Hoc networks," *IEEE Globecom '05*, Dec. 2005.

- [61] W. Su, Z. Safar, and K. J. R. Liu, "Systematic design of space-frequency codes with full rates and full diversity," *IEEE Wireless Commun. and Networking Conf.*, Mar. 2004.
- [62] M. Brehler and M. K. Varanasi, "Asymptotic error probability analysis of quadratic receivers in Rayleigh-fading channels with applications to a unified analysis of coherent and noncoherent space-time receivers," *IEEE Trans. Inform. Theory*, vol. 47, no.6, pp. 2383-2399, Sep. 2001.
- [63] O. Y. Takeshita and D. J. Costello, Jr., "New classes of algebraic interleavers for turbo-codes," *IEEE Intl. Symp. on Inform. Theory*, vol. 9, p. 419, Aug. 1998.
- [64] J. Foerster, et. al, "Channel modeling sub-committee report final," IEEE 802.15-02/490, Nov. 18, 2003.
- [65] A. A. M. Saleh and R. A. Valenzuela, "A statistical model for indoor multipath propagation," *IEEE J. on Selected Areas in Commun.*, vol. 5, no. 2, pp. 128-137, Feb. 1987.
- [66] W. C. Jakes, *Microwave Mobile Communications*. Piscataway, NJ: IEEE Press, 1993.
- [67] B. L. Hughes, "Optimal space-time constellation from groups", *IEEE Trans. Inform. Theory*, vol. 49, pp. 401-410, Feb. 2003.
- [68] M. K. Byun and B. G. Lee, "New bounds of pairwise error probability for space-time codes in Rayleigh fading channels", *IEEE Proc. WCNC 2002*, pp. 89-93. Mar. 2002.

- [69] H. F. Lu, Y. Wang, P. V. Kumar, and K. M. Chugg, “On the performance of space-time codes”, *IEEE Proc. Inform. Theory Workshop 2002*, pp. 49-52. Oct. 2002.
- [70] J. Wang, M. P. Fitz, and K. Yao, “Differential unitary space-time Modulation for a large number of receive antennas”, *Signals, Systems and Computers Conference*, vol. 1, pp. 565-569, Nov. 2002.
- [71] J. Wang, M. K. Simon, and K. Yao, “On the optimum design of differential unitary space-time modulation”, *to appear in IEEE Trans. Commun.*
- [72] T. Himsoon, W. Su, and K. J. R. Liu, “Matrix rotation based signal design for differential unitary space-time modulation”, *IEEE Proc. WCNC 2004, Atlanta, GA, Mar. 2004.*
- [73] Z. Liu, and G. B. Giannakis, “Block differentially encoded OFDM with maximum multipath diversity,” *IEEE Trans. Wireless Commun.*, vol. 2, pp. 420-423, May 2003.
- [74] B. Hassibi and M. Khorrami, “Fully-diverse multiple-antenna signal constellations and fixed-point-free Lie groups,” *IEEE Trans. Inform. Theory*, submitted.
- [75] R. A. Horn and C. R. Johnson, *Topics in Matrix Analysis*, New York: Cambridge Univ. Press, 1994.
- [76] W. Su, Z. Safar, and K. J. R. Liu, “Full-rate full-diversity space-frequency codes with optimum coding advantage,” *IEEE Trans. Inform. Theory.*, vol. 51, pp. 229-249, Jan. 2005.

- [77] T. Himsoon, W. Su, and K. J. R. Liu, "Single-block differential transmit scheme for frequency selective MIMO-OFDM systems," *IEEE Wireless Commun. and Networking Conf.*, Mar. 2005.
- [78] O. Y. Takeshita and D. J. Costello, Jr., "New classes of algebraic interleavers for turbo-codes," *IEEE Intl. Symp. on Inform. Theory*, vol. 9, p. 419, Aug. 1998.
- [79] Q. Ma, C. Tepedelenlioğlu, and Z. Liu, "Full diversity block diagonal codes for differential space-time-frequency coded OFDM," *IEEE Global Telecommun. Conf.*, vol. 2, pp. 868-872, Dec. 1-5, 2003.
- [80] T. Himsoon, W. Su, and K. J. R. Liu, "Single-block differential transmit scheme for frequency selective MIMO-OFDM systems," *IEEE WCNC*, vol. 1, pp. 532-537, Mar. 2005.
- [81] W. Su and K. J. R. Liu,, "Differential space-frequency modulation for MIMO-OFDM systems via a smooth logical channel," *IEEE Global Telecommun. Conf.*, Dec. 2004.
- [82] J. Foerster, et. al, "Channel modeling sub-committee report final," IEEE802.15-02/490, Nov. 18, 2003.
- [83] A. A. M. Saleh and R. A. Valenzuela, "A statistical model for indoor multipath propagation," *IEEE J. on Selected Areas in Commun.*, vol. 5, no. 2, pp. 128-137, Feb. 1987.
- [84] R. A. Horn and C. R. Johnson, *Topics in Matrix Analysis*, New York: Cambridge Univ. Press, 1994.

- [85] K. L. Clarkson, W. Sweldens, and A. Zheng, "Fast multiple antenna differential decoding," *IEEE Trans. Commun.*, vol. 49, pp. 253-261, Feb. 2001.
- [86] M. Brehler and M. K. Varanasi, "Asymptotic error probability analysis of quadratic receivers in Rayleigh-fading channels with applications to a unified analysis of coherent and noncoherent space-time receivers," *IEEE Trans. Inform. Theory*, vol. 47, no.6, pp. 2383-2399, Sep. 2001.
- [87] W. Pam Siritwongpairat, W. Su, K. J. R. Liu, "Characterizing performance of multiband UWB systems using Poisson cluster arriving fading paths," *IEEE SPAWC*, pp. 264-268, Jul. 2005.
- [88] M. K. Simon and M.-S. Alouini, "A unified approach to the probability of error for noncoherent and differentially coherent modulations over generalized fading channels," *IEEE Trans. Commun.*, vol. 46, no. 12, pp. 1625-1638, Dec. 1998.
- [89] D. G. Brennan, "Linear diversity combining techniques," *Proceedings of the IEEE*, vol. 91, no. 2, pp. 331-356, Feb. 2003.
- [90] M. K. Simon, S. M. Hinedi, and W. C. Lindsey, *Digital Communication Techniques—Signal Design and Detection*. Englewood Cliffs, NJ: Prentice Hall, 1994.
- [91] J. N. Laneman, G. W. Wornell, and D. N. C. Tse, "An efficient protocol for realizing cooperative diversity in wireless networks," in *Proc. IEEE Intl. Symp. Inform. Theory, (ISIT)*, Washington, DC, Jun. 2001.

- [92] M. Janani, A. Hedayat, T. E. Hunter and A. Nosratinia, "Coded cooperation in wireless communications: space-time transmission and iterative decoding," *IEEE Trans. Signal Processing*, vol. 52, pp. 362-370, Feb. 2004.
- [93] W. Su, A. K. Sadek, and K. J. R. Liu, "SER performance analysis and optimum power allocation for decode-and-forward cooperation protocol in wireless networks" in *Proc. IEEE WCNC 2005*, vol. 2, pp. 984-989, Mar. 2005.
- [94] A. K. Sadek, W. Su, and K. J. R. Liu, "Multi-node cooperative communications in wireless networks," in *Proc. IEEE SPAWC 2005*, New York city, NY, Jun. 2005.
- [95] P. Tarasak, H. Minn, and V. K. Bhargava, "Differential modulation for two-user cooperative diversity systems," *IEEE Global Comm. Conf. (GLOBECOM)*, Dallas, TX, Nov. 2004.
- [96] R. F. Pawula, "Generic error probabilities," *IEEE Trans. Commun.*, vol. 47, no. 5, pp. 697-702, May 1999.
- [97] H. Stark and J. W. Woods, *Probability and Random Processes with Applications to Signal Processing*. Upper Saddle River, NJ: Prentice Hall, 2001.
- [98] Q. Zhao and H. Li, "Performance of differential modulation with wireless relays in Rayleigh fading channels," *IEEE Commun. Letters*, vol. 9, no.4, pp. 343-345, Apr. 2005.
- [99] T. Himsoon, W. Su, and K. J. R. Liu, "Differential transmission for amplify-and-forward cooperative communications," *IEEE Signal Processing Letters*, vol. 12, pp. 597-600, Sept. 2005.

- [100] I. S. Gradshteyn, I. M. Ryzhik, and A. Jeffrey, *Table of Integrals, Series, and Products*. San Diego, CA: Academic Press, 1994.
- [101] J.-H. Chang and L. Tassiulas, "Maximum lifetime routing in wireless sensor networks," *IEEE/ACM Trans. on Networking*, vol. 12, no. 4, pp. 609-619, Aug. 2004.
- [102] M. Bhardwaj, T. Garnett, and A. P. Chandrakasan, "Upper bounds on the lifetime of sensor networks," *Proc. of the Int. Conf. on Commun.*, vol. 3, pp. 785-790, June 2001.
- [103] H. Zhang and J. Hou, "On deriving the upper bound of lifetime for large sensor networks," *Proc. MobiHoc*, pp. 121-132, 2004.
- [104] Z. Hu and B. Li, "On the fundamental capacity and lifetime limits of energy-constrained wireless sensor networks," *10th IEEE Proc. of Real-Time and Embedded Technology and Applications Symposium*, pp. 2-9, May 2004.
- [105] R. J. Marks, A. K. Das, and M. El-Sharkawi, "Maximizing lifetime in an energy constrained wireless sensor array using team optimization of cooperating systems," *Int. Joint Conf. on Neural Networks*, pp. 371-376, May 2002.
- [106] I. Maric and R. D. Yates, "Cooperative broadcast for maximum network lifetime," *Conf. on Inform. Sciences and Systems*, vol. 1, pp. 591-596, 2004.
- [107] P. Floreen, P. Kaski, J. Kohonen, and P. Orponen, "Multicast time maximization in energy constrained wireless networks," *ACM/IEEE Mobicom 2003 Workshop on Foundations of Mobile Computing*, Sept. 2003.

- [108] Y. T. Hou, Y. Shi, H. D. Sherali, and S. F. Midkiff, "On energy provisioning and relay node placement for wireless sensor networks," *IEEE Trans. on Commun.*, vol 4, pp. 2579-2590, Sept. 2005.
- [109] J. W. Craig, "A new simple and exact result for calculating the probability of error for two-dimensional signal constellations," *IEEE MILCOM*, pp. 25.5.1-25.5.5, 1991.
- [110] H. Kellerer, U. Pferschy, and D. Pisinger, *Knapsack problems*, Springer, New York, 2004.